GEOLOGICAL SURVEY OF NAMIBIA

MINISTRY OF MINES AND ENERGY

TECTONICS AND SEDIMENTATION OF A LATE PROTEROZOIC DAMARAN CONVERGENT CONTINENTAL MARGIN, KHOMAS HOCHLAND, CENTRAL NAMIBIA

by

PETER A. KUKLA

MEMOIR 12

1992

***Front cover*:** Sedimentary cycles in the Kuiseb Formation of the Khomas Hochland. View southwestwards from the farmroad on the farm Tsawisis 308 towards one of the mountains (16°13′15″E, 22°44′37″S) bordering the Kaan river. The 200 m-high hillside consists of Kuiseb Formation psammites and pelites which are organized into two thickening-upward cycles, each approximately 100 m thick. The top of the cycles is formed by thick psammitic units (bed thickness up to 5 metres) which constitute the two marked ridges in the centre and in the top part of the mountain.

MINISTRY OF MINES AND ENERGY

GEOLOGICAL SURVEY OF NAMIBIA

Director: R. McG. Miller

MEMOIR 12

Tectonics and sedimentation of a Late Proterozoic Damaran Convergent Continental Margin, Khomas Hochland, Central Namibia

by

Peter A. Kukla

Editor: Clare Kennedy Galloway

Typesetting and layout: J. Angermund

Obtainable from the Geological Survey
P.O. Box 2168, Windhoek, 9000, Namibia

	Price
Local (+ GST)	R 20.00
Abroad Post Free	R 25.00

ISBN 0 86976 245 1

ABSTRACT

The Late Proterozoic Damara Orogen (750-450 Ma) in Namibia forms part of the Pan-African mobile belt system which bisects southern Africa. The Khomas Trough in the inland branch of the orogen comprises thick multiply-deformed metagreywackes and metapelites of the Kuiseb Formation. Minor lithologies are graphite schists, calc-silicates and scapolite schists. The Matchless Amphibolite Member is structurally emplaced within the sequence and contains tholeiitic, mid-ocean ridge-type metavolcanic rocks, including pillow lavas and breccias, as well as ultramafic lithologies and metagabbroic lenses. Pelagic graphite schists, pelitic schists and a marble unit are intercalated within the metabasic rocks. Original sedimentary structures, turbidite facies, the vertical facies distribution of progradational and retrogradational cycles, and the lateral extent of major sedimentary units indicate that psammitic parts of the sedimentary protoliths have been deposited as turbidites on an elongate submarine fan. Geochemical signatures suggest that an active continental margin source to the northeast of the present-day Khomas Trough supplied the vast amounts of clastic sediment. The regional structural pattern is characterized by five phases of deformation with folds verging consistently to the southeast. The structural regime is markedly heterogeneous and is associated with thrusting which developed elongate thrust slices traceable laterally for at least 150 km. Metamorphic index minerals indicate lower to upper amphibolite facies conditions but partial melting occurred in some areas along the northern margin of the Khomas Trough.

These features are explained in a tectono-sedimentary model which involves the evolution of a Late Proterozoic accretionary prism, here named the Khomas Hochland accretionary prism, within a convergent continental margin setting. Rift initiation took place along old tectonic weakness zones between the Congo and Kalahari Cratons. This was followed by the formation of oceanic crust in the Khomas Sea which was an appreciably-

sized oceanic basin with a minimum width of hundreds of kilometres. Subsequent convergence and subduction of oceanic crust beneath the Congo Craton in a northwesterly direction produced an oceanic trench which contained the westward-prograding elongate submarine fan. Pelagic sedimentation occurred contemporaneously within the basin. Basalts including a high proportion of pillow lavas and associated massive sulphide ore deposits formed at the mid-ocean ridge. The accretionary prism evolved through the offscraping of the trench sediments together with some pelagics from the oceanic plate and accretion against the Congo cratonic margin. Early folding and thrusting occurred within the prism during this accretionary stage. Continental collision of the Congo and Kalahari Cratons resulted in the formation of a northwards-steepening thrust pile with an overall imbricate fan geometry. Subsequent phases of compressional deformation involved initially thrusting and folding in a southeasterly direction, which was followed at a late stage by right-lateral strike-slip dislocation along the Okahandja Lineament. The Matchless Amphibolite was most probably emplaced during the abduction of the accretionary prism onto the Kalahari Craton. Thermal relaxation subsequent to subduction led to prolonged amphibolite facies regional metamorphism with the peak occurring late in the deformational history. Heterogeneous geothermal gradients in the Khomas Trough are interpreted to be due to differential uplift. The post-tectonic Donkerhuk Granite intruded along the Okahandja Lineament, which is interpreted to represent the former backstop of the accretionary prism.

Lithologies, structural styles, time sequence of events and the size of the Khomas Hochland accretionary prism may be compared with the Palaeozoic Southern Uplands accretionary prism of Scotland, the Cretaceous Chugach terrain in Alaska and the Shumagin region of the modem Aleutian Trench. Several aspects, such as the inferred width of the Khomas Sea, the scarcity of arc magmatics to the north, the lack of recognition of fore-arc basin deposits, early compressional stresses, extensive sediment loading, and the intercalation of metabasalts, turbidites, pelagics and massive sulphide deposits all point to the shallow subduction of young, buoyant and hot oceanic crust. A comparison to the southern Peru - Chile Trench may be drawn.

TABLE OF CONTENTS

1. INTRODUCTION

1.1 Preamble 1
1.2 Location 1
1.3 Objectives of study 1
1.4 Previous work 2
1.5 Methods of investigation 2

2. GEOLOGICAL SETTING

2.1 Pre-Damaran Basement 3
2.2 Stratigraphy of the Damara Sequence and its radiometric ages 4
2.2.1 Overview of the Damara Stratigraphy 4
2.2.2 Stratigraphy of the Central Zone and the Southern Margin Zone 5
2.2.3 Stratigraphy of the Khomas Trough 6
2.3 Deformation, crustal structure and metamorphism of the Damara Sequence 7

3. SEDIMENTOLOGY

3.1 Introduction 9
3.2 Description of lithotypes 9
3.2.1 Quartz-plagioclase-mica schist (psammite)/ greywacke 9
3.2.2 Mica-quartz-plagioclase schist (pelite and metasiltstone)/mudstone and siltstone 9
3.2.3 Graphitic mica-quartz-plagioclase schist/ carbonaceous mudstone 9
3.2.4 Marble and tremolite schist/carbonate 10
3.2.5 Calc-silicate rock/impure carbonate 10
3.3 Geochemical characterization of psarnmites, pelites and meta-siltstones 10
3.4 Sedimentary structures and palaeocurrents 12
3.5 Turbiditic and pelagic facies 15
3.5.1 Medium- to very thick-bedded psammite facies (facies class 1) 15
3.5.2 Very thick- to thin-bedded graded psam-mite/pelite facies (facies class 2) 16
3.5.3 Thin-laminated metasiltstone facies (facies class 3) 17
3.5.4 Very thick- to thin-bedded pelite facies (facies class 4) 18
3.5.5 Impure metacarbonate facies (facies class 5) ..19
3.5.6 Thin- to very thick-bedded graphite schist facies (facies class 6) 20
3.5.7 Marble and tremolite schist facies (facies class 7) 21
3.6 Vertical facies sequences and sedimentary cycles 22
3.7 Facies models 24
3.8 Depositional setting of the Khomas Trough 28
3.8.1 Previous sedimentation models 28
3.8.2 Geochemical constraints on the source area of Kuiseb metagreywackes 28
3.8.3 Interpretation of elongate submarine-fan and basin-plain depositional environments 29
3.8.4 Discussion of other possible depositional environments 31
3.9 Palaeo-environmental synthesis 32

4. STRUCTURAL GEOLOGY OF THE KHOMAS TROUGH

4.1 Introduction 33
4.2 Structural characteristics of domains 33
4.2.1 Domain A 34
4.2.2 Domain B 35
4.2.3 Domain C 39
4.2.4 Domain D 41
4.2.5 Late fractures 44
4.3 Contact relationships of meta3ediments and migmatites with the Donkerhuk Granite 45
4.4 The recognition of heterogeneous strain and thrusting 46
4.4.1 Heterogeneous strain 46
4.4.2 Major high-strain zones 46
4.4.3 Summary and conclusions 50
4.5 Kinematic interpretation and time sequence of deformational events 54
4.5.1 D_1 phase of deformation 55
4.5.2 D_2 phase of deformation 55
4.5.3 D_3 phase of deformation 56
4.5.4 Later phases of deformation 58
4.5.5 Strike-slip displacement along the northern margin of the Khomas Trough 58
4.5.6 Aspects of strain determinations 58

4.5.7 Consideration of previous studies: a correlation of deformation events in the Khomas Trough 60
4.6 Structural evolution of the Khomas Trough fold-and-thrust belt 60

5. THE MATCHLESS AMPHIBOLITE

5.1 General setting of the Matchless Amphibolite 62
5.2 Lithologies, mineral assemblages and textures 62
5.3 Stratigraphic and structural relationships 62
5.3.1 Stratigraphy 62
5.3.2 Structure 65
5.4 Classification of metabasic rocks 66
5.5 Tectonic setting of the Matchless Amphibolite with special regard to the development of the Khomas Trough 68

6. METAMORPHISM

6.1 Introduction 70
6.2 Mineral textures and relationships to structural elements 70
6.2.1 Pelites 70
6.2.2 Calcareous lithologies 72
6.3 Mineral assemblages 72
6.4 Mineral compositions 75
6.5 The P-T evolution of metamorphism 78
6.5.1 Qualitative estimation of P-T conditions 78
6.5.2 Geothermometry and geobarometry 79
6.5.3 Summary of the P-T conditions in the Khomas Trough 81

7. TECTONICS AND SEDIMENTATION OF A LATE PROTEROZOIC CONVERGENT CONTINENTAL MARGIN

7.1 Previous geodynamic models for the evolution of the inland branch of the Damara Orogen 83
7.2 The tectono-sedimentary evolution of the Khomas Trough 83
7.2.1 Rifting and spreading phase 83
7.2.2 Early subduction phase 84
7.2.3 Accretion phase 84
7.2.4 Collision phase 85
7.2.5 Ancient and modem analogues 87

8. ACKNOWLEDGEMENTS

9. REFERENCES

APPENDIX

I. XRF-analyses of metasediments
II. XRF-analyses of metabasites
III. Microprobe-analyses

1. INTRODUCTION

1.1 Preamble

Geoscientific investigations in Precambrian orogenic belts are seriously hampered by penetrative deformation, metamorphic recrystallization and the lack of biostratigraphic control. In metasedimentary sequences this may result in the obliteration of delicate sedimentary structures which are essential for palaeo-environmental interpretations. Consequently, sedimentary facies analysis, which provides one of the most important tools in looking into the evolution of these orogenic belts, together with structure and other geoscientific approaches, has not been undertaken in many Precambrian orogens.

The Damara Orogen is one of the best-preserved Late Proterozoic orogenic belts worldwide and is therefore crucial for the understanding of later Precambrian tectonics. Nevertheless, palaeo-environmental studies in this belt and especially in the important southern part have so far mainly concentrated on stratigraphic aspects. In this respect the Damara Orogen is no different from other Precambrian belts. In acknowledging the problem, this study introduces a sedimentary facies analysis to the area and together with results obtained from other geoscientific disciplines, attempts a multidisciplinary approach to provide an insight into the evolution of the orogen as a whole.

1.2 Location

Rocks assigned to the Late Proterozoic Damara Sequence in Namibia are exposed within a NNW-trending coastal branch and a NE-trending inland branch (Fig. 1.1). The Khomas Trough of the southern inland branch extends from the Namib desert in the southwest to the Kalahari desert in the northeast. Figure 1.1 shows important geographical features including the Khomas Hochland. The Late Proterozoic Damaran rocks are well exposed at the western end of the Khomas Hochland, which represents the immediate interior of the "Great Escarpment", originating from erosional processes (Ward, 1987) associated with the Cretaceous break-up of Gondwanaland. This area conse-quently provides good surface exposure, whereas the outcrop situation deteriorates rapidly towards the east because of the undissected flat erosional topography associated with the Cretaceous Kalahari basin (Fig. 1.1).

The main study area is a north-south trending traverse near the Great Escarpment about 120 kilometres west of Windhoek (Figs 1.1 and 1.2).

1.3 Objectives of study

The Late Proterozoic Khomas Trough comprises metasedimentary and metabasic rocks of the Kuiseb Formation and its evolution plays an important role in our understanding of the Damara orogenic belt as a whole. The present study attempts to characterize the metasedimentary and metabasic rocks encountered by means of sedimentological, structural, petrographic, mineralogical and geochemical methods. This leads to the modelling of the geotectonic evolution of the

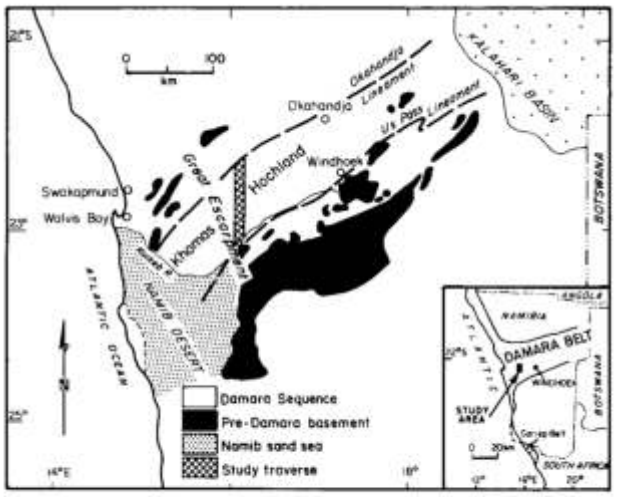

Fig. 1.1: Location of the study area in the inland branch of the Damara Orogen in Namibia.

Khomas Trough with particular focus on the sedimentary palaeoenvironments and the structural evolution of this area during the Pan-African orogeny in Namibia.

1.4 Previous work

Pioneering publications on the geology of the Khomas Trough are those of Gevers (1963) and Martin (1965). Lithostratigraphic aspects of the Kuiseb Formation in the Khomas Trough have been catalogued by the South African Committee for Stratigraphy (SACS, 1980), Miller (1983b) and Hoffmann (1983). Structural studies in parts of the eastern Khomas Trough were undertaken by Gevers (1963), Smith (1965), Hälbich (1970, 1977), Porada and Wittig (1975), Kasch (1975, 1983c) and Blaine (1977). Miller (1979), Sawyer (1981,1983) and Preussinger (1987,1990) studied the structural geology of selected areas in the western Khomas Trough and in the vicinity of the Okahandja Lineament. No detailed facies analysis of the Kuiseb Formation has been undertaken in this part of the southern Damara Orogen prior to this study although preserved sedimentary features (e.g. graded bedding) have been reported from limited areas by Miller (1979), Downing (1983) and Preussinger *et al.* (1987). Initial studies on the thermal evolution of the Damara Orogen as a whole have been undertaken by Hoffer (1977,1983), Behr *et al.* (1983) and Hartmann *et al.* (1983). Sawyer (1981), Kasch (1983b, 1987) and Preussinger (1990) studied the metamorphism of certain areas in the western and eastern Khomas Trough. Geochemical studies of metasediments and amphibolites have been undertaken by Miller (1983c), Miller *et al.* (1983), Schneider (1983), Schmidt and Wedepohl (1983), Breitkopf and Maiden (1987) and Phillips *et al.* (1989). The nature of the massive sulphide deposits associated with the Matchless Member of the Kuiseb Formation has been studied by Killick (1983), Klemd *et al.* (1987, 1989), Breitkopf and Maiden (1988), Preussinger (1990) and Klemd and Okrusch (1990). Little geochronological work has been undertaken and this has mainly concentrated on

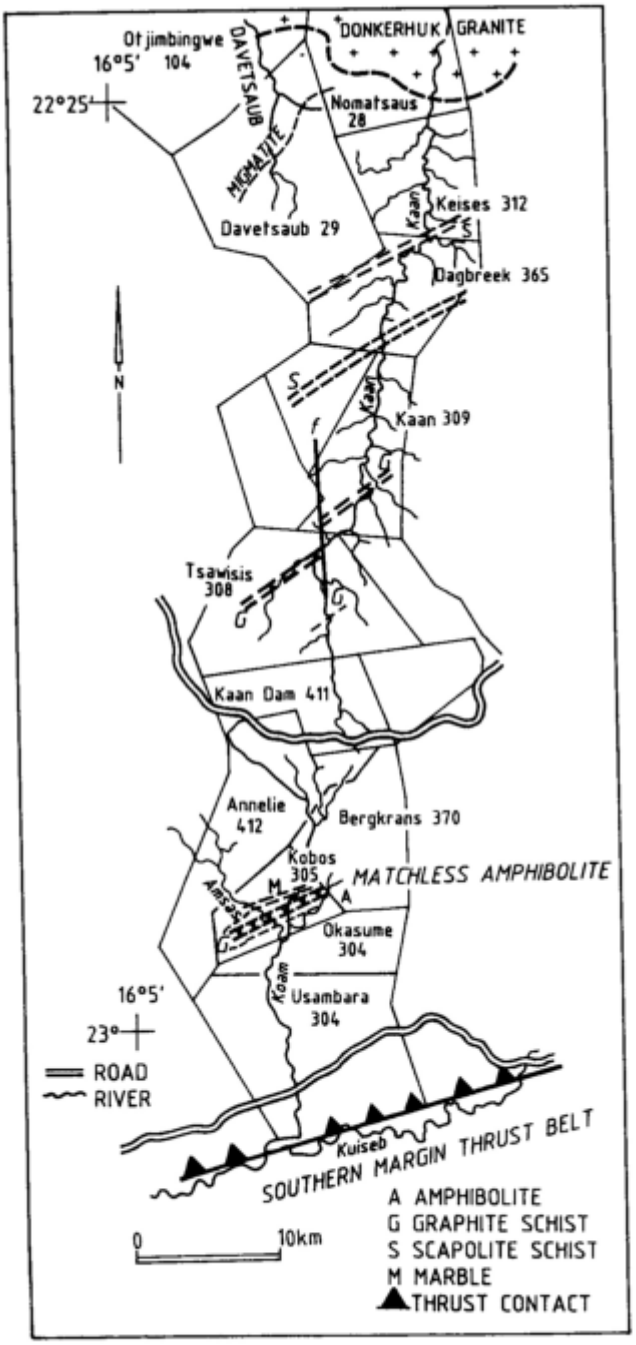

Fig. 1.2: Map of the study traverse showing important marker units, major ephemeral rivers and farm boundaries.

the post-tectonic Donkerhuk Granite and the Kuiseb Formation migmatites (Kröner and Hawkesworth, 1977; Blaxland *et al.*, 1979; Kukla *et al.*, 1990a; Kukla, 1991) as well as on some metasediments (Hawkesworth *et al.*, 1983; Haack, 1983; Kukla, 1991). Kröner (1982) obtained a Rb/Sr isochron from rocks associated with the Matchless Member. A seismic line has been shot and interpreted by Green (1983) and Baier *et al.* (1983) in the eastern Khomas Trough.

Geotectonic models for the evolution of the Damara Orogen as a whole, which incorporate the Khomas Trough, have been proposed by several authors. In summary, the discussion on the geodynamic evolution of the inland branch has concentrated on whether or not oceanic crust has formed, to be subsequently subducted during continental convergence. Aulacogen-related models have been favoured by Martin and Porada (1977), Porada (1983) and Kröner (1982). Limited ocean models have been proposed by Miller (1983b) and Breitkopf (1986) and major ocean models by Blaine (1977), Hartnady (1978), Kasch (1979, 1983a), Barnes and Sawyer (1980) and Downing and Coward (1981).

1.5 Methods of investigation

The main study area is an 80 km-long traverse north to south across the Khomas Hochland west of Windhoek, along ephemeral river valleys (Kaan, Amsas, Koam and Davetsaub rivers) (Fig. 1.2). Only the deeply incised riverbeds associated with the Khomas Hochland Escarpment provide detailed outcrop. Apart from these, exposure is obscured by weathering and gravel cover. In order to trace important stratigraphic and structural marker horizons, these have been mapped along strike from the Namib desert in the west into the Khomas Hochland further east. Important information of large-scale structures has additionally been obtained from Landsat images and aerial photographs.

To gain further regional constraints, the field areas of Sawyer (1981) and Preussinger (1987) in the Gorob district of the Namib desert, as well as the Okahandja - Windhoek profile of Hälbich (1977), have been studied for comparison.

In order to unravel the sedimentological and structural evolution of the Kuiseb Formation, a large number of detailed profiles and sequences were measured along the 80 km-long study traverse. Since no work on the sedimentology and the depositional palaeoenvironments had previously been undertaken, lithotypes were mapped and characterized, original sedimentary structures were documented and a detailed facies analysis was carried out.

A large number of structural data were collected. These were processed together with thin section information m order to interpret the structural evolution and associated compressional directions.

A total of 132 samples of metasediments and 14 samples of amphibolites and metagabbros was analysed by X-ray fluorescence (XRF) analysis for major and trace elements. A sample of marble was analysed by X-ray diffraction (XRD) to identify calcite and dolomite contents.

Mineralogical and petrographic studies were based on about 200 thin sections. Selected samples from different metamorphic zones were chosen for microprobe analyses which were carried out during research leave at the Mineralogy Institute of the University of Würzburg, Germany.

With regard to the origin of the graphite schists and a marble horizon of the Kuiseb Formation several samples were analysed for carbon (^{13}C) and oxygen (^{18}O) isotope contents at the Schonland Research Centre for Nuclear Sciences at the University of the Witwatersrand.

2. GEOLOGICAL SETTING

The Damara Orogen forms part of the Pan-African mobile belt system (Clifford, 1967; Shackleton, 1976; Miller, 1983a; Martin, 1983) which largely surrounds but also bisects the African continent (Fig. 2.1). Two structural types of Pan-African belts have been recognized: (1) belts with thermally and tectonically rejuvenated, older Precambrian basement, such as suggested for the Zambezi and Mozambique Belts (Martin, 1983; Muhongo, 1990); and (2) Late Proterozoic "geosynclines" which have passed through a stage of subsidence and sediment accumulation. The Damara Orogen belongs to the latter type. It consists of a NNW-trending, 150 km-wide coastal branch and a NE-trending, 400 km-wide inland branch (Figs 2.1 and 2.2). Most of the geological research has concentrated on the more easily accessible and more completely preserved inland branch.

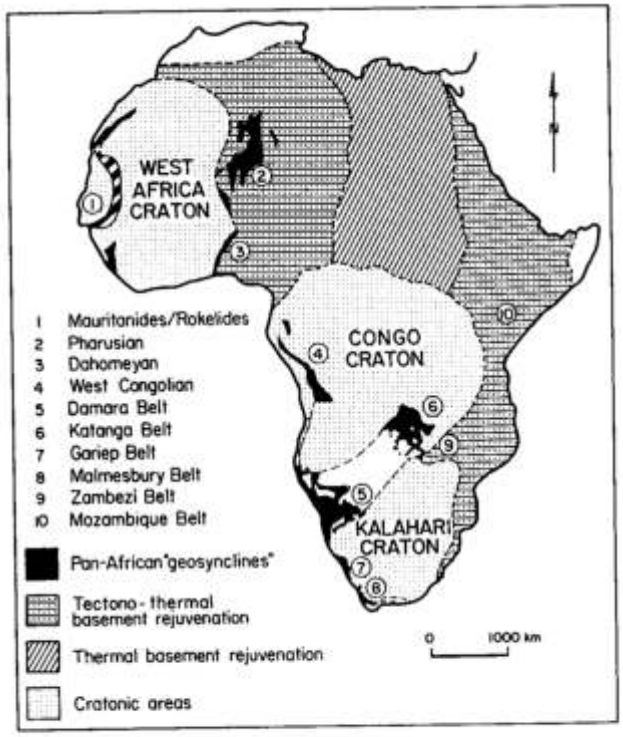

Fig. 2.1: Pan-African orogenic belts and terranes of basement rejuvenation (modified from Porada, 1983).

The southern extension of the Damara Orogen is formed by the Gariep Belt and the Malmesbury Belt (Fig. 2.1; Miller, 1983b; Hartnady *et al.*, 1985). Geophysical features suggest that the inland branch extends further to the east into the Katanga and Zambezi Belts (Reeves, 1978; Hartnady *et al.*, 1985) to form a triple junction with the Mozambique Belt in eastern Africa (Fig. 2.1). It has been suggested that the western limit of the Damara Orogen is represented by the Ribeira Orogen of Brazil (Porada, 1979) but regional and geochronological constraints also indicate that the more southerly Dom Feliciano Belt may be regarded as Damara-equivalent (Cordani *et al.*, 1990).

The Damara Orogen has been subdivided into several tectono-stratigraphic zones, mainly on the basis of stratigraphy, structure, metamorphic grade, magmatic rocks and radiometric age (Miller, 1983a). These are, from north to south (Fig. 2.2): the Kaoko Zone (KZ) (in the coastal branch), the Northern Platform (NP), Northern Zone (NZ), Central Zone (CZ), Okahandja Lineament Zone (OLZ) , Southern Zone (SZ), Southern Margin Zone (SMZ) and Southern Foreland (SF) in the inland branch. The OLZ and SZ are together often referred to as the Khomas Trough (e.g. Martin, 1965; Martin and Porada, 1977), a terminology which is also used in this study. Zone boundaries are in most cases major thrusts, faults and lineaments as indicated in Figure 2.2.

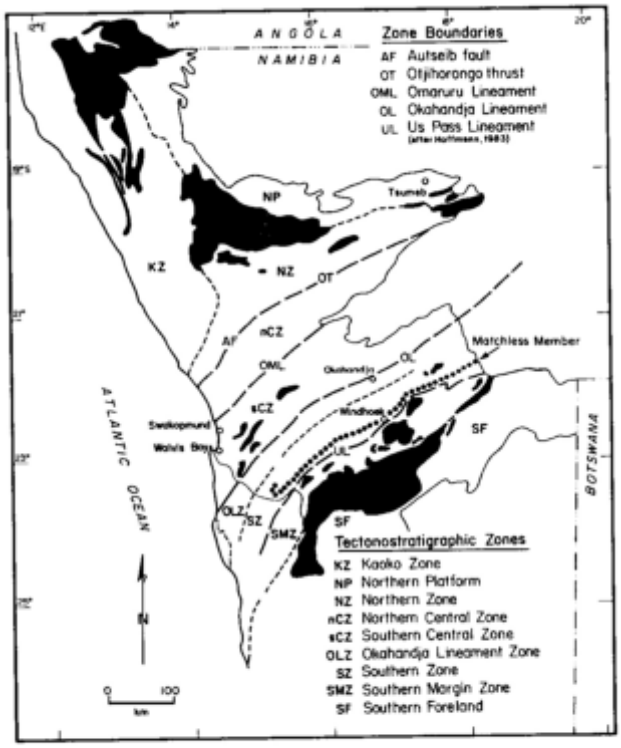

Fig. 2.2: Tectono-stratigraphic zones of the Damara Orogen (from Miller, 1983b).

2.1 Pre-Damaran Basement

The pre-Damaran basement is largely granitic and is exposed to the north and south of the orogen as well as in several inliers in the centre (Fig. 2.2). Radiometric ages are very variable, however, showing the oldest ages in the order of 2000 Ma in the Central Zone (1955±20 Ma,a U-Pb zircon date by Briqueu *et al.*, 1980) and the youngest ages in the order of 1000 Ma in the southern part of the orogen (961±23 Ma, a Rb/Sr whole rock date of Esquevin and Menendez, 1975, in the eastern Khomas Trough; 1049±28 Ma, a Rb/Sr whole rock date of Pfurr *et al.*, 1990, in the Southern Margin Zone).

TABLE 2.1: Lithostratigraphy of the Damara Sequence (from Martin, 1983, based on SACS, 1980).

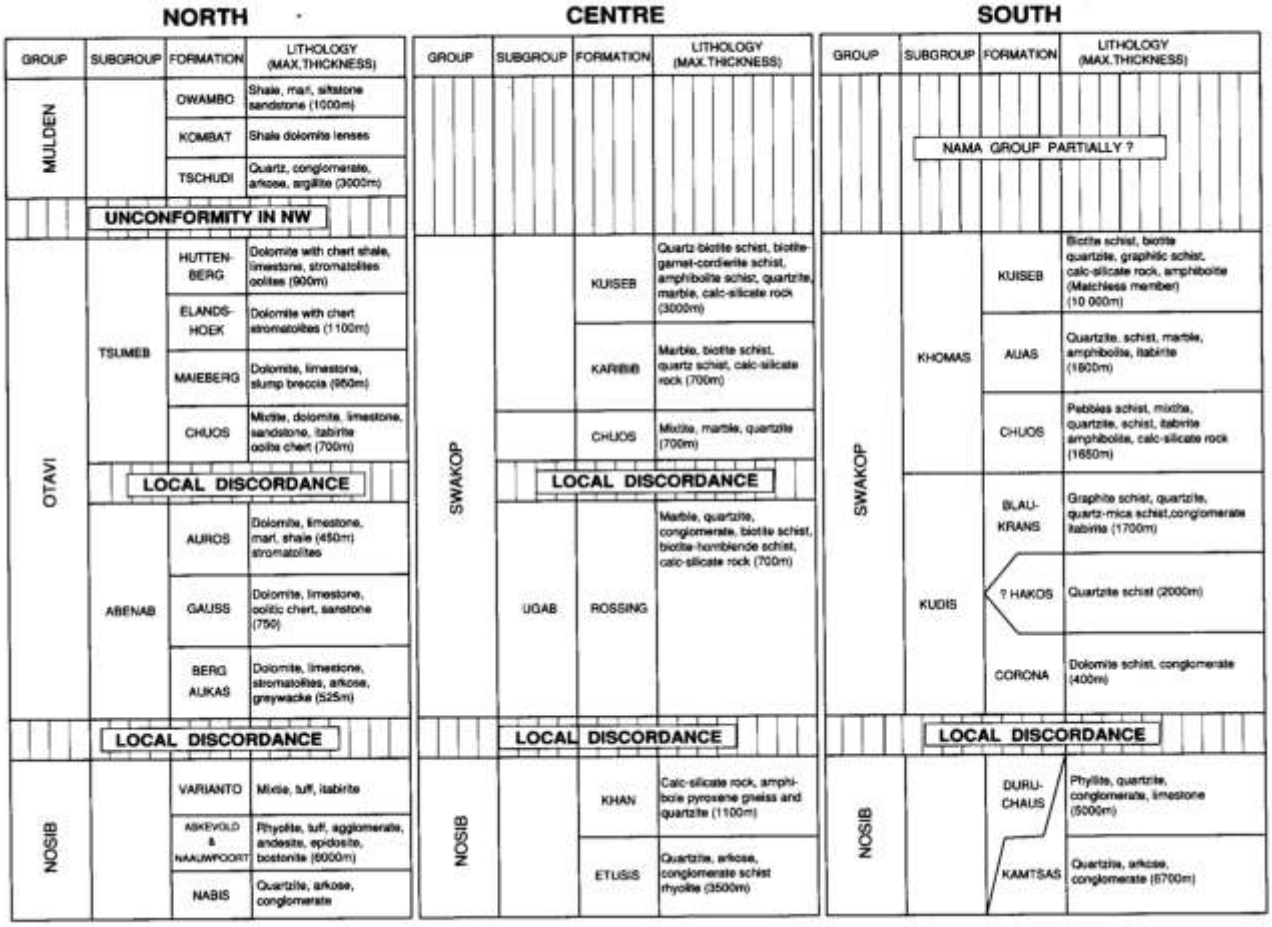

2.2 Stratigraphy of the Damara Sequence and its radiometric ages.

2.2.1 Overview of the Damara Stratigraphy

The stratigraphy in the inland branch shows a marked asymmetrical arrangement of rock types. This is indicated in Table 2.1 which shows subdivisions and correlations as suggested by the South African Committee for Stratigraphy (SACS, 1980). Most important in interpreting the Damara Sequence is the occurrence of a number of unconformities which define several unconformity-bound sequences within the stratigraphic column (Table 2.1).

The earliest sediments and volcanic rocks of the Damara Sequence belong to the Nosib Group (Table 2.1) which discordantly overlies pre-Damaran basement. The Nosib Group comprises a wide spectrum of mainly fluviatile deposits and alkalic to acid volcanic rocks. Thick and widespread rhyolites of the Naauwpoort Formation in the Northern Zone are considered to represent a time marker for the early evolution, i.e. rifting, of the orogen (Miller, 1983b) at 750±65 Ma (U-Pb zircon ages, Miller and Burger, 1983). The initiation of rifting is considered by Miller (1983b) to pre-date the Oas Syenite which intruded Nosib sediments at 840±12 Ma (Rb-Sr whole rock age, Kröner, 1982). The sequences of the Nosib Group show rapid changes in rock types and depositional facies within and across tectono-stratigraphic zones (Table 2.1).

The Nosib Group is unconformably overlain by the Otavi Group in the north and the Swakop Group in the centre and south (Table 2.1). The Abenab, Ugab and Kudis Subgroups still show a considerable variety of rock types and facies. Calcareous sequences predominate in the north and more clastic sequences in the south (Table 2.1). The inconformity at the base of the Chuos Formation is of regional importance and this formation is the most important chronostratigraphic marker within the orogen (Tables 2.1 and 2.2). Above the Chuos unconformity, sedimentary sequences are much more coherent and laterally extensive. Thick carbonates are developed in the north (Tsumeb Subgroup), thinner carbonates with some amphibolites and clastics in the centre (Khomas Subgroup of the Central Zone) and mostly clastic sequences with some amphibolites in the south (Khomas Subgroup of the Southern and Southern Margin Zones).

The Otavi Group is unconformably overlain on the Northern Platform by thick clastic sediments of the Mulden Group (Miller, 1983b). Carbonate and mixed clastic-carbonate sequences of the zones further south are overlain by clastic sediments of the Khomas Subgroup which represents the youngest stratigraphic unit (Table 2.1).

There are few geochronological constraints on the depositional history of the Damara Sequence. Most radiometric ages have been derived from pre-, syn-, and post-tectonic magmatic rocks, mostly granite intrusions. Mineral dates from metasedimentary rocks give a spectrum of "ages" from about 530 to < 200 Ma, reflecting metamorphic processes and isotopic re-equilibrations (e.g. Miller, 1983b; Miller and

Grote, 1988; Haack and Martin, 1983; Kukla, 1991). Damaran sediments have been intruded by post-tectonic granites and the Rb-Sr whole rock age of 458±8 Ma (Kröner and Hawkesworth, 1977) of the youngest of these intrusions, the Rössing alaskite in the Central Zone, is considered to mark the end of the Pan-African events in Namibia (Miller, 1983b).

TABLE 2.2: Comparison of lithostratigraphic classifications of the Southern Margin Zone by Hoffmann (1983) and SACS (1980) (from Hoffmann, 1983).

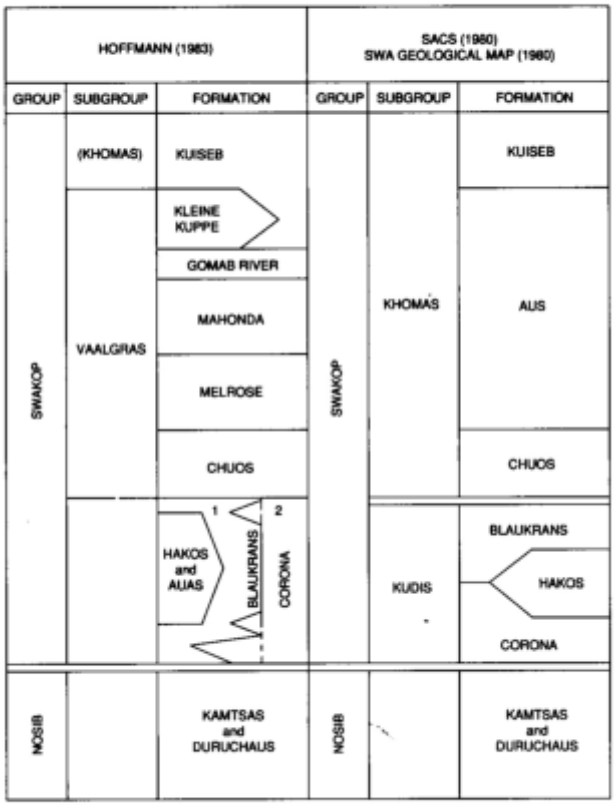

1: Allochthonous nappes
2: Parautochthonous Samara-Dagbreek Thrust Zone

2.2.2 Stratigraphy of the Central Zone and the Southern Margin Zone

The Khomas Trough of the Damara Sequence is bounded to the north by the Central Zone and to the south by the Southern Margin Zone (Fig. 2.2; Table 2.2). A rock-relationship diagram illustrates the local stratigraphies within the tectono-stratigraphic framework of the southern Damara Orogen (Fig. 2.3). The stratigraphy of the Southern Margin Zone is based on Hoffmann (1983) who revised the SACS (1980) stratigraphy subsequent to detailed mapping in this area (Table 2.2). To underline important stratigraphic changes, time-equivalent sequences across the zones are described below. The sequences are unconformity-bound and the important chronostratigraphic marker is the Chuos Formation of the Swakop Group.

(a) The Nosib Group

In the Central Zone, sediments of the Nosib Group rest unconformably on Abbabis basement gneisses, schists, amphibolites and marbles (Smith, 1965) with an approximate age of 2000 Ma (Briqueu *et al.*, 1980). Extensive fluviatile deposits of the Etusis Formation are represented by metamorphosed quartzites, arkoses and conglomerates (Fig. 2.3) which underlie and interfinger with feldspathic quartzites and quartz-biotite schists of the Khan Formation (Smith, 1965; Jacob, 1974).

In the Southern Margin Zone (Fig. 2.3), quartzites, arkoses and conglomerates of the Kamtsas Formation were deposited on about 1050 Ma - old basement gneisses and amphibolites. The basement close to the boundary with the Khomas Trough has been structurally emplaced and contains serpentinite bodies (Barnes, 1982).

As a facies of the Kamtsas Formation, the Duruchaus Formation (Martin, 1965; Hälbich, 1970; Schalk, 1970) comprises fine-grained psammites, pelites, carbonates, meta-evaporites and some conglomerates (Löffler and Porada, 1987; Hoffmann, 1987) and it has been interpreted to represent playa-sabkha type, lacustrine (Behr *et al.*, 1983) as well as fluviatile (Löffler and Porada, 1987) deposits.

(b) The Swakop Group

This Group has been subdivided into the Ugab and the Khomas Subgroups in the Central Zone which have been correlated with the Kudis and the Vaalgras + Khomas Subgroups of the Southern Margin Zone, respectively (Hoffmann, 1983; Tables 2.1 and 2.2). The only stratigraphic unit in the Khomas Trough is the Kuiseb Formation of the Swakop Group (Fig. 2.3).

Both the Ugab and Kudis Subgroups are characterized by a considerable lithological variability. The former contains dolomite, quartzite, quartz-biotite schist, calc-silicate rocks, gneisses and amphibolites of the Rössing Formation in the Central Zone (Fig. 2.3). The time-equivalent Kudis Subgroup of the Southern Margin Zone comprises marbles (Corona Formation), quartz-mica schists and graphite schists (Blaukrans Formation), interbedded quartzites and graphite schists (Hakos Formation), and thick quartzites with interbedded graphite layers of the Auas Formation. This succession has been interpreted by Hoffmann (1983) to have been deposited in progressively deepening marine environments.

The Khomas Subgroup in the Central Zone comprises the Chuos, Karibib, Tinkas and Kuiseb Formations (Fig. 2.3). The Chuos Formation has long been recognized and was interpreted early on as being glacial in origin (Gevers, 1931). It shows a major discordance at its base and Henry *et al.* (1986) reported that Chuos metasediments rest in places on Khan, Etusis and basement rocks. Rock types developed are mainly glacial diamictites and minor feldspathic quartzites, marbles and iron formations (Henry *et al.*, 1986; Badenhorst, 1987). The overlying shelf sequence of the Karibib Formation consists predominantly of dolomitic marble; schist and marl are subordinate. Towards the Khomas Trough the Karibib marbles interfinger with calc-silicates and fine-grained graphitic schists of the Tinkas Formation which outcrops along the Okahandja Lineament in the southwestern Central Zone. Porada and Wittig (1983) have interpreted this succession as calcareous, slope turbidites. An amphibolitic unit has been described

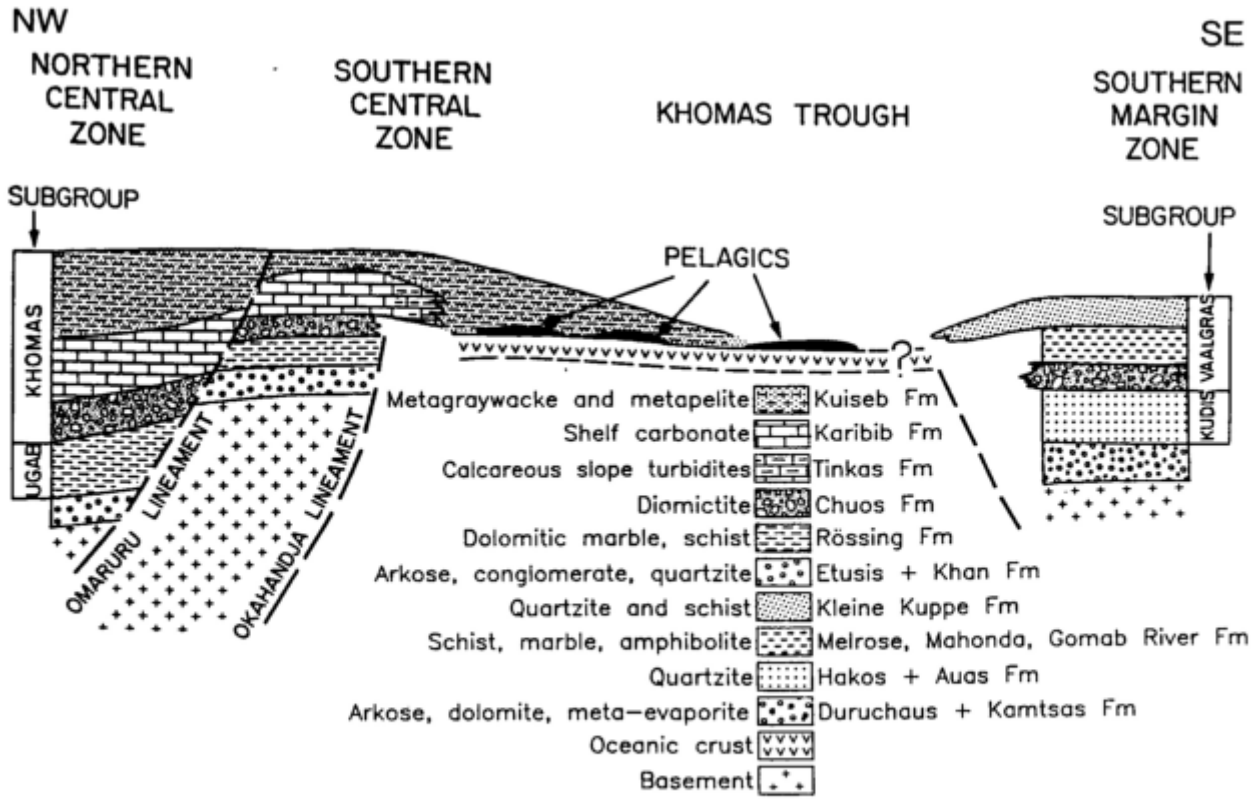

Fig. 2.3: Rock-relationship diagram of the Khomas Trough and adjacent areas in the Damara Orogen. Stratigraphic contacts are emphasized in their palinspastic context. Correlations and terminology of the Southern Margin Zone and the southern and northern Central Zone are after Hoffmann (1983), Henry *et al.* (1990) and Badenhorst (1987) respectively.

from stratigraphic positions within the Karibib Formation (Smith, 1965) and the Tinkas Formation just north of the Otjimbingwe Granite (De Kock, 1985). The uppermost unit in the Central Zone is the Kuiseb Formation which comprises pelites, metagreywackes and calc-silicates.

The Khomas Subgroup of the Southern Margin Zone has been subdivided by Hoffmann (1983) into the Vaalgras Subgroup, comprising the Chuos, Melrose, Mahonda, Gomab River and Kleine Kuppe Formations, which are structurally overlain by Khomas Subgroup sediments (Tables 2.1 and 2.2). The Chuos Formation in this zone has been used for correlation across the Khomas Trough. Hoffmann (1983) reported pebble-bearing, semi-pelitic, light grey mica schists, pelitic schists, quartzites, metabasic rocks and iron formations, which conformably overlie rocks of the Kudis Subgroup. This is in contrast to the inconformity in this position suggested by SACS (Table 2.2; 1980). The Melrose Formation consists of green garnet-chlorite schists and subordinate quartzites, calcareous schists and marbles which occasionally interfinger with quartzites, schists, amphibolites and marbles of the Mahonda Formation. The Gomab River Formation occurs as a thin unit at the northern boundary of the Southern Margin Zone. It comprises dark amphibole schist, minor mica schist and marble and the former "Red Band Quartzite" (De Kock, 1934; Hälbich, 1970) which has been named "Hartelust Rhyolite Member" by Miller (1983b). The Kleine Kuppe Formation consists of intercalated, thin-bedded micaceous quartzites and schists as well as occasional thin amphibolite bands. Hoffmann (1983) interpreted the Vaalgras Subgroup to represent slope (Chuos Formation) and ocean-basin (Melrose and Kleine Kuppe Formations) deposits. Contacts with the overlying Kuiseb Formation pelites and meta-greywackes are structural.

2.2.3 Stratigraphy of the Khomas Trough

In the study area, the Khomas Trough is bounded to the north by the post-tectonic Donkerhuk Granite (Fig. 2.4). Further to the west, however, Porada and Wittig (1983) have established an interfingering of the Khomas Trough metasediments with the Tinkas Formation of the Central Zone (Fig. 2.3). The only formal stratigraphic unit in the Khomas Trough is the Kuiseb Formation of the Swakop Group (Fig. 2.3). Rock types present are mainly metasediments such as metagreywackes, meta-siltstones, pelites, graphite schists, scapolite schists, calc-silicates and a marble unit. Also part of the Kuiseb Formation is the Matchless Member (SACS, 1980), a 350 km-long and up to 3 km-wide zone (Miller, 1983b) of metamorphosed mafic volcanic and intrusive rocks which are interposed with the metasediments. Also associated with the Matchless Member are ultramafic rocks (Barnes, 1982).

Mapping within the Khomas Trough has now shown that the sequence comprises several stratigraphic and structural marker horizons (Fig. 2.4). These are: (1) the Matchless Member, in this study referred to as the Matchless Amphibolite, which is associated with a graphite schist and a marble unit; (2) a thick pelitic unit north of the Matchless Amphibolite; (3) a graphite schist unit several tens of metres thick

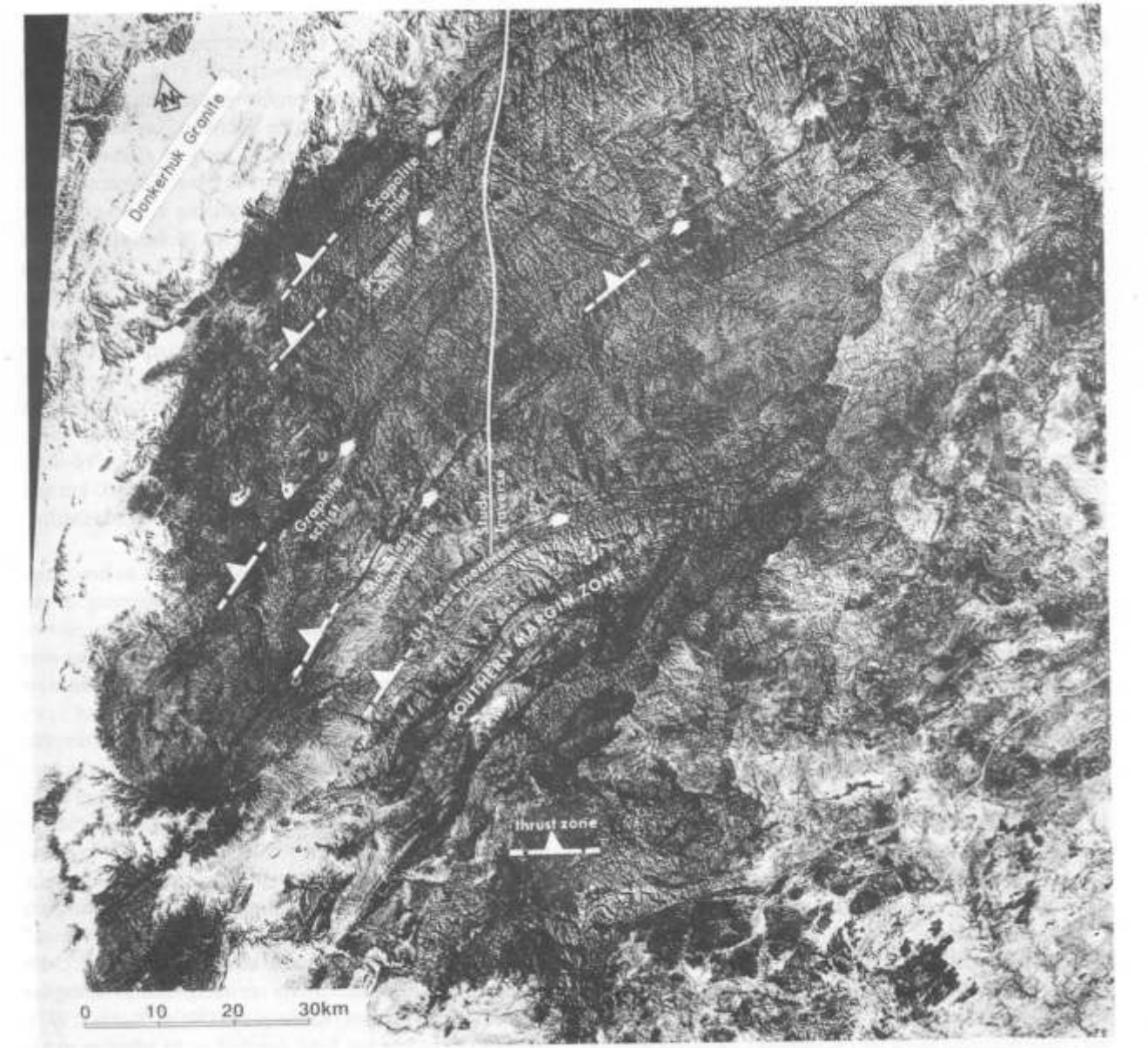

Fig. 2.4: Landsat image of the central and western Khomas Trough showing lithological and structural marker units. Note their lateral extent (reproduced with permission of the Satellite Applications Centre of the CSIR).

which is associated with a thin tremolite schist in the centre of the trough; and (4) two pelitic successions (several hundreds of metres thick) which were scapolitized during late-stage metamorphism (Fig. 2.4). The marker horizons are of regional importance since they may be traced for more than 150 kilometres laterally along strike. The Landsat image of the Khomas Trough confirms and emphasizes this extreme lateral persistence of the markers (Fig. 2.4). It will be shown in Chapters 3 and 5 that these markers also designate the position of thrust-bound sequences.

Radiometric dating of Kuiseb Formation rocks in the Khomas Trough has mostly produced ambiguous results which are probably due to isotopic re-equilibration during regional metamorphism (Hawkesworth *et al.*, 1983) leading for example to Rb-Sr whole rock ages in the order of 550-490Ma (Hawkesworth *et al.*, 1983; Kukla, 1991). A Rb/Sr whole rock date of 765±37 Ma is listed by Hawkesworth *et al.* (1981) for the Matchless Amphibolite.

2.3 Deformation, crustal structure and metamorphism of the Damara Sequence

The Damara Sequence throughout the inland branch has been subjected to varying degrees of deformation involving folding, thrusting and faulting. As with the stratigraphic asymmetries, structural patterns also vary markedly across the orogen (Coward, 1983; Henry *et al.*, 1990). Generally, intensity of deformation increases southwards from gently open, upright folds on the Northern Platform into tight, locally recumbent, northward-verging folds and thrusts in the Northern Zone (Frets, 1969; Miller, 1983b). Further south, complex interference patterns of upright to northerly - and southerly-inclined, tight and locally recumbent folds occur in the Central Zone (Smith, 1965; Jacob, 1974; Blaine, 1977; Sawyer, 1981; Coward, 1983; Miller, 1983b). Folds are tight to isoclinal and upright close to the Okahandja Lineament, passing into southeastward-verging, open and isoclinal folds in the Khomas Trough (Smith, 1965; Hälbich, 1977; Kukla

et al., 1988). Several phases of deformation, which are associated with folding, thrusting, faulting and cleavage formation, have been discerned within the Khomas Trough. Fold vergences are consistently to the southeast and axes generally trend northeast except at the Okahandja Lineament.

The Okahandja Lineament (Fig. 2.2) is a monoclinal downfold of the Damaran succession along the southern edge of the Central Zone (Miller, 1983b). It constitutes a major structural break which shows early and late strike-slip displacements (Downing and Coward, 1981) and which has been interpreted by Miller (1979) to represent an early, repeatedly rejuvenated, fundamental structure of the orogen. Thrusting increases southwards and complex thrust and nappe systems involving pre-Damaran basement and ultramafic bodies occur in the Southern Margin Zone (Hoffmann, 1983). The Schlesien-Amerongen Line (Hartnady, 1978) or Us Pass Lineament (Hoffmann, 1983) is a prominent zone along the northern margin of the Southern Margin Zone (Figs 2.2 and 2.4) which contains nappes of basement and ultramafic rocks and thrusts, the Hartelust Rhyolite Member. It has also been considered to represent a major tectonic boundary which might be connected and traced into the Mwembeshi shear zone of the Zambezi Belt, as such representing a transcontinental Pan-African shear zone (Unrug, 1990). The northern edge of the Southern Foreland has been deformed into open- to tight-folds but deformation dies out further to the south (Ahrendt *et al.*, 1977; Weber *et al.*, 1983).

Very little geophysical data are available from the Damara Orogen. Aeromagnetic surveys have confirmed and defined lineaments and lineament zones (Corner, 1983) that form the boundaries of the tectono-stratigraphic zones shown in Figure 2.2. Results support the hypothesis that the lineaments are associated with downfolding of stratigraphic sequences (Miller, 1983b). The most severe downfolding may have occurred along the Okahandja Lineament with the Central Zone being uplifted relative to the Khomas Trough in the order of 20 km (Miller, 1983b; Corner, 1983). An aeromagnetic survey of Botswana (Reeves, 1978) clearly shows a major tectonic belt connecting the inland branch with the Katanga and Zambezi Belts (Fig. 2.1). Three northeast-trending seismic profiles in the Central Zone, the eastern Khomas Trough and the Southern Foreland, respectively, show complicated crustal sections (Green, 1983; Baier *et al.*, 1983). In the Central Zone, Damaran cover rocks and basement are indistinguishable in a 15 km-thick upper crustal section. The depth of the Moho is interpreted to be between 36 and 47 km (Green, 1983). The Khomas Trough profile was set up along strike from the Windhoek area to the east. It shows a 3 km-thick low-velocity section on top, followed by denser material down to the 50 km-deep Moho (Green, 1983). Palaeomagnetic data suggest that there was initially no separation of the Congo and Kalahari Cratons during the Late Proterozoic (Piper *et al.*, 1973; McWilliams and Kröner, 1981). The resolution of data, however, allows a separation of approximately 800 km and there are no data for the period from 730 to 700 Ma (Miller, 1983b).

The Damaran rocks have been subjected to low-, medium-, and high-grade metamorphism. Mapping of regional metamorphic isograds by Hoffer (1977) has shown that these describe a concentric distribution around an area close to Walvis Bay where partial melting associated with the highest temperatures has occurred. The studies of Sawyer (1981) and Kasch (1983b) confirmed that metamorphic temperatures increased and pressures decreased inward towards the Central Zone, with the highest pressures of up to 11 kbar obtained in the southern Khomas Trough. Metamorphism in the Khomas Trough reached the upper amphibolite facies with partial melting occurring along the northern margin. The migmatites of the Kuiseb Formation in this area have been reinterpreted to represent "*in situ*" migmatization during regional metamorphism and U-Pb monazite ages of about 520 Ma are interpreted as dating the peak of metamorphism (Kukla *et al.*, 1990a; Kukla, 1991). No agreement has yet been reached as to whether metamorphism in the Damara Orogen was a single prograde event (Jacob, 1974; Hoffer, 1977) or had several peaks, as suggested by Sawyer (1981) and Kasch (1983b).

3. SEDIMENTOLOGY

3.1 Introduction

A large part of the present outcrop surface in the Southern Damara Orogen comprises rocks of the Kuiseb Formation within the Khomas Trough. No detailed sedimentological studies have, however, previously been undertaken because of the supposed monotony of the sequence and because of its structural and metamorphic overprint. It is therefore the aim of this chapter to present data from measured sections taken across the Khomas Trough and to combine these in a model of depositional palaeo-environments. The most likely tectonic settings in which the sedimentary precursors of the Kuiseb metasediments might have accumulated, and suitable provenance areas, are also discussed. Since the Kuiseb schists represent metamorphosed rocks, the present-day lithotypes will primarily be introduced. For convenience the interpretation of their probable sedimentary precursor rocks is added to the headings of section 3.2.

3.2. Description of lithotypes

3.2.1 Quartz-plagioclase-mica schist (psammite)/greywacke

Psammites are most abundant throughout the Khomas Trough. The light grey to dark grey quartz-plagioclase-mica schists vary from below 10 cm up to 5 m in thickness and are mineralogically uniform. The metamorphic texture is schistose. Quartz forms polygonal grain boundaries indicating recrystallization and the quartz-plagioclase matrix is fine- to medium-grained (<0.5 mm). Other mineral phases are largely dependent on the metamorphic grade in various parts of the traverse and include plagioclase, biotite, muscovite, chlorite, scapolite and minor amounts of tourmaline, epidote, sphene, zircon and apatite.

3.2.2 Mica-quartz-plagioclase schist (pelite and metasiltstone)/mudstone and siltstone

Pelites are also abundant throughout the Khomas Trough whilst meta-siltstones only occur in the central part of the traverse. Both rock types are principally mica (biotite-muscovite)-quartz-plagioclase schists with unit thicknesses ranging from below 10 cm to more than 10 m. Depending on the metamorphic grade and the bulk-rock geochemistry, the minerals garnet, staurolite, kyanite, andalusite, sillimanite, chlorite, scapolite as well as minor amounts of tourmaline, epidote, sphene, zircon and apatite are also present.

3.2.3 Graphitic mica-quartz-plagioclase schist/carbonaceous mudstone

Units of graphite schists are developed particularly in the central and southern part of the traverse. The amount of graphite ranges between 20% and nearly 100% within pelitic schists with streaked texture. Additional components

TABLE 3.1: Chemical compositions of psammites and pelites of the Kuiseb Formation along the study traverse in the western Khomas Trough (samples were reduced in a jaw crusher and tungsten carbide mill, and prepared as pressed pellets and fused discs in the Department of Geology, University of the Witwatersrand). SD = standard deviation.

Psammites Khomas Trough					Pelites Khomas Trough				
Element	mean (n=70)	min	max	SD	Element	mean (n=62)	min	max	SD
SiO_2 (wt %)	72.40	68.12	75.65	1.62	SiO_2 (wt %)	57.85	39.93	68.23	5.57
TiO_2	.85	.49	1.19	.15	TiO_2	1.01	.78	1.55	.15
Al_2O_3	11.19	9.35	13.11	.74	Al_2O_3	18.06	13.35	25.90	2.73
Fe_2O_3*	5.06	3.35	6.34	.59	Fe_2O_3*	8.18	1.42	12.11	1.77
MnO	.08	.06	.15	.02	MnO	.10	.01	.18	.03
MgO	2.03	1.39	3.48	.36	MgO	4.24	.67	7.88	1.21
CaO	1.70	.71	5.07	.73	CaO	1.58	.11	8.86	1.78
Na_2O	2.78	1.62	3.94	.46	Na_2O	1.65	.59	4.31	.75
K_2O	2.16	1.26	3.95	.46	K_2O	4.51	.32	7.87	1.31
P_2O_5	.19	.10	.27	.04	P_2O_5	.21	.07	.35	.05
Cr (ppm)	77	60	101	9.55	Cr (ppm)	125	85	187	20.90
Ni	27	14	51	6.49	Ni	49	23	79	12.50
Rb	85	34	127	15.99	Rb	180	14	381	57.65
Sr	146	58	396	69.78	Sr	114	40	388	70.99
Ba	462	185	949	147.89	Ba	752	79	1486	275.76
V	99	70	124	11.19	V	191	121	304	38.53
Y	33	17	45	4.83	Y	39	26	64	7.36
Zn	71	13	121	17.13	Zn	117	14	212	42.61
Nb	10	4	15	1.96	Nb	14	6	20	2.64
Zr	243	125	384	66.92	Zr	202	152	291	27.33
Co	12	7	18	2.11	Co	18	6	32	4.56
Cu	26	6	142	29.97	Cu	42	6	235	46.82

*total Fe as Fe_2O_3

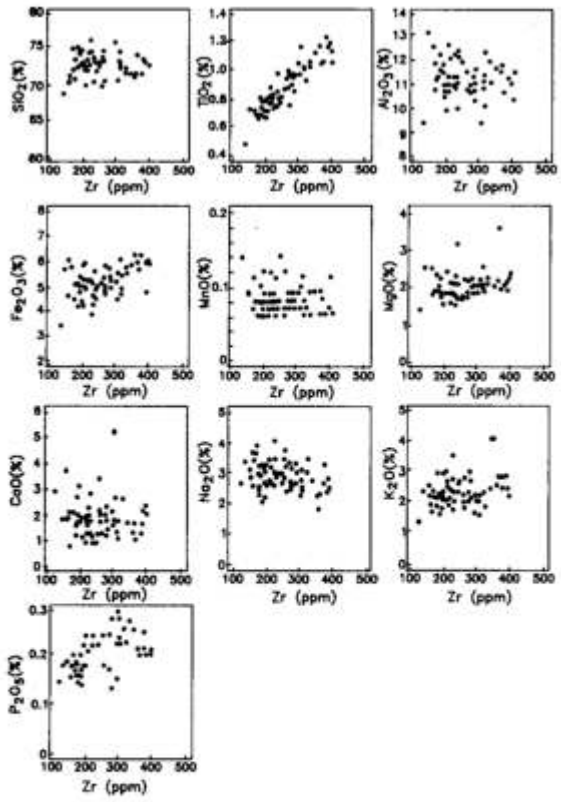

Fig. 3.1: (A) Geochemical variation diagrams showing major elements of psammite analyses plotted against an immobile parameter Zr. Note the good correlations with TiO_2 and P_2O_5.

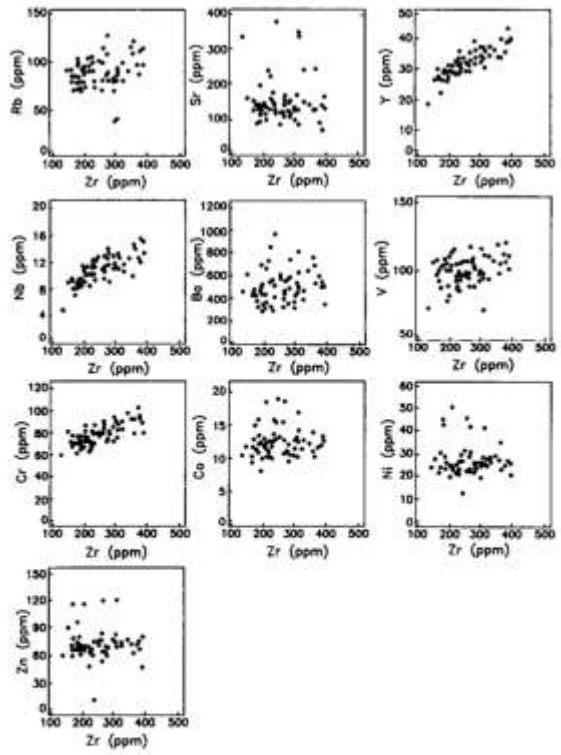

Fig. 3.1: (B) Geochemical variation diagrams showing minor elements of psammite analyses plotted against an immobile parameter Zr. Note the good correlations with Y, V, Nb and Cr.

(with decreasing frequency) are biotite, muscovite, quartz, plagioclase and chlorite as well as andaluslte in the appropriate metamorphic zones. The schists contain appreciable numbers of pyrite grains.

3.2.4 Marble and tremolite schist/carbonate

A marble unit up to 2 m thick in the hanging wall sequence of the Matchless Amphibolite is composed mainly of fine-grained dolomite and some calcite as well as minor amounts of quartz and muscovite. A deeply-weathered layer of rock, up to 1 m thick, which contains mostly tremolite and some biotite and quartz «5%) occurs in the centre of the Khomas Trough.

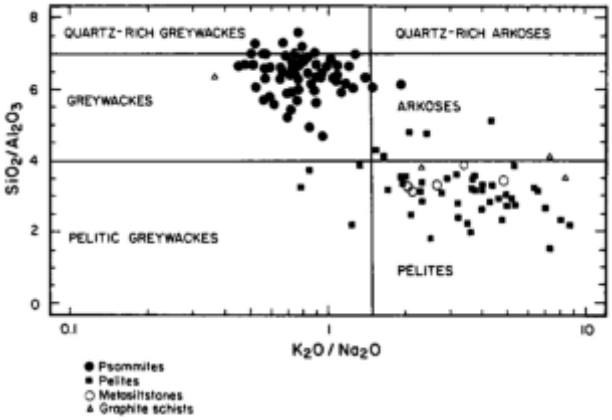

Fig. 3.2: Geochemical grid for discriminating clastic sedimentary protoliths after Wimmenauer (1984), with Kuiseb metagreywackes, pelites, metasiltstones and graphite schists plotted.

3.2.5 Calc-silicate rock/impure carbonate

Calc-silicate rocks occur as a relatively minor component of the sequence throughout the area. These form bodies with a large variety of shapes and mineralogical compositions, e.g. layers, spindles, nodules segregations and veins. Mineral components encountered are: quartz, plagioclase, garnet, hornblende, biotite, muscovite, diopside, zoisite, calcite, scapolite, epidote, chlorite, sphene, rutile, apatite and tourmaline within a partly blastomylonitic matrix.

3.3 Geochemical characterization of psammites, pelites and meta-siltstones

A brief geochemical characterization of the Kuiseb schists was undertaken in order to support the thin-section and sedimentological data. This also helps to constrain later considerations of a suitable source area. Layers of psammites, pelites and meta-siltstones were sampled along the study traverse and subsequently analysed by XRF whole-rock analysis for 23 major and trace elements. The data are presented in Table 3.1 which gives mean, minimum and maximum element concentrations as well as the standard deviation of the 132 samples analysed. The full analyses are given in Appendix I.

One of the major geochemical problems encountered in resedimented and metamorphosed terranes is secondary-element mobilities. Studies in other parts of the Khomas Trough have indicated certain mobilities of major and minor elements (Miller, 1983c; Phillips *et al.*, 1989). This is also confirmed by geochemical studies of Häussinger (1990) who compared unaltered Kuiseb schists from the present study area with altered Kuiseb schists from the Gorob massive sulphide deposit in the Namib desert. Elements plotted against an "immobile" TiO_2/Zr ratio (Häussinger and Kukla, 1990) show mostly good correlations in the case of the Khomas Trough. In the consideration of possible source areas, the psammites have been chosen for further investigations. This is because pelites usually show more significant changes during metamorphism than the mineralogically and chemically more uniform psammites. Secondly, it will be shown later in this chapter that, in contrast to the psammites, the precursors of the pelites were formed under different depositional processes.

The element Zr is thought to have been transported mostly as the heavy mineral zircon with other sand grains and consequently major and minor elements have been plotted against Zr as the "immobile" parameter in Figure 3.1. Respective element mobilities are shown in this type of variation diagram and in this case they demonstrate good correlations and small variations of inter-element ratios of TiO_2, P_2O_5, Y, Nb, Cr, and partly Fe_2O_3 and V with Zr. This does not necessarily assume that Zr was constant but it tests whether parts of the group including Zr could have been immobile. Phillips *et al.* (1989) have shown from investigations in the Kuiseb schists of the eastern Khomas Trough that most of the above elements are also reasonably constant if plotted

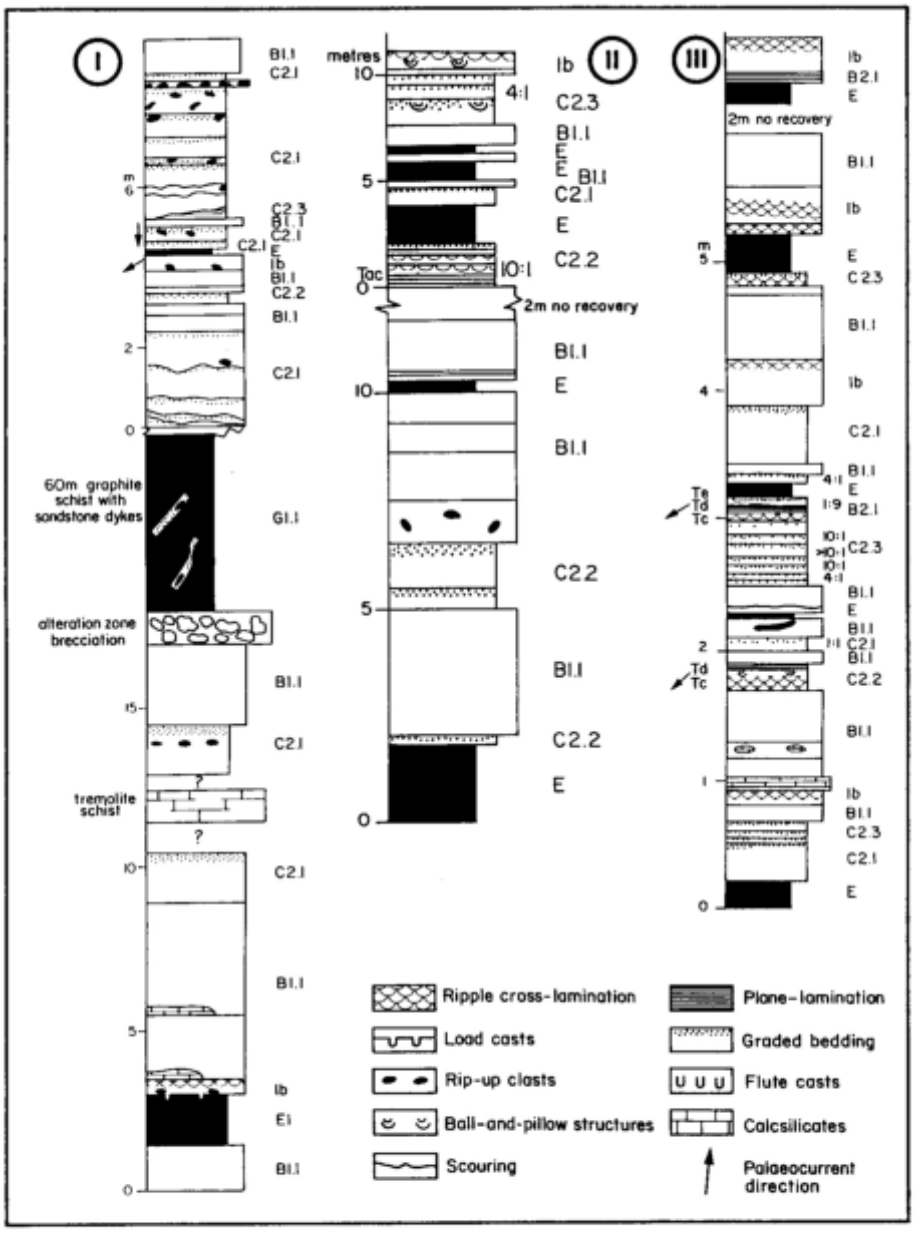

Fig. 3.3: Representative measured sections I-V showing range of sedimentary structures preserved, Bouma sequences and palaeocurrent directions in the Kuiseb Formation. For facies classification according to Pickering *et al.* (1986) see section 3.5. Positions of profiles are indicated in Figure 3.12.

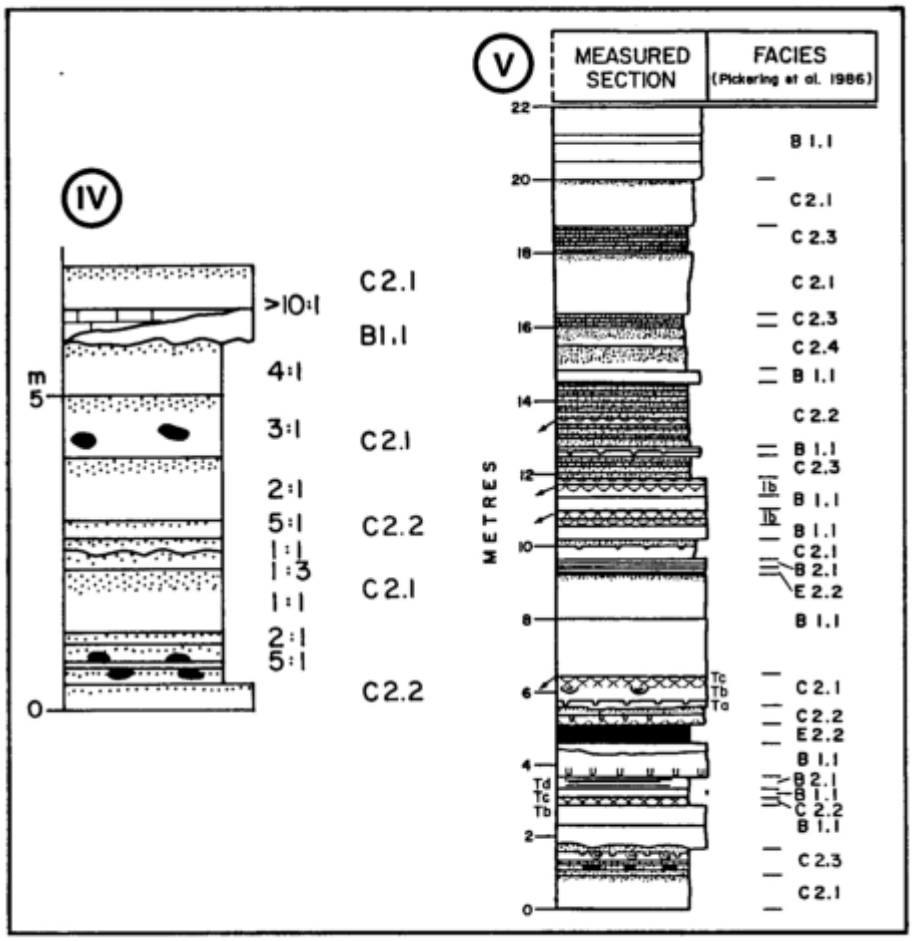

Fig. 3.3 (continued)

against Ti in pelitic rock types.

The geochemical grid of Wimmenauer (1984) classifies sedimentary protoliths by means of K_2O/Na_2O and SiO_2/Al_2O_3 ratios (Fig. 3.2). Although element mobilities especially for K and Na may be expected (Fig. 3.1), the diagram clearly distinguishes geochemically "pelites" and "greywackes". Data points in the arkose field are samples with slightly higher quartz contents due to veining. The more pelitic character of the siltstones is also indicated in this diagram.

3.4 Sedimentary structures and palaeocurrents

(a) Sedimentary structures

Short sections were measured in detail throughout the study traverse on a variety of scales from centimetres upwards. With the exception of the southern-most part of the area, sedimentary structures have been detected throughout the Kuiseb Formation rocks. Sedimentary logs from outcrops with the best-preserved sedimentary structures are shown in Figure 3.3. Measured section data showed that bed thicknesses may be defined according to the scheme employed by Mutti and Ricci Lucchi (1975) with very thick beds greater than 100 cm; thick beds, 40-100 cm; medium beds, 10-40 cm; and thin beds 1-10 cm. In terms of measured bed thicknesses it is to be expected in a deformed terrane that tectonic thinning affects the analysis. Sedimentary structures do, however, act as strain markers and may indicate a low degree of internal deformation if original shapes are largely preserved. Additionally, it will be shown elsewhere (see Chapter 4) that layer-parallel extension played a minor role within low-strain zones in the Khomas Trough.

Initially, the primary nature of the layering in which the above lithotypes are organized is confirmed by sharp bases and tops of beds, graded beds and various erosional features (Fig. 3.3). Graded beds are more quartz- and feldspar-rich at the base and more mica-rich at the top, representing a metamorphosed compositional grading (Fig. 3.4, A) reflecting a sand- to mud-rich transition in a normally-graded unit. Furthermore, structural fabrics mostly cross-cut and refract at bedding surfaces and bedding - fabric relationships therefore allow structural way-up control of both folds and measured sections within the traverse. Sedimentary structures such as graded bedding confirm stratigraphic "way-up". This terminology will be employed in the following sections.

Bedding is generally very uniform laterally although observations are limited by outcrop size. In the case of the psammites, internal bed forms present are: (1) massive, structureless; (2) plane-laminated; and (3) cross-laminated. Small-scale trough cross-lamination (Fig. 3.4, B and C) has been recognized in several outcrops and occurs both within discrete psammitic layers and in graded units which form part of Bouma sequences.

Load casts are common, with a maximum width of 10 cm

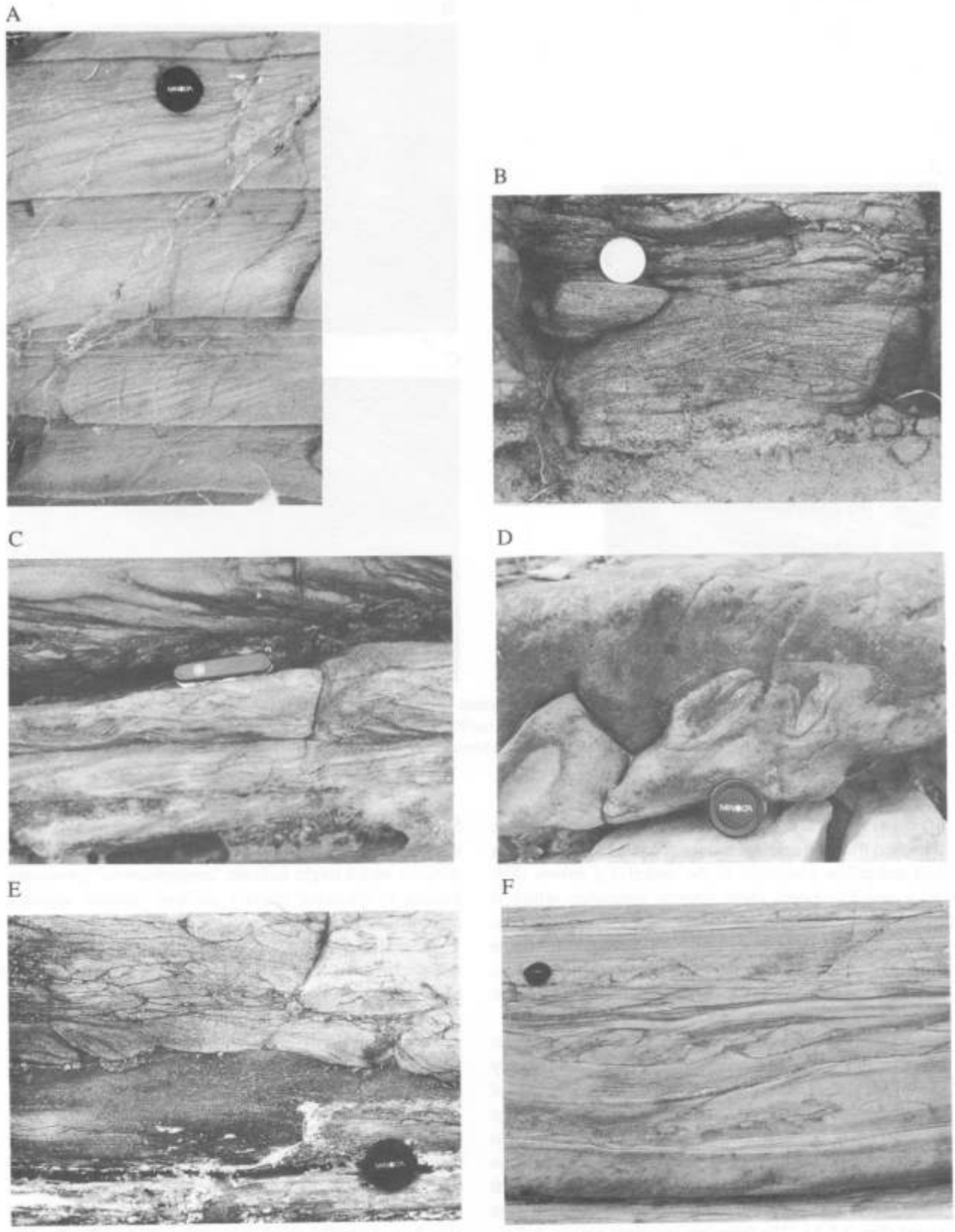

Fig. 3.4: (A) Graded layering in medium-bedded facies C2.2 turbidite (facies terminology after Pickering *et al.*, 1986). Note the crosscutting relationship between the metamorphic-banding cleavage (oblique) and bedding (horizontal). Lens cap is 4.9 cm in diameter. Farm Tsawisis 308. (B) Trough cross-lamination in a facies B2.2 turbidite. Coin is 2.5 cm in diameter. Farm Dagbreek 365. (C) Trough cross-lamination and flute casts (above the pocket knife) in facies B turbidites. Pocket knife is 8.5 cm long. Farm Dagbreek 365. (D) Overturned load structures in a medium-bedded facies C turbidite. Farm Kaan 309. (E) Metagreywacke layer showing extreme loading. Farm Dagbreek 365. (F) Flame structures and ball-and-pillow structures in medium-bedded facies C turbidites. The first major cleavage crosscuts the various structures confirming their sedimentary origin. Lens cap is 4.9 cm in diameter. Farm Dagbreek 365.

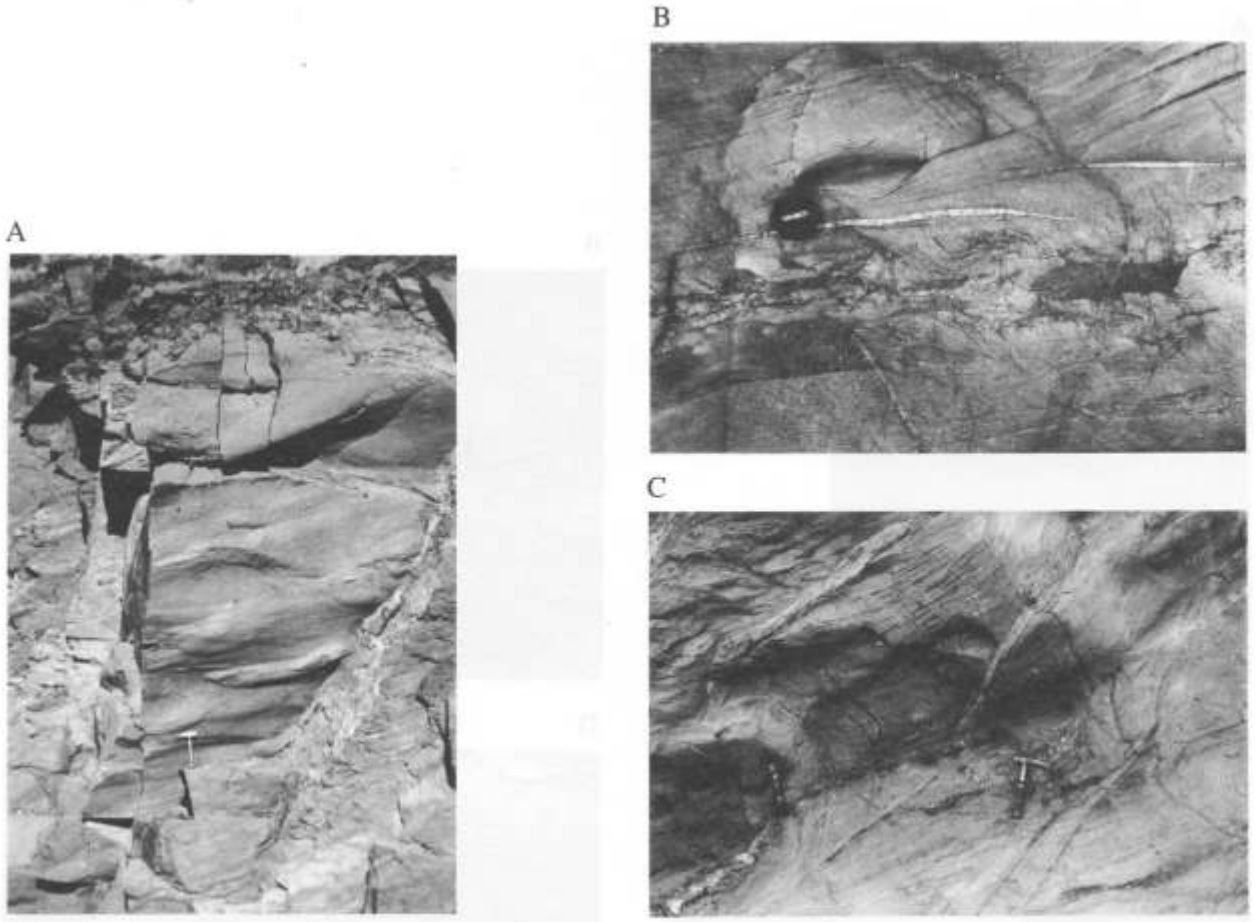

Fig. 3.5 : (A) Large flute casts at the underside of a facies B (class 1b of this study) turbidite. Palaeocurrents indicate current flow towards the southwest. Khomas Hochland Pass, farm Garums 300. (B) Graphite schist rip-up clasts in a thick-bedded facies C turbidite. Lens cap is 4.9 cm in diameter. Farm Kaan 309. (C) Metasandstone dykes in a thick, mud-dominated facies C2.4 turbidite. Farm Kaan 309.

(Fig.3.4, D). In some cases the loads have became detached from the original sediment and form load balls or ball-and-pillow structures in the underlying pelites (Fig. 3.4, E and F). Loads show internal lamination which is parallel at the margins but contorted towards the centre. Laminations of underlying strata are deformed by flame structures which are associated with the loads (Fig. 3.4, F). Extreme loading has led in some cases to layers which comprise an accumulation of load balls (Fig. 3.4, E).

A variety of erosional structures is present, namely flute casts, small-scale scours and channels (Fig. 3.3). Bilaterally symmetrical flute casts are preserved on the undersides of massive psammitic layers. The flutes commonly range from 10 cm to 20 cm in length and from 5 cm to 10 cm in width and depth (Fig 3.4, C). In one particular outcrop at the Khomas Hochland road, however, mega-flutes with a length of about I m and a width and depth of 20 cm to 50 cm were found (Fig. 3.5, A). The flutes are excellent way-up indicators and they have also been used to determine palaeocurrent directions.

Scour surfaces and channels are developed throughout the traverse. These erosional features are evident where mostly massive psammitic layers truncate earlier bedding surfaces (Fig. 3.3, IV and V). Only a few channels have, however, been found with both margins exposed and these show a maximum depth of about 3 m and a width of 5 m.

Some thick psammitic units, reaching a thickness of more than 10 m, are subdivided by bedding-parallel joint-like surfaces which might indicate “amalgamation” (processes leading to erosional contact surfaces between adjacent psammitic beds).

In several outcrops, rip-up clasts of pelite and graphite schist up to a few centimetres in length and width have been observed within psammitic lithologies. Rip-up clasts of graphitic schist are incorporated into psammites and meta-siltstones (Fig. 3.5, B) at the graphite schist sequence on the farm Kaan, thus confirming the primary sedimentary origin of this unit.

In the centre of the traverse, “sandstone” (psammite) dykes are preserved in thick-bedded graded sequences and in the thick graphite schist on the farm Kaan. One particular outcrop exhibits exceptionally well-preserved dykes which are up to 2 m long and 30 cm wide. Dyke walls are both straight and parallel-sided or irregular and undulating. The dykes lead from the psammitic base of thick graded units and may be traced through the silty-pelitic top upwards, where they link with the psammitic base of the overlying graded unit (Fig. 3.5, C). Internal structures of the dykes are contorted if compared with the outside texture. Similar structures may be observed at the graphite schist on the farm Kaan. There, however, the dykes occur isolated within the graphite schist and they contain graphitic clasts.

(b) Palaeocurrents

Palaeocurrent determinations have been made in some outcrops where three-dimensional orientations of flute casts and sets of trough cross-laminae could be measured. The measurement of palaeocurrents was facilitated by the fact that the sedimentary structures are preserved in zones of low strain. In these zones, sequences are usually upward-facing and the fold axes of the main fold phase are horizontal with the axial plane dipping northwestwards (330°/45°).

The second phase of deformation in these zones is represented only by a reorientation of micas, and small-scale folds related to this phase also have horizontal fold axes co-linear with the previous main fold phase. This meant that the restoration of palaeocurrents involved a straightforward small-circle rotation on the stereonet. Although only a few palaeocurrent orientations from flute casts and trough cross-beds could be obtained, they show a remarkable uniformity throughout the traverse (Fig. 3.6). Orientations indicate current flow from the east-northeast to the west-southwest (230° -250°).

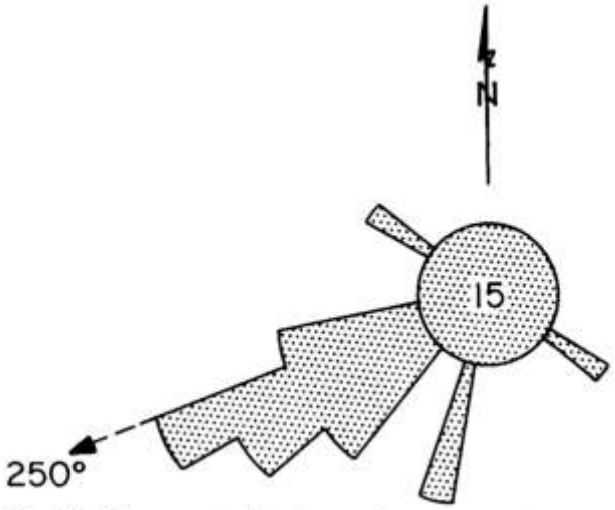

Fig. 3.6: Palaeocurrent data from various measured sections throughout the Khomas Trough. Palaeocurrent directions determined from sets of cross-laminae and flute casts (n = 15).

	THIS STUDY Facies Class	Pickering et al. (1986) Facies Class	Mutti & Ricci Lucchi (1975) Facies
2m	Facies Class (1) medium- to very thick-bedded psammites a) massive, structureless b) massive, "organized" c) parallel-stratified d) cross-stratified	B 1.1 – B 2.1 B 2.2	A1 or B1 B2 B1 –
2m	Facies Class (2) graded psammite/pelite couplets a) very thick- to thick-bedded b) medium-bedded c) thin-bedded d) very thick- to thick-bedded, mud-dominated	C 2.1 C 2.2 C 2.3 C 2.4	C2 D2 D1 –
0,5 m	Facies Class (3) thin-laminated metasiltstones	D 2.1	D1
2m	Facies Class (4) thin- to very thick-bedded pelites a) structureless b) "organized"	E 1 or G E 2 or G	thin- to medium-bedded D or G

Fig. 3.7: Summary of the turbidite facies classification of this study compared with other studies.

3.5 Turbiditic and pelagic facies

The recognition of sedimentary structures within graded units in the present study area proves that parts of the Kuiseb schists are organized in classical Bouma sequences (Bouma, 1962). These units are therefore hydrodynamically interpreted as having been deposited by turbidity currents, being one end member of "sediment gravity flows" as defined by Middleton and Hampton (1973, 1976). The development of graded bedding has previously been used in isolation to infer that the sedimentary precursors of the Kuiseb schists were deposited by turbidity currents (Miller *et al.*, 1983; Preussinger *et al.*, 1987).

In consequence, sedimentary facies may be defined in the Kuiseb schists and be compared with current classification schemes of marine clastic sediments. The most widely used classification is the "turbidite facies and facies associations" scheme of Mutti and Ricci Lucchi (1972, 1975). New research data from the past decade have led Pickering *et al.* (1986) to a reclassification of ancient and recent deep-water sediments. Figure 3.7 gives an overview of the turbidite facies classes established in this study and these are compared with the schemes of Mutti and Ricci Lucchi (1975) and Pickering *et al.* (1986). In extending Gressly's (1838) original application of facies, Selley (1976) defined the parameters of facies, namely lithology, sedimentary structures, palaeontology, geometry and palaeocurrent patterns. These are only partly applicable, however, to deformed and metamorphosed Phanerozoic and Proterozoic rocks. The major attributes used to define facies in the Kuiseb schists are lithologies, bedding style, vertical bed thickness distribution, variations in psammite/pelite ratio and sedimentary structures. On the basis of these characteristics, the metasediments within the Khomas Trough are grouped into seven facies classes, representing both turbidite and pelagic facies which are characterized and hydrodynamically interpreted below. Additional data have led to an extension of a facies classification scheme given by this author in an earlier publication (Kukla *et al.*, 1988).

3.5.1 Medium- to very thick-bedded psammite facies (faciesclass 1)

This facies class includes psammitic layers which are not part of a Bouma sequence. It is subdivided into (a) massive, structureless psammites; (b) massive, "organized" psammites; (c) parallel-stratified psammites; and (d) cross-stratified psammites.

(a) Massive, structureiess psammites

The structureless psammites have sharp and planar bounding surfaces and range in thickness from 15 cm upwards, commonly to about 3-5 m (Fig. 3.8, A). Psammitic units which are 5 m to 15 m thick commonly show signs of amalgamation. Graded layering has not been observed. This facies would best be compared with facies B 1.1 "thick/medium-bedded disorganized sands" of Pickering *et al.* (1986). (In the Mutti and Ricci Lucchi (1975) scheme, however, these psammites could be assigned to both facies A1, which includes medium- to coarse, often amalgamated sandstones, and to more "organized facies B 1 sands". In contrast, facies A of Pickering *et al.* (op.cit.) only contains gravels and pebbly sands). *Interpretation*: Depositional processes assigned

to this facies are high-density turbulent flows (Mutti and Ricci Lucchi, 1975; Pickering *et al.*, 1986; Lowe, 1982). The psammites are similar to mostly structureless facies S_3 sands of Lowe (1982), who interpreted deposition from high-concentration turbidity currents by suspension sedimentation. Some liquefied flow deposits closely resemble these S_3 divisions but would contain generally fine-grained sand and coarse silt (Lowe, 1982). Within this facies the effect of tractional processes, developed beneath turbidity currents and typical for "proximal" turbidites and Bouma T_a divisions, must also be considered.

(b) Massive, "organized" psammites

Abundant within the sections measured are psammites which have a massive texture if compared with other facies in this facies class (see below) but which contain sedimentary structures (Fig. 3.3). Bed thicknesses range from 10 cm to about 3 m but are mostly in the order of 70 cm. Most commonly the layers which are up to 70 cm thick contain trough cross-lamination in the upper 10 cm. Load casts and flute casts do occur on bases (Fig. 3.4, C). Erosional channels and scours detected within the traverse are mostly developed within this facies class. Sandstone dykes and rip-up clasts have also been observed. This facies compares well with Mutti and Ricci Lucchi's (1975) facies B2 turbidites. Pickering *et al.* (1986), however, do not address a facies which includes massive, ungraded psammites containing a variety of sedimentary structures. *Interpretation*: This facies might indicate the transition from high-density suspension flow to residual low-density currents whose cross-lamination confirms continued rapid fallout from suspension. This process was suggested by Lowe (1982) and is manifest in units comprising his S_3 and T_t divisions.

(c) Parallel-stratified psammites

This facies is poorly developed within the area. The beds are 10-35 cm thick and show flat, planar upper and lower surfaces. No sedimentary structures have been observed. This facies is compared with plane-laminated facies B 1 of Mutti and Ricci Lucchi (op.cit) and with facies B2.1 of Pickering *et al.* (op.cit). *Interpretation*: Within turbidite sequences, this facies is interpreted as traction carpet deposits, comprising "horizontal" lamination and inverse grading (Lowe, 1982; Pickering *et al.*, 1986; Hiscott and Middleton, 1979). The latter feature, however, has not been observed in the metamorphosed Kuiseb schists.

(d) Cross-stratified psammites

A cross-stratified psammitic layer which is not part of a Bouma sequence has only been observed in one outcrop (Fig. 3.4, B). The layer is 20 cm thick, trough cross-laminated and the top and basal contacts are sharply defined. This facies is the only facies of completely cross-laminated meta-sandstone layers and compares principally with facies B2.2 of Pickering *et al.* (1986). Caution must be applied, however, in terms of the grain size, since this facies is only assigned to medium- to granule-grade sands, an evaluation which cannot strictly be made in metamorphic rocks. *Interpretation*: It has been pointed out by various authors that discrete cross-stratified layers might be attributed to tractional processes beneath dilute turbidity currents or bottom currents (Mutti and Ricci Lucchi, 1972; Lowe, 1982; Pickering *et al.*, 1986).

3.5.2 Very thick- to thin-bedded graded psammite/pelite facies (facies class 2)

The psammite-pelite couplets of facies class 2 show a wide range of psammite/pelite ratios from 10:1 to 1:10. Graded layering generally characterizes this facies and sedimentary structures within Bouma sequences are abundant Four subfacies have been distinguished (Fig. 3.7) based mainly on bed thickness, which may initially appear to be an arbitrary criterion. Measurements have shown, however, that certain sedimentary structures are associated with specific bed thicknesses and these agree broadly with the subdivision scheme employed by Pickering *et al.* (1986).

(a) Very thick- to thick-bedded psammite/pelite couplets range in thickness from 40 cm to 170 cm (Fig. 3.8, B). Psammite/pelite ratios in well-developed graded beds vary between 1: 1 and 10: 1 but commonly are about 4: 1. Sedimentary structures found in this facies are primarily sets of trough cross-laminae which contribute to partial Bouma sequences that are mostly T_{abc} divisions, although complete Bouma divisions have also been found (Fig. 3.8, C and D). Additional structures are rip-up clasts, scour surfaces, load casts, load balls and flame structures. This facies is compared with facies C2 of Mutti and Ricci Lucchi (1975) and with facies C2.1 of Pickering *et al.* (1986).

(b) Medium-bedded graded units are abundant in measured sections (Fig. 3.3). The beds are 10-25 cm thick and psammite/pelite ratios range widely between 10: 1 and 1: 10 with an average of 1: 1. Bouma sequences are mainly T_{bcd} divisions lacking the lower massive psammite, but T_{cd} and T_{ac} divisions have also been found. Sedimentary structures are comparable to those in the previous subfacies. This facies is compared with facies C2.2 of Pickering *et al.* (op.cit) and facies D_2 of Mutti and Ricci Lucchi (op. cit).

(c) Thin-bedded graded layers are up to 10 cm thick and are characterized by a dominant pelitic top (Fig. 3.8, E) with psammite/pelite ratios usually $<<1$. Bouma sequences often start with trough cross-laminated T_c units within overall T_{cde} sequences. No additional sedimentary structures have been found. This facies is comparable with facies C2.3 of Pickering *et al.* (1986) and facies D1 of Mutti and Ricci Lucchi (1975). *Interpretation*: Facies 2 very thick- to thin-bedded graded layers represent the "classic" turbidites described by Walker (1976) and depositional processes therein have been interpreted by many workers (Bouma, 1962; Piper, 1978; Walker, 1978; Stow and Bowen, 1980). High-concentration turbidity currents with rapid settling seem the predominant depositional processes within this facies but low-concentration currents produce thin-bedded units and decreasing psammite/pelite ratios.

(d) Graded layers which are dominated by pelitic lithologies and which are 50 cm to more than 2 m thick have been observed in a few outcrops across the traverse. Psammitic bases are rather irregular and commonly show load struc-

tures. The pelitic parts of the units are laminated with alternations of pelites and meta-siltstones. On the farm Kaan, spectacular meta-sandstone (psammite), dykes have developed from the lower psammitic layer through the pelitic part, finally to join the psammite of the overlying graded unit (Fig. 3.5, C). This facies is compared with facies C2.4 of Pickering *et al.* (1986). *Interpretation*: Pickering and Hiscott (1985) attributed this unusual facies to large-volume, high-concentration turbidity currents confined within small basins. In this model the thick silt-mud layers are formed by rapid settling of floes within a highly concentrated mud cloud. Piper (1978) pointed out the occurrence of thick turbiditic mud beds overlying sands with partly gradational contacts in channel to levee environments. He also cited ponding in basins as a possible mechanism to accumulate turbiditic thin sand/thick mud couplets.

3.5.3 Thin-laminated metasiltstone facies (facies class 3)

This facies is only developed in the central part of the study traverse. The classification as siltstones seems appropriate because of the thin-laminated character of sedimentary layering, and the modal compositions which point towards equal proportions of quartz and mica. The sequences comprising this facies are all very similar so that only one facies type, namely graded stratified meta-siltstones, has been established.

The sedimentary units comprising this facies are typically 20 cm to 350 cm thick. Within these, single metasiltstone layers are internally well-laminated (i.e. silt and clay laminations) with bed thicknesses ranging from I mm to 2 cm (Fig. 3.8, F). Only very few sequences comprise up to 7 cm-

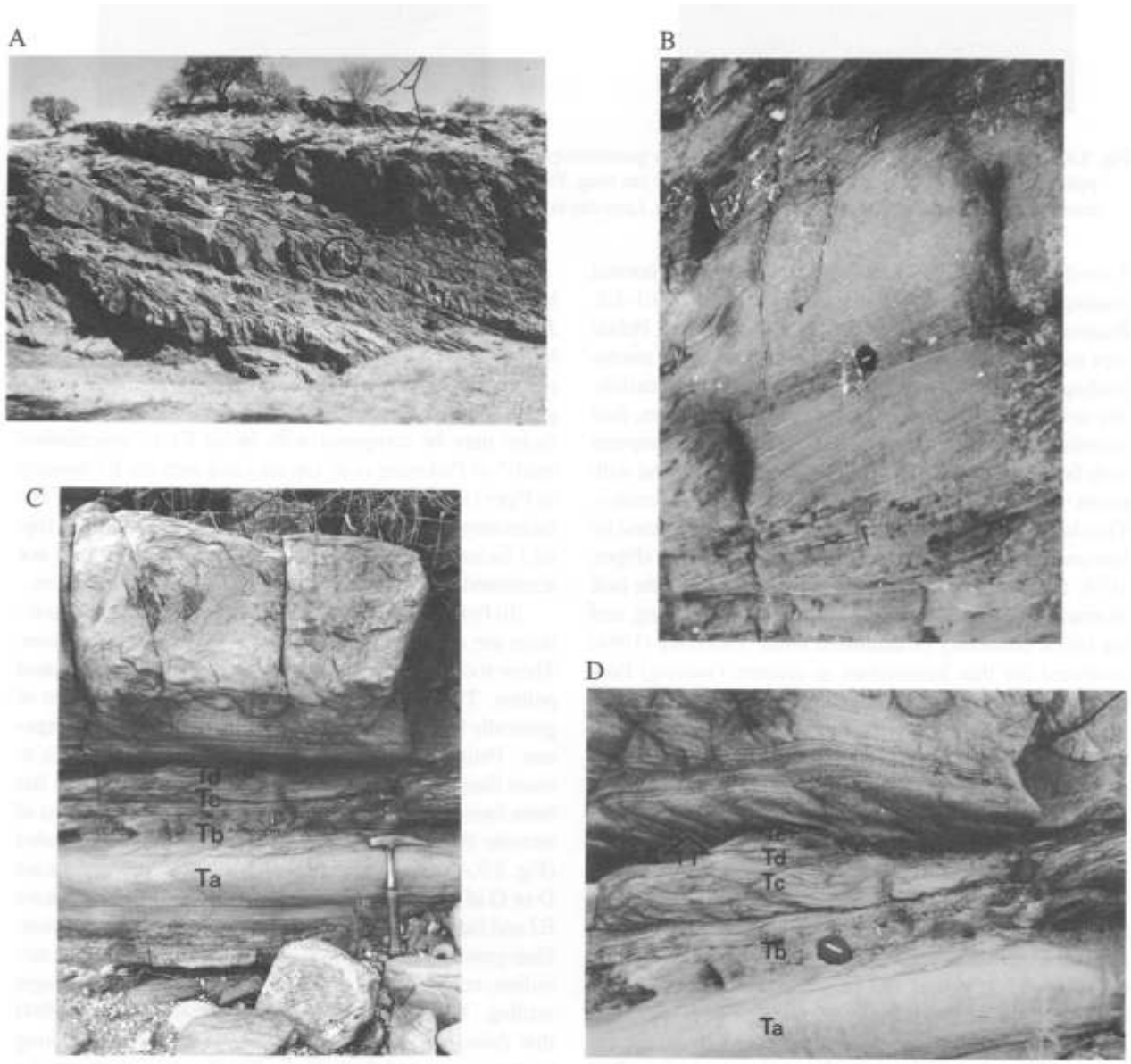

Fig. 3.8: (A) Thick-bedded facies B turbidites. Height of scale (circled) is 1.7 m. Farm Usambara 304. (B) Thick-bedded facies C2.1 graded psammite/pelite turbidites. Beds are overturned. Farm Kaan 309. (C) Complete Bouma sequence developed in a facies C2.1 turbidite underlying a thick-bedded facies B psammite. Farm Dagbreek 365. (D) Complete Bouma sequence developed in a facies C2.1 turbidite overlying a medium-bedded facies B psammite and underlying a medium-bedded facies C2.2 turbidite containing flute casts (see arrow). Farm Dagbreek 365.

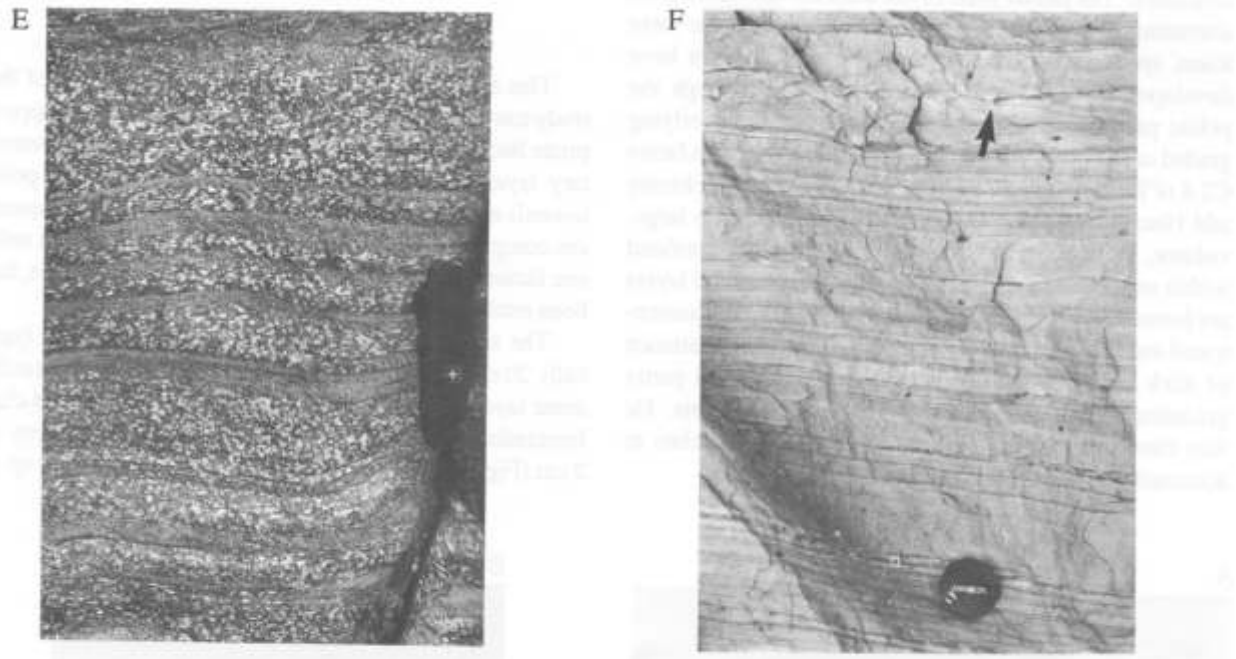

Fig. 3.8: (E) Thin-bedded facies C2.3 turbidite with low psammite/pelite ratios. Note the selective development of sillimanite in the pelitic tops; beds are overturned. Pocket knife is 8.5 cm long. Farm Keises 312. (F) Fine-laminated facies D2.1 metasiltstones containing small load structures (indicated by arrow). Lens cap is 4.9 cm in diameter. Farm Kaan 309.

thick layers. The majority of the beds show normal grading with psammite/pelite ratios in the order of 3:1-1:2. Bouma sequences comprise mostly T_{de} divisions. Pelitic tops are in some cases graphitic. Bases often show micro-loading and flame structures. Cross-lamination is occasionally developed in the lower quartz-rich parts of layers, thus constituting Bouma T_{cde} turbidites. This facies compares with facies D_1 of Mutti and Ricci Lucchi (1975) and with facies D2.1 of Pickering *et al.* (1986). *Interpretation*: Thin-laminated siltstones are interpreted to have formed by low-concentration, low-velocity turbidity currents (Piper, 1978; Stow and Piper, 1984). This is confirmed by the lack of erosive features, the thin bed thickness, the grading, and the lateral continuity of laminated units. Pickering (1984) attributed the thin laminations to discrete (waning) flow events with an accompanying depositional sorting process as described by Stow and Bowen (1978). An increase of this facies together with mud turbidites towards distal parts of a sedimentary basin has been pointed out by Piper (1978).

3.5.4 Very thick- to thin-bedded petite facies (facies class 4)

This facies comprises pelitic layers which are not part of graded psammite/pelite couplets and it is subdivided into (a) structureless pelites and (b) "organized" pelites. The classifications of Pickering *et al.* (op.cit.) and Mutti and Ricci Lucchi (op.cit.) distinguish a variety of mud subfacies using additional components such as colour, organic carbon content, terrigenous input, degree of bioturbation and grain size. These cannot be evaluated in the pelites of the Kuiseb schists. A further problem encountered is the preservation potential of pelitic units which would have been preferentially eroded.

(a) Structureless pelites mostly occur in units where bedding is poorly defined. The thickness varies from about 20 cm to several metres. No sedimentary structures have been found and the layers are mostly coarsely recrystallized pelites with biotite and chlorite (depending on metamorphic grade and bulk composition) as the main constituents. This facies may be compared with facies E1.1 "structureless muds" of Pickering *et al.* (op.cit.) and with the E3 division of Piper (1978). The thin- to medium-bedded pelites of this facies may be compared with Mutti and Ricci Lucchi's (op. cit.) facies D or facies G pelites. These authors have not accounted, however, for pelitic layers thicker than 60 cm.

(b) Pelites which show some degree of internal organization are assigned to the second group within this facies. These rocks may best be described as graded, laminated pelites. The grading varies from silt to mud with ratios of generally less than 1:3 but transitions are very often ambiguous. Pelite layer thicknesses range from below 10 cm to more than 10 m. One unit which is about 30 m thick has been found in the centre of the traverse but a component of tectonic thickening through repetition cannot be excluded (Fig.3.9, A). This facies may also be compared with facies D or G of Mutti and Ricci Lucchi (op.cit.) and with facies E2 and facies G of Pickering *et al.* (op.cit.). *Interpretation*: Fine-grained sediment may generally be deposited as turbidites, contourites and as a result of pelagic-hemipelagic settling. It has been pointed out by Stow and Piper (1984) that these processes strongly interact and overlap during both transport and deposition. Structureless muds may be interpreted as resulting from nepheloid settling through the water column finally to be reworked by deep-sea bottom currents (Gorsline, 1984). This facies may also result from ponding of thick, dilute turbidity currents as suggested by Pickering *et al.* (1986). Piper (1978) pointed out that the internal organization of muds is

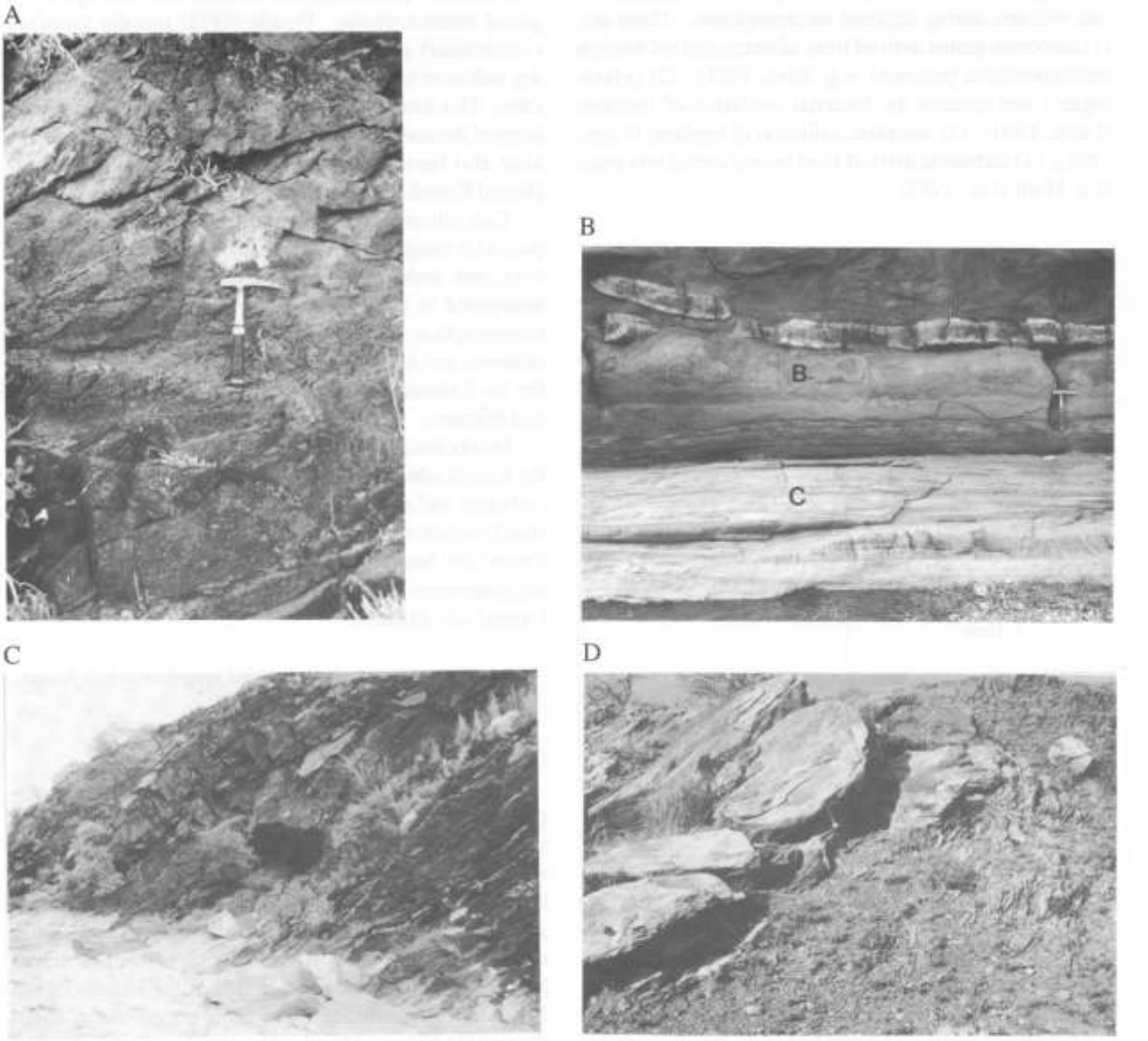

Fig. 3.9 : (A) Very thick-bedded (10 m) facies E pelites. Farm Keises 312. (B) Calc-silicate layer and spindles (facies class 5) in thick-bedded facies B turbidite above facies C turbidite. Farm Dagbreek 365. (C) Very thick-bedded pelagic graphite schist facies (facies class 6). Height of outcrop is about 10 m. Farm Kaan 309. (D) Dolomitic marble facies (facies class 7) on top of a graphite schist in the hangingwall of the Matchless Amphibolite (stratigraphic top towards the left). Hammer for scale. Farm Annelie 412.

largely dependent on the deceleration of the turbidite flow concerned. Thin facies E2 turbidites may therefore be deposited through grain-by-grain settling or aggregate settling within low-concentration turbidity currents (Pickering *et al.*, 1986).

3.5.5 Impure metacarbonate facies (facies class 5)

(a) Description

Metacarbonate-rich lithologies occur widely within the Khomas Trough as calc-silicates and have been described previously (e.g. Gevers, 1963; Hälbich, 1970; Porada, 1973; Preussinger, 1987). A large variety of geometries of these units has been observed in the present study area such as: (a) well-defined layers up to 40 cm thick that are parallel to bedding (Fig. 3.9, B); (b) cigar-shaped spindles up to several metres long and 40 cm thick that are either aligned along bedding planes or oriented between bedding and the S_2 cleavage (Fig. 3.9, B); (c) small nodules up to several cm long and wide; (d) diffuse concentrations of calcareous lithologies within cleavage domains; and (e) calc-silicate veins discordant to bedding. The occurrence of the calc-silicates is almost exclusively restricted to psammitic lithologies and in particular to the basal parts of facies 1 turbidites and the structureless Bouma T_a division of facies 2 turbidites. Furthermore, finely-dispersed calcareous material is preferentially deposited within the troughs of cross-laminated psammites. This feature has also been observed in the Ugab area in northwestern Namibia where much less de-formed and metamorphosed equivalents of the Kuiseb schists crop out.

(b) Interpretation

There are several possibilities which would account for

the origin of the carbonate leading to the formation of calc-silicates during regional metamorphism. These are: (1) carbonate grains derived from adjacent shelves through resedimentation processes (e.g. Stow, 1984); (2) pelagic organic precipitation by bacterial oxidation of methane (Faure, 1986); (3) inorganic oxidation of methane (Faure, 1986); (4) carbonate derived from hydro thermal processes (e.g. Mottl *et al.*, 1983).

TABLE 3.2: Stable isotope data from graphite schists and dolomitic marble. For sample localities see Figure 3.12. (All samples refer to bulk-rock analyses. Mass-spectrometric measurements were undertaken with a VG micromass 602 C. The samples were reacted with 100% H_3PO_4 at 25°C to liberate CO_2; analyses were carried out at the Schonland Research Centre for Nuclear Sciences, University of the Witwatersrand).

SAMPLE NO.	SAMPLE DESCRIPTION	$\sigma^{13}C$ (% PDB)	$\sigma^{13}O$ (% PDB)
PK 852	Graphite schist, Kwaggafontein farm	- 20.4	
PK 954	Graphite schist, Annelie farm	- 19.6	
PK 825	Dolomitic marble, Annelie farm	- 4.3	- 15.8
PK 866	Dolomitic marble, Annelie farm	- 9.0	- 15.7

The wide distribution of calc-silicates in the Khomas Trough and the striking confinement of these lithologies to psammites, which are part of turbiditic sequences, imply that calcareous sediment formed part of the resedimentation processes during deposition of the siliciclastics. Therefore possibility (1) is strongly favoured for the origin of the carbonate. Stow (1984) described decreasing amounts of carbonate upward from Bouma T_b to T_e divisions in cores taken from the Angola basin. The redeposition of fine-grained carbonate sediment (aragonite and Mg-calcite) from shelf areas into adjacent ocean basins has frequently been described; from the Bahama Banks, for example, by Neumann and Land (1975) and Heath and Mullins (1984). Transport distances of 200 km or more from the nearest carbonate source have been reported (Berner and Honjo, 1981). Organic or inorganic precipitation of carbonate from seawater should have produced a more random distribution of carbonate within the variety of lithologies in the Khomas Trough. These processes may, however, not totally be excluded, since carbonate formed by pelagic precipitation may also have been involved in resedimentation processes (e.g. bottom currents) from the site of original deposition. There is no evidence for hydro thermal processes in large parts of the Khomas Trough which excludes possibility (4).

Processes leading to the formation of the various geometries of calc-silicates may comprise diagenesis (including concretionary processes), deformation and subsequent regional metamorphism. Porada (1973) initially proposed concretionary processes within an originally $CaCO_3$-bearing sediment to account for the formation of the calc-silicates. This interpretation is acceptable for the spindles and some of the nodules; well-developed carbonate concretions have also been observed in less-deformed and metamorphosed Kuiseb Formation schists in the U gab area.

Calc-silicate layers and calc-silicate lithologies deposited in troughs of cross-laminated psammites have, however, not undergone concretionary processes and are interpreted to represent resedimented deposits. Regional metamorphism has formed the various mineral assemblages observed and element mobilization processes may account for the formation of calc-silicate assemblages along veins and fractures.

In conclusion, the occurrence of metacarbonate rocks in the Kuiseb schists implies that sediments comprising mixed carbonate and siliceous grains have also been deposited by resedimentation processes. Some of the calcareous lithologies have been subjected to concretionary processes during diagenesis. Regional metamorphism has subsequently formed calc-silicates.

3.5.6 Thin- to very thick-bedded graphite schist facies (facies class 6)

(a) Description

This facies is closely associated with sequences comprising turbidite facies classes 1 to 4. Graphite schists have been found mainly in the south and central parts of the traverse, especially in the vicinity of the Matchless Amphibolite. Units are usually between 1 m and 10 m thick but a graphite schist with a thickness of about 60 m in outcrop is developed on the farm Kaan (Fig. 3.9, C). This thick-bedded graphite schist and one unit in the vicinity of the Matchless Amphibolite have been traced along strike through the Khomas Hochland into the Namib desert, proving the regional distribution of this facies. The graphite schists show very little internal organization, except of some of the graphitic tops in the thin-laminated metasiltstone facies. On the farm Kaan, psammitic dykes which contain graphitic clasts are developed within the thick graphite schist. Pyrite is abundant within the graphite schists.

(b) Stable isotope analysis

In a first step towards the interpretation of the graphite schists, stable isotope geochemistry has been applied in order to prove or disprove the organic origin of these rocks. The thick graphite schist on the farm Kaan and one unit close to the Matchless Amphibolite have been analysed and the data, given in Table 3.2, show a very homogeneous distribution of ^{13}C indicating a considerable enrichment of up to 20‰ ^{12}C relative to unaltered marine limestones.

(c) Interpretation and discussion

This graphite schist facies is compared with facies G ("hemipelagic pelites") of Mutti and Ricci Lucchi (1975) and with facies group G ("biogenic oozes, hemipelagites and chemogenic sediments") of Pickering *et al.* (1986).

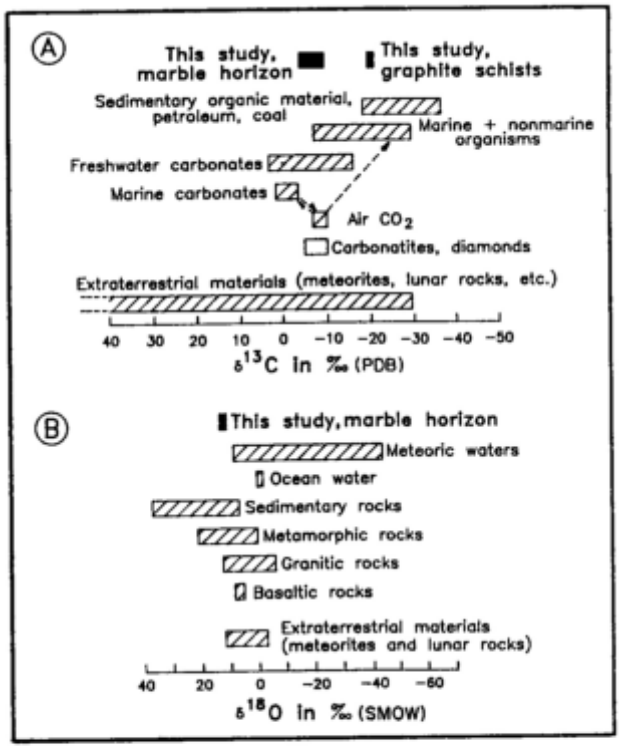

Fig. 3.10: Diagram comparing ^{13}C (A) and ^{18}O (B) data from graphite schists and marble in the Khomas Trough with carbon and oxygen isotope distributions of the lithosphere and hydrosphere (from Hoefs, 1980).

The carbon isotope data obtained for the graphite schists are in accordance with published data of potentially analogous biogenic precursors of such rocks (Hahn-Weinheimer, 1966; Hoefs, 1980). Analyses of Hahn-Weinheimer (1966) on Precambrian and Cambrian metamorphosed graphite schists are divided by her into one group, with a considerable depletion in ^{13}C (average -25‰) being interpreted as compatible with a biogenic origin of these rocks and a second group with ^{13}C-values of up to -7‰ interpreted as bearing a probable crustal signature. The average ^{13}C-value of about -20‰ fits well into data sets for sedimentary organic material as is shown by Figure 3.10, A. The graphite might have developed by the progressive loss of hydrogen from organic compounds, leading to the recrystallization of the residual carbon as graphite (Faure, 1986). A mechanism involving the (abiogenic) reduction of CO_2 or of carbonates would have produced an enrichment in ^{13}C with a shift towards positive values of the $^{13}C/\ ^{12}C$ ratio.

The interpretation of "black shales" preserved in the rock record is still problematic. Arthur *et al.* (1984) summarize the three most frequently used variables which are considered to be most significant for black shale development: (a) variations in the supply of marine and terrigenous organic matter from surface productivity, fluvial discharge, redepositional processes and settling from nepheloid-layers; (b) variation in the rate of sedimentation and hence rate of burial of organic matter; and (c) variation in bottom water oxygenation within an oxygen-minimum zone. Graphitic schists occur within distinct parts of the study area and are intercalated with turbidite facies sequences. The sequence stratigraphically above the graphite schist on the farm Kaan shows especially-well preserved sedimentary structures which are part of turbidite facies (Fig. 3.3,1), High pyrite contents indicate reducing conditions. The most likely processes which would account for this change in facies are initial changes in supply of organic matter (e.g. by increasing plankton productivity) and/or oxygen depletion associated with volcanic activity, e.g. as represented by the Matchless Amphibolite. Both these processes may lead to temporary extensions of oxygen-minimum zones into the deep-sea zone which might even explain the occurrence of black shales near the Mid-Atlantic ridge (Tissot *et al.*, 1980), in the deep Atlantic Cape Verde basin (Arthur *et al.*, 1984) and the Angola basin off the southwest African coast (Stow and Dean, 1984).

Taking the case of the Angola basin, Stow and Dean (1984) pointed out that oxygen concentrations change periodically in sediment and bottom waters. This leads to anoxic conditions both in the basin and on the continental margin. Analyses of black shale sequences in the Atlantic ocean have shown that both turbiditic and pelagic processes operate throughout their deposition (Arthur *et al.*, 1984).

3.5.7 Marble and tremolite schist facies (facies class 7)

(a) Description

Rocks of this facies have only been found in association with the Matchless Amphibolite (marble) and stratigraphically below the graphite schist on the farm Kaan (tremolite schist). The marble horizon is up to 2 m thick and is developed on top of a 10 m-thick graphite schist and has been traced laterally over several kilometres (Fig. 3.9, D). The marble is internally massive, the matrix consisting mainly of finely-recrystallized dolomite and some calcite. The tremolite schist is about 1 m thick and is extremely weathered. It has been included with this facies because metamorphic assemblages indicate that it formed from dolomite during prograde metamorphism (Winkler, 1979).

(b) Stable isotope analysis

Stable isotope techniques have been used to elucidate the primary (organic pelagic) or secondary (chemogenic, hydro thermal) origin of the marble layer at the Matchless Amphibolite. Oxygen data (Table 3.2, Fig. 3.11, B) give constant ^{18}O-values around -16‰. This represents an enrichment in ^{18}O compared with average ocean water (Fig. 3.10, B) but a marked depletion if compared with data for Upper Proterozoic marine carbonates (Veizer and Hoefs, 1976). The BC-values for carbon isotopes range between -4‰ and -9‰ (Table 3.2, Fig. 3. 11 ,A) which represent a depletion in BC compared with marine carbonates (Hoefs, 1980).

(c) Interpretation and discussion

In comparison with the graphite schists, the interpretation of the carbon and oxygen data of the dolomitic marble horizon poses more of a problem. Land (1980) concluded that the marked depletion in ^{18}O of ancient dolomites compared with recent dolomites has either developed by primary precipitation (which is rather rare) or by replacement, either at elevated temperatures or from fluids depleted in ^{18}O relative to SMOW. Oxygen isotopic compositions may

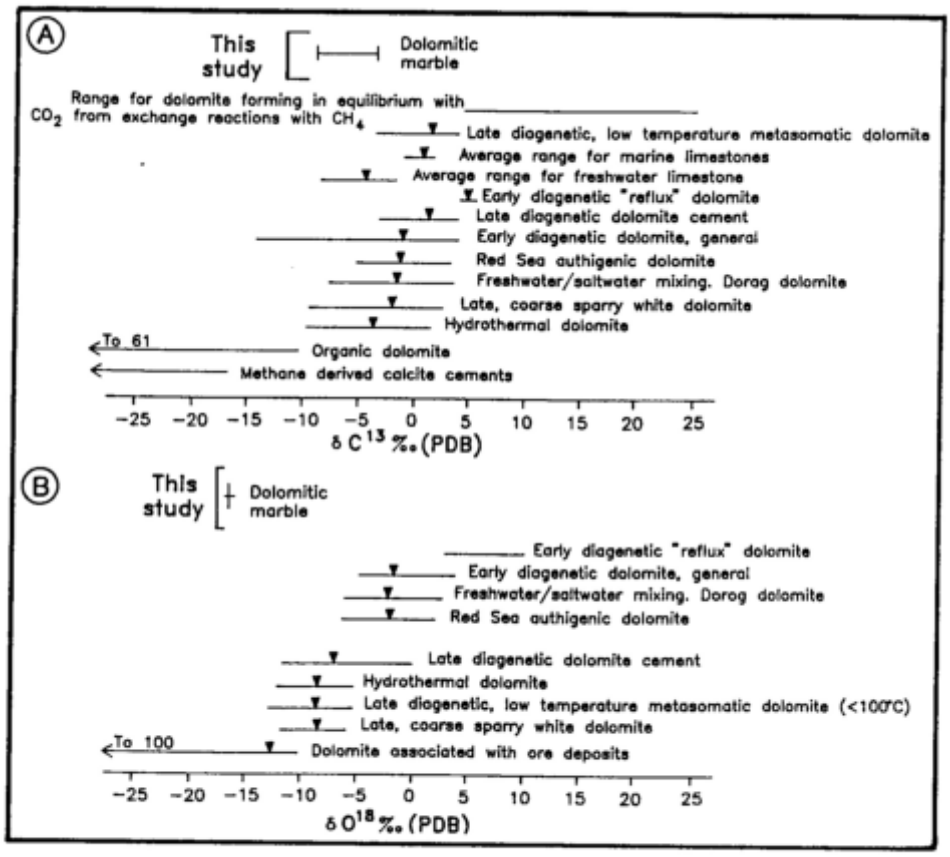

Fig. 3.11: Diagram comparing ^{13}C (A) and ^{18}O (B) data from the dolomitic marble at the Matchless Amphibolite with other species of dolomite (from Mattes and Mountjoy, 1980).

change during subsequent processes, such as hydro thermal alteration, and under the influence of meteoric waters (Cocker *et al.*, 1982; Fig. 3.11, B). On the other hand, Valley (1984) reported that during metamorphism, volatilization and fluid exchange tend to decrease ^{18}O but only on a scale of 1-3‰ between lower-greenschist and granulite facies. Carbon isotopic compositions are more difficult to alter due to the higher insolubility of CO_2 (Land, 1980). Since a freshwater origin as well as the participation of terrestrial organic carbon towards formation of the marble, seem unlikely in terms of the deep marine sedimentary facies encountered in the Khomas Trough, a mechanism to deplete ^{13}C to the values observed was probably involved. This decrease in ^{13}C towards values characteristic for "juvenile carbon" in carbonatites and diamonds (Fig. 3.10, A) might be a result of diagenetic processes (Mattes and Mountjoy, 1980; Land, 1980) or due to hydro thermal alteration, which includes the possibility of fumarolic activity (Faure, 1986).

In conclusion, both data sets may be regarded from two points of view: if compared with recent and ancient "organic" limestones, both heavy isotopes are depleted, but compared to ocean seawater as well as meteoric, connate and formation waters, ^{18}O is enriched and ^{13}C is enriched with regard to sedimentary organic carbon. Possible explanations for the origin of the marble horizon are: (l) resedimentation processes involving shelf carbonates; and (2) precipitation and/or replacement of carbonate, involving marine organic CO_2 or CO_2 from hydro thermal/fumarolic activity. Possibility (l) may be excluded due to the pelagic sedimentary facies surrounding the marble. Therefore "*in situ*" precipitation of carbonate from seawater, probably in the vicinity of the Matchless Amphibolite shortly after its extrusion, is considered better to explain the isotope signatures obtained.

3.6 Vertical facies sequences and sedimentary cycles

(a) Vertical facies sequences

The facies described above occur within characteristic facies sequences throughout the Khomas Trough. Since the comparison with the turbidite facies classes of Pickering *et al.*. (1986) has been drawn in section 3.5, their facies will be referred to for convenience in the following section. A representative sample of measured sections is presented in Figures 3.12 and 3.13. This shows that vertical facies sequences mostly involve very thick -bedded (north) to thin-bedded (south) facies B layers which are associated: with facies C and E at the northern margin of the Khomas Trough (Figs 3.12, 3.13, 3.14, A and B); with facies C, D and partly E in the centre (Figs 3.9, B, 3.12, 3.13, 3.14, C); and with facies E and partly C in the south (Figs 3.12, 3.13, 3.14, D). Also in the centre of the traverse, facies C is associated with facies D. In the south and centre of the trough, pelagic facies G graphite schists are intercalated within turbiditic facies B and C (Fig. 3.3,1). The turbiditic carbonate facies is distributed throughout the traverse and is preferentially associated with facies Band C psammites.

The development of bed thicknesses of psammites and pelites shows similar trends for both rock types in the north

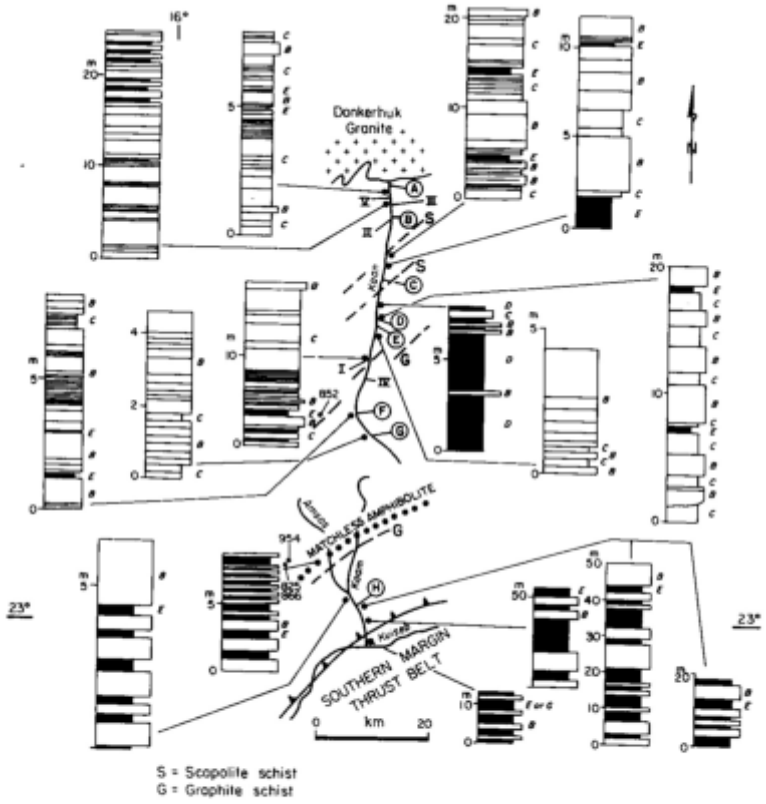

Fig. 3.12: Representative selection of measured sections along the study traverse showing facies distribution. Note the increase of pelagic facies southwards. Pelites shaded black; Psammites blank. Also indicated are positions of measured sections in Figures 3.3 (roman letters) and 3.13 (circled letters).

and centre of the Khomas Trough, but different trends in the south. This is expressed by a decrease in psammite layer thickness to a maximum of about 20 em in the south, whilst pelitic units increase in thickness to several metres (Fig. 3.12). An exception is found in a limited area on the farm Okasume where thicker beds are developed (Figs 3.12 and 3.13, H). It is due to the greater differential weathering of the pelitic units that measured sections have a recording bias. They preferentially contain information from the psammitic parts of each sequence and therefore do not reflect psammite/pelite percentages on a larger scale along the traverse. Figure 3.12, however, indicates the increase of pelitic percentage in the southern part of the Khomas Trough.

In addition to the change in bed thickness it is important to note that there is a pronounced change in sedimentary features occurring in the centre of the traverse. Sedimentary structures are commonly developed in sequences north of the upper Koam canyon (Figs 3.12, G and 3.13). To the south, however, only graded layering appears to be preserved.

(b) Sedimentary cycles

Further analyses of measured sections have shown that facies sequences are organized into sedimentary cycles which are developed on all scales. Cyclicity on a kilometre scale is already conspicuous in the landscape which exhibits a regular alternation of zones with smooth topography and scarce outcrop which contrast with rough, steep topographies with abundant outcrop. Mapping along the traverse and along some sections west towards the Namib desert has revealed that these topographical changes are related to sedimentary facies changes from major pelite-dominated to psammite-dominated successions, respectively. The major cyclic sequences are also visible on the Landsat image of the area (Fig. 2.4) and they may be traced laterally for at least 100 km. Their distribution along the study traverse is shown in Figure 3.15. Medium-scale cycles have proven to be difficult to evaluate in measured sections due to outcrop preservation, but could be mapped in the landscape where they are well shown (Fig. 3.16, A-D). The medium-scale cycles are between 200 m and 500 m thick and the measured cycles have been incorporated into the large cycles in Figure 3.15.

Small-scale cycles vary in thickness from 2 m to 30 m and are nested within the medium-scale cycles. Bed thickness plots of some selected outcrops are given in Figure 3.13. These confirm that the northern part of the Khomas Trough comprises two major thinning-upward sequences (Figs 3.15, 3.16, E), the southern one of which, however, includes minor thickening-upward cycles (Fig. 3.15).

Towards the south a wide zone of nested thickening-upward cycles follows (Figs 3.13, 3.15, 3.16, F and G), to be succeeded by non-cyclic successions in the south (Figs 3.12, 3.15). A small zone containing thickening-upward cycles is incorporated within the latter zone (Figs 3.15, 3.16, D).

Since the Kuiseb schists are strongly deformed and metamorphosed, a considerable amount of internal folding is developed within the sedimentary cycles. Notwithstanding this

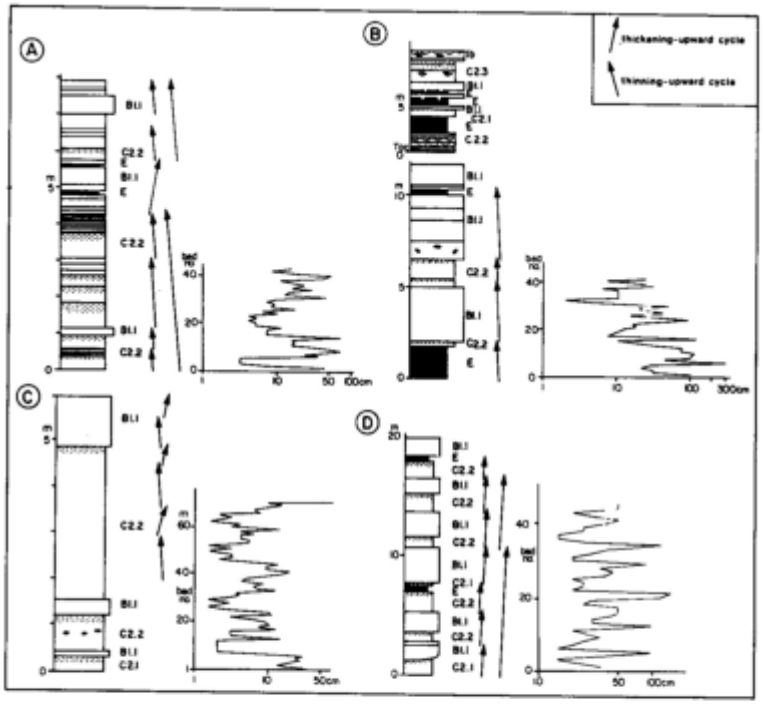

Fig. 3.13: Representative measured sections showing facies analysis, sedimentary cycles and bed thickness plots. Diagrams from A to H confirm the change from small-scale thinning-upward to thickening-upward cycles from north to south. Positions of sections are indicated in Figure 3.12.

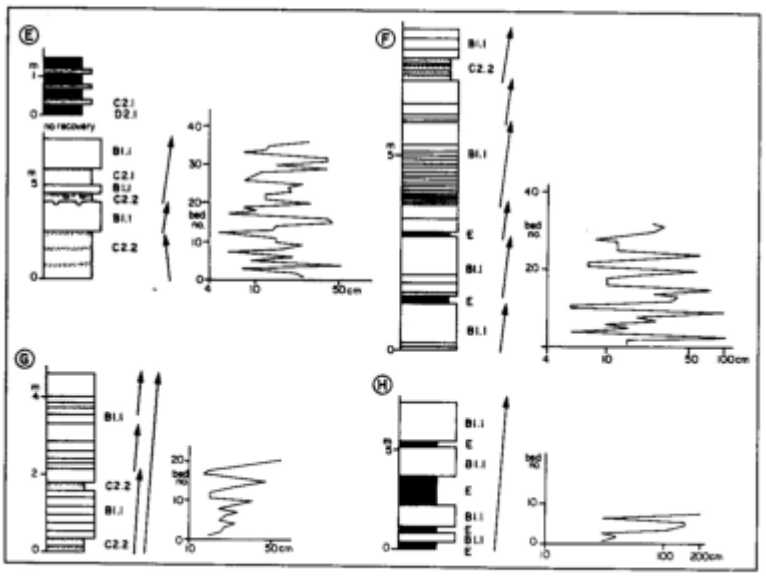

Fig. 3.13: (continued)

strong but widely coaxial deformation, sequential lithofacies changes have been shown to occur on all scales. Therefore, the major large-scale cycles are regarded as coherent stratigraphic units which extend for more than 100 km laterally.

3.7. Facies models

Most of the seven facies described above may be interpreted in terms of facies models for turbidites and pelagic sediments. The turbidites in the Khomas Trough are largely accommodated within the medium-grained turbidite model (terminology of Stow, 1986 and Pickering *et al*., 1986). This involves the classical Bouma (1962) sequence and represents the depositional model for most of facies C and partly facies B and D (Fig. 3.7). The well-known five Bouma divisions are T_a to T_e. It seems, however, that incomplete sequences (top-absent, mid-absent, base-absent etc.) are the rule. This also formed the basis of the facies subdivisions into immature facies (B1, C1) and mature facies (B2, C2) by Pickering *et al.* (1986). Most of the sand-rich turbidites (facies C) are deposits of high-concentration turbidity currents in contrast to low-concentration currents of facies D. Tractional processes playa role where flows are underladen (Pickering *et al.*, 1986).

The fine-grained turbidite model (Stow and Piper, 1984) represents much of facies D and E (Fig. 3.7). In this model

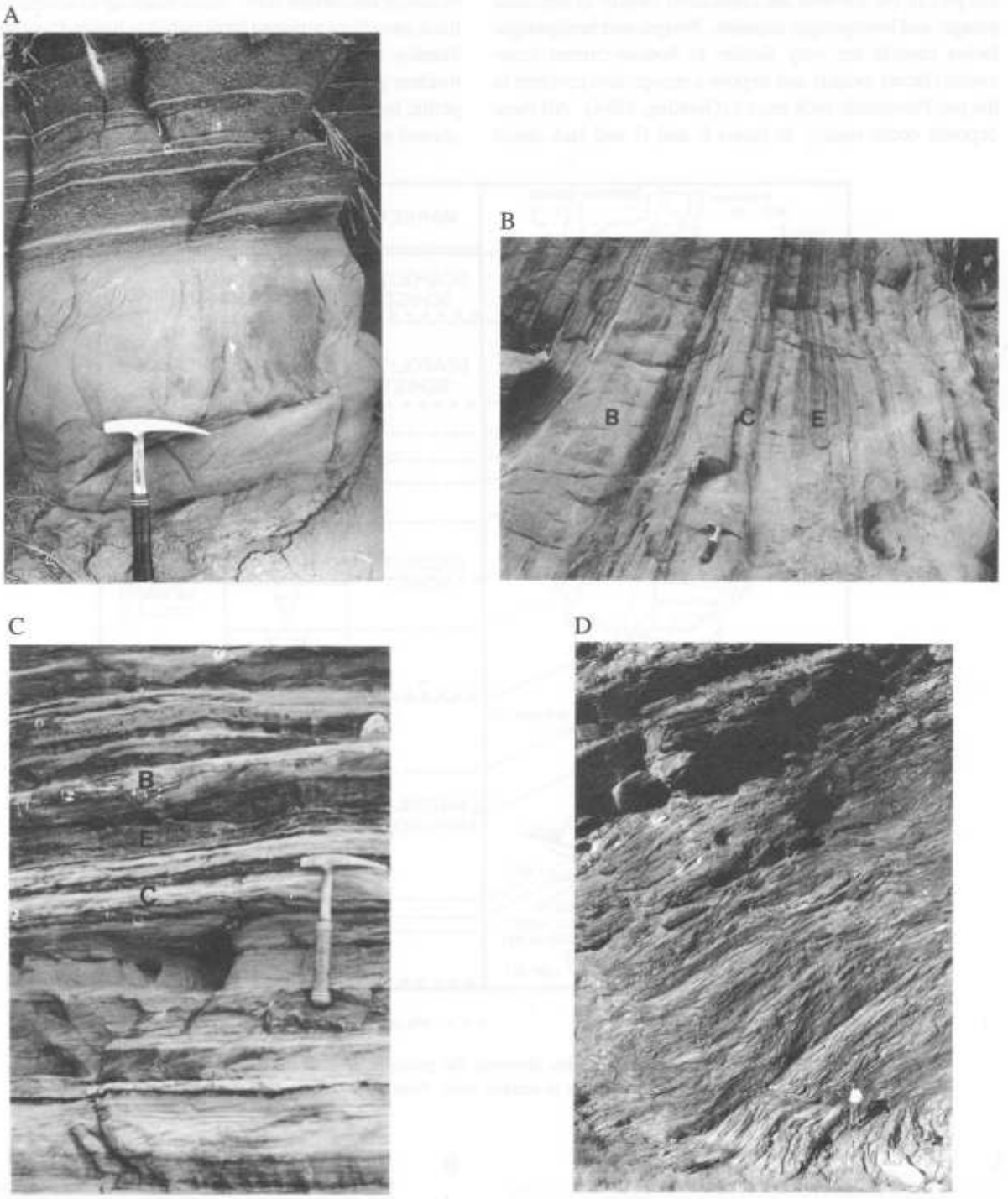

Fig. 3.14 : (A) Thick-bedded facies B turbidite underlying facies E turbidite, northern Khomas Trough, farm Keises 312. (B) Facies B, C and E turbidites in the northern Khomas Trough, farm Keises 312. (C) Facies B, C and E turbidites in the central Khomas Trough, farm Dagbreek 365. (D) Thin-bedded facies E turbidites below the Matchless Amphibolite in the southern Khomas Trough. Height of scale is 1.8 m. Farm Kobos 305.

graded, silt-laminated muds pass upward into graded muds and finally into ungraded muds. These sequences have been described by Piper (1978) and Stow and Shanmugam (1980). Again in this facies, complete sequences are the exception and top-, mid-, and base-absent units occur. Waning current velocities account for the grading, and the alternation of silt and mud laminae originated from depositional sorting of silt grains from clay flocs due to shear in the bottom boundary layer (Stow and Bowen, 1980).

Resedimented carbonates have become incorporated with the clastic depositional system in the Khomas Trough. Whilst fine-grained carbonate material would have tended to disperse in the water column and settle out with the pelagic background sediments (Stow, 1986), the sand- and silt-grade carbonates have been deposited with the turbidity currents, to produce a mix which was metamorphosed to calc-silicate rocks.

Pelitic successions more than 100 m thick in the south-

ern part of the traverse are considered largely to represent pelagic and hemipelagic deposits. Pelagic and hemipelagic facies models are very similar to bottom-current (contourite) facies models and impose a recognition problem in the pre-Palaeozoic rock record (Gorsline, 1984). All these deposits occur mainly in facies E and G and lack direct evidence for current flow. Since muds up to several metres thick have been reported from turbidite basins ("unifites" of Stanley, 1981) it is extremely difficult to distinguish structureless pelitic turbidites, pelagic/hemipelagic pelites and pelitic bottom-current deposits, especially in the metamorphosed sequences described here.

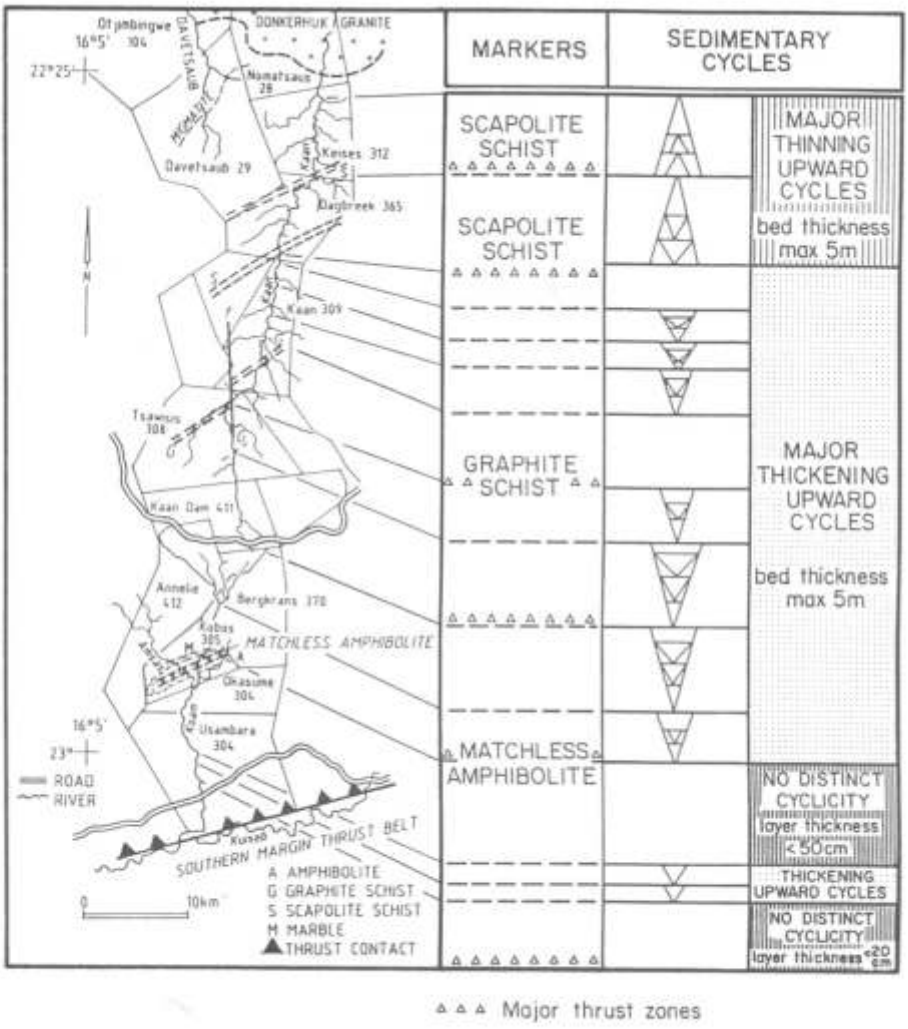

Fig. 3.15: Map of the study traverse showing the position of major sedimentary cycles and non-cyclic sequences in relation to marker units. Note the decrease of bed thicknesses from north to south.

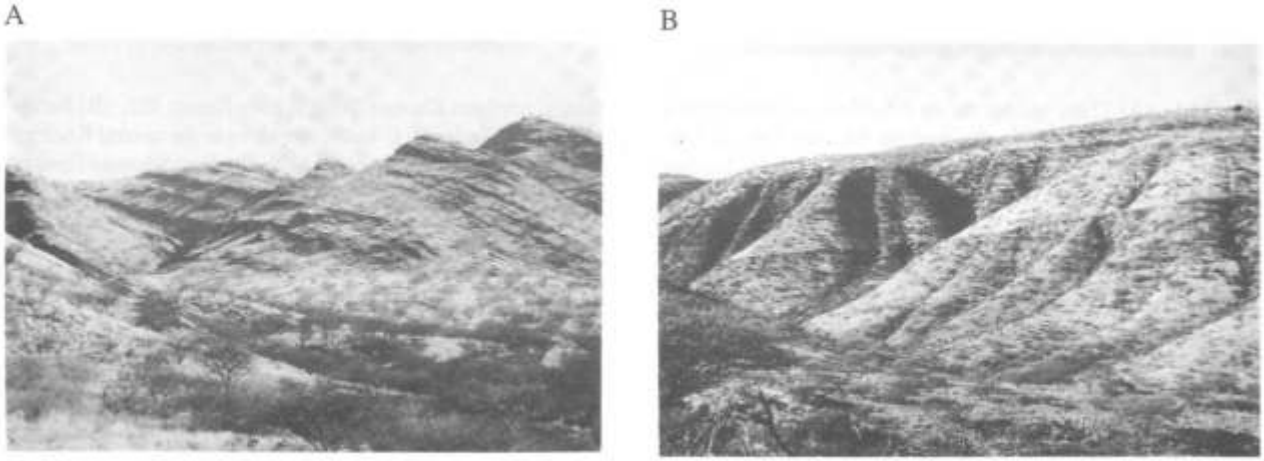

Fig. 3.16: (A) Several thickening-upward cycles, approx. 50 m thick, etched in the landscape. Farm Dagbreek 365. (B) Thickening-upward cycles, approx. 200 m thick. Farm Kaan 309.

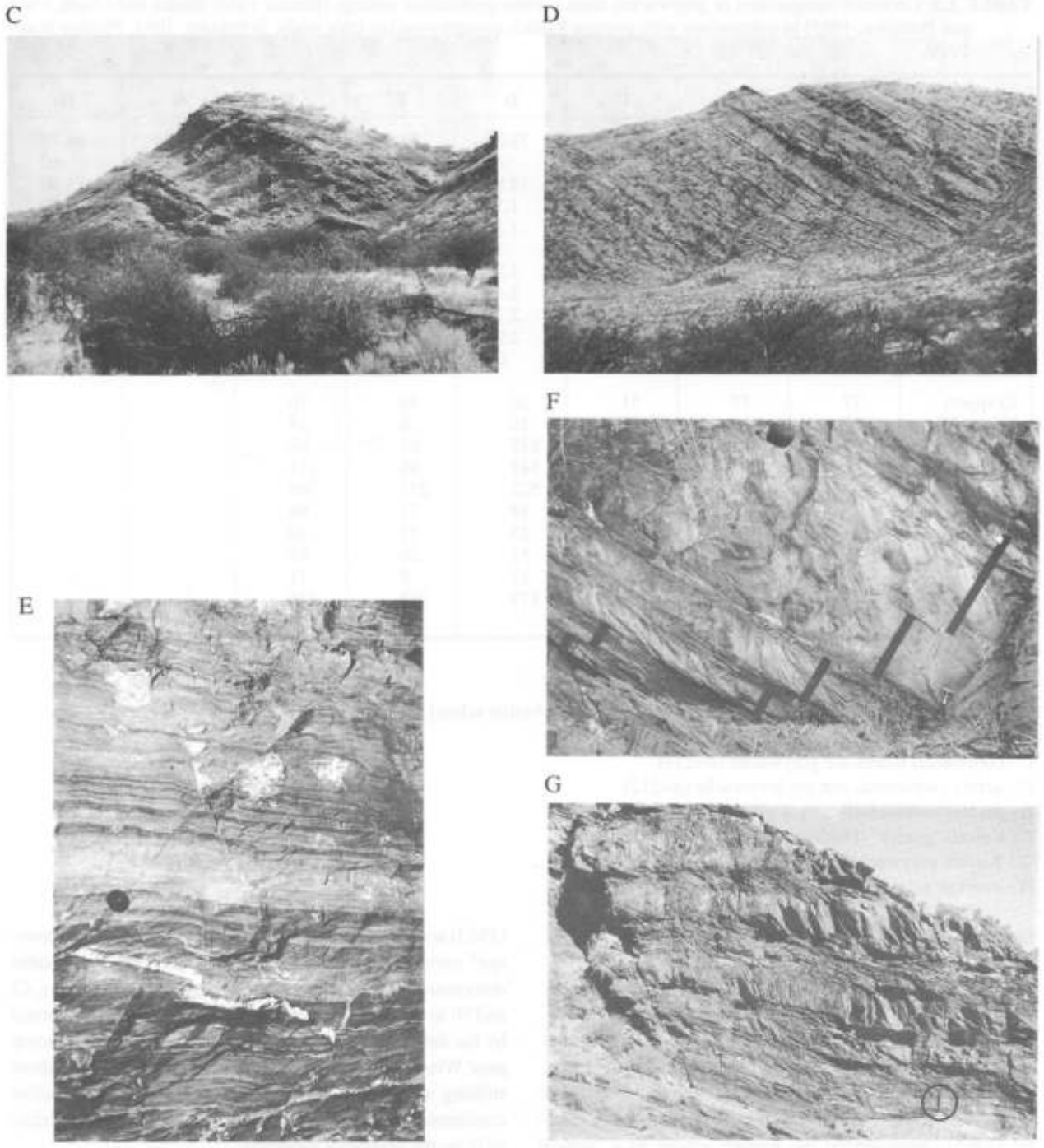

Fig. 3.16: (C) Thickening-upward cycles, approx. 100 m thick. Farm Tsawisis 308. (D) Thickening-upward cycles, intercalated with thick non-cyclic basin-plain sequences of the southern Khomas Trough (compare with Fig. 3.13). Farm Okasume 304. (E) Small-scale thinning-upward cycles. Psammitic lithologies are light coloured, pelites are dark. Beds thin towards the stratigraphic top (top of the photograph). Farm Dagbreek 365. (F) Small-scale thickening-upward cycle (3.5 m). See bed thickness plot in Figure 3.13,D which also contains this cycle. Individual beds are demarcated by bars. Hammer for scale. Farm Tsawisis 308. (G) Thickening-upward cycle (approx. 15 m thick) within lobe sequence of the southern Khomas Trough. Sledge hammer for scale (circled) is 59 cm long. Farm Okasume 304.

Further facies models encountered in the literature are slides and slumps (Woodcock, 1976), debrites (Thornton, 1984) and coarse-grained turbidites (Lowe, 1982). There is no evidence for slides, slumps or debris-flow deposits in the Khomas Trough to date. Although the sediments have been considerably recrystallized during metamorphism, it may be postulated that original grain sizes have not exceeded sand size. It is rather unlikely that a conglomeratic precursor recrystallized during metamorphism to produce the fine and medium "grain sizes" encountered in the study area. The relative uniformity of grain size is a regional feature. Some authors have, however, suggested that some of the carbonate-bearing nodules and spindles described above under the metacarbonate facies represent original sedimentary clasts

TABLE 3.3: Chemical composition of greywackes from various geotectonic settings (Bhatia, 1983; Bhatia and Crook, 1986 and Pettijohn, 1963) in comparison with average Kuiseb metagreywackes (this study; Schneider, 1983; Phillips *et al.*, 1989).

	A	B	C	D	E	F	G	H
SiO_2 (wt %)	72.40	58.83	70.69	73.86	81.95	71.79	70.54	66.70
TiO_2	.85	1.06	.64	.46	.49	.93	.78	.60
Al_2O_3	11.19	17.11	14.04	12.89	8.41	11.71	12.10	13.50
FeO	nd	5.52	3.05	1.58	1.76	5.03	3.19	3.50
Fe_2O_3*	5.06	1.95	1.43	1.30	1.32	nd	1.63	1.60
MnO	.08	.15	.10	.10	.05	.08	.10	.10
MgO	2.03	3.65	1.97	1.23	1.39	2.23	2.24	2.10
CaO	1.70	5.83	2.68	2.48	1.89	1.58	2.73	2.50
Na_2O	2.78	4.10	3.12	2.77	1.07	2.28	2.84	2.90
K_2O	2.16	1.60	1.89	2.90	1.71	2.17	1.76	2.00
P_2O_5	.19	.26	.16	.09	.12	.18	.18	.20
Cr (ppm)	77	37	51	26	39	76		
Ni	27	11	13	10	8	24		
Rb	85	18	67	115	61	88		
Sr	146	637	250	141	66	114		
Ba	462	370	444	522	253	389		
V	99	131	89	48	31	96		
Y	33	20	24	25	27	40		
Zn	71	89	74	52	26	67		
Nb	10	2	9	11	8	11		
Zr	243	96	229	179	298	238		

*total Fe as Fe_2O_3 in Kuiseb schists

A - Kuiseb metagreywacke (this study; quartz-plagioclase-biotite schist) (n=70)
B - oceanic island-arc greywacke (n=82)
C - continental island-arc greywacke (n=257)
D - active continental-margin greywacke (n=212)
E - passive continental-margin greywacke (n=123)
F - Kuiseb "gneiss" (Phillips *et al.*, 1989; n=17)
G - Kuiseb greywacke (Schneider, 1983; n=57)
H - average greywacke (Pettijohn, 1963; n=61)

(De Waal, 1966; Preussinger *et al.*, 1987).

3.8 Depositional setting of the Khomas Trough

3.8.1 Previous sedimentation models

For the Khomas Trough, interpretations of the sedimentation patterns have only been speculative in the past. Martin (1965) characterized the Kuiseb schists as a "typical eugeosynclinal assemblage". Miller (1979) initially demonstrated graded bedding and he concluded that the "flysch sediments" were deposited by turbidity currents. This has subsequently been confirmed by several authors (e.g. Downing, 1983; Preussinger *et al.*, 1987). Without presenting data, Downing (1983) speculated upon a submarine fan environment for the Kuiseb schists.

3.8.2 Geochemical constraints on the source area of Kuiseb metagreywackes

With regard to a possible source area, chemical compositions of the Kuiseb metagreywackes of this study (see section 3.3) of Schneider (1983) and of Phillips *et al.* (1989), are compared in Table 3.3 with greywackes from different geotectonic settings on the basis of data compiled by Bhatia (1983) and Bhatia and Crook (1986). Also given are "average" greywacke analyses from Pettijohn (1963). The table demonstrates unusually high average contents of TiO_2, Cr and Ni in the Kuiseb metagreywackes which are confirmed by the data of Phillips *et al.* (1989) who studied an outcrop near Windhoek in detail. The overall compositions show striking similarities to continental island-arc and active continental-margin greywackes which is confirmed particularly by the immobile elements.

Within Crook's (1974) classification, based on SiO_2 and Na_2O/K_2O contents, the Kuiseb metagreywackes classify as quartz-intermediate Andean-margin greywackes. Roser and Korsch (1986) have also analysed greywackes from different tectonic settings and have tried to characterize these by means of major element ratios. The Kuiseb data have been plotted into one of their diagrams and this confirms an active continental-margin source for the precursor (Fig. 3.17). Although major elements have been modified during metamorphism, the variation diagrams (Fig. 3.1) show that K_2O, Na_2O and SiO_2 have been enriched. Pettijohn (1975) pointed out that K_2O and Na_2O increase with increased maturity of the terrigenoclastic sedimentary rock. It may therefore be expected that K_2O/Na_2O ratios were originally lower, a fact which emphasizes even more, considering Figure 3.17, the probable active-margin deri-

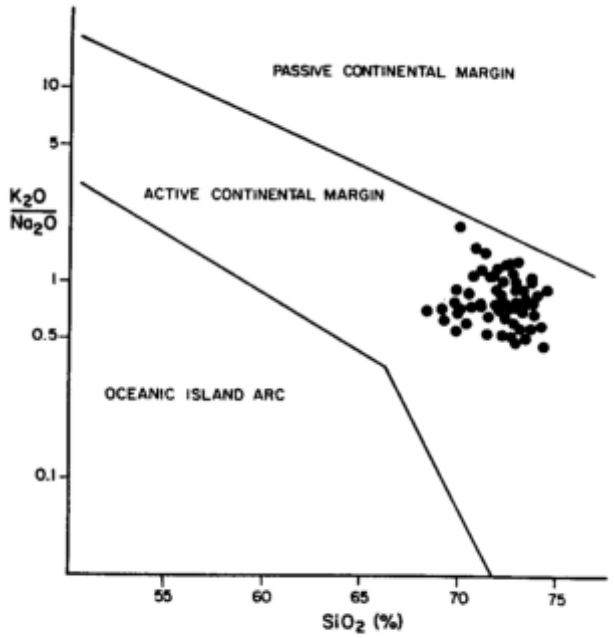

Fig. 3.17: Major element plot distinguishing tectonic settings of sandstone-mudstone suites (after Roser and Korsch, 1986).

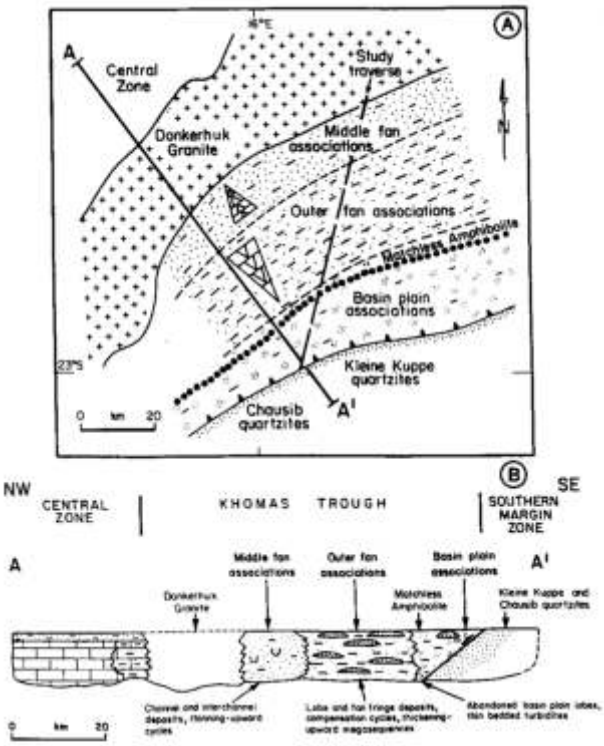

Fig. 3.18: (A) Map of depositional palaeoenvironments interpreted for the Khomas Trough. Middle fan and outer fan deposits of an elongate submarine fan system as well as basin-plain deposits are developed in the north, centre and south respectively. (B) Schematic profile through the southern inland branch of the Damara Orogen showing palaeoenvironmental setting and facies associations in the present-day Khomas Trough and in adjacent areas. Note the position of the Matchless Amphibolite.

vation of the Kuiseb metagreywackes.

These results, suggesting that an active continental margin with both volcanic and plutonic magmatic suites contributed considerably towards the precursor of the Kuiseb metagreywackes in the Khomas Trough, are not in accordance with the findings of Miller *et al.* (1983) who studied the geochemistry of the Kuiseb schists along a traverse between Okahandja and Windhoek. Based on the geochemical maturity index of Pettijohn (1975) the authors concluded that a southern and central group in the Khomas Trough are related to a passive margin provenance, whereas a northern group has been supplied by a northerly-situated rhyolite-rich source.

3.8.3 Interpretation of elongate submarine-fan and basin plain depositional environments

By the very nature of the metamorphosed Kuiseb Formation metasediments, comparison must be made between the sedimentary features recognized and those facies associations already described from more recent turbidite sequences. Within marine environments, three fundamental "facies associations" (Nelson and Nilsen, 1984) or "environments" (Stow, 1986) have been identified: slope aprons, submarine fans and basin plains. The facies and facies models which have been documented and summarized above are interpreted to indicate submarine-fan environments and basin-plain environments. The lateral extent of marker horizons, the consistent palaeocurrents from the northeast parallel with the tectonic strike, the size of sedimentary cycles and the uniformity in lithologies and grain sizes strongly suggest a mixed-sediment elongate fan system (Nelson and Nilsen, 1984).

Interpreting submarine-fan facies associations from "proximal" to "distal" has limitations. Various authors have put emphasis on the problems arising from the comparison of modern fan settings with those of ancient fans (Normark *et al.*, 1983/84; Shanmugam *et al.*, 1988). This is initially a problem of study approaches, since modern fan research deals mainly with morphologic aspects and shallow drill cores. Subsequently the turbidite facies scheme of Mutti and Ricci Lucchi (1972), developed on an ancient mixed-sediment fan (Nelson and Nilsen, 1984), has been applied to modern fan settings. Ancient fans, on the other hand, are interpreted from vertical facies sequences which are dependent on outcrop preservation. Large-scale morphologic features which help to confirm a fan shape are extremely difficult to evaluate. In the rock record it is difficult to recognize channels on a smaller scale, although they are such an important feature of fan settings, as has been pointed out by Normark *et al.* (1983/84) and Shanmugam *et al.* (1988).

Interpretation of sedimentary sequences in the Khomas Trough is made with the background that the succession is subdivided into individual thrust-bound sequences (this will be shown in Chapter 4). However, having taken internal folding into account during the taking of measurements in the field, it is implicit that facies relationships are largely intact within the individual slabs. The fold style and southeast-directed vergences have produced thick, upright fold limbs with upward-facing sequences and only very narrow overturned limbs. Stratigraphic relations between adjacent slabs, however, are unknown and considerable parts of the fan sys-

tem might be missing but are more probably repeated.

The distribution and organization of facies and vertical facies sequences, together with cyclic patterns as shown in Figures 3.12, 3.13 and 3.15, are interpreted to document middle-fan and outer-fan depositional environments of an elongate submarine fan in the north and centre of the Khomas Trough. Basin-plain deposits are developed in the south (Fig. 3.18). Since there is no evidence for coarse-grained, conglomerate facies A (Pickering *et al.*, 1986; Mutti and Ricci Lucchi, 1975) on a larger scale as well as for facies F "chaotic deposits" (Pickering *et al.*, 1986; Mutti and Ricci Lucchi, 1975), it is inferred that inner-fan environments and slump and slide deposits have not been developed on the line of this traverse or have not been preserved. Inner-fan depositional environments are typically small and closely situated to the feeding source of elongate fans (e.g. Nelson, 1983/84) and may therefore easily be obliterated or developed laterally in ancient orogenic settings.

In the northern part of the Khomas Trough, middle-fan depositional environments of an idealized fan system (Nelson and Nilsen, 1984) are indicated by the dominance of thick-bedded over thin-bedded turbidites within an overall thinning-upward trend. Irregular alternations of thinning - and thickening-upward cycles, together with small channels and incomplete Bouma sequences suggest, however, the widespread occurrence of interchannel deposits (Nelson and Nilsen, 1974; Stow, 1986).

Facies features from the centre of the trough, outlined above, are consistent with outer-fan lobe (in the sense of Mutti and Ricci Lucchi, 1972) and fan-fringe facies associations (summaries in Nelson and Nilsen, 1984 and Shanmugam and Moiola, 1988). The small-scale thickening-upward cycles (up to 5 m thick) most probably represent compensation cycles as described by Mutti and Sonnino (1981). Regarding cyclicity, Stow (1986) has pointed out that proximal sandy lobes tend to show thickening-upward sequences in contrast to distal sandy and muddy lobes which show more symmetrical sequences.

Sedimentary sequences in the southern part of the Khomas Trough, from several kilometres north of the Matchless Amphibolite to the Southern Margin Zone, document the transition from outer-fan lobes to fan-fringe and basin-plain successions (Fig. 3.18). In favour of this interpretation are: (1) thin-bedded turbidites intercalated with pelagic deposits; (2) the overall decreasing bed thickness of turbidites towards the southern margin of the Khomas Trough; and simultaneously, (3) the increasing thickness of large-scale pelagic successions (pelites and graphite schists) to a scale of up to a hundred metres towards the south, reflecting the preponderance of hemipelagic and pelagic sedimentation over turbiditic processes. The narrow zone which comprises thick psammitic beds organized within thickening-upward cycles intercalated within the basin-plain succession (Figs 3.12 and 3.18) might be explained either by structural interposition or by an episode of outbuilding of a lobe sequence into the distal environments. This would be similar to one of the basin-plain lobes described by Pickering (1981) from the Late Proterozoic Kongsfjord turbidite system and by Ricci Lucchi and

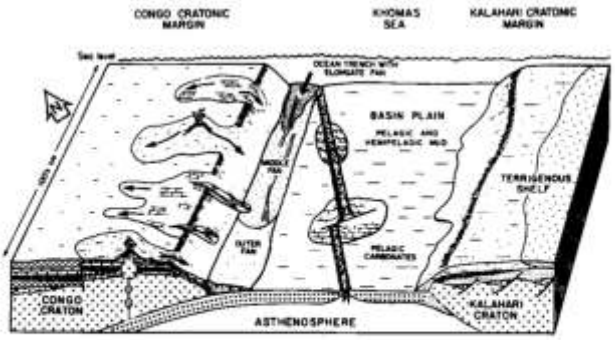

Fig. 3.19: Palaeoenvironmental model of the Khomas Trough. The elongate Khomas Fan is fed primarily from a mixed volcanic-plutonic active continental-margin source which is situated to the northeast of the present Khomas Trough. Pelagic and hemipelagic sedimentation dominates the basin plain towards the south. Continental platform and slope sedimentation, partly in submarine fans, occurs on the Congo and Kalahari Cratons on either side of the Khomas Sea.

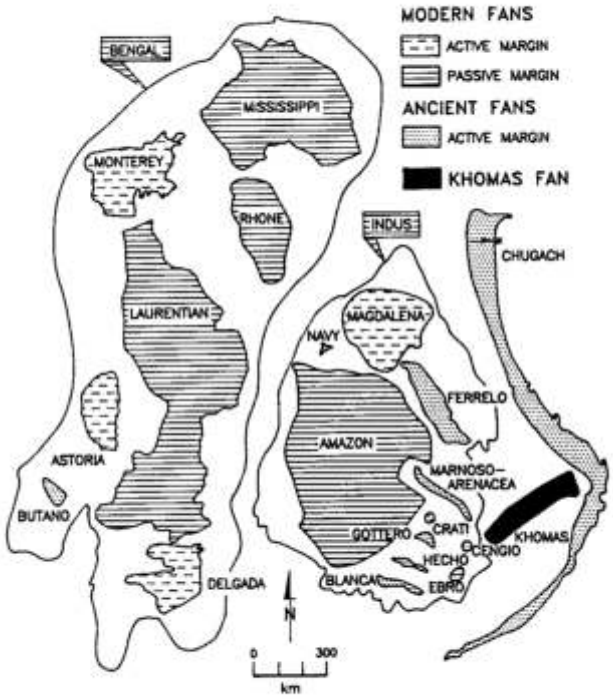

Fig. 3.20: Comparison of the size and shape of the present-day outcrop of the Khomas Fan with other ancient and modern fan systems (modified after Barnes and Normark, 1983/84).

Valmori (1980) from the Italian Apennines.

There are most probably levee, interchannel and contourite environments intercalated in various parts of the succession. Facies D deposits in the centre of the Khomas Trough are especially likely candidates for interchannel deposits in the outer fan. Levees, interchannels and thin-bedded basin-plain turbidites are, however, very similar in depositional patterns (Nelson and Nilsen, 1984) and therefore great uncertainties accompany interpretations in an ancient terrain.

Comparing the assignment of cyclicity to various submarine fan facies associations on modem and ancient fans in various studies shows that there are considerable dissimilarities. There seems to be only partial consensus in recognizing the larger-scale thinning-upward trends as inner- and middle-fan environments as opposed to thickening-upward

TABLE 3.4: Comparison of tectonic settings, sizes, thicknesses and shapes of modern (above the double line) and ancient (below the double line) fans (from Barnes and Normark, 1983/84). Note that ancient fans are almost exclusively situated at active continental margins as pointed out by Bouma *et al.* (1985).

NAME	BASIN SETTING type of margin, type of crust	LENGHT, WIDTH [RADIUS] (km)	MAX. THICKNESS (m)	SHAPE	REFERENCE
1. Amazon	P, O	700 min, 250-700	4200	elongated partial cone	Normark *et al.*, 1983/84
2. Astoria	A, O	250 min, 130	2200	trapezoidal	Normark *et al.*, 1983/84
3. Bengal	P, O	2800, 1100	>5000	elongated	Normark *et al.*, 1983/84
4. Cap Ferret	P, C	[75]	1800	elongated dissymmetric	Coumes *et al.*, 1983
5. Crati	A, C	16, 4-5	30	elongated	Normark *et al.*, 1983/84
6. Delgada	T, O	[>350]	3000	elongated bi-lobed	Normark *et al.*, 1983/84
7. Ebro	P, C	100, 50	370	oval	Normark *et al.*, 1983/84
8. Indus	P, O	1500, 960 max	>3000	fan	Normark *et al.*, 1983/84
9. La Jolla	T, C	40, 50	1600	pear shaped	Graham & Bachman, 1983
10. Laurentian	P, O	500 min - 1500 max, 200-400	2000	elongated, lobate	Normark *et al.*, 1983/84
11. Magdalena	A, O	[230]	3000	trapezoidal fan	Normark *et al.*, 1983/84
12. Mississippi	P, C/O	540, 570	4000	conical	Normark *et al.*, 1983/84
13. Monterey	T, O	400, 250	2000	quarter cone	Normark *et al.*, 1983/84
14. Navy	T, C	[40]	900	elongate basins	Normark & Piper, 1972
15. Nicobar	A/T, O	[2200]	3000	triangular	Bowles *et al.*, 1978
16. Nile	P, C	280, 500	>3000	fan	Maldonado & Stanley, 1978
17. Nitinat	A,O	260, 80	1000	triangular	Stokke *et al.*, 1983/84
18. Rhone	T, C/O	440, 210	1500	elongated	Normark *et al.*, 1983/84
19. San Lucas	P, O	[60]	1000	rectangular	Normark, 1970
20. Blanca	T, C	215, 30	1000	elongated	Normark *et al.*, 1983/84
21. Brae	P, C	overlapping fans each [5-10]	600	slope-apron elongated	Normark *et al.*, 1983/84
22. Butano	S, C	80, 40	3000	elongated ellipsoidal	Normark *et al.*, 1983/84
23. Cengio	A, C	6.4, 4.8	170	arcuate	Normark *et al.*, 1983/84
24. Chugach	S, O	2000, 100	10000	narrow prism	Normark *et al.*, 1983/84
25. Ferrelo	A, O	340, 65	1800	elongated	Normark *et al.*, 1983/84
26. Gottero	A, O	[30, 50]	1500	semicircle	Normark *et al.*, 1983/84
27. Hecho	A, C	175, 40-50	3500	elongated	Normark *et al.*, 1983/84
28. Marnos-Arenacea	A, C	Major-25-50, 6-15 Minor-20-25, 4-10	1000	elongated	Normark *et al.*, 1983/84
29. Khomas	A, O	425, 100	?(>5000)	elongated	this study

abbreviations: (a) type of margin: A-accretionary; P-passive; T-transform; S-subduction.
(b) type of crust: C-continental; O-oceanic.

trends of outer-fan environments. In view of the widespread symmetrical sequences occurring in the Khomas Trough, the compilation of "typical" vertical sequences of turbidites and associated sequences by Stow (1985) shows that regular cyclicity, which occurs preferentially in proximal environments, is rather the exception. In outer-fan and distal environments, symmetrical sequences or non-cyclic sequences are widespread features (Stow, 1985).

3.8.4 Discussion of other possible depositional environments

The basic turbidite sedimentation systems within the marine realm are slope aprons, radial fans, elongate fans in trenches and open basins, and extended deep-sea channel systems. Slope aprons, as well as radial fan systems (summaries e.g. in Nelson and Nilsen, 1984 and Stow, 1986), can be ruled out for the Khomas Trough based on the following reasons: (1) the lateral extent and the consistency of major sedimentation units; (2) the overall vertical facies distribution with uniform (metamorphic) psammite grain sizes probably reflecting original sedimentary grain sizes, and mostly regular bedding surfaces; (3) the lack of proximal slope and inner-fan deposits; (4) the uniform longitudinal palaeocurrent distribution; and (5) the present-day size of the Khomas Trough which is larger than most radial fans described in the literature.

Stow *et al.* (1983/84) have pointed out that fans with elongate shapes also develop in trench floor settings (compared to elongate open-basin fans) due to structural confinement and if a large sediment source exists. An ancient example is the Cretaceous Chugach terrane in Alaska (Nilsen and Zuffa, 1982). Underwood and Bachmann (1982) have shown that trenches may contain debris aprons, elongate fans, axial

channel deposits and unchannelized turbidite sheet flows. It has furthermore been emphasized by Nelson and Nilsen (1984) that there are also striking similarities in source debris and depositional patterns amongst elongate trench fans, elongate open-basin fans and deep-sea channel turbidites. The authors further emphasize that source muds for these trench fans may be high in organic content due to deposition at depths coincident with oxygen minimum layers in the ocean.

3.9. Palaeo-environmental synthesis

A palaeo-environmental interpretation of the Khomas Trough has to take the following regional aspects into account (Fig. 2.3): Towards the south of the Khomas Trough, continental margin sediments of the Upper Damara Sequence of the Kalahari Craton have been interpreted to partly represent slope to deep-water turbidites deposited on small fans (Porada and Wittig, 1983; Hoffmann, 1983). On the Congo Craton in the north, calcareous platform sediments are overlain by younger clastic sequences. Along the cratonic margin calcareous turbidites form slope facies associations which have been deposited within radial submarine fan systems, according to Porada and Wittig (1983). Margins both north and south of the Khomas Trough have thus been interpreted as platform and slope settings which contain partly turbiditic deep-water sediments (Fig. 2.3).

This study proposes the following palaeo-environmental setting for the Khomas Trough (Fig. 3.19): Clastic sedimentation probably commenced during divergent plate movements in the Southern Damara Orogen (e.g. Miller, 1983b; Henry *et al.*, 1990). The lithofacies and facies associations described in the previous sections indicate that turbidity currents within a submarine fan, here named Khomas Fan, were the main depositional processes within the Khomas Sea which separated the Congo and Kalahari Cratons. The turbidites carried a preponderately clastic load but some calcareous material, which was most probably derived from the adjacent shelf to the north, was included in the flows. The sediment load was effectively transported laterally, parallel to the basin margins, from the northeast to the southwest. This type of longitudinal, long-distance sediment transport is best interpreted by deposition within an elongate submarine fan as shown in Figure 3.19. "Proximal" to "distal" relationships occur from north to south confirming the development and preservation of middle-fan, outer-fan and basin-plain depositional environments through time. The mass-flow processes were accompanied by contemporaneous pelagic and hemipelagic settling but part of the pelagic and hemipelagic sediment has also been involved in resedimentation processes during progressive development of the basin. Various graphite schists intercalated with turbiditic as well as pelagic facies probably originated from both pelagic settling and transport of organic carbon-rich detritus by turbidity currents into oxygen-deficient, anoxic parts of the Khomas Sea where they were deposited as black shales.

Palaeocurrent data confirm that the main source for the clastic sediment was situated towards the northeastern end of the present Khomas Trough (Fig. 3.19).

Geochemical patterns show a volcanic source influence and point towards continental island-arc and/or active continental margin derivation of the precursor greywackes. Judging from these data the most probable provenance areas are either the Proterozoic mobile belts in the east (Lufilian Arc, Zambezi Belt), or, alternatively, a volcanic arc feeding in from the Central Zone (Fig. 3.19).

The width and depth of the initial Khomas Sea has repeatedly been a controversial issue and speculations have been based on overall geotectonic models of the Damara Orogen. The sedimentological data presented here suggest that the basin was wide enough to accommodate thick submarine-fan and basin-plain sequences. Furthermore two contrasting depositional environments, clastic and calcareous, were operating on opposite margins of the basin. No evidence for deposition above wave base, such as symmetric-asymmetric ripples or hummocky cross-stratification, is present. Facies C turbidites with base-truncated Bouma T_{bcde} divisions, confirm the basinal nature of deposition, as does the lack of sedimentary structures together with thin-bedded turbidites and thick pelagic pelites in the southern Khomas Trough. Carbonates indicate deposition above carbonate compensation depth (CCD) but judging from present-day CCD levels between 4000 m and 5500 m water depth, as well as from the interpreted slope successions at adjacent margins, the water depth of the original depository was well in excess of 1500 m (average base of continental slope; Cook *et al.*, 1982). This estimate is in accordance with data obtained from modern elongate fans on passive and active continental margins (Nelson and Nilsen, 1984).

A comparison with modern and ancient elongate fans shows the considerable size and the shape of the proposed Khomas Fan (Fig. 3.20; Table 3.4). It is interesting in terms of possible tectonic settings that modern studies describe both passive margin fans (e.g. Bengal, Indus, Amazon; Fig. 3.20) and active margin fans (e.g. Astoria, Crati, Magdalena, Zodiac). In strong contrast to this most of the ancient fans (Mamoso-Arenacea, Gottero, Ferrelo, Chugach, Butano, Jackford Formation/Pennsylvanian, Torlesse Terrane, Eastern Alps; Table 3.4) are interpreted as situated at proposed active margins (Bouma *et al.*, 1985). Many of these active margin fans are furthermore elongate in shape and are interpreted to have developed in oceanic trenches. Exceptions are the slope-apron system of the Brae Oil field in the North Sea (Stow, 1985) and possibly the Late Proterozoic Kongsfjord submarine fan-slope delta system (Pickering, 1985).

In conclusion, the above shows that the facies and the facies associations in the Khomas Trough compare well with published elongate submarine-fan settings. The vertical and lateral facies distribution, the high percentage of metasediments which indicates a large sediment supply and the inferred shape of the Khomas Fan are similar to elongate trench fans developed at active continental margins. Ancient examples are the Cretaceous Chugach terrain in Alaska (Nilsen and Zuffa, 1982), the Middle Phanerozoic Torlesse terrain in New Zealand (MacKinnon and Howell, 1983/84), the Early Palaeozoic of the Central Appalachians (Lash, 1986) and the Cretaceous Shimanto Belt in Japan (Taira *et al.*, 1982).

4. STRUCTURAL GEOLOGY OF THE KHOMAS TROUGH

4.1 Introduction

Structural studies along the study traverse examined the overall deformation pattern in order to help constrain the tectonic setting of the Khomas Trough. The studies benefited from the fact that almost continuous exposure exists along the river sections. Detailed structural analyses in the Khomas Trough were first undertaken by Gevers (1963) and Smith (1965) in the vicinity of the Donkerhuk Granite southwest of Okahandja, followed by Hälbich (1970,1977), Blaine (1977) and Sawyer (1981). Hälbich (1977) studied the Khomas Trough between Okahandja and Windhoek, 100 km to the east of the present study traverse. A reconnaissance study by Hälbich (op.cit.) in the western Khomas Trough was largely based on aerial photographs. Kasch (1975, 1983c) studied the Kuiseb Formation east of Windhoek in the Omitara area, whilst Sawyer (1981) and Preussinger (1987, 1990) concentrated on the structural style of the Gorob mining area in the Namib desert, 150km southwest of the present study traverse.

In the study area, five phases of deformation have been discerned, four of which are associated with cleavage development. Changes in fabric development which sometimes coincide with changes in fold morphology allow subdivision into four structural domains, labelled A, B, C, and D. "Domain" here is used in the grammatical and physical sense of a region which has been affected by a unitary influence. The characteristics of domains, i.e. fabric elements and folds, will be described in section 4.2, and the contact of the Kuiseb metasediments with the Donkerhuk Granite in section 4.3. Structural discontinuities play an important role in the deformation history and these will be discussed separately in section 4.4. The gross structural style and the timing of deformational events (section 4.5) are interpreted in a unitary structural model for the Khomas Trough in section 4.6.

Since there is no general classification scheme on the terminology of fabric elements, "foliation" is used in the current text to describe generally planar surfaces of structural origin. Following the subdivision of cleavage types by Hobbs *et al.* (1976), axial-planar foliations are represented in the study area by metamorphic banding cleavages and crenulation cleavages. Transposed foliations in the southern part of the traverse represent the second major group. Penetrative cleavage is a more general term used for fabrics which are characterized by the preferred alignment (newly crystallized and/or re-oriented) of a particular mineral species. The nomenclature of Fleuty (1964) is used for fold shapes (i.e. open, close, tight). Where more accurate measurements were taken, Ramsay's (1967) fold classification is employed.

The earliest planar element developed in most parts of the traverse is original sedimentary bedding, defined by graded and non-graded units, as well as plane bedding and a variety of other sedimentary structures documented in Chapter 3. Sedimentary bedding is referred to as So. As far as other structural elements are concerned the terminology of Turner and Weiss (1963) is used where S_n characterizes planar, penetrative fabrics, L_n linear penetrative fabrics and F_n folding of fabrics. The age order of consecutive fabric generations is denoted by suffixes 1,2,3,4. The deformations identified are labelled D_1 to D_5 and they are characterized and defined by the following structural elements: (1) D_1 by an S_1 cleavage and F_1 folds; (2) D_2 by an S_2 cleavage, an L_2 lineation and F_2 folds; (3) D_3 by an S_3 cleavage and F_3 folds; (4) D_4 by an S_4 cleavage and F_4 folds; and (5) D_5 by F_5 folds. It is important to note that D_1 structural elements in the southern part of the traverse could not conclusively be established for the northern part. There is evidence, however, that the structural elements which are associated with D_2 are developed throughout the traverse and this therefore serves as a structural datum or benchmark. These relationships, nomenclatures and the occurrences of planar elements and folds within the particular domains are summarized in Table 4.1.

TABLE 4.1: Summary of planar fabrics and folds encountered in domains A-D along the study traverse.

	Planar elements				Folds				
Domain A	$S_{0,1,2,3}$			S_4				F_4	F_5
Domain B	S_1	S_2	S_3	S_4	F_1	F_2	F_3	F_4	
Domain C		S_2	S_3		?	F_2	F_3		
Domain D		S_2	S_3	S_4		F_2	F_3	F_4	

4.2 Structural characteristics of domains

The problems of correlating structures, microstructures and metamorphic assemblages in multiply-deformed terranes has repeatedly been pointed out (e.g. Spry, 1963; Williams, 1985). To obtain a relative timing of events in an area, as many "positive" relationships as possible have to be taken into consideration. In this study area, the following lines of evidence have been used to distinguish consecutive phases of cleavage development and fold formation:

(1) preferred orientation and character of planar and linear fabric elements;

(2) overprinting of planar and linear fabrics of earlier folds;

(3) crystallization and recrystallization of metamorphic minerals and theirrelationships to the foliations present (see Chapter 6);

(4) styles of meso scopic and macroscopic folds;

The first two of the above criteria define the four domains which are shown in Figure 4.1. In comparison with an earlier publication of Kukla *et al.* (1988), it is apparent that on the basis of additional data a new subdivision of the traverse has been made (Table 4.2). The structural profile along the study traverse (Fig. 4.2) indicates that on the basis of fold style a further subdivision is possible. This has been omit-

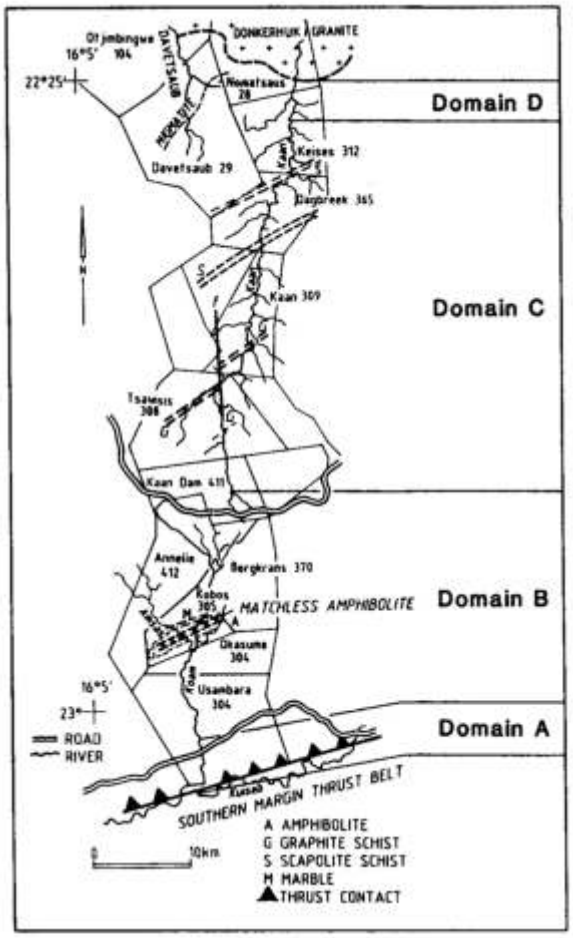

Fig. 4.1: Map of the study traverse showing geographical locations of structural domains A-D.

TABLE 4.2: Comparison of the subdivision of the study traverse into domains A-D of this study with an earlier study of Kukla *et al.* (1988).

Domain	E	D	C	B	A	Kukla *et al.*, 1988
Domain	D		C	B	A	Kukla, this study

ted because fabric elements in this area represent a more reliable "first order" structural marker. The fold geometry is much more dependent on the mechanical and rheological state of the rocks during the folding process (Ramsay and Huber, 1987).

The symbols used for various structural elements are summarized in Table 4.3. Generally, orientations of axial planes give strike, angle of dip and dip direction (i.e. 030°/40°NW). Orientations of linear elements are recorded by azimuth and angle of plunge (i.e. 060°/11°). All structural data are presented on a Schmidt lower-hemisphere stereographic net.

4.2.1 Domain A

This domain covers approximately the area between the confluence of the Koam and Kuiseb fivers at the southern margin of the Khomas Trough and the Us Pass road in the north (Fig. 4.3).

(a) Planar fabrics

The southern most part of the traverse is characterized by a distinct subparallel orientation of planar fabric elements. Judging from other parts of the traverse where original bedding is evident, it is inferred that lithological contacts between metagreywackes and pelites in this do-main also represent original sedimentary layering. Since there is evidence for three penetrative fabrics in the adjacent domain B (Fig. 4.1), subparallel planar elements in this domain are inferred to constitute an $S_{0,1,2,3}$ composite cleavage. The mean orientation of this fabric is 052°/36°NW. It is mainly defined by the parallel to subparallel alignment of chlorite, muscovite and biotite which encloses staurolite, kyanite and garnet (Fig. 4.4, A). Within the composite cleavage domains, symmetrical boudinage occurs, which is associated with quartz-chlorite-ankerite segregations within the extensional spaces. The composite cleavage is overprinted by a weak S_4 crenulation cleavage in pelitic lithologies (Fig. 4.4, B). The crenulation fabric dips moderately to steeply northeast (133°/84°NE).

(b) Linear elements

Throughout the domain, a prominent L_{2A} mineral lineation comprising elongate biotite aggregates, is developed on composite cleavage surfaces. Although data show considerable scatter, there is a major cluster with a mean orientation of 336°/40°. A partial girdle representing an anticlockwise shift of orientations from north-northwest towards west-northwest appears to occur towards the north of the domain (Fig. 4.3). However, to the east of the study traverse close to the Us Pass, an S_4 crenulation cleavage has been observed with a biotite lineation comparable in characteristic and orientation with the west-northwesterly trends just described. The possibility can therefore not be excluded that in fact two different generations have been measured. Left -lateral shearing along the southern margin of the Khomas Trough may, on the other hand, also account for this observed shift of linear element orientations.

A second type of linear element is represented by deformed quartz-chlorite-carbonate concretions which are up to several tens of centimetres long set mostly in pelitic lithologies. The long axes of these concretions are parallel to the fold axes in this area which are oriented 057°/5°.

(c) Folds

No major folds have been observed within this domain. Fold structures occurring are D5 asymmetric and monoclinal kink folds, as defined by Ramsay and Huber (1987). The composite cleavage is deflected from its original orientation within kink bands which are 10-100 cm wide. Axial surfaces (kink planes) dip 20°-60° towards 156° which is opposite to the northwest-dipping attitude of the regional cleavage. Quartz-filled dilation spaces occur parallel to the kinked surfaces (Fig. 4.5) and kinking is closely associated with joint planes. No direct relationship of kink folds with fabric elements could be observed but the kinking occurred subsequent to faulting events which displaced the S_4 cleavage.

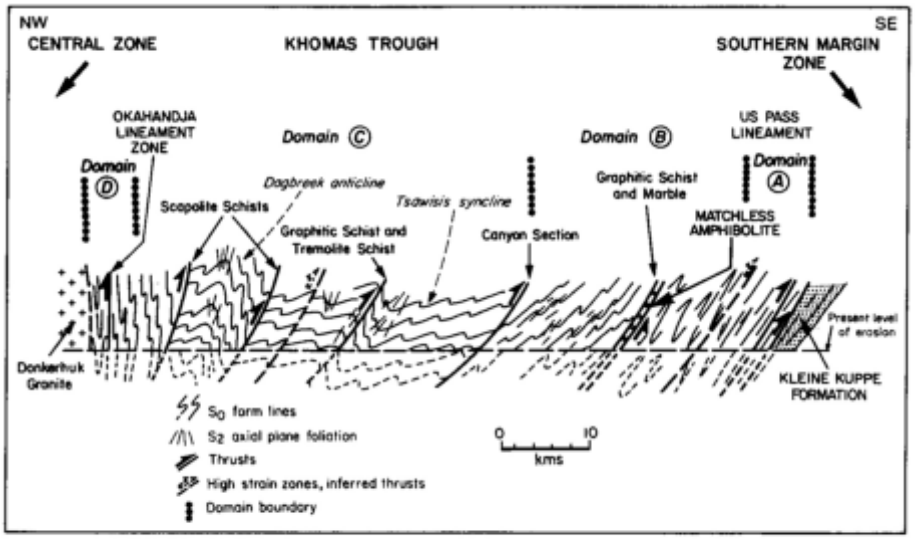

Fig. 4.2: Structural profile across the Khomas Trough showing the size and the style of major D_2 folds.

TABLE 4.3: Summary of the symbols used for various structural elements.

PLANAR ELEMENTS			
Sedimentary layering, strike and dip	S_0	x	x
Metamorphic foliation	S_1	○	○
Metamorphic foliation	S_2	△	△
D_2 axial plane		▲	▲
Metamorphic foliation	S_3	⧖	⧖
D_3 axial plane		⧗	⧗
Crenulation cleavage	S_4	□	□
D_4 axial plane		■	■
D_5 axial plane (Kink folds, only axial plane readings)		✳	✳
Antiform axial surface trace (north dipping)			
Synform axial surface trace (north dipping)			
Exposed normal fault (with dip tick)			
Exposed reverse or thrust fault (triangle on upper sheet)			
Inferred reverse or thrust fault (triangle on upper sheet)			
Thrust zone (triangle on upper sheet)			
LINEAR ELEMENTS			
D_2 fold hinge line (with azimuth and angle of plunge)			
D_3 fold hinge line (with azimuth and angle of plunge)			
D_4 fold hinge line (with azimuth and angle of plunge)			
D_5 kink fold hinge line (with azimuth and angle of plunge)			
D_2 mineral lineation	L_{2A}	✱	
Intersection line S_0/S_2	L_{2B}	⁂	
Long axes of calc-silicate spindles		●	

4.2.2 Domain B

Various generations of fabric elements and folds are discernible within this domain and in domains C and D towards the north. Five planar elements and several linear elements can be distinguished, including bedding. The domain covers an area from the Us Pass road in the south to the northern part of the farm Kaan Dam (Fig. 4.6). The Matchless Amphibolite is situated in the centre of this domain.

(a) Planar fabrics

Bedding S_o can readily be defined from original layering. This is evident in parts of the sequence where graded bedding occurs. Graded layers which provide younging evidence are more quartz- and feldspar-rich at the base and more mica-rich at the top, representing a metamorphosed compositional grading. The orientation of bedding is variable but generally trends northeast and dips moderately towards the northwest (054°/40°NW). In contrast to bedding S_o, the earliest structural fabric is an S I compositional banding with alternating quartz-rich and mica-rich layers oriented obliquely to bedding (Fig. 4.7, A).

Because of later refolding (Fig. 4.7, B) there is no consistency in the orientation of S_1 which is strongly transposed within S_2 cleavage domains to be preferentially preserved as a crenulation in F_2 fold hinges (Fig. 4.8). The fabric dips both towards the southeast (050°/30°SE) and the northwest (060°/30°NW; Fig. 4.6). The S_1 fabric is characterized by an early generation of biotites which may be enclosed and wrapped around by later biotites developed in S_2. Further evidence for S_1 comes from early quartz veins (Fig. 4.7, C) and calc-silicate layers which parallel S_0 and which are folded by D_1 and subsequently by D_2 (Fig. 4.7, B).

The second recognizable structural fabric (S_2) is a strong, penetrative cleavage throughout the domain and a metamorphic banding cleavage in which 50 and 5 I are partly transposed by D_2 (Fig. 4.7 ,A) in the centre and north. The S_2 fabric dips moderately (30°-40°) to the northwest (060°) and occurs axial-planar to F_2 folds. Fanning of the cleavage and refraction at psammite - pelite contacts is common. The character of the S_2 fabric changes with the lithology, shown by the widths of the quartz-feldspar-rich and the mica-rich bands which vary from less than one millimetre to about one centimetre. S_2 is defined by the preferred alignment of biotite and chlorite constituting either a penetrative foliation or a wavy to anastomosing network (Fig. 4.8). Calc-silicate spindles from several centimetres to several tens of centimetres in size, are mostly oriented with their long axes parallel to S_2.

S_3 is a rather unevenly distributed fabric, especially in the southern part of this domain. The mean orientation in the centre and north is 050°/30°NW (Fig. 4.6). The fabric is best

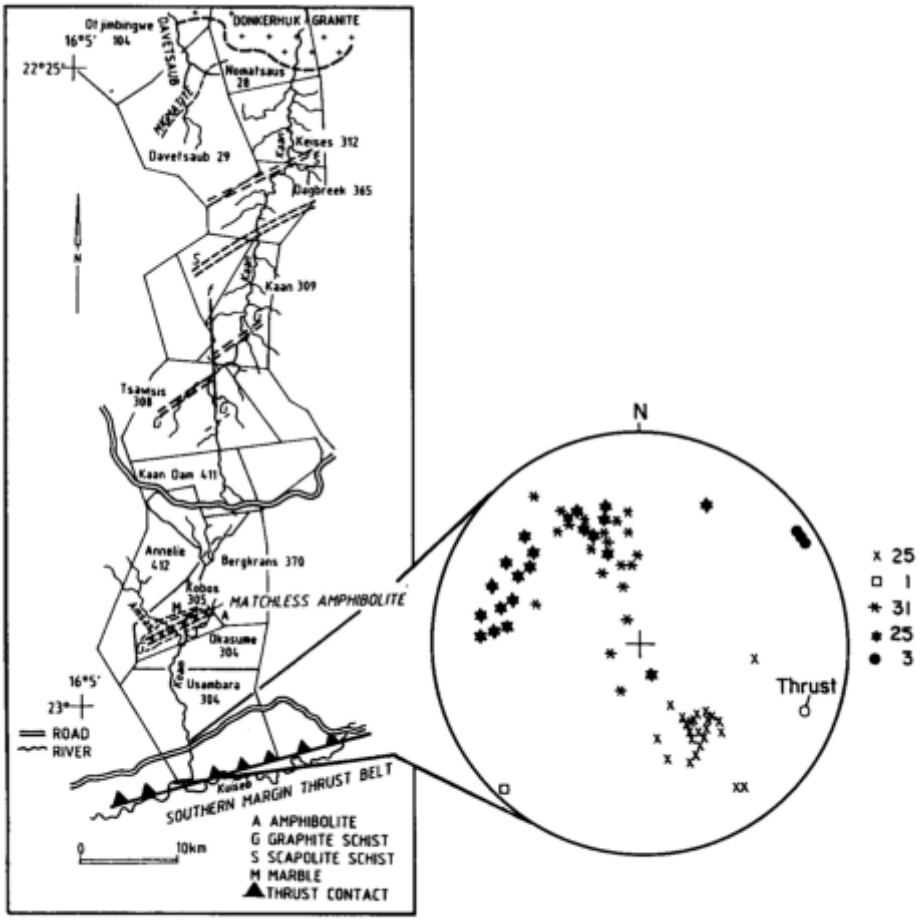

Fig. 4.3: Map of the study traverse showing a selection of structural data for domain A. See Table 4.3 for explanation of symbols; key gives number of measurements.

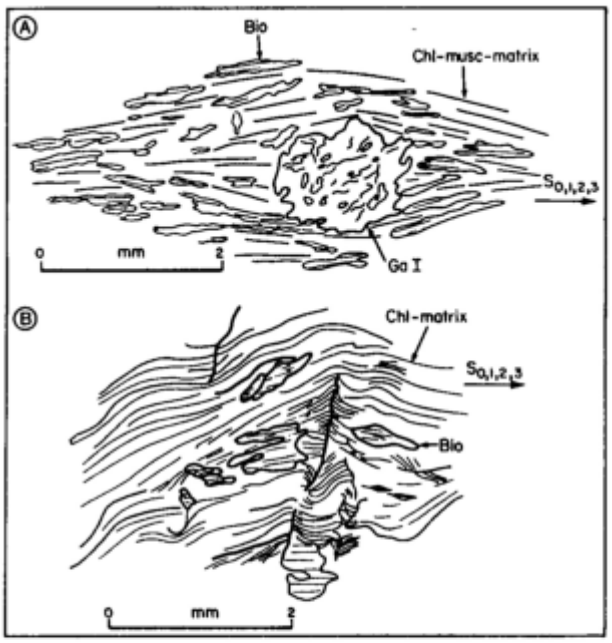

Fig. 4.4: Microtextures in domain A. Tracings from thin sections showing: (A) $S_{0,1,2,3}$ composite cleavage illustrating the parallel to subparallel alignment of biotite within a chlorite-muscovite matrix enclosing garnet I (specimen PK 855, farm Usambara 304, south of Us Pass road); (B) Chlorite-biotite schist showing S_4 crenulation cleavage developed within the $S_{0,1,2,3}$ composite cleavage. Note microfaults at hinge lines (specimen PK 140, farm Usambara 304, south of Us Pass road).

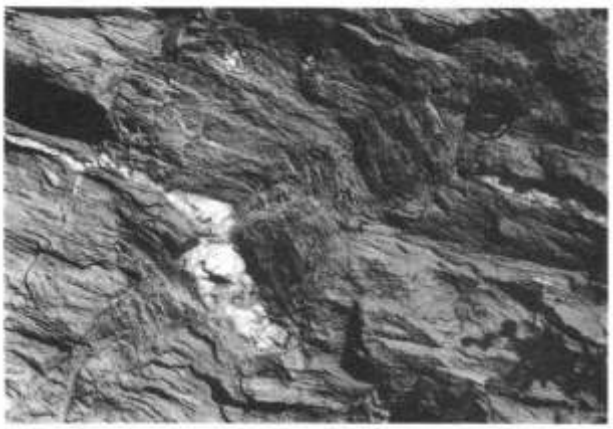

Fig. 4.5: Small-scale (D_5) kink band in domain A, showing quartz-filled dilation space parallel to the $S_{0,1,2,3}$ composite cleavage. Lens cap for scale is circled. Farm Usambara 304, south of Us Pass road.

developed in narrow shear zones where folding of S_2 by D_3 occurs (Fig. 4.7, D and E). Notably, in the hinges of F_3 folds, S_3 constitutes a penetrative biotite fabric which encloses the S_2 fabric.

An S_4 crenulation cleavage occurs in the highly pelitic lithologies (Fig. 4.7, C and E). The orientation of this fabric is variable (Fig. 4.6) and it describes a clockwise rotation from orientations of 010°/40°-60°NW in the south to 060°/60°-80°NW close to the Matchless Amphibolite where

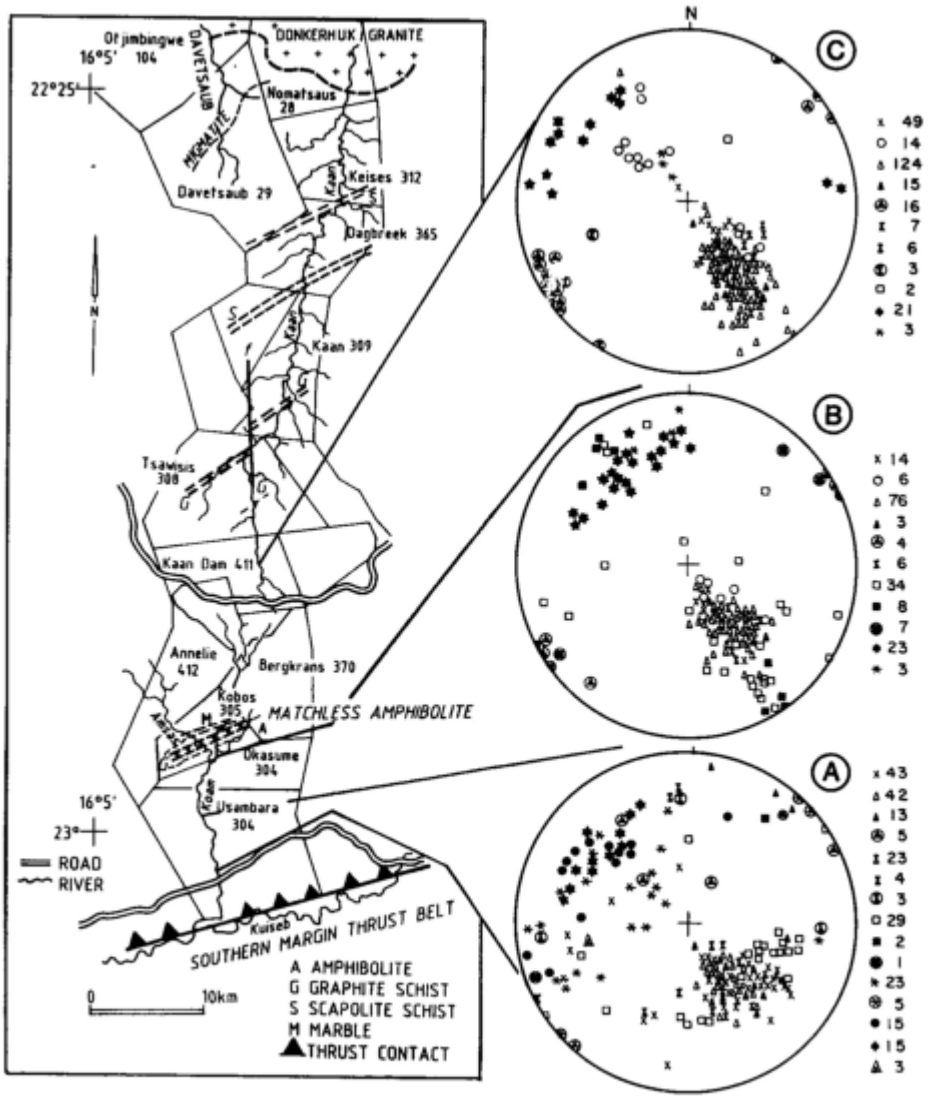

Fig. 4.6: Map of the study traverse showing a selection of structural data for the southern (A), central (B), and northern (C) part of domain B. See Table 4.3 for explanation of symbols; key gives number of measurements.

the fabric is exceptionally strongly developed (Fig. 4.6, A and B).

(b) Linear elements

There are several linear elements present in this domain. The most distinct is a mineral lineation which plunges 20°-40° towards 320° on S_2 planes and which is therefore designated L_{2A}. Minerals defining L_{2A} are mainly biotite but also plagioclase and amphiboles at the Matchless Amphibolite. A second lineation, L_{2B}, is the S_0/S_2 intersection with an orientation of 060°/0°. In the south and centre of the domain, the long axes of small calc-silicate spindles constitute a lineation which plunges at 30°-50° towards 315° down-dip on S_2 planes (Fig. 4.6, A). At the Matchless Amphibolite the long axes of pillow structures plunge 330°/35° forming a down-dip lineation on S_2 planes, together with the elongated plagioclase porphyroblasts they contain. In the southern part of the domain on the farm Usambara, the long axes of quartz-chlorite-carbonate concretions are oriented 250°/10° (Fig. 4.6, A).

(c) Folds

D_2 structures represent the major fold phase in this domain. Folds are developed on all scales varying from em-scale intrafolial folds to isoclinal folds with wavelengths of up to 250 m. Quartz veins and calc-silicate layers which parallel So are folded by D_2 to form intrafolial folds within S_2 cleavage domains (Fig. 4.7, B and C). Folds with wavelengths of several metres are isoclinal with axial planes dipping mostly northwest (050°/20°-60°NW), although some folds with northeast-dipping axial planes with a considerable spread of orientations occur in the southern-most part of the domain (Fig. 4.6, A and B). The majority of the fold axes plunge subhorizontally towards the northeast and the southwest but steeply-plunging axes also occur (Fig. 4.6, A and B). Intrafolial D_2 folds and isoclinal folds with wavelengths of up to 5 m are particularly well developed within metasedimentary sequences intercalated with the Matchless Amphibolite. D_2 folds with wavelengths of 15-20 m and amplitudes of tens of metres are spectacularly developed and well exposed in a canyon section of the upper course of the

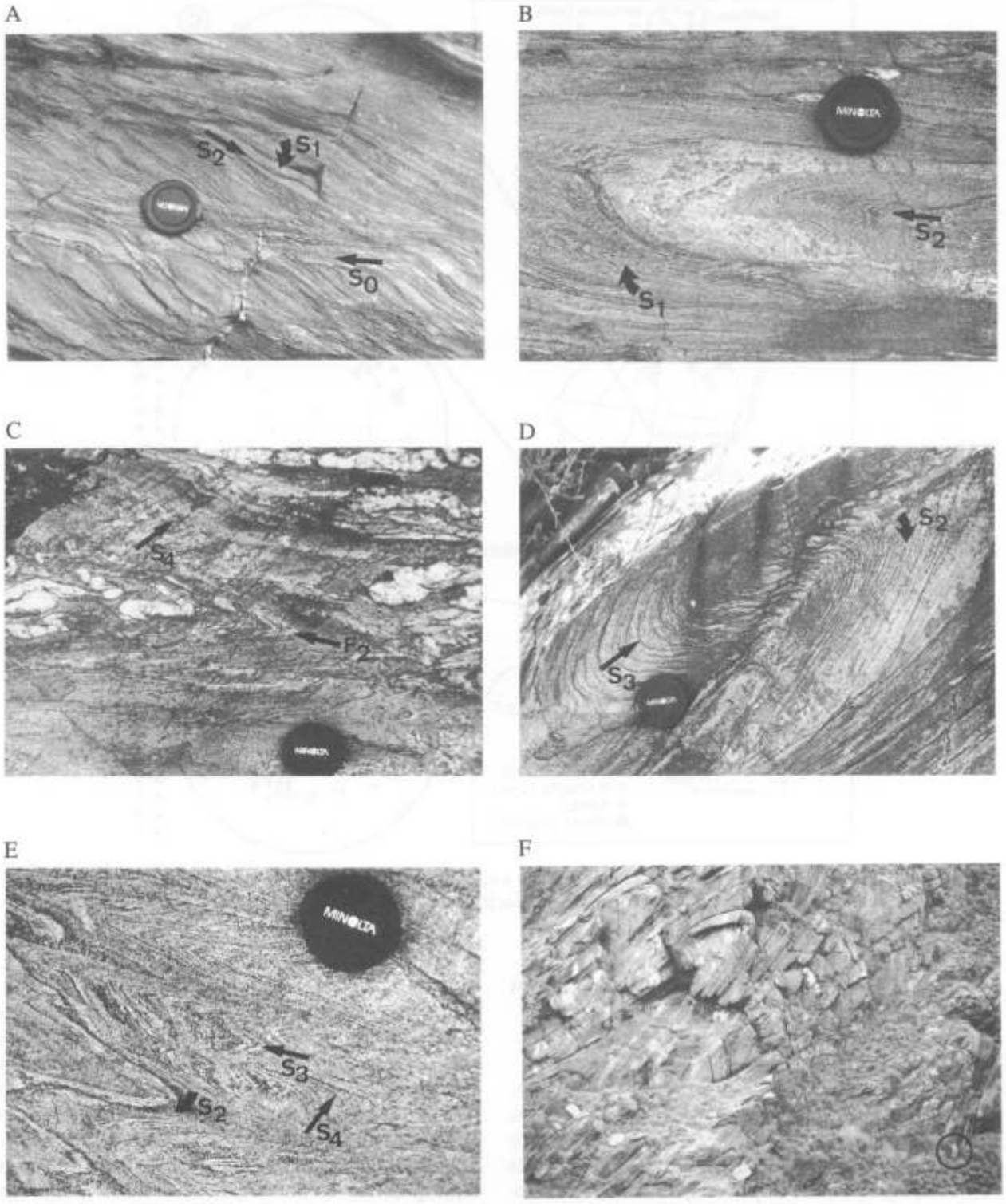

Fig. 4.7: (A) Transposition of S_1 and refraction of S_2 at lithological contacts S_0 (indicated by arrows). Sedimentary younging indicated by graded layering is towards the bottom of the photograph. Locality Koam canyon, farm Annelie 412. (B) Calc-silicate layer folded within pelitic lithologies, representing intrafolial D_2 fold within S_2 cleavage domains. Folded and transposed S_1 fabric also indicated by arrow. Farm Usambara 304, north of Us Pass road. (C) Photograph showing intrafolial D_2 folds within the S_2 cleavage and an overprinting S_4 crenulation cleavage in pelitic schist. Farm Usambara 304, north of Us Pass road. (D) Narrow shear zone in psammitic lithologies showing small-scale F_3 fold. The biotite fabric constituting the S_2 cleavage is deformed about the fold and the penetrative S_3 cleavage is developed in the fold hinge. Koam canyon, farm Annelie 412. (E) Photograph showing overprinting relationships of deformations D_2-D_4 in narrow shear zone in pelitic lithologies. S_2 is folded by D_3 which developed small-scale F_3 folds and a penetrative S_3 cleavage; these are overprinted by the S_4 crenulation cleavage. All planar fabrics are indicated by arrows. Matchless Amphibolite sequence, farm Annelie 412. (F) Flattened, concentric D_2 folds (class 1C; Ramsay, 1967) in the Koam canyon section. Height of scale (circled) is 1.7 m. Farm Annelie 412.

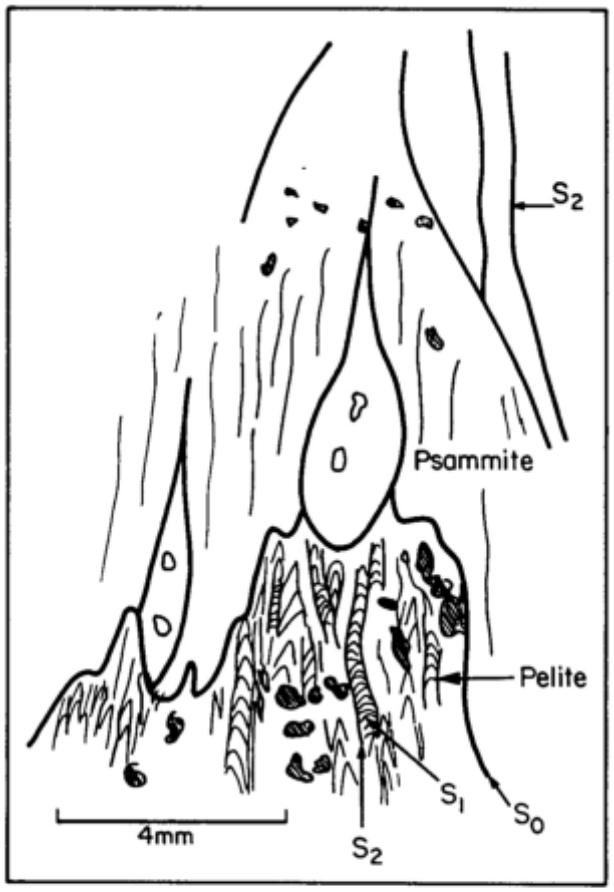

Fig. 4.8: Tracing from thin section showing hinge area of minor F_2 fold developed in pelitic lithologies. The S_1 fabric is transposed and crenulated within S_2 domains. S_2 constitutes an anastamosing network within psammitic lithologies (specimen PK 86/57, farm Kaan Dam 411, near Khomas Hochland road).

Koam river (Figs. 4.9 and 4.10). These folds are flattened concentric folds (class 1C; Ramsey, 1967) which are tight to isoclinal, inclined, and horizontally to shallowly plunging in attitude (Fig. 4.7, F; Fig. 4.9). Axial planes are oriented 040°/40° -60°NW and fold axes plunge at low angles both towards 235° and 050° -060° (Fig. 4.6, C). Way-up criteria to determine major D_2 fold closures are provided by bedding - cleavage relationships. Detailed mapping of the canyon section has shown that the wavelengths of the major folds are in the order of 5 km. Overturned limbs, however, are very narrow confirming that mainly right-way-up sequences are developed within this part of the Khomas Trough.

Downward-facing D_2 folds have been detected at three localities (Figs. 4.9 and 4.10) of the Koam canyon section (Kukla *et al.*, 1989). It is essential for the recognition of downward-facing direction that sedimentary structures, providing way-up criteria, are combined with fabric elements. Two lines of evidence were used to define downward-facing: (i) sedimentary younging indicated by graded bedding and (ii) bedding - cleavage relationships with respect to D_2 folds. Figures 4.7, F and 4.11 demonstrate the structural style of part of the canyon section where downward-facing has been detected. The S_1 cleavage has been refolded and strongly transposed into S_2 (Figs. 4.7, A and 4.10) so that F_1 fold closures have been largely obscured.

Orientations of S_1 in the canyon section consequently have variable dip directions both to the northwest and the southeast (Fig. 4.9).

F_3 folds are cm- to m-scale, tight to isoclinal, asymmetric folds which are developed in narrow shear zones (Fig. 4.7, D and E). They have gently- to moderately-plunging fold axes (250°/14°-40°) and axial planes which dip moderately to steeply towards the northwest (059°/43°-63°NW) and the southeast (059°/25°SE; Fig. 4.6).

Axial planes of cm-scale, close-tight crenulation folds (Fig. 4.7, C and E) dip moderately towards both the northwest and the southeast with axes plunging subhorizontally towards the northeast and the southwest (Fig. 4.6, B).

Kink bands of monoclinal kink folds are up to two metres wide and are occasionally brecciated. Axial planes dip both towards the southeast and the northeast (Fig. 4.6, A).

4.2.3 Domain C

This domain covers a wide area between the Upper Koam river canyon on the farm Annelie up to the central part of the farm Keises (Fig. 4.12). In this domain only D_2 and D_3 structural elements are evident according to the nomenclature of previous domains (Table 4.1). However, one downward-facing D_2 fold has been detected in the centre of this domain which might suggest the presence of an earlier D_1 phase of folding.

(a) Planar fabrics

Bedding is evident throughout the domain and a variety of sedimentary structures has been described (Chapter 3). So strikes uniformly towards the northeast and dips both towards the northwest and the southeast (Fig. 4.12).

The first recognizable fabric element is the S_2 cleavage which is similar in character to that described in domain B. S_2 is a strong, pervasive, narrow to widely spaced and wavy to anastomosing metamorphic banding with quartz-feldspar-rich and mica-rich (biotite and muscovite) cleavage domains (Fig. 4.13, A and B). Fanning of the cleavage and refraction at psammite - pelite contacts are common (Fig. 4.13, C). The S_2 fabric is axial-planar to the dominant F_2 folds in this domain and it varies according to the orientation of the folds, but generally trends towards the northeast (Fig. 4.12).

S_3 occurs within the southern part of the domain in narrow shear zones but is more strongly developed towards the north where it is dominant in major high-strain zones. The fabric is penetrative (Fig. 4.13, D) and is characterized by a newly-formed biotite generation which encloses the S_2 fabric. In units of low competence such as the graphite schist on the farm Kaan, however, S_3 is rather a strong crenulation cleavage. Orientation data for S_3 indicate a shift from northeasterly trends (050°/30°-50°NW) to north-northeasterly trends (030°/30°NW) towards the north of the domain, demonstrated by the stereoplots in Figure 4.12.

(b) Linear elements

Within shear zones, mineral lineations of elongate biotite and garnet are occasionally developed, showing a wide

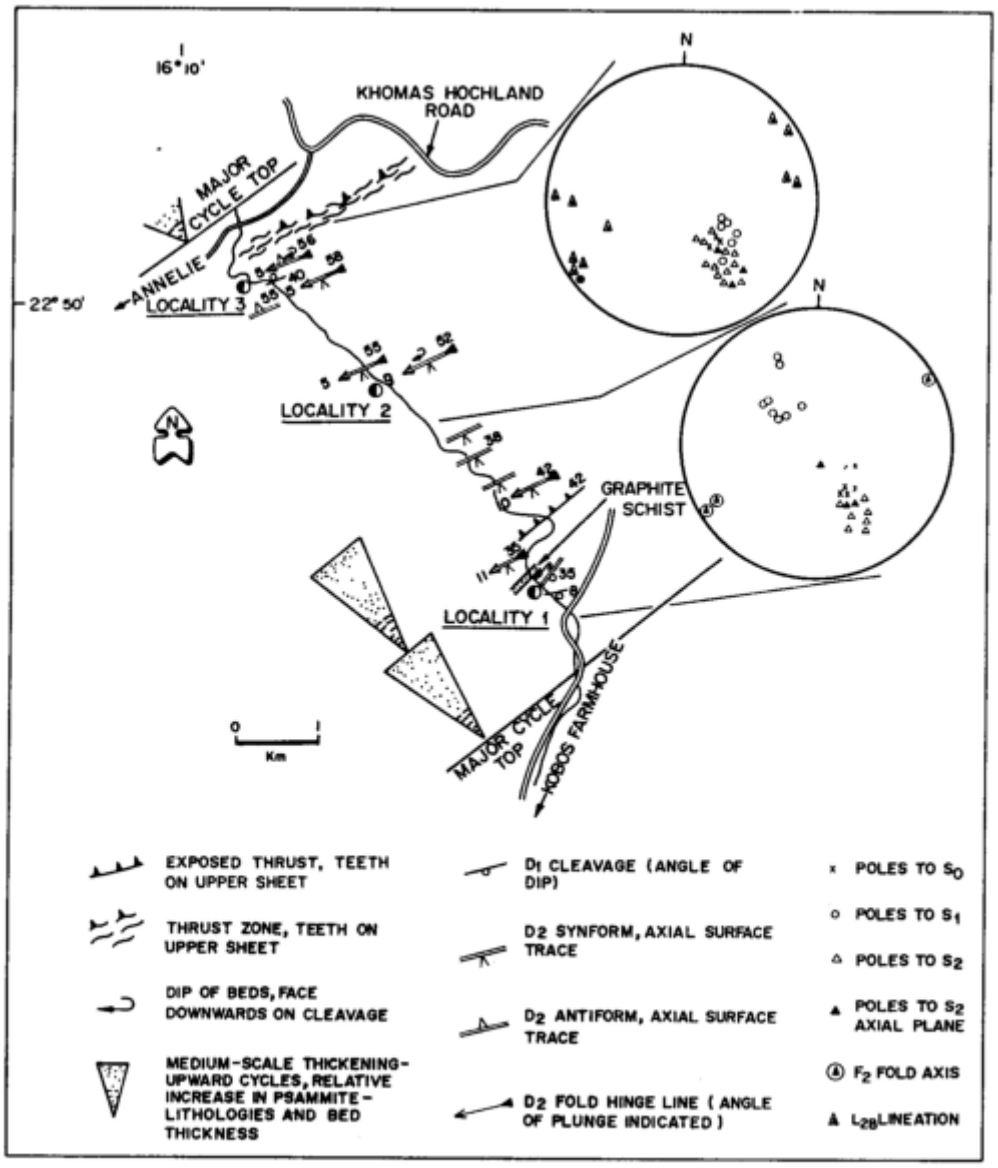

Fig. 4.9: Map of the Koam canyon section on the farm Annelie 412 showing localities with D_2 downward-facing structures and stereonet data. Major sedimentary cycles are also indicated.

spread of orientations (Fig. 4.12, C). A northeast-trending S_0/S_2 intersection lineation also occurs. Furthermore, the long axes of calc-silicate spindles are elongated parallel to the D_2 fold axes (Fig. 4.12, A and B). An example of the occurrences, sizes and orientations of calc-silicate spindles in an open asymmetric fold on the farm Kaan is shown in Figure 4.14.

(c) Minor folds

F_2 folds are open to tight in the northern part of the domain and on the steep limbs of some major fold structures. In contrast, a pronounced open asymmetric fold style occurs in the centre and south. Figures 4.13 (E and F), 4.14 and 4.15 illustrate examples of open asymmetric folds on the upright limb of a major fold structure on the farm Kaan. In contrast, Figure 4.16 shows tight folding associated with the steep limb of the major syncline on the farm Tsawisis. Axial planes become steeper towards the north as limbs tighten (Fig. 4.12, A-C). Fold axes plunge at low angles both towards the northeast and southwest (050°110° and 230°/10°) but within zones of high strain, axes plunge up to 20° towards 050°. Wavelengths of asymmetric folds are in the order of 20-50 m in the shallow limbs and of 5-10 m in the steep limbs of larger structures (Figs. 4.15 and 4.16). There is evidence for a D_2 downward-facing fold towards the top of the scapolite schist sequence on the farm Dagbreek. This is based on the relationship of graded bedding which provides way-up criteria and the attitude of the S_2 cleavage (Fig. 4.17, E). The presence of this fold indicates that folding and overturning of fold limbs occurred prior to D_2. This may therefore be seen as evidence for a D_1 phase of deformation in this part of the Khomas Trough.

F_3 folds are developed on a centimetre- to metre-scale in narrow high-strain zones (Fig. 4.13, G). In these zones, tight to isoclinal F_3 folds largely overprint earlier structures. Typical features of D_3 folding and overprinting relationships of D_3 on D_2 are well developed in the southern scapolite schist (Fig. 4.12) and are illustrated in Figure 4.17. The orientations of fold axes and axial planes change from south to north within this domain.

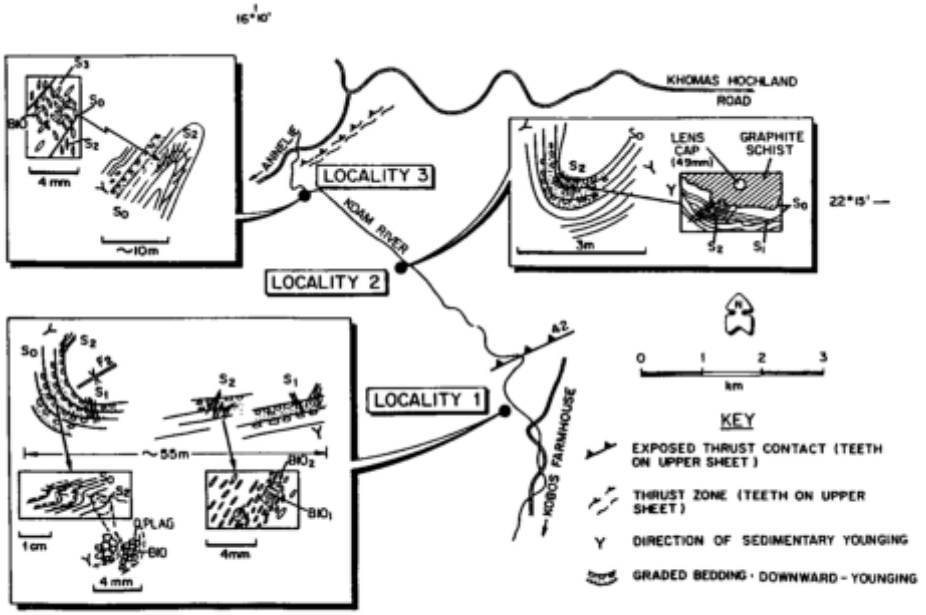

Fig. 4.10: Map of the Koam canyon section showing sketches of downward-facing structures and related thin-section information. Note particularly the direction of sedimentary younging with respect to the S_2 axial-planar cleavage, which indicates downward-facing. Abbreviations: Q, quartz; PLAG, plagioclase; BIO, biotite. See Table 4.3 for explanation of symbols. Farm Annelie 412.

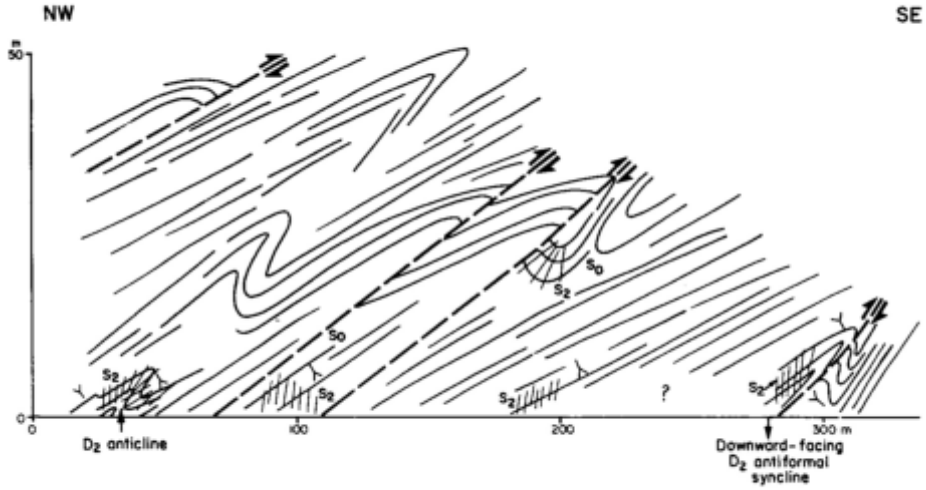

Fig. 4.11: Structural sketch illustrating the style of D_2 folding in the Koam canyon section. S_0 and S_2 form lines are indicated. Note sedimentary younging evidence. Farm Annelie 412.

Axial planes of F_3 folds change from 060°/50°NW in the south to 030°/30°NW at the scapolite schists, and fold axes change from 060°/10° in the south to 036°/10°-20° in the north (Fig. 4.12).

(d) Major folds

Major F_2 folds have been detected in this domain and they are indicated by the bedding - cleavage relationships on minor structures. Characteristically the major folds are open and asymmetric with shallowly- to moderately-dipping southern limbs and steep northern limbs. The major fold structures as shown in Figure 4.2 are: (1) the Tsawisis syncline in the south; (2) a zone of open, asymmetric folding on the upright limb of a major synclinal structure in the centre; (3) the Dagbreek anticline between the two scapolite schist sequences; and (4) a zone of isoclinal folding in the northern part of the domain. The fold hinges of the major structures are situated in the most psammitic part of the respective areas. It can be seen in Figure 4.2, however, that parts of the limbs of the major folds are missing due to the presence of structural discontinuities which will be described separately below.

4.2.4 Domain D

This domain extends from the centre of the farm Keises to the southern margin of the Donkerhuk Granite (Fig. 4.18). The establishment of this domain is based on the recognition of an S_4 crenulation cleavage and a clockwise rotation of fabric elements. Additionally, axial planes of deformation

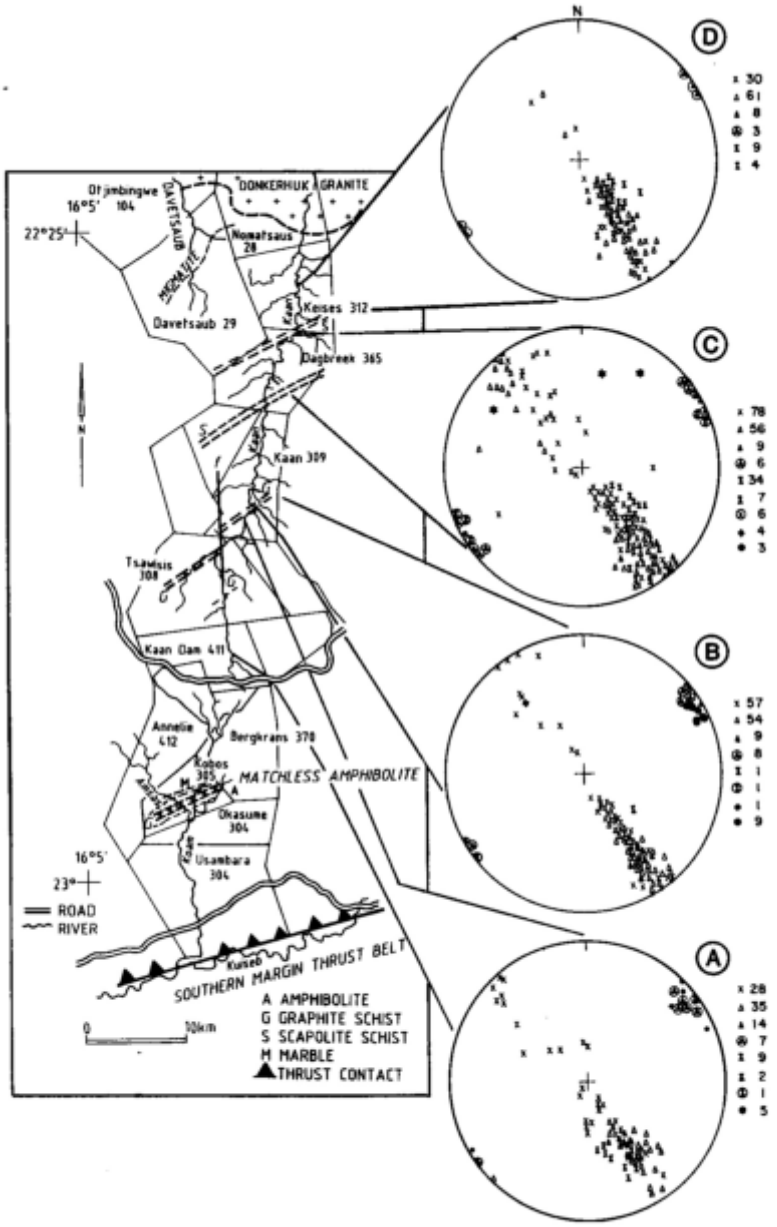

Fig. 4.12: Map of the study traverse showing a selection of structural data for domain C from south (A) to north (D). See Table 4.3 for explanation of symbols; key gives number of measurements.

phases D_2 to D_4 are steeply inclined to upright and fold axes plunge moderately in the north of the domain. The northern margin of the Khomas Trough is defined by the Donkerhuk Granite in this area.

(a) Planar fabrics

As in domain C, original bedding is confirmed by a variety of sedimentary structures. S_2 is a widely spaced biotite foliation with sillimanite (fibrolite) knots oriented parallel to and situated within the mica-rich cleavage domains. The fabric changes orientation from westerly trends in the south (086°/10°-90°NW) to east-southeasterly trends in the north (102°/50°-90°NE). The S_2 fabric is folded by D_3 within narrow shear zones in a manner similar to that described in domain C (Fig. 4.19, A and B). S_3 is a spaced cleavage which is axial-planar to F_3 folds. This biotite fabric is developed throughout the domain but especially in high-strain zones as in domain C. Orientations are similar to S_2 and also trend east-southeasterly in the north. Sillimanite knots, which usually parallel S_2, have been bent (transposed) partly into S_3 orientations. Within highly pelitic lithologies a symmetric crenulation cleavage is developed which here is designated S_4 (Fig. 4.19, C).

Generally, data plots of fabric elements indicate a more uniform coaxial distribution in the south of the domain, but a wide spread of orientations for respective fabric elements occurs in the north (Fig. 4.18).

(b) Linear elements

There are only occasional S_0/S_2 intersection lineations preserved which plunge 280°/10°-40° in the north of the domain (Fig. 4.18).

(c) Folds

The vergence of minor fold structures together with bedding - cleavage information indicates that the domain is situ-

ated on the overturned limb of a major D_2 anticlinal closure located to the north. (Fig. 4.2). Observed D_2 folds are open to tight to isoclinal in the south and strongly isoclinal in the north, with wavelengths decreasing from 10-20 m to 5 m respectively. Axial planes of these flattened concentric F_2 folds (class 1 C; Ramsay, 1967) change clockwise from 074°/40°-

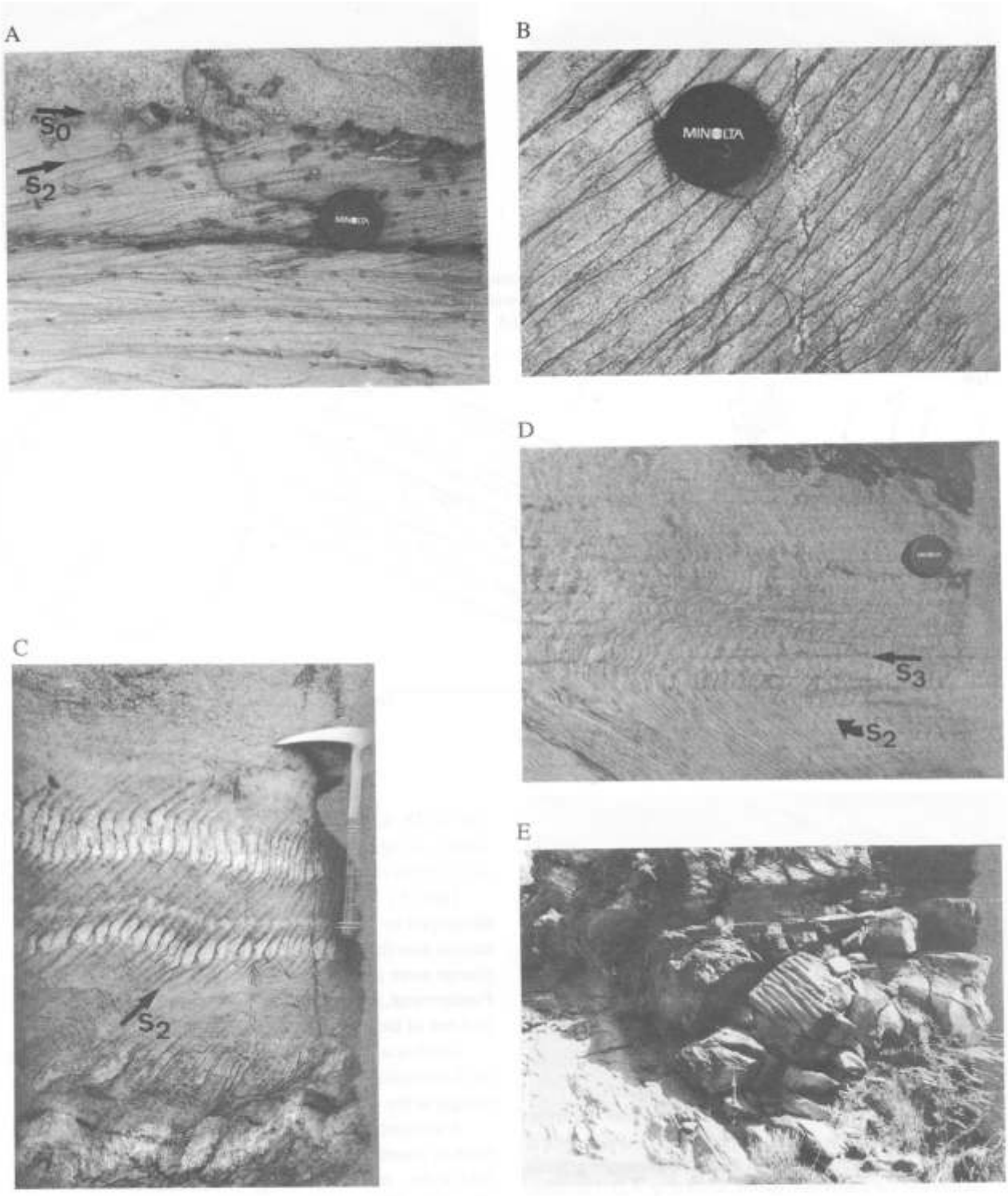

Fig. 4.13: (A) Photograph showing the strong development of the S_2 metamorphic banding cleavage (indicated by arrow) in pelitic lithologies. Note the alignment of staurolite porphyroblasts within the cleavage domains and along bedding S_0 (indicated by arrows). Locality is at the northern boundary of the farm Kaan 309. (B) Anastomosing S_2 biotite fabric in calc-silicate rich psammite, northern scapolite schist, farm Keises 312. (C) Refraction of the S_2 metamorphic banding cleavage at lithological contacts between psammites and calc-silicate layers. Locality in the centre of the farm Keises 312. (D) S_2 metamorphic-banding cleavage superimposed by intense S_3 spaced fabric in high-strain zone of the southern scapolite schist on the farm Dagbreek 365. (E) Open asymmetric SE-verging F_2 fold in mainly psammitic lithologies on the southern, shallow-dipping limb of the Tsawisis syncline (see Fig. 4.2). S_0 is demarcated by dashed line. Hammer for scale. Domain C, farm Tsawisis 308.

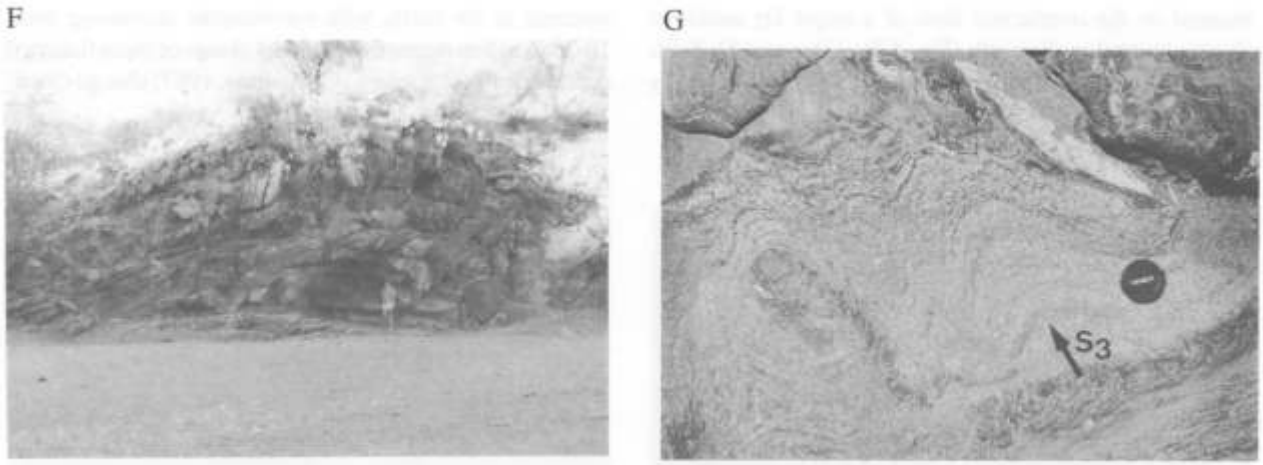

Fig. 4.13: (F) Open F_2 fold in psammitic schist on the southern margin of domain C. North is towards the left of the photograph, the height of the scale is 1.7 m. Farm Kaan Dam 411. (G) Metre-scale isoclinal F_3 folds with axial-planar S_3 penetrative fabric in shear zone in the southern scapolite schist on the farm Dagbreek 365.

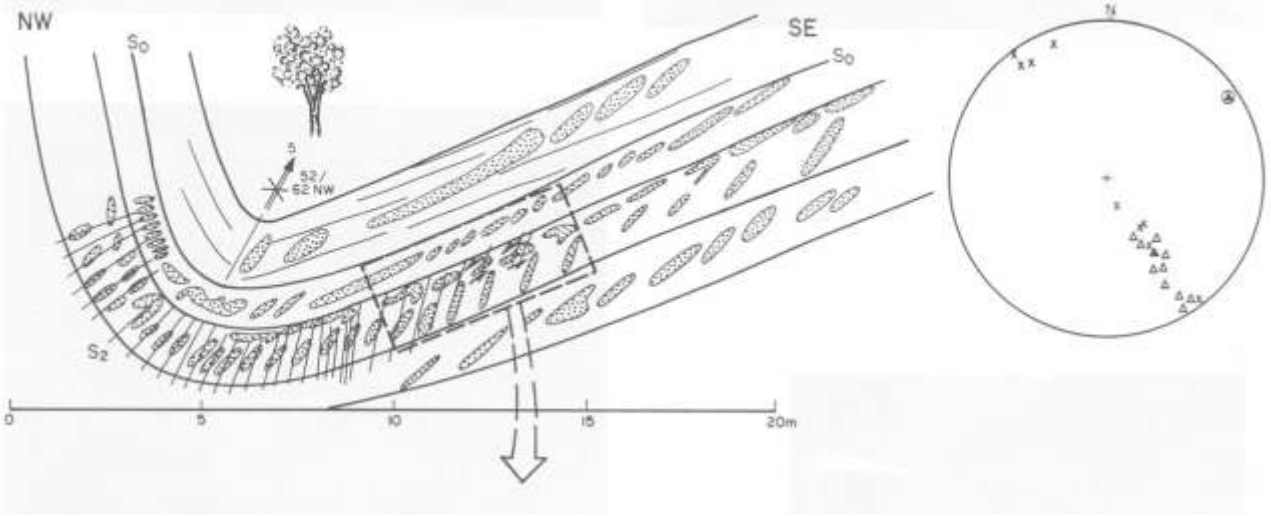

Fig. 4.14: Diagram showing sketch, photograph and stereoplot of an open asymmetric D_2 fold in the area between the graphite schist and the southern scapolite schist (Fig. 4.2). The orientation and shape of calc-silicate layers and spindles respective to S_0 and S_2 is strongly dependent on their positions within the fold. Shear processes parallel to S_0 are also indicated. See Table 4.3 for explanation of symbols. Farm Kaan 309.

50°NW in the south to 106°/65°NE in the north; fold axes change from 080°/10° to 106°/30°-40° respectively (Fig. 4.18). The more steeply-plunging attitude of D_2 fold axes in the northern part of this traverse stands out against the usually horizontal to subhorizontal orientations elsewhere along the traverse.

Tight F_3 folds with wavelengths of up to 5 m have developed in shear zones (Fig. 4.19, D, E and F) and orientations also rotate clockwise (Fig. 4.18). F_3 fold axes also plunge more steeply in this domain (Figs. 4.18 and 4.19, F). Furthermore, downward-facing F_3 folds have been detected and one of these structures is shown in Figure 4.19, D.

Small-scale (tens of centimetres) F_4 folds are related to the S_4 crenulation cleavage and occur towards the northern margin at the contact with the Donkerhuk Granite.

A structural section from the southern part of this domain is presented in Figure 4.20 showing fabric elements, fold styles, and overprinting relationships of deformation phases D_2, D_3 and D_4.

4.2.5 Latefractures

Late-stage joints and faults are considered together here since their characteristics are similar in all domains. A minor feature occurring in domain A is post-D_4 joint sets with subvertical northeasterly strikes. The two major fault sets occurring in the Khomas Trough appear prominently on the

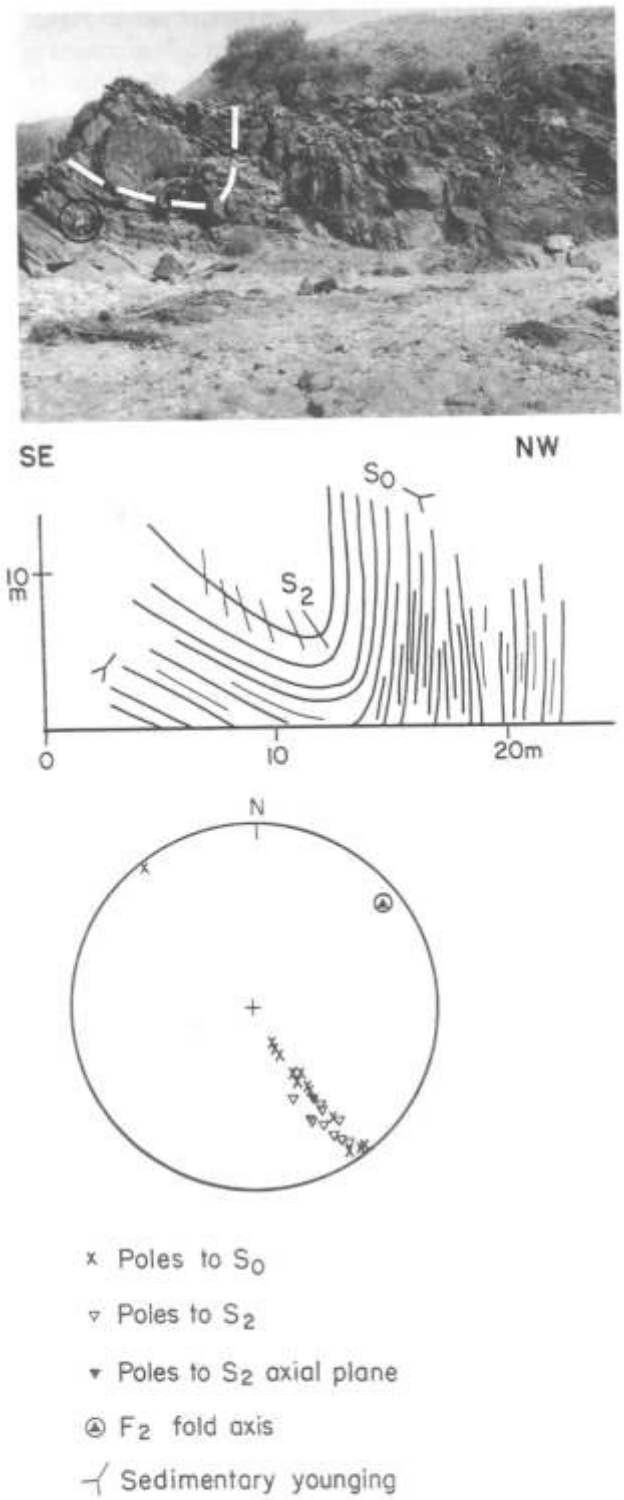

Fig. 4.15: Diagram showing sketch, photograph and stereoplot of an open asymmetric D_2 fold in the area between the graphite schist and the southern scapolite schist (Fig. 4.2). Younging evidence is based on sedimentary structures. Bedding is demarcated by dashed line. Height of scale (circled) is 1.7 m. Farm Kaan 309.

Landsat image of the Khomas Trough (Fig. 2.4). One set is oriented subvertically and trends north-south and the second set is also orientated subvertically and trends northwest-southeast. A north-south trending fault is recognizable all along the course of the Kaan river and displaces the graphite schist on the farms Kaan and Tsawisis by several hundreds of metres. This is accompanied by brecciation, silicification, quartz mobilization and iron-staining. The northwest striking fault set formed the Koam canyon but only minimal displacement is evident since structural elements and lithologies can be traced across it. Senses of movement are largely dextral in both sets. The time of formation of both fault sets was after the intrusion of the Donkerhuk Granite which has been partly displaced by the faulting.

4.3 Contact relationships of metasediments and migmatites with the Donkerhuk Granite

The northern margin of the Khomas Trough in the study area is defined by the contact with the Donkerhuk Granite. Structural relationships between this granite and the metasediments with regard to the time of granitic emplacement have been discussed by many authors (e.g. Reuning, 1923; Gevers, 1963; Martin, 1965; Smith, 1965; Hälbich, 1970; Jacob, 1974; Faupel, 1974; Nieberding, 1976). These studies have concluded that the granite intruded after deformation into the Kuiseb metasediments where it caused the formation of migmatites (Fig. 4.21, A and B). In this study, the structural relationships between migmatites, metasediments, and granitic phases have been investigated.

Generally, migmatites occur around the Donkerhuk Granite in well defined zones covering several km^2. The western boundary of one of these zones is shown in Figure 4.18 on the farm Davetsaub where investigations have been undertaken. This figure illustrates that no migmatites are developed in the Kaan river section.

The following features are important with respect to the northern margin of the study area: (1) metasediments are coarsely recrystallized only several hundreds of metres to the south of the granite contact in the Kaan river section; (2) deformational features in the metasediments include a strong S_4 crenulation cleavage, F_2 and F_3 folds with plunging fold axes and steeply-inclined axial surfaces as well as downward-facing F_3 folds; (3) the migmatitic areas contain xenoliths of metasediments and calc-silicates (Fig. 4.21 ,B); (4) xenoliths of coarse-grained metasediment within the white, two-mica granite contain the S_2, S_3 and S_4 cleavages as well as ptygmatic folds (Fig. 4.21, C); (5) thin pegmatite veins and granite apophyses are folded by the S_4 crenulation cleavage (Fig. 4.21, D and E); and (6) migmatitic areas contain pegmatite phases of the granite with sharp crosscutting contacts (Fig. 4.21, F).

In conclusion, field observations along the northern boundary of the Khomas Trough show that the main granite intrusion occurred after the main deformation events which affected the Khomas Trough. Coarser grain sizes of Kuiseb metasediments in a narrow zone bounding the granite indicate a certain thermal influence of the pluton. In some areas, however, migmatites extend up to several kilometres south of the granite contact. Structural relationships which show pegmatites crosscutting the migmatites with sharp contacts confirm that migmatites formed before the emplacement of the Donkerhuk Granite. These findings are interpreted to favour an "*in situ*" migmatization by the regional metamorphism which preceded the intrusion. This is preferred to models of the above authors which explain

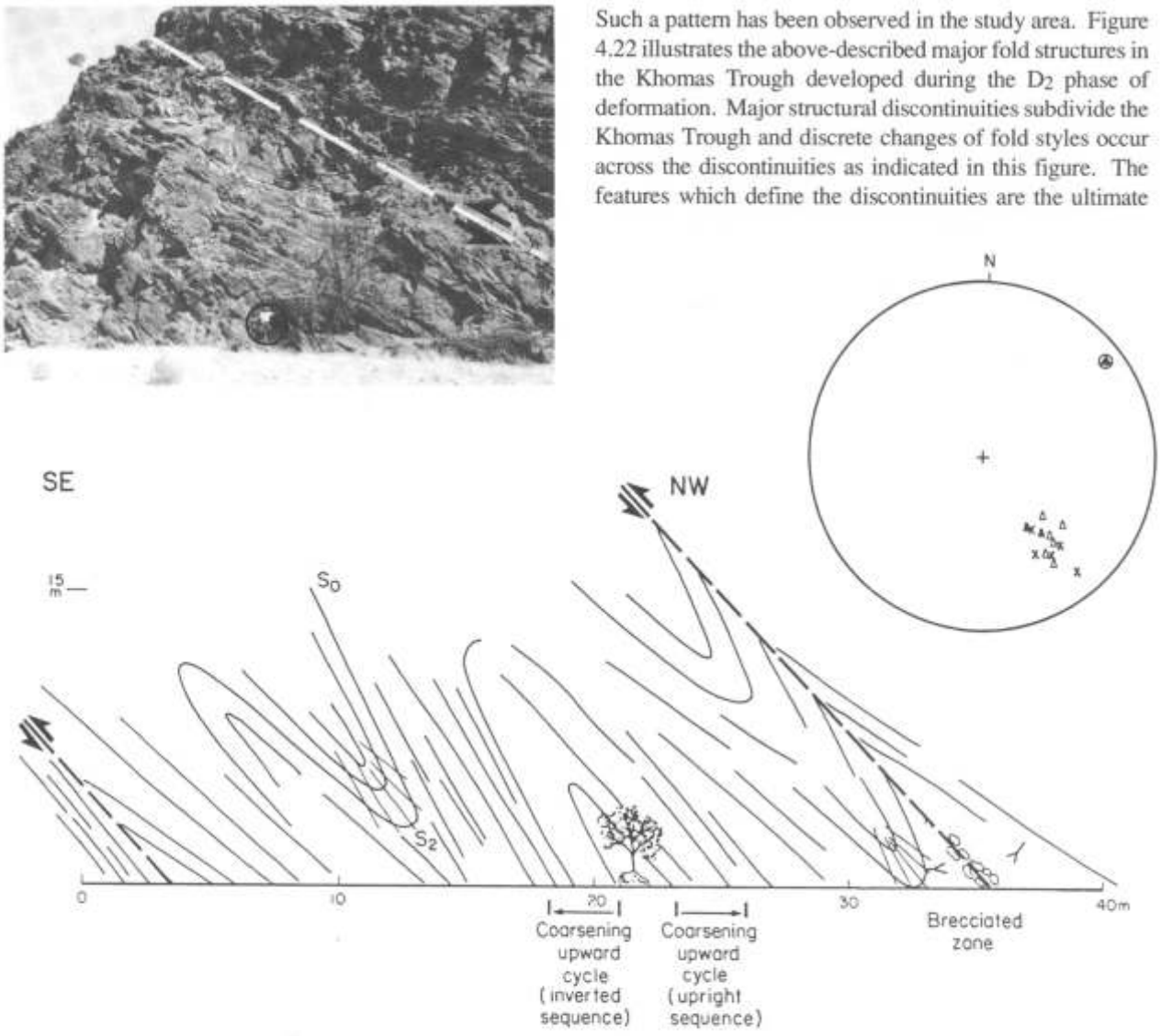

Fig. 4.16: Diagram showing sketch, photograph and stereoplot of tight to isoclinal SE-verging D_2 folds on the northern, upright to overturned limb of the Tsawisis syncline (Fig. 4.2). In order to compare sketch and photograph, reference may be made to the thrust indicated. Note also sedimentary younging evidence. See Table 4.3 for explanation of symbols. Height of scale (circled) is 1.8 m. Farm Tsawisis 308.

the migmatization by melting and injection during the intrusion of the Donkerhuk Granite.

4.4 The recognition of heterogeneous strain and thrusting

4.4.1 Heterogeneous strain

The distribution of strain throughout the traverse is distinctly heterogeneous in the sense of Ramsay (1967). Multi-layered sequences are especially receptive to strain variations in lithologies with different physical properties. Heterogeneity is developed on all scales. On a small scale, it is expressed in the differential development of fabrics in more competent quartz-rich (low-strain) and more incompetent mica-rich (high-strain) lithologies. On a large scale, strain variations may be expressed in particular high-strain zones which alternate with discrete zones of low strain.

Such a pattern has been observed in the study area. Figure 4.22 illustrates the above-described major fold structures in the Khomas Trough developed during the D_2 phase of deformation. Major structural discontinuities subdivide the Khomas Trough and discrete changes of fold styles occur across the discontinuities as indicated in this figure. The features which define the discontinuities are the ultimate expression of heterogeneous deformation within the Khomas Trough.

4.4.2 Major high-strain zones

Characteristics of the most important of the discontinuities outlined in Figure 4.22 are described below from south to north.

a) Southern-most Khomas Trough

Thrust faulting is clearly evident at the contact between the Kleine Kuppe quartzites and schists and the Kuiseb Formation schists just north of the confluence of the Koam and Kuiseb rivers (Fig. 4.3). At this locality a large number of northeast-trending thrust faults dip at shallow to steep angles towards the northwest. The faults cut out lithological units and produce typical wedge-shaped outcrop patterns. They are characterized by silicified and brecciated zones and the presence of iron-staining. When enclosed by two

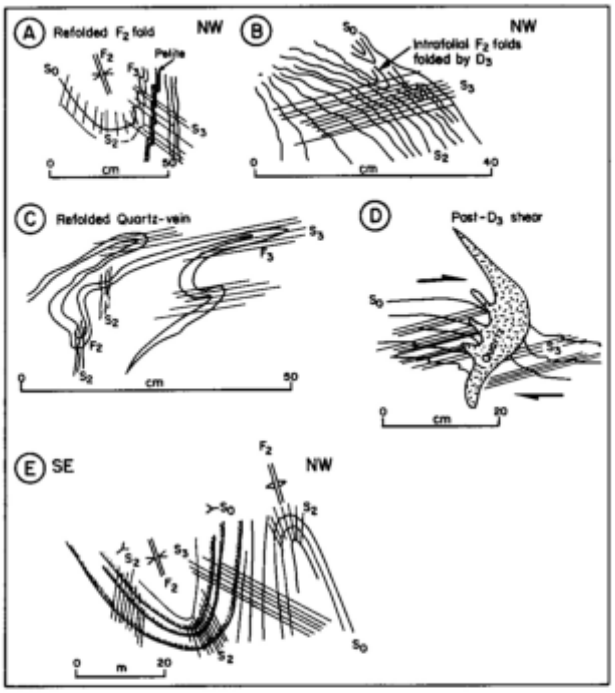

Fig. 4.17: Structural sketches showing D_2 and D_3 features of the southern scapolite schist on the farm Dagbreek 365 (see Fig. 4.2). (A) Tight F_2 syncline partly refolded by D_3. Note superimposition of S_2 by S_3. (B) Intrafolial minor F_2 folds situated on the overturned limb of a larger D_3 syncline. (C) Refolded quartz vein showing the development of minor F_2 and F_3 folds. (D) Penetrative S_3 cleavage and post-D_3 shear underlined by quartz segregation. (E) Downward-facing D_2 fold confirmed by sedimentary younging evidence and overprinting relationships of D_3 on D_2. The development of this fold suggests the presence of a D_1 deformation prior to D_2 in this part of the study traverse. See Table 4.3 for explanation of symbols.

fault planes, small-scale duplex-type structures indicate a southeasterly-verging shear sense (Fig. 4.23, A and B). The occurrence of drag folds on the upper sheet of faults also confirms the contractional style of the faulting. Associated with the faults are small-scale shear zones (comprising the composite cleavage which is sigmoidally shaped) and some deformed quartz segregations (Fig. 4.23, C and D). These quartz segregations act as small-scale strain markers and confirm the reverse attitude of the observed thrust faults.

b) Matchless Amphibolite

Heterogeneous strain is particularly well developed within the Matchless Amphibolite, which is situated in thick pelitic sequences. The heterogeneity is initially expressed by the alternation of low-strain zones and high-strain zones on a metre-scale. This is best illustrated by the shapes of pillow structures which range between original spheroidal and extremely elongated structures. The main fabric element is the S_2 cleavage which is axial-planar to isoclinal F_2 folds. Fold axes of these folds plunge more steeply (up to 25°) towards the northeast if compared with sequences north and south of the Matchless Amphibolite (Figs. 4.6 and 4.24). Elongated biotites and hornblendes form a pronounced northwest-plunging lineation. This lineation is best developed within the Matchless Amphibolite if compared to elsewhere along the traverse. Long axes of pillow structures also plunge to the northwest. S_3 is a penetrative biotite fabric which overprints S_2 in intercalated biotite schists. The S_4 crenulation cleavage is exceptionally well developed within this sequence (Fig. 4.24).

Stratigraphic relationships within the Matchless Amphibolite are strongly connected with the development of reverse faults. These have been observed throughout the sequence but they are much more pronounced at the base (Fig. 4.25, A). The main thrusting event occurred prior to D_3, which is evident from the shearing of the S_2 fabric and the unaffected S_3 cleavage (Fig. 4.25, C).

Post-D_3 thrusting, however, has also been observed. Orientations of thrust planes are largely parallel to F_2 axial surfaces at 040°-055°/35°-50°NW. Some thrusts are associated with breccia bands, silicification and iron-staining (Fig. 4.25, A). Thrust faults are generally associated with shear zones in which the S_2 fabric shows a sigmoidal pattern (Fig. 4.25, B). Metagabbros in the vicinity of thrusts are also strongly sheared (Fig. 4.25, D). More information on the stratigraphic implications within the Matchless Amphibolite due to thrusting will be given in Chapter 5. Important to note at this stage, however, is the occurrence of a 15 m-thick graphite schist and an overlying, 2 m-thick marble unit at the top of the Matchless Amphibolite (Fig. 4.22).

c) Koam canyon section

Geological features are well exposed in this northwest-trending, 6 km-long canyon on the farm Annelie (Fig. 4.9). Three phases of deformation (D_1, D_2 and D_3) are recognized in this area. Strain is also heterogeneous, shown by superimposed folding and thrusting. The structural fabrics and folds have been described above (section 4.2, domain B) and structural data are summarized in Figure 4.9. The earliest phase of thrusting is evident in the southern canyon where the crosscutting S_2 fabric post-dates a thrust fault (Fig. 4.26).

A major phase of thrusting occurred after the formation of F_2 folds and the S_2 cleavage. This is shown by the development of shear zones which show sigmoidally curved S_2 fabric elements and by sheared-out D_2 synclines and anticlines. Figure 4.11 illustrates the shearing-out of major limbs of tight to isoclinal F_2 folds. A pronounced L_2 biotite lineation plunging moderately towards the northwest on S_2 foliation surfaces occurs in the vicinity of the high-strain zones in the sequence. Within these zones, D_2 downward-facing structures which are unique in this part of the overall study traverse have been observed (Figs. 4.9, 4.10, 4.11). The downward-facing structures have been interpreted by Kukla *et al.* (1989) to have originated from early D 1 folding and thrusting which created overturned limbs. This was followed by D_2 folding and rejuvenated thrusting to develop the downward-facing structures (Fig. 4.27). Centimetre- to metre-scale F_3 folds are confined to the narrow shear zones which developed in the less competent lithologies (Fig. 4.7, D). A major structural discontinuity is indicated towards the northern end of the canyon section (Fig. 4.22). This is shown by a change from open asymmetric folds on the north side of the discontinuity to folds on the south side in which the bedding/cleavage relationships confirm

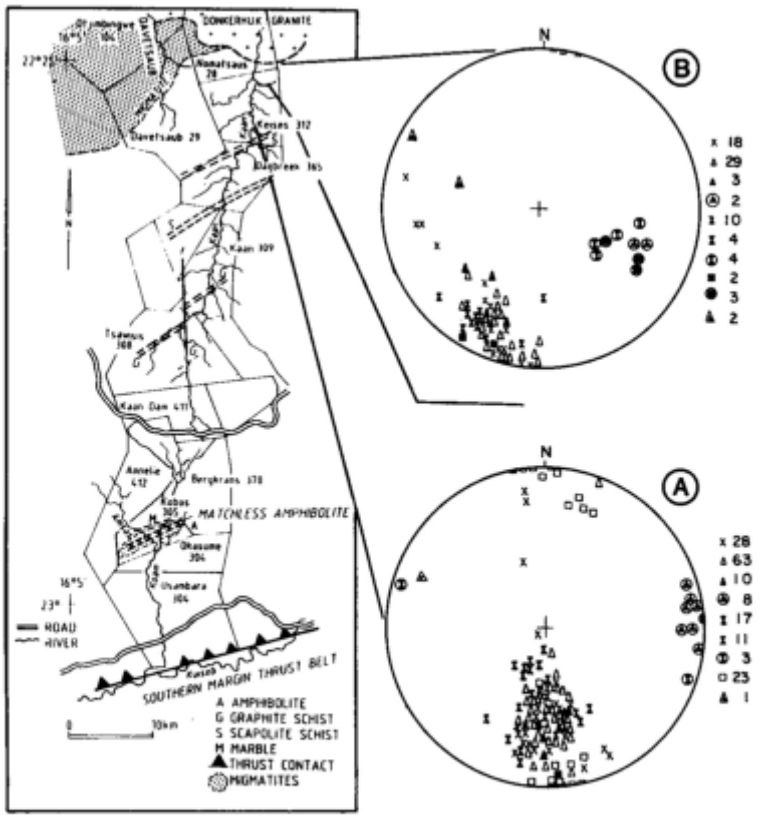

Fig. 4.18: Map of the study traverse showing a selection of structural data for the south (A) and the north (B) of domain D. See Table 4.3 for explanation of symbols; key gives number of measurements.

the presence of antiforms in which overturned limbs have been eliminated. These antiforms pass southward into tight to isoclinal overturned folds (Fig. 4.11).

d) Graphite schist

The area of the thick graphite schist on the farm Kaan in the centre of the Khomas Trough (Fig. 4.22) is a further high-strain zone. A one metre-thick tremolite schist occurs at the base of the approximately 60 m-thick graphite schist. The tremolite schist has been interpreted previously to have formed from a dolomitic precursor during metamorphism (see Chapter 3.5.7). A thrust fault with an orientation of 075°/40°NW has been observed at the base of the sequence and is shown by the shearing-out of an F_2 synclinal fold (Fig. 4.28, A and B). This zone is characterized by shearing although observations are more limited due to the uniform lithology of the graphite schist. In thin section, however, strongly elongated quartz may be seen within a highly-sheared S_2 foliation matrix (Fig. 4.28, C). A further feature is the isoclinal character of the F_2 folds which is unusual compared with the open folds north and south of this zone (Figs. 4.12; 4.13, E and F; 4.28, C). Additionally, F_2 fold axes in this zone plunge at steeper angles (20°) towards the northeast. In contrast to these D_2 features, F_3 fold axes maintain their horizontal to subhorizontal attitude throughout domain C. The latter, together with the crosscutting S_3 cleavage (which is a strong crenulation cleavage in the graphite schist) indicates that the thrusting event occurred pre-D_3.

An inferred thrust zone is situated between the graphite schist and the southern scapolite schist in domain C (Fig. 4.22). Since features of this zone are similar to those in the scapolite schists further north, they will be covered with the following description of the scapolite schist.

e) Scapolite schists

The two scapolite schist sequences occur in the northern part of domain C and they will be considered together, because charactelistics are similar (Fig. 4.22). Each of these zones is several hundred metres wide and contains overwhelmingly pelitic lithologies. D_2 and D_3 structural elements comprising cleavages and folds have been encountered. F_2 folds and the S_2 cleavage have, however, been strongly refolded and overprinted by D_3 within prominent shear zones where s-c band shearing occurs (Fig. 4.29, A). The usually competent calc-silicate spindles and layers are extremely folded and sheared into adjacent lithologies. The shearing and associated thrusting has led to D_2 downward-facing structures at the top of the sequence (Fig. 4.17, E) and to plunging F_2 fold axes (Fig. 4.29, B). Generally, the S_3 spaced cleavage is most strongly developed within this zone (Fig. 4.13, D) where it crosscuts dislocation zones which contain refolded and sheared D_2 structures. This indicates that the main thrusting event also occurred pre-D_3. In parts of the sequence, plunging D_3 fold axes have been observed and this suggests that syn- to post-$_{D3}$ faulting has also occurred if the lack of evidence for a strong D_4 fold phase in this area is considered. Some bedding-parallel fault surfaces have been observed along which massive scapolitization, brecciation and occasionally iron-sulphide mineralization occur (Fig. 4.29, C). Some of the observed features, especially the al-

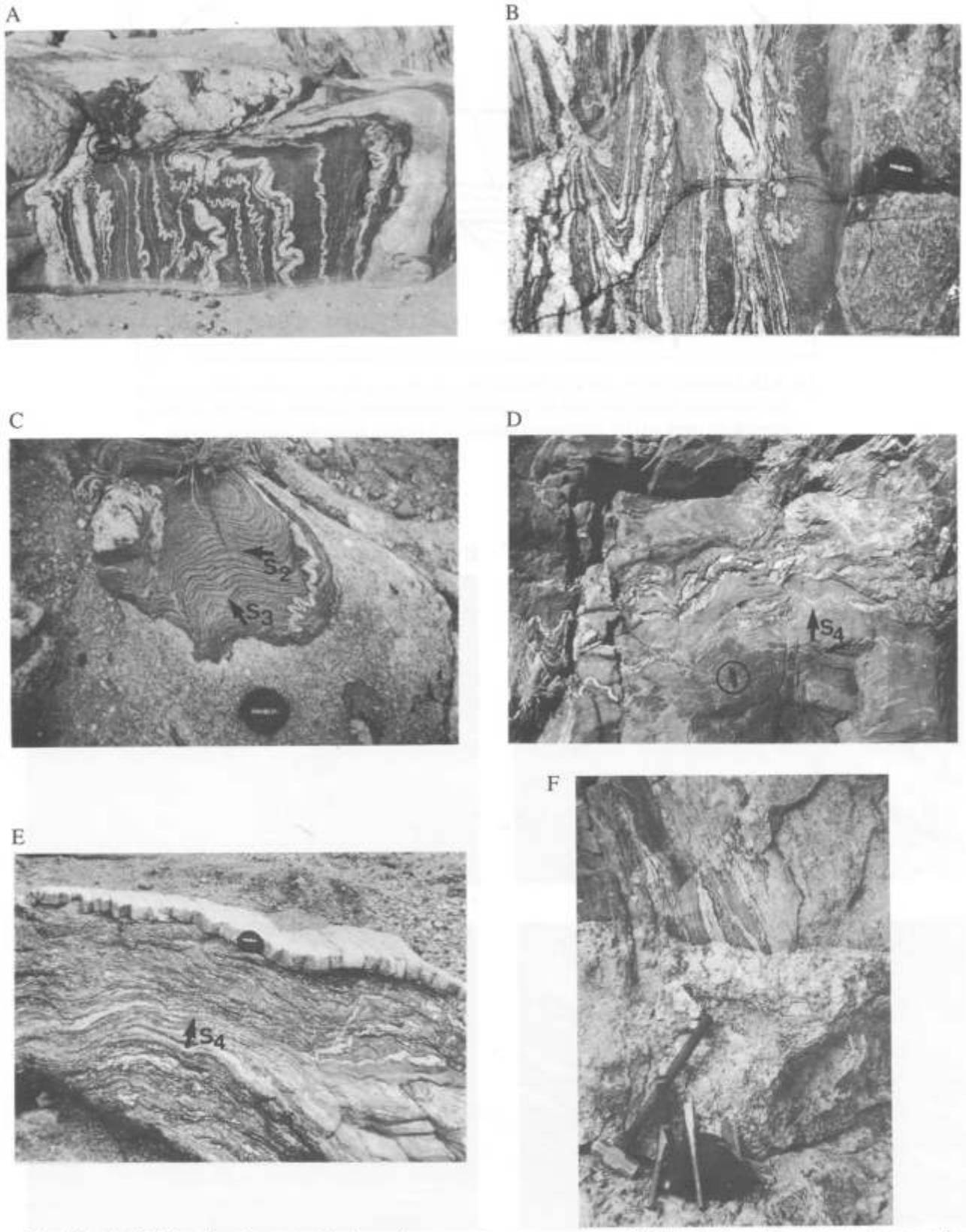

Fig. 4.21: (A) Kuiseb schist migmatites showing palaeosome and neosome, ptygmatic folding, and granitic apophyses. Lens cap for scale is circled. Davetsaub river, farm Nomatsaus 28. (B) D_2 synform in Kuiseb schist migmatites. Note boudinage in the centre of the photograph. Davetsaub river, farm Davetsaub 29. (C) Xenolith of Kuiseb Formation pelitic schist in granite comprising S_2 and S_3 cleavages (indicated by arrows) and ptygmatic folds. Farm Davetsaub 29. (D) Photograph showing pegmatite veins of the Donkerhuk Granite folded by D_4. The S_4 crenulation cleavage is demarcated. Pocket knife for scale (8.5 cm long) is circled. Kaan river, farm Keises 312. (E) Photograph showing granitic apophysis in pelitic schist folded by D_4. The orientation of the S_4 crenulation cleavage is indicated by arrow. Davetsaub river, farm Davetsaub 29. (F) Photograph showing sharp contact between crosscutting pegmatite (lower part of the photograph) and Kuiseb schist migmatites (upper part of the photograph). Davetsaub river, farm Davetsaub 29.

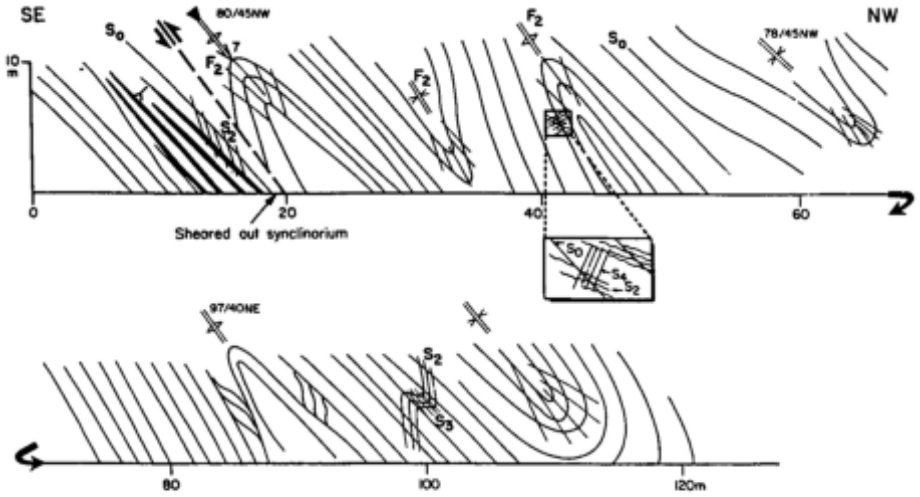

Fig. 4.20: Structural profile illustrating tight to isoclinal, moderately- to steeply-dipping D_2 folds with axial-planar S_2 fabric. Superimposed are the S_3 and S_4 fabrics in this low-strain zone in the southern part of domain D. See Table 4.3 for explanation of symbols. Farm Keises 312.

ternation of high- and low-strain zones and the refolding of F_2 folds by D_3, may be seen in Figure 4.30, which is a structural profile across the northern scapolite schist on the farm Keises (Figs. 4.18 and 4.22). The abrupt changes from areas with preponderant D_2 folding to areas with strong D_3 folding are especially note-worthy. A further important feature contributing towards the interpretation of these scapolite zones is the abrupt change of fold styles on a large scale on both the northern and southern sides of the discontinuities. This is conspicuous in the landscape and is illustrated in Figure 4.22, which shows that subhorizontal limbs of open asymmetric folds occur on the southern sides but steep to overturned limbs of isoclinal folds occur in the north.

f) Northern Khomas Trough

The central and northern parts of domain D, designated the Okahandja Lineament Zone (Miller, 1983b) in Figure 4.22, are characterized by mostly pelitic sequences. The S_2 fabric and D_2 folds have been refolded within shear zones which has led to the formation of D_3 downward-facing folds (Fig. 4.19, D). Parallel-sided shear zones with the development of F_3 folds and a strong S_3 cleavage are illustrated in Figure 4.31. A structural cross-section shown earlier (Fig. 4.20) demonstrates the shearing-out of overturned F_2 limbs by thrusting in the central part of the farm Keises. The Schmidt net in Figure 4.31, B indicates an unusually wide spread of poles to cleavages as well as the steeply-inclined attitude of the axial planes in this area. A post - D_4 feature in this area is the clockwise rotation of structural elements (Fig. 4.18).

4.4.3 Summary and conclusions

Most of the above-described individual high-strain zones throughout the study traverse share features which are the ultimate expression of heterogeneous deformation in the Khomas Trough. The following characteristics are common to most of the discontinuities described.

(1) The discontinuities are zones which are several hundreds of metres wide and they are situated particularly in the thickest pelitic successions of the Khomas Trough. Thrust faulting has been directly observed mainly through the displacement of fold limbs which have been sheared-out at the southern margin of the traverse, the Matchless Amphibolite, the Koam canyon section, the graphite schist on the farm Kaan, and the scapolite schists. Pronounced mineral lineations down-dip on axial-planar foliation surfaces are associated with the southeasterly-directed thrusting. Small-scale strain markers such as sheared pre-thrusting fabrics, quartz layers and calc-silicate spindles, confirm the reverse attitude of the observed discontinuities. The earliest thrusting occurred during the D_1 phase of deformation but major thrusting was associated with the D_2 and D_3 phases of deformation which are evident in all high-strain zones described. Late shearing and thrusting post-dating D_3 is indicated in the Matchless Amphibolite sections and the scapolite schists. The above features confirm the contemporaneity of folding, cleavage formation and thrusting.

(2) The discontinuities are zones of concentrated shear. On a small scale, ductile shearing is indicated in thin section and in outcrop by cm- to m-wide zones, where pre-shear foliations are deflected and sigmoidally shaped. In some cases, layer-parallel s-c band shearing is developed which also indicates the heterogeneity of strain during fold development. Apart from enhanced retrograde reactions there is very little evidence for changes in metamorphic conditions within the shear zones, since the peak of metamorphism outlasted the major deformation phases (Chapter 6). Strain determinations, shear zone geometries and compressional directions are difficult to evaluate since shear zones are largely parallel-sided within the overall northeast-trending tectonic grain of the orogen. The intense refolding of the S_2 metamorphic banding cleavage and the largely unaffected S_3 cleavage confirm the pre-D_3 age of major shearing within the high-strain zones.

(3) With respect to the main fold phase D_2, discrete and rather abrupt changes of fold styles occur across the discontinuities, separating isoclinally from openly folded zones. This may be seen in the centre and the northern part of the traverse, where shallow- and steep-dipping bedding sur

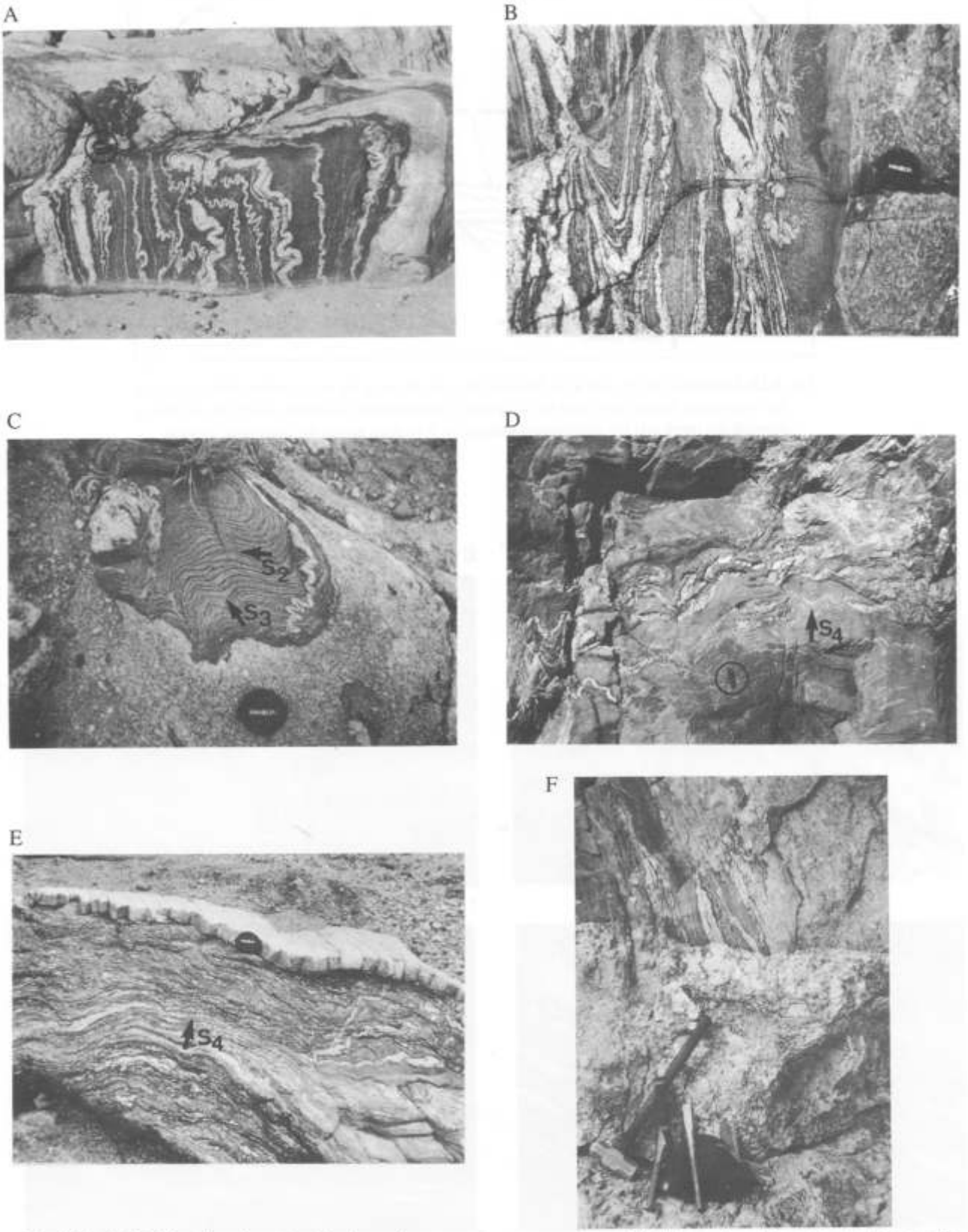

Fig. 4.21: (A) Kuiseb schist migmatites showing palaeosome and neosome, ptygmatic folding, and granitic apophyses. Lens cap for scale is circled. Davetsaub river, farm Nomatsaus 28. (B) D_2 synform in Kuiseb schist migmatites. Note boudinage in the centre of the photograph. Davetsaub river, farm Davetsaub 29. (C) Xenolith of Kuiseb Formation pelitic schist in granite comprising S_2 and S_3 cleavages (indicated by arrows) and ptygmatic folds. Farm Davetsaub 29. (D) Photograph showing pegmatite veins of the Donkerhuk Granite folded by D_4. The S_4 crenulation cleavage is demarcated. Pocket knife for scale (8.5 cm long) is circled. Kaan river, farm Keises 312. (E) Photograph showing granitic apophysis in pelitic schist folded by D_4. The orientation of the S_4 crenulation cleavage is indicated by arrow. Davetsaub river, farm Davetsaub 29. (F) Photograph showing sharp contact between crosscutting pegmatite (lower part of the photograph) and Kuiseb schist migmatites (upper part of the photograph). Davetsaub river, farm Davetsaub 29.

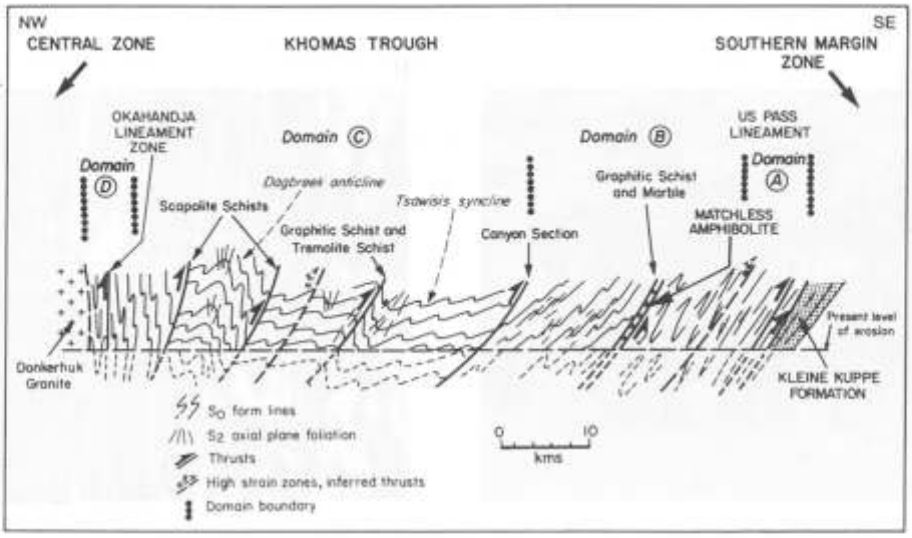

Fig. 4.22: Structural profile across the Khomas Trough showing the organization of the sequence into individual thrust slices after the D_2 phase of deformation. Note the structural steepening towards the north and the pronounced changes in fold style across the individual thrusts.

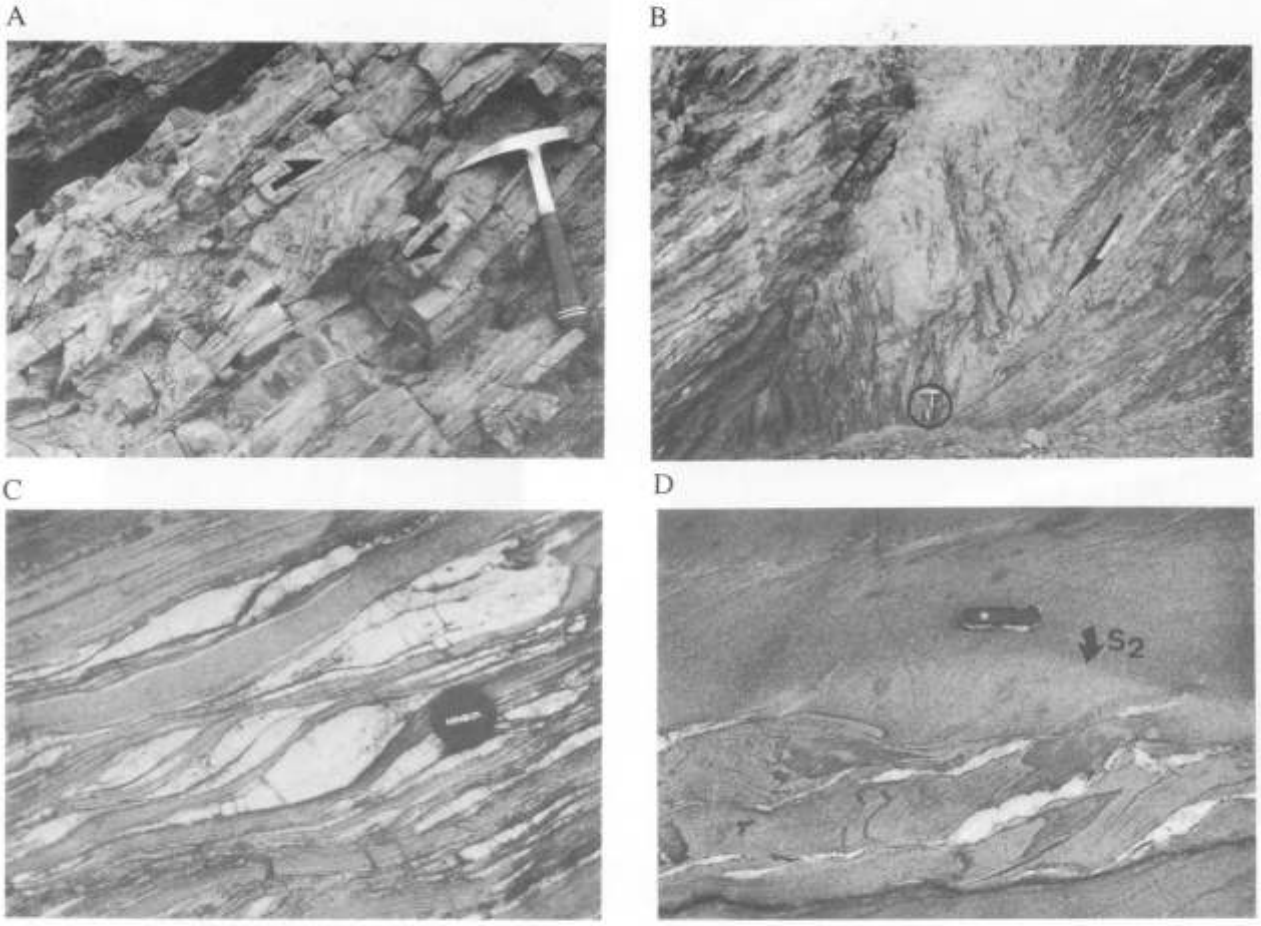

Fig. 4.23: (A) Small-scale, southeast-verging thrust fault within Kleine Kuppe Formation pelites and quartzites, about 500 m north of the confluence of the Koam and Kuiseb rivers on the farm Usambara 304. (B) Southeast-verging thrust faults in Kuiseb Formation pelites, several hundreds of metres north of the confluence of the Koam and Kuiseb rivers on the farm Usambara 304. Hammer for scale is circled. (C) Photograph showing shear zone near thrust fault indicated by sigmoidally shaped quartz segregations within $S_{0,1,2,3}$ composite cleavage in chlorite schist. Farm Usambara 304. (D) Small-scale shear zone comprising sigmoidally shaped S_2 fabric and intrafolial D_2 folds. Pocket knife is 8.5 cm long. Farm Okasume 304.

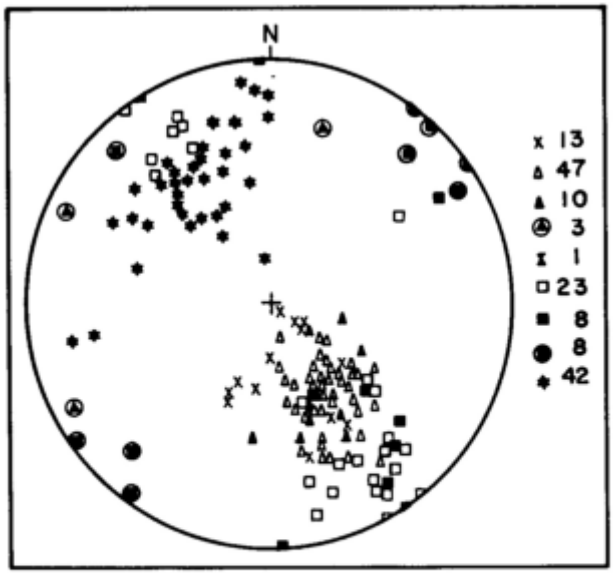

Fig. 4.24: Stereonet showing structural data from metasediments and amphibolites within the Matchless Amphibolite. See Table 4.3 for explanation of symbols; key gives number of measurements.

faces on the respective northern and southern sides of the discontinuities, exhibit a distinct ramp and flat geometry.

(4) Within the high-strain zones there is a remarkable development of structures associated with the D_3 phase of deformation. The S_3 fabric and tight to isoclinal F_3 folds, only scarcely developed in low-strain zones and restricted to metre-scale shear zones, dominate within these high-strain zones. Original sedimentary features are largely obliterated and D_2 fold structures and fabric elements are strongly overprinted to become uneven in geometry and intensity. The above is in strong contrast to adjacent low-strain zones where sedimentary structures are remarkably well preserved and F_2 folds with the associated penetrative S_2 axial-planar foliation form the main structural elements. Orientations of planar and linear structural elements vary considerably within the high-strain zones which is especially evident from the plunging attitude of F_2 fold axes. This is unusual if compared to the commonly horizontal to subhorizontal plunges of fold axes in low-strain zones of the Khomas Trough.

(5) Downward-facing D_2 and D_3 structures along the study

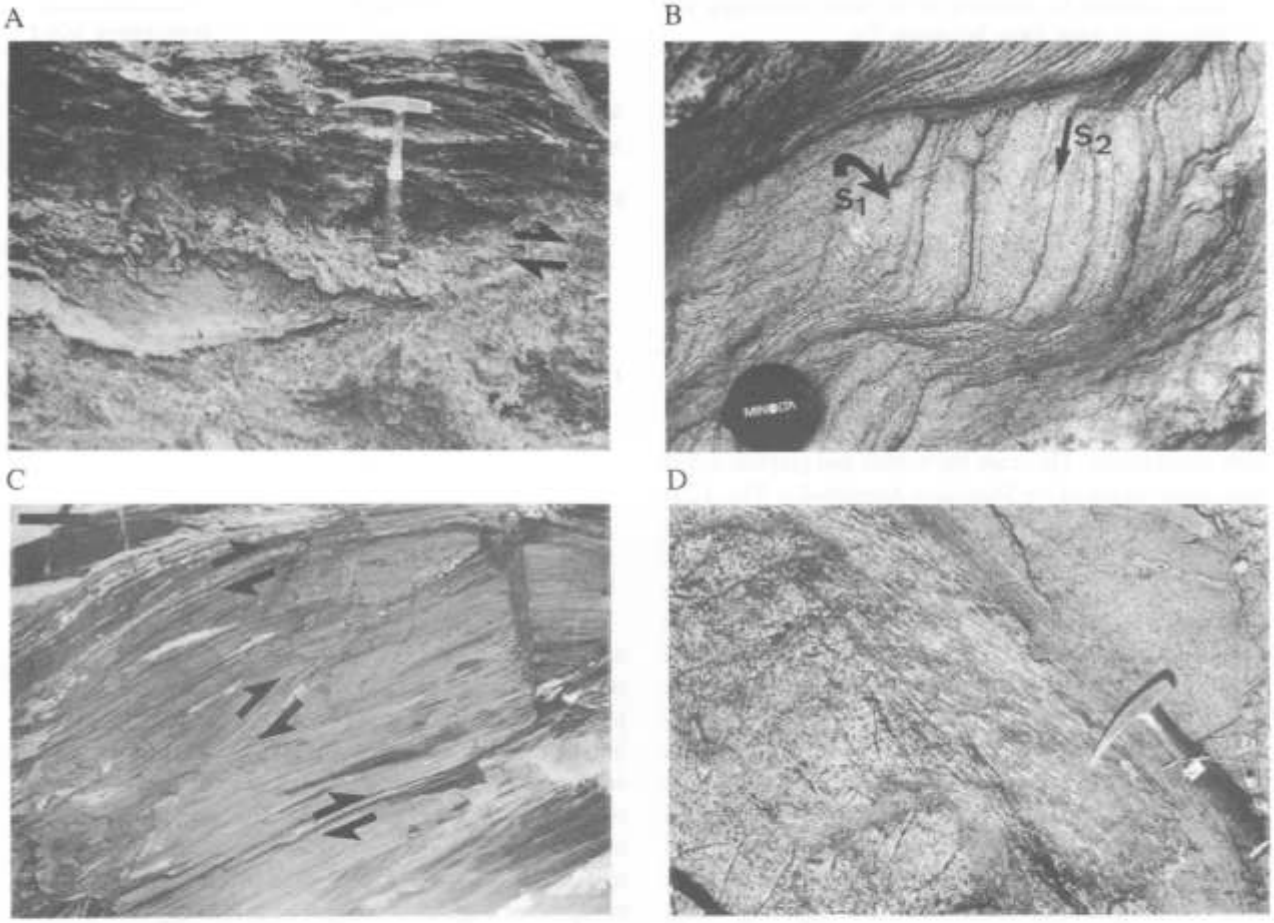

Fig. 4.25: (A) Major thrust fault (décollement) situated in 10 m-thick graphite schist at the base of the Matchless Amphibolite. Thrusting is accompanied by brecciation and silicification. For detailed profile see Figure 5.5. Amsas river, Farm Kobos 305. (B) Shear zone of D_2 age in pelitic schist associated with the graphite schist thrust zone shown in Figure 4.25,A. Photograph shows sigmoidally shaped S_2 metamorphic banding cleavage in which S_1 is strongly transposed (indicated by arrows). Amsas river, farm Kobos 305. (C) Southeast-verging thrust zone of post-D_2 age developed in type I amphibolites of the Matchless Amphibolite. Waterfall profile (see profile A in Figure 5.1), farm Annelie 412. Scale bar is 0.5 m. (D) Shear zone in metagabbro of the Matchless Amphibolite. Koam river, farm Kobos 305.

Fig. 4.26: Southeast -verging pre-D_2 thrust fault in psammitic and pelitic schist in the southern Koam canyon. This thrust zone is clearly crosscut by the S_2 metamorphic banding cleavage which suggests D_1 thrusting in this area. Brecciation and silicification occur. Farm Bergkrans 370.

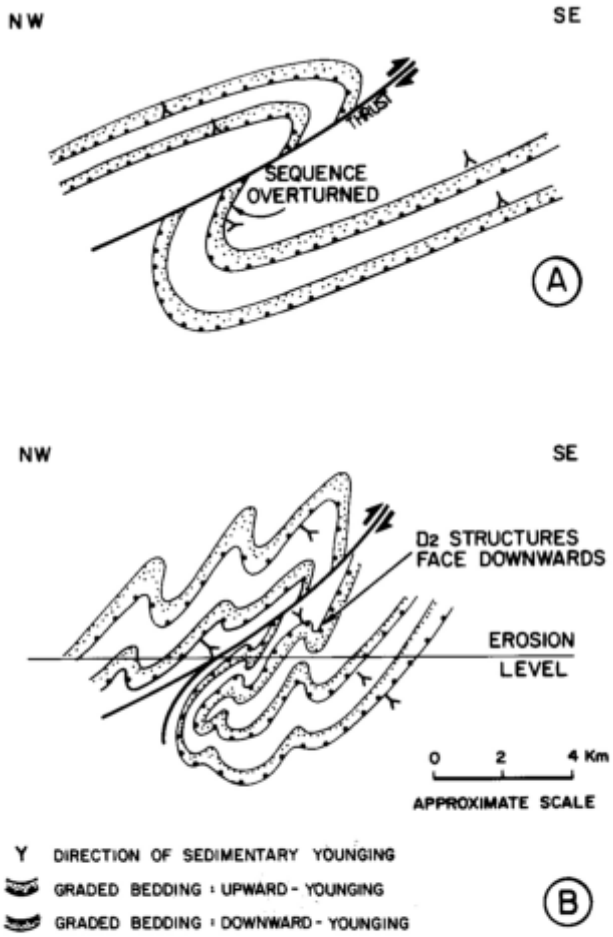

Fig. 4.27: Schematic diagram of the model for the development of downward-facing structures along the Koam canyon section. (A) Early (D_1) folding and thrusting, creating overturned limbs. (B) D_2 folding, rejuvenated thrusting and subsequent development of downward-facing structures. Note that folds produced in the overturned sequence are downward-facing. (From Kukla *et al.*, 1989).

traverse are exclusively confined to the observed high-strain zones, i.e. the Koam canyon section, the hanging wall of the southern scapolite schist, and the northern margin of the Khomas Trough.

(6) In the case of the two scapolite schists, the scapolitization of the originally plagioclase-bearing wallrock occurred post-D_3. The massive enrichment along fractures as well as the chlorine-rich compositions of the scapolites (Chapter 6.4) indirectly point to the presence of tectonic weakness zones which hosted fluid movement.

(7) There are similar lithologies present in two of the high-strain zones. These are the marble and graphite schist association on top of the Matchless Amphibolite (Fig. 4.22) and the tremolite schist - graphite schist association in the centre of the traverse (Fig. 4.22). Striking lithological similarities also characterize the two scapolite schists which comprise calc-silicate rich and pelitic sequences. These are suggestive of geological repetition of units which could ideally have been used as décollement planes within the sequence.

In conclusion, these high-strain zones are interpreted as major shear and thrust zones, situated in pelitic sequences. The individual thrust slices may be traced over more than 150 km along strike (Fig. 2.4) and they define, together with the northwards-steepening attitude of structures, an overall imbricate fan geometry in the Khomas Trough (Fig. 4.22). With respect to this structural setting and the similar lithologies occurring in some of the thrust zones, it may be speculated that the individual thrusts are all related to a major décollement surface at depth.

4.5 Kinematic interpretation and time sequence of deformational events

The correlation of structural elements along the traverse uses the S_2 foliation as a time datum because this fabric is a recognizable metamorphic banding cleavage and is axial-planar to F_2 folds of varying style. The following kinematic interpretation is structured according to the proposed time sequence of events as evident from several successive stages of cleavage and fold formation. This does, however, not necessarily imply discrete and independent phases of deformation through time. Lithological contacts are interpreted to represent original bedding, which is in any case evident from original sedimentary structures preserved through large parts of the traverse. Structural elements encountered and their correlation along the study traverse are represented in Table 4.1.

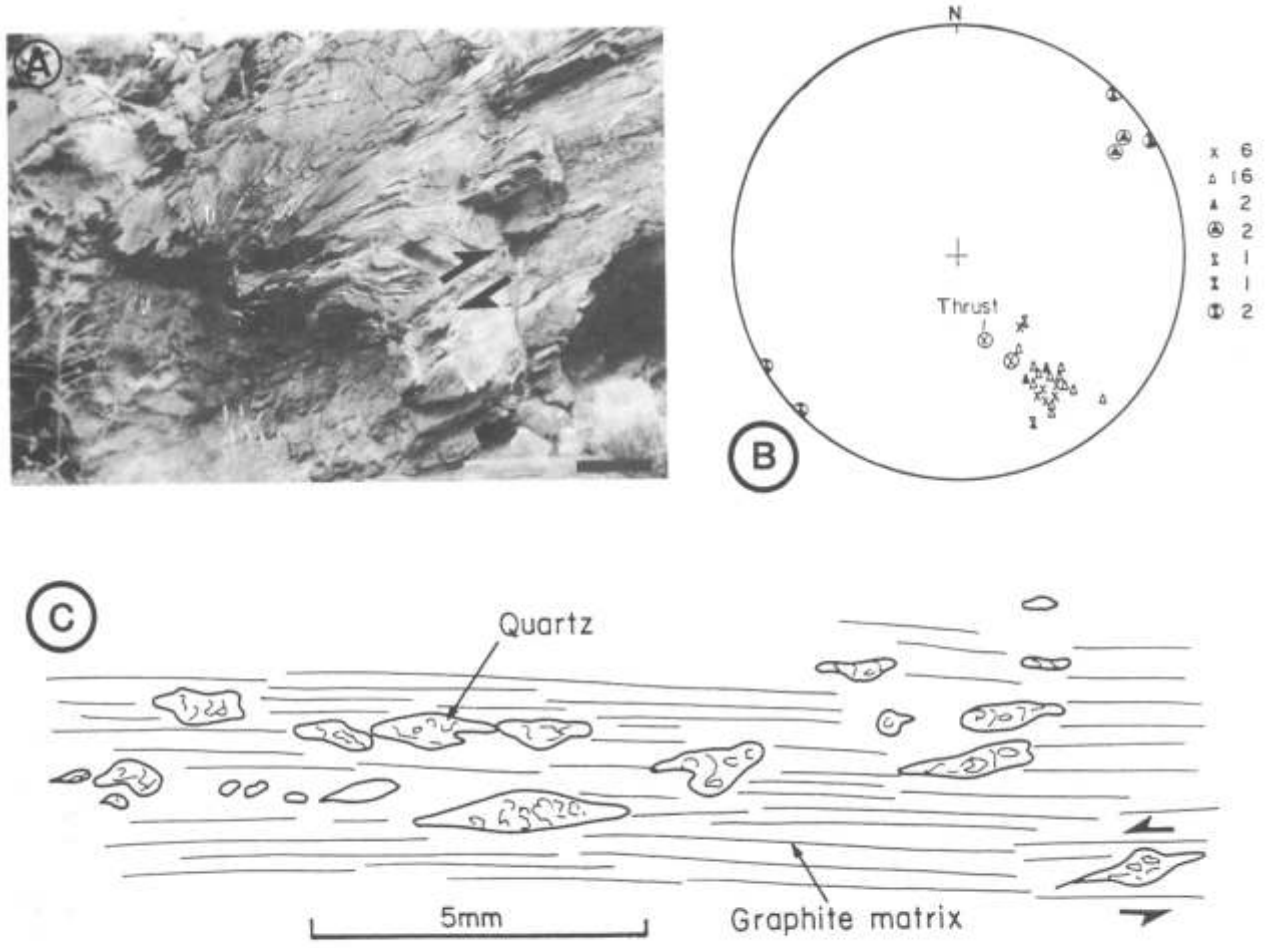

Fig. 4.28: Diagram showing photograph, sketch and stereoplot of structural features in the graphite schist in the centre of the Khomas Trough. Kaan river, farm Kaan 309. (a) Photograph showing pre-D_3 thrust fault and sheared-out synform at the base of the graphite schist. Thrust zone is brecciated and iron-stained. (b) Stereonet data for the graphite schist sequence. See Table 4.3 for explanation of symbols. (c) Tracing from thin section showing elongated and sheared quartz in highly sheared graphitic matrix.

4.5.1 D_1 phase of deformation

The first phase of deformation is mostly evident in the southern part of the Khomas Trough. D_1 is represented by a northeasterly-trending metamorphic banding cleavage which is defined by an early biotite generation of metamorphic origin. S_1 has been intensely overprinted and transposed during subsequent deformation phases. This process would account for the lack of recognition of F_1 folds which even in domain B are of a regional scale. In other medium-grade metamorphic terrains, transposition and obscuring of D_1 fold closures by later phases of deformation has been widely documented (Turner and Weiss, 1963; Hobbs *et al.*, 1976). Lines of evidence suggesting the development of F_1 fold closures are the northerly- and southerly-inclined attitude of S_1 and the presence of D_2 downward-facing structures in domain B and the southern scapolite schist in domain C. The latter have formed through the refolding of overturned F_1 limbs during D_2. This, together with silicified and brecciated zones which are crosscut by S_2, demonstrates that thrusting had already been initiated during D_1 and that these thrusts were inherited by later deformation phases. Cleavage data confirm that S_1 formed within the overall coaxially consistent stress regime of the Khomas Trough. The structural style and the character of the cleavage indicate that it formed under an overall compressive regime.

4.5.2 D_2 phase of deformation

The second phase of deformation has been labelled D_2 on the basis of the S_2 fabric which is always a strong, penetrative metamorphic banding cleavage, with quartz-feldspar and mica-rich domains and which is axial-planar to second generation folds throughout the area. S_2 trends northeast and dips northwest with the exception of high-strain shear zones where orientations vary. Calc-silicate spindles are preferentially oriented parallel or subparallel to this fabric. Wide spacing of the cleavage in psammites and narrow spacing in pelites indicates a lithological control of the cleavage formation.

The style of D_2 folds varies throughout the Khomas Trough from intrafolial to isoclinal in the south through open in the centre to isoclinal in the north. The major fold structures which are indicated in Figure 4.22 are thrust bounded. Rather abrupt changes of fold styles occur across the thrust zones. The consistent southeasterly vergence, the subhorizontal fold axes and the corresponding axial-planar cleavage indicate that the folds have formed within a compressive regime. The formation of open, asymmetric folds in the low-strain zones in the centre might be attributed to: (1) an oblique angle be-

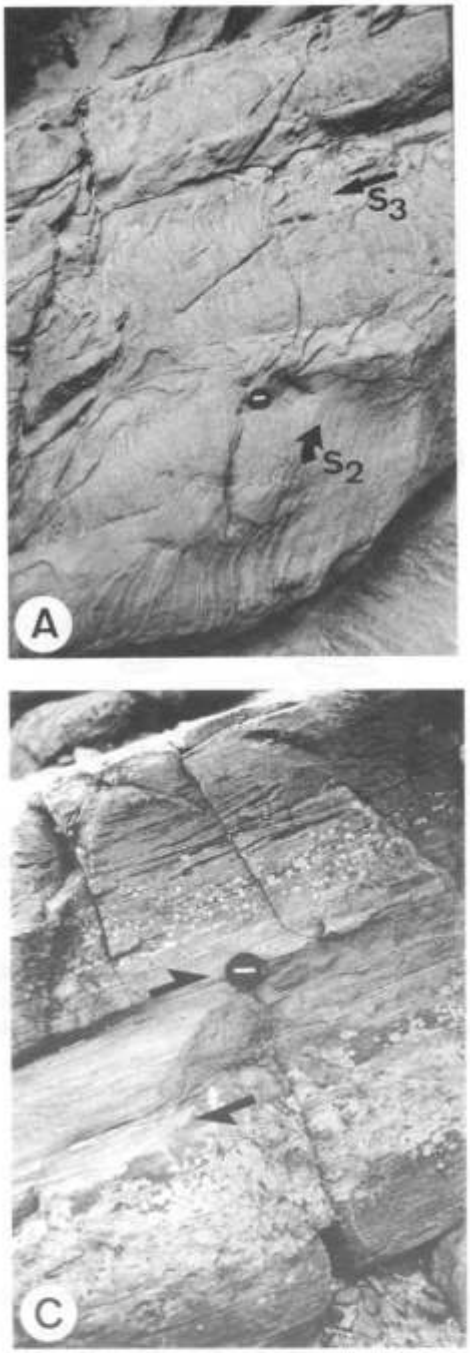

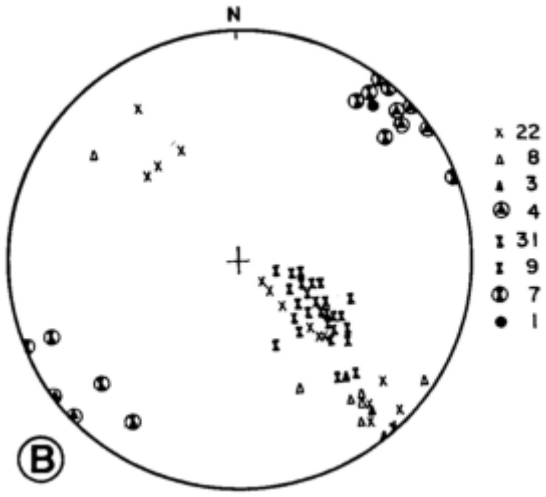

Fig. 4.29: Shearing and thrusting in the southern scapolite schist sequence, farm Dagbreek 365. (A) Strong s-c band shearing of S_2 by D_3. S_2 metamorphic banding cleavage and orientation of S_3 cleavage parallel to D_3 shear zones are indicated by arrows. (B) Structural data for the scapolite schist sequence. See Table 4.3 for explanation of symbols; key gives number of measurements. (C) Brecciated and silicified bedding-parallel fault which is part of a D_2 thrust zone. Western flank of "Kuduspitze" mountain, farm Dagbreek 365.

tween layering and the maximum shortening direction; (2) southeast-directed shear, and (3) southeast-directed translation during fold development. The first possibility is ruled out since there is no evidence for non-coaxial folding in this area. Shear deformation within the low-strain zones is only evident on a minor scale. It is therefore more conceivable that these particular folds developed during southeastward-directed translation with possibly additional shear components participating in this process. The extreme coaxiality of structures confirms the constancy of the principal axis of shortening throughout the deformational history of the Khomas Trough. The existence of intrafolial D_2 folds in domain B occurring in association with isoclinal D_2 folds confirms that considerable layer-parallel extension has occurred after layer-parallel shortening. Distinct mineral elongations of mainly biotite and amphiboles occur in domains A and B. Since the direction of maximum extension will be close to perpendicular to the fold axis, the lineations most likely represent extensional down-dip lineations within S_2 planes. The remarkable development of these lineations at the southern margin of the Khomas Trough, the Matchless Amphibolite and the scapolite schists in the north, speak in favour of formation parallel to the direction of tectonic transport in thrust zones as described by Hobbs *et al.* (1976).

A major phase of thrusting occurred during this stage of the structural evolution. The thrust zones are high-strain zones and simple shear deformation plays a major role as is evident from non-coaxial deformation. Observed shear senses are mostly directed towards the southeast. It is mainly the overprinting relationships of D_3 features on D_2 which indicate that the main thrusting period occurred late during D_2, most probably representing the culmination of this D_2 deformation. The lack of mylonites might indicate that folding and thrusting occurred contemporaneously, a feature pointed out by Lewis *et al.* (1988). The orientations of thrust zones also confirm the steepening of structural elements towards the north to develop an overall imbricate fan geometry as indicated in Figure 4.22.

Finally the coaxial and subhorizontal attitude of structures developed in low-strain zones is related to simple shear deformation, whereas pure shear produced plunging attitudes of structural elements in high-strain zones during the subsequent D_3 deformation.

4.5.3 D_3 phase of deformation

The structural patterns which characterize the third deformation differ from those of the D_2 phase. The S_3 cleavage and F_3 folds have developed preferentially within zones of high strain. The penetrative S_3 biotite fabric is a spaced cleavage and tight to isoclinal metre-scale F_3 folds have only developed within these high-strain zones. The style and scale

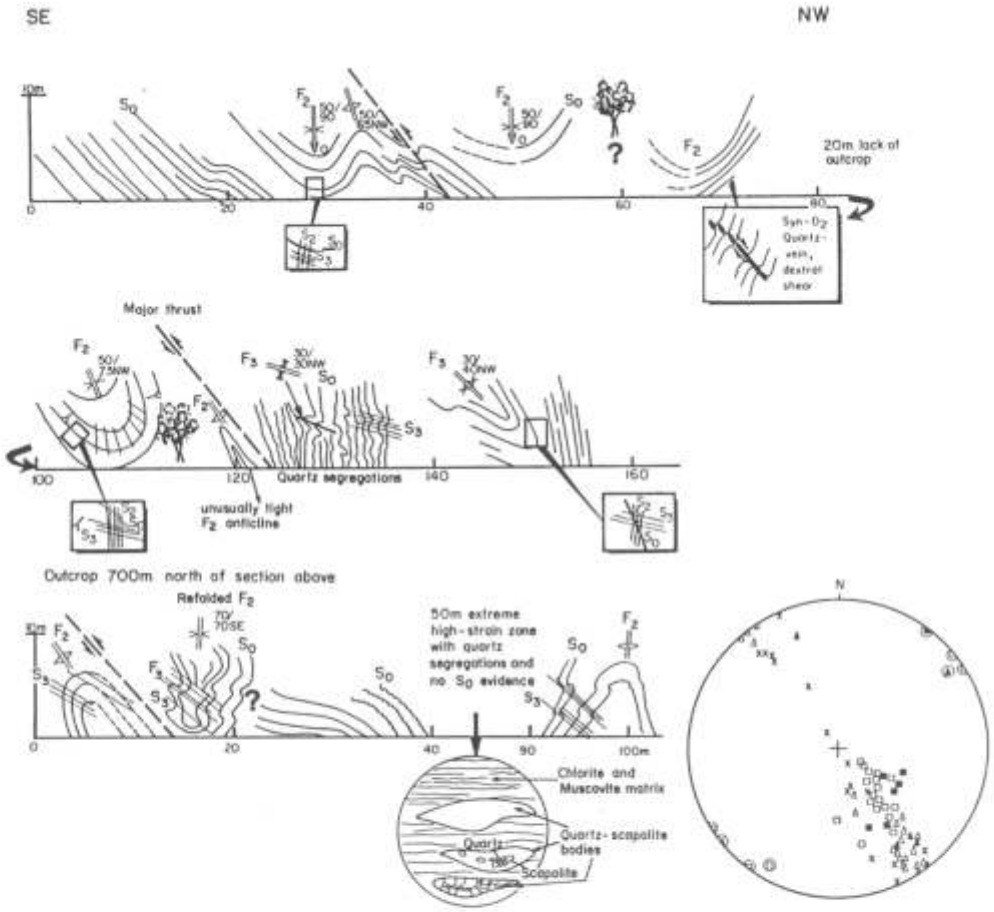

Fig. 4.30: Structural profile across the northern scapolite schist sequence on the farm Keises 312. Diagram illustrates overprinting relationships of D_3 on D_2 in association with thrust faults. Structural data along the profile are given in stereonet. See Table 4.3 for explanation of symbols.

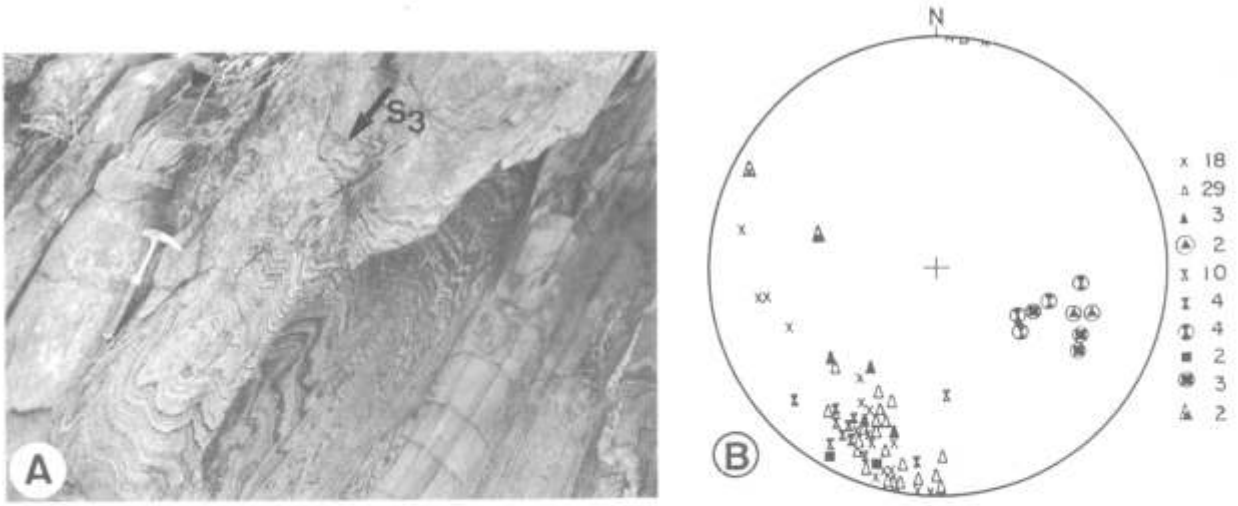

Fig. 4.31: (A) Photograph of parallel-sided D_3 shear zone containing F_3 folds and a pervasive S_3 spaced cleavage. S_0 and S_2 are intensely folded. Note parallelism of S_0, S_2 and S_3 on either side of the shear zone. Northern margin of the farm Keises 312. (bB Stereonet showing structural data for the northern part of domain D (see Fig. 4.18). Note wide spread of data, clockwise rotation of structural elements compared with domains A-C, and plunging fold axes. See Table 4.3 for explanation of symbols; key gives number of measurements.

of folding and the development of plunging F_2 and F_3 fold axes indicate that shear processes played a major role during and after D_3. Downward-facing D_2 folds originated through the refolding of overturned D_2 limbs during D_3. Sillimanite knots which were formed during D_2 have been partly re-oriented into the S_3 cleavage. The participation of fluid phases during deformation in high-strain zones is illustrated by the post-D_3 scapolitization of metasediments in the north. The above aspects indicate that the D_3 deformation had a mainly compressional character.

The features outlined for the D_1, D_2 and D_3 deformations show that fold formation, cleavage formation and thrusting occurred continuously through time, emphasized by the inheritance of the major thrusts from one phase to the next. The structural evolution of the Khomas Trough is therefore interpreted to be one of progressive deformation.

4.5.4 Later phases of deformation

S_4 crenulation cleavages and related small-scale F_4 folds are only developed at the southern and northern margin of the study traverse. The symmetric and asymmetric fabric only occurs in the most pelitic lithologies, where it overprints earlier planar fabrics. An early generation of Donkerhuk pegmatites as well as some granite apophyses are folded D_4.

Asymmetric and monoclinal kink folds, designated as D_5 structures in Table 4.1, with southerly-dipping axial surfaces are a particular feature of the southern part of the traverse up to the Matchless Amphibolite. The kink folds clearly post-date the crenulation cleavage. The development of kink folds has been attributed to the principal compressive stress directions being parallel to the folded surface and cleavage planes (Donath, 1961). It is therefore probable that the kinks developed by late-phase fault movements directed towards the southeast. The restriction of the kink folds to the southern part of the traverse may have been pressure controlled such that kink band formation only occurred at pressures above 3 kbar as shown by experiments of Anderson (1974).

4.5.5 Strike-slip displacement along the northern margin of the Khomas Trough

The clockwise rotation of structural elements in domain D is the youngest deformation discernible in this area. This rotation has been explained as having been caused by the intrusion of the Donkerhuk Granite (Faupel, 1974) or by late right-lateral strike slip movement (Gevers, 1963; Blaine, 1977) in the vicinity of the Okahandja Lineament (Miller, 1979). These findings are in contrast to a study by Downing and Coward (1981) in which they postulated a sinistral strike-slip movement along the Okahandja Lineament, based on a southwest - northeast oriented extension lineation in the Central Zone and the Okahandja Lineament Zone.

A compilation of data from several studies in the vicinity of the Donkerhuk Granite (Gevers, 1963; Smith, 1965; Faupel, 1974; Hälbich, 1977; Blaine, 1977; Sawyer, 1981; Preussinger, 1987) has been undertaken by the writer. This has revealed that rotation of structural elements is not confined to the respective outcrop limits of the granite. It is therefore concluded that the clockwise rotation occurred post-D_4 within a right-lateral transpressional strike-slip regime, according to the mechanism described by Sanderson and Marchini (1984). Since some granite apophyses have been folded by D_4 it is conceivable that strike-slip displacement and granite intrusion were approximately contemporaneous.

4.5.6 Aspects of strain determinations

Strain determinations within the Khomas Trough have been undertaken previously by Hälbich (1977) who obtained a total amount of 67% shortening, studying selected folds and calc-silicate spindles in the Okahandja - Windhoek profile. Sawyer (1981) used folds, deformed pebbles, vari¬olites and amphibolite pillows for his strain determinations and presented a rough estimate of 50-80% shortening for the Khomas Trough. Within the Kuiseb schists, markers to determine strain quantitatively are extremely rare. Calc-silicate bodies of spindle shape are widespread and it has previously been shown that their maximum elongation is parallel to the regional fold axes in the Y-direction of the strain ellipsoid. These bodies do not, however, appear to be suitable for strain analysis since they represent originally calcareous lithologies which have been subjected to concretionary processes and metamorphism, as pointed out in Chapter 3. Pillow bodies within the Matchless Amphibolite were used by Sawyer (1981) and they are also studied here to give an initial overview of the types of strain involved during deformation. The profile from which data were obtained is shown in Figure 5.2. The pillows are considered to have had originally spherical or near-spherical shape which is confirmed by the X:Y:Z data of certain pillows in zones of low strain. In contrast to the calc-silicate spindles, the maximum direction of extension, X, of the pillows, is perpendicular to the regional strike. The intermediate elongation, Y, parallels the regional fold axes. Strain data and calculations are compiled in Table 4.4 which gives the number of two- and three-dimensional readings as well as the maximum, minimum, and average extension and shortening. The initial size of the assumed spherical pillows has been calculated from the X:Y:Z ratios, with Z=1.

The results in Table 4.4 indicate that shortening in the Z direction averages 47%, ranging from 20% to 63%. Extension towards X is most pronounced and the wide range of values for both extension directions demonstrates the variability of imposed strain rates. High-strain and low-strain zones on a metre-scale within the Matchless Amphibolite (see Chapter 5.3.2) are respectively represented by maximum and minimum values of extension. Shortening estimates, however, are regarded as minimum values since competent pillows within an incompetent amphibole-carbonate-plagioclase matrix most probably react to compressive stress to a certain extent by internal deformation. They might therefore record different strain from that of the bulk of the rock, a factor pointed out by Hobbs *et al.* (1976) as being valid for most lithological markers. Additionally, several successive stages of shortening which have not been separated are likely to be recorded within the pillows. Three-dimensional measurements have been plotted on a Flinn diagram (Fig. 4.32). The ellipsoids are oblate and in the field of apparent flattening. The data confirm a large flattening strain imposed and k-values from 0 to 1 imply a complex deformation history involving flattening-type deformation with volume loss and plane-strain deformation in a simple shear environment High- and low-strain domains are additionally confirmed by these data indicating progressive incremental shortening.

TABLE 4.4: Strain data for deformed pillow structures in locality A (Fig. 5.1) at the Matchless Amphibolite. Values given are averages, minima and maxima for extension and shortening obtained from three-dimensional (n=6) and two-dimensional (n=23) measurements (formulas after Hobbs *et al.*, 1976: p. 33).

	$\bar{y}$	$\bar{y}$	$\bar{z}$	$k=\frac{R_{xy}^{-1}}{R_{yx}^{-1}}$
pillows (n=6)	4.3	2.9	1	0.02-1.05
extention (mean) (max./min.)	107% (13%/58%)	70% (116%/36%)		
shortening (mean) (max./min.)			-47% (-61%/-35%)	
pillows (n=23)		3.3	1	
extension (mean) (max./min.)		81% (170%/22%)		
shortening (mean) (max./min.)			-45% (-63%/-20%)	

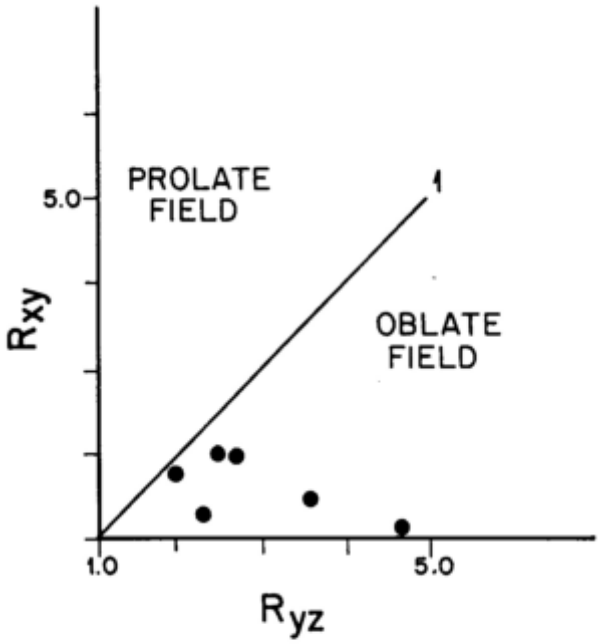

Fig. 4.32: Flinn diagram showing data from strain measurements of pillow structures within the Matchless Amphibolite. Pillows plot into the oblate field indicating a flattening-type deformation.

4.5.7 Consideration of previous studies: a correlation of deformation events in the Khomas Trough

With the increasing number of data obtained from studies in various parts of the Damara Orogen it is tempting to combine these to correlate deformation events over larger areas. It has frequently been shown in other folded terranes that it is highly tenuous to correlate structural elements over such large areas. In acknowledging this problem, a correlation of structural elements is nevertheless proposed in the case of the Khomas Trough. This is based on a few detailed structural studies which have been undertaken in previous years. In order to improve the confidence level of such a correlation, the study areas of Hälbich (1977) in the east and of Sawyer (1981) and Preussinger (1987) in the Namib Desert Park in the west have additionally been studied by the writer. The correlation is based mainly on the character of foliations, the associations of mineral assemblages with particular deformation periods (see Chapter 6.2) and on fold styles. The proposed correlation is summarized in Table 4.5.

A weakly-developed and transposed S_1 fabric has been reported by all authors except Hälbich (1977) and its existence is acknowledged in Table 4.5. The D_2 phase involved the formation of a penetrative metamorphic banding cleavage, tight to isoclinal folds, thrusts, and an L_2 down-dip mineral lineation. This phase is also associated with the growth of a variety of metamorphic index minerals (Chapter 6.2), all features which are similar to Hälbich's (op.cit.) D_1 phase (Table 4.5). Structural elements of subsequent deformation phases also seem to be comparable throughout the Khomas Trough and show regional importance, including the D_4 phase which is mostly represented by crenulation cleavages and associated open folds. Sawyer's (1981) D_5 and D_6 deformations are minor phases of kink folds comparable to the late-phase kinking event described from the present study. Finally, it is important to point out that there is considerable disagreement on the timing of structural elements between the Central Zone, the Okahandja Lineament Zone, and the Khomas Trough. Whilst Miller and Hoffmann (1981) postulated two earlier deformation phases in the Central Zone, Sawyer

TABLE 4.5: Proposed correlation of deformation phases of various studies in the Khomas Trough. Note that Sawyer (1981) suggests contemporaneous deformation of the Central Zone, Okahandja Lineament Zone and the Khomas Trough. Abbreviations: CZ, Central Zone; OLZ, Okahandja Lineament Zone; KT, Khomas Trough.

Namib desert / Gorob mine		Okahandja-Windhoek Section	Upper Black Nossob River area	Khomas Hochland Escarpment
Sawyer 1981 CZ-OLZ-KT	Preussinger 1987 KT	Hälbich 1977 OLZ-KT	Kasch 1986,1987 Eastern KT	Kukla 1991 (this study) Western KT
D_1	D_1		D_1	D_1
D_2	D_2	D_1	D_2	D_2
D_3	D_3	D_2	D_3	D_3
D_4	D_4	D_3	D_4	D_4
D_5				D_5
D_6				

TIME ↓

(1981) presented evidence that all three zones experienced the same deformation episodes, as shown in Table 4.5.

4.6 Structural evolution of the Khomas Trough fold-and-thrust belt

Various authors have previously speculated upon the structural evolution of the Khomas Trough. Only very little research, however, has been undertaken to study in detail the deformation features within the Khomas Trough to finally present an evolutionary synthesis. Gevers (1963) characterized the "Khomas Highlands" as a tightly folded synclinorium of schists with largely isoclinal folds. Hälbich (1977) based the timing of deformation events "in the absence of marker horizons" on fold styles and subdivided the area into a northern belt with discernible major fold structures and a southern belt with a preponderant schistosity. He drew the boundary in the area of the graphite schist on the farm Kaan of this study. Hälbich (op.cit.) further defined two major synclinal structures (Berlin and Gorogoneib synclines) in the northern Khomas Trough on the basis of photographic interpretation. These cannot be confirmed since the suggested synclinal axes are in fact geographically located within the scapolite schist zones which have proved to separate openly from isoclinally folded areas, with a thrust zone situated in the supposed hinge area.

In conclusion, the structural investigations within this study have revealed the following structural patterns. An initial phase of deformation (D_1) was associated with the formation of folds and a biotite foliation and was accompanied by thrusting. A major deformation period, labelled D_2, involved the formation of: (1) penetrative axial-planar cleavages; (2) tight to isoclinal and open asymmetric folds; (3) downward-facing folds in previously overturned strata; and (4) thrust faults. The cleavage formation parallel to the XY plane of the finite strain ellipsoid was accompanied by the formation of folds of various styles. Folding, thrusting and southeastward-directed structural translation occurred contemporaneously. The major compression was directed towards the northwest and elongation occurred along D_2 axes towards the northeast. This major regional deformation was followed by the D_3 deformation, which was a phase of intensified shear within high-strain zones. A strong spaced cleavage and isoclinal F_3 folds were formed preferentially in these zones. Fluid movement along the D_3 thrusts is indicated by the scapolitization in the northern Khomas Trough. The patterns of the D_1, D_2 and D_3 phases of deformation show that the structural evolution is one of progressive deformation. Late phases of deformation include the formation of crenulation cleavages (D_4) and the formation of kink-folds (D_5) which might indicate layer-parallel faulting. The emplacement of the Donkerhuk Granite took place during these late deformation events and right-lateral strike-slip faulting occurred along the northern margin of the Khomas Trough, indicating an oblique compression direction relative to the margins of the Central Zone. Prominent north south- and northwest-trending fault sets clearly post-date the Donkerhuk Granite and have been attributed a Karoo age by Behr *et al.* (1983).

The above features show that the Khomas Trough deformational history involves several deformation phases which are characterized by contemporaneous folding and thrusting throughout the structural evolution. This has developed laterally extensive, northward-steepening thrust slices within an overall imbricate fan geometry with probably repeated sedimentary sequences. The thrust zones, which are situated in pelitic schists, graphite schists, and amphibolites, have been a locus of both thrusting and shearing throughout the protracted history of the Southern Damara Orogen. This structural style shows striking similarities to the imbricate thrust fan and duplex geometries which have been reported from many compressional fold-and-thrust belts worldwide

(e.g. Boyer and Elliot, 1982; Park, 1988). Examples of these are, amongst others, the Caledonides of Britain, the Alps, the Himalayas, the Appalachians as well as parts of the Pan-African of Mozambique (Shackleton and Ries, 1984) and Marocco (Saquaque *et al.*, 1989). This comparison is especially valid when the distinct changes of structural styles across the thrust slices in the Khomas Trough are considered.

5. THE MATCHLESS AMPHIBOLITE

5.1 General setting of the Matchless Amphibolite

The Matchless Member (SACS, 1980) of the Kuiseb Formation forms a linear outcrop which may be traced for more than 350 km along strike from the Namib desert in the southwest to the Steinhausen area in the northeast (Fig. 2.4). The Matchless Member sequence, here termed the Matchless Amphibolite, consists of interlayered amphibolites (mainly), metagabbros and metasediments. In other areas west and east of the study traverse, Alpine-type ultramafic bodies are also associated with the Matchless Amphibolite (Barnes, 1982).

Several economically important massive sulphide ore bodies and prospects such as Gorob, Hope, Matchless, Kupferberg, Otjihase and Ongombo occur within the sequence. Studies by Finnemore (1978), Sawyer (1981), Barnes (1982), Killick (1983), Miller (1983c), Schmidt and Wedepohl (1983), Breitkopf and Maiden (1987, 1988), Preussinger (1987, 1990) and Klemd *et al.* (1987, 1989) have concentrated mainly on the geochemistry and the ore-forming processes within the Matchless Amphibolite. The main concerns of this study, however, are aspects of the stratigraphic and structural relationships of various metabasic and metasedimentary rock types. Unusually well-preserved outcrops in the study area (Fig. 5.1 ,A) have allowed mapping of several correlative river profiles along strike.

5.2 Lithologies, mineral assemblages and textures

The mafic rock types may be distinguished on the basis of textures and mineral assemblages into: type I, massive, epidote-rich amphibolite; type II, banded, carbonate-rich amphibolite; and type III, coarse-grained amphibolite, i.e. metagabbro. Amphibolitic breccias have also been encountered in the present study. The amphibolites are associated with chlorite schists, pelitic and psammitic schists, graphite schists, and a thin marble unit.

Type I amphibolites are massive, epidote-rich and form units which comprise mostly pillow lavas. Modal compositions are dominated by green and blue-green hornblende, plagioclase and epidote. Minor constituents are chlorite, sphene, clinozoisite, opaque grains, biotite, calcite and quartz. Calcite is much less common than in type II amphibolites and occurs mostly in small layers or segregations, together with chlorite and epidote. Pillow structures which have also been described from other parts of the Matchless Amphibolite (Sawyer, 1981; Miller, 1983c; Breitkopf and Maiden, 1987; Preussinger, 1987) are abundant in all measured sections. They occur as spheroidal to elongated bodies which are separated by seams of epidote amphibolite forming the inter-pillow fillings (Fig. 5.1 ,B).

Type II amphibolites are parallel- to wavy-banded and carbonate-rich. The banding consists of alternations of light bands comprising plagioclase-epidote-calcite-quartz assemblages and dark bands comprising green hornblende-epidote-calcite-quartz-plagioclase assemblages with minor biotite and chlorite (Fig. 5.1, C). Hornblende within the matrix and opaque minerals define the predominant S_2 structural fabric, whereas large hornblende crystals overgrow the S_4 crenulation cleavage.

Type III amphibolites (metagabbros) are coarse-grained and mineralogically uniform, containing mainly porphyroblasts of green hornblende, plagioclase and calcite. Minor constituents are epidote, sphene, chlorite and opaque minerals. Grain sizes are coarse, but a distinct zoning towards finer-grained margins has been observed in association with shear zones (Fig. 5.1, D). Metagabbro lithologies form lensoid, round and irregularly shaped bodies within the amphibolites and at the contacts to metasediments. Sizes are variable from a few metres to several tens of metres in length and width. In one case, a "bleached" margin to the pelitic host rock has developed. The contact zone is extremely fine-grained showing the assemblage quartz-plagioclase-hornblende-chlorite-biotite-epidote. Similar features in other areas along the Matchless Amphibolite have been interpreted as "chilled" intrusive margins (Preussinger, 1987; Breitkopf and Maiden, 1987).

Amphibolite breccias have been found in parts of the sequence containing clasts several tens of centimetres long or aggregates comprising hornblende and chlorite in a matrix of both type: I and type II amphibolites (Fig. 5.1, E). Cherts occur as several-cm-long "clasts" in type I amphibolites in the structural footwall of the Matchless Amphibolite on the farm Annelie (Fig. 5.1, F).

Associated with the amphibolites are extremely fine-grained chlorite schists, chlorite-hornblende schists and biotite schists. These comprise mainly chlorite, epidote, biotite, hornblende and opaque minerals. Minor constituents are plagioclase, calcite, quartz, garnet, sphene and clinozoisite.

Several graphite schists are associated with the Matchless Amphibolite and a distinct dolomitic marble unit occurs in the hanging wall of the sequence.

Field observations, such as the conformable intercalation of metasediments with amphibolites, the lateral extent of the fine- to medium-grained amphibolites and the recognition of pillow lavas, suggest that the amphibolites were derived from mafic extrusive rocks. The interpretation of the metagabbros as metamorphosed mafic intrusives is based on partly-developed bleached marginal zones with sediments and amphibolites, and on coarser-grained cores compared with the rims. The metagabbros, however, have mostly been subjected to structural displacement and dismemberment which will be discussed later.

5.3 Stratigraphic and structural relationships

5.3.1 Stratigraphy

Three traverses within the Matchless Amphibolite sequence have been studied in detail and these are shown in Figure 5.2. The measured sections confirm that the overall structural thickness of the Matchless Amphibolite is in the order of 1500 m in this area. There are basically three major units developed: (1) a structurally lower unit consisting of

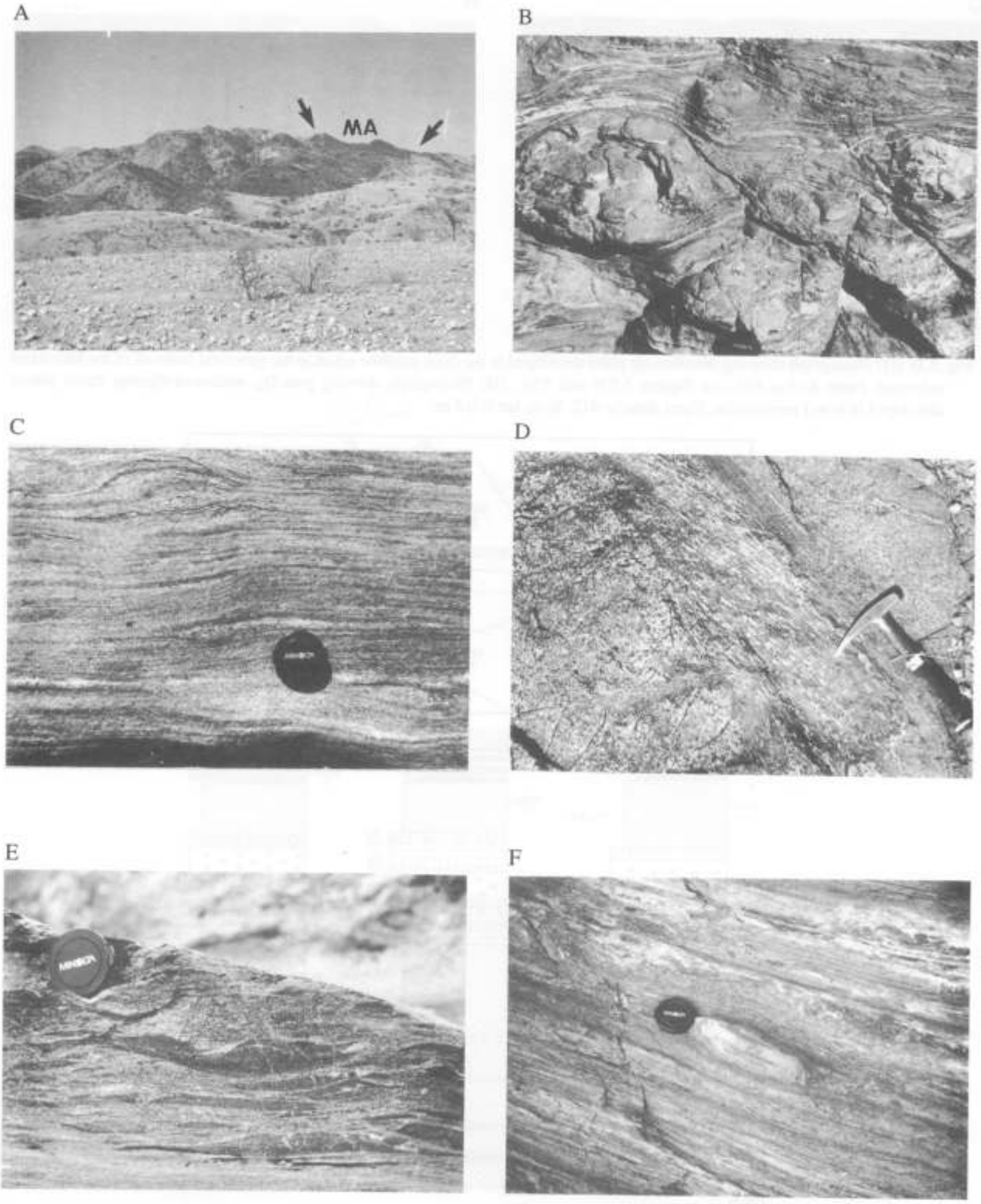

Fig. 5.1: (A) Photograph showing the Matchless Amphibolite (indicated by arrows) as a prominent feature in the landscape on the farm Annelie 412 (see profile A in Figure 5.2). (B) Slightly deformed pillow structures wrapped around by extremely sheared pillows and inter-pillow fillings in type I amphibolites. Farm Annelie 412 (profile A in Figure 5.2); lens cap is 4.9 cm in diameter. (C) Carbonate-rich, banded type II amphibolite. Farm Kobos 305 (profile B in Figure 5.2). (D) Photograph showing structurally emplaced metagabbro body in type I amphibolite. Note extremely sheared margins, emphasized by plagioclase elongation. Amsas river profile, farm Kobos 305. (E) Photograph showing amphibolitic breccia, consisting of elongated, massive, type I amphibolite clasts within type II amphibolite matrix. Farm Kobos, Amsas river (profile B in Figure 5.2). (F) Chert nodules developed in type I amphibolite in the footwall of the Matchless sequence on the farm Annelie 412 (see Figure 5.4).

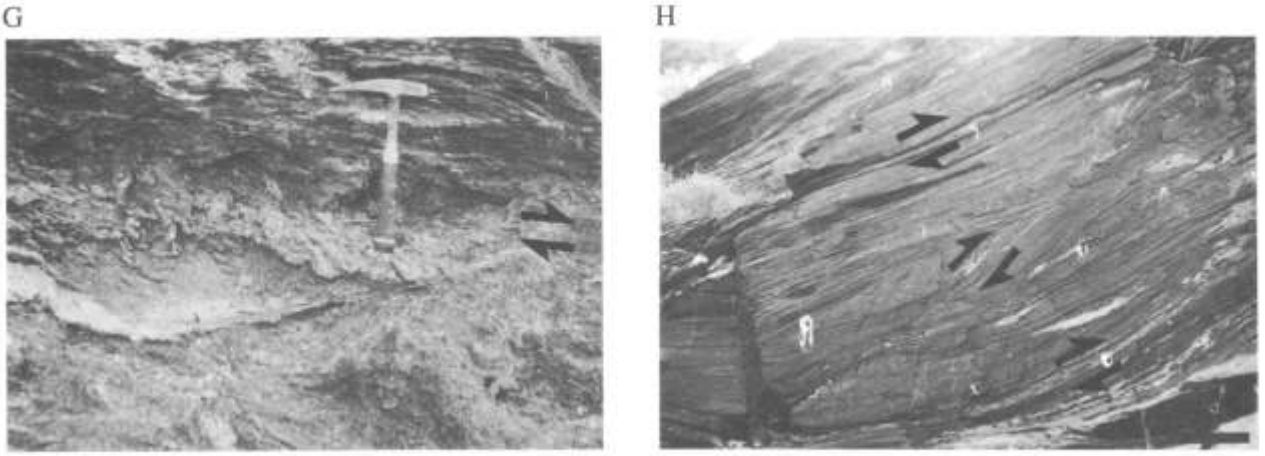

Fig. 5.1: (G) Photograph showing décollement plane developed in the thick graphite schist in the structural footwall of the Matchless sequence. Farm Kobos 305 (see Figures 5.2,B and 5.5). (H) Photograph showing post-D_2, northwest-dipping thrust planes developed in type I amphibolite. Farm Annelie 412. Scale bar is 0.5 m.

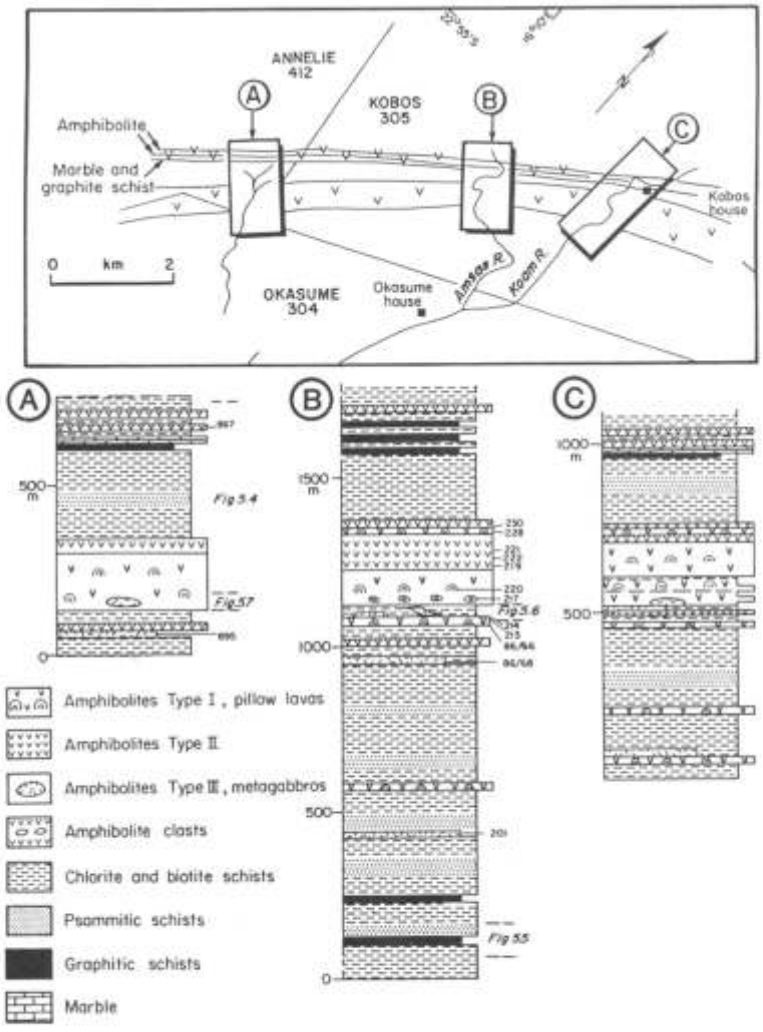

Fig. 5.2: Map and detailed measured sections A - C along the Matchless Amphibolite. Also shown are positions of geochemistry samples within the Annelie (A) and Amsas (B) river profiles and locations of Figures 5.4 - 5.7.

intercalated graphite schists, pelitic schists and minor psammitic schists, metagabbros and amphibolites; (2) a middle unit comprising massive and banded amphibolites as well as some metagabbros; and (3) an upper unit with intercalated pelitic schists, graphite schists, a marble unit and amphibolites (Fig. 5.2).

A comparison of the sections in Figure 5.2 shows that metagabbro bodies occur preferentially in the lower parts of the sequence, mostly at contacts of amphibolites with sediment. Carbonate-rich type II amphibolites occur in the upper parts

and pillow lavas mostly in the massive middle unit together with breccias. Graphite schists and graphitic pelites up to several metres thick occur in the structural footwall of the sequence. A thick graphite schist unit in this position has also been described from the Gorob area further to the west (Sawyer, 1981; Preussinger, 1990). The meta-sediments throughout the studied sections are mainly pelitic with, however, a strong predominance of chlorite schists.

Bed thicknesses do not exceed 15 cm. Graded layering provides way-up criteria indicating mostly right-way-up and some inverted sequences. In the upper part of the Matchless sections, the marble unit is up to 2 m thick and occurs rather continuously along strike for more than 10 km (Fig. 5.2). The layer is strongly boudinaged which most likely accounts for the occasional non-recognition of this unit as in traverse B (Fig. 5.2). The occurrence and thickness of graphite layers in the structural hanging wall varies along strike.

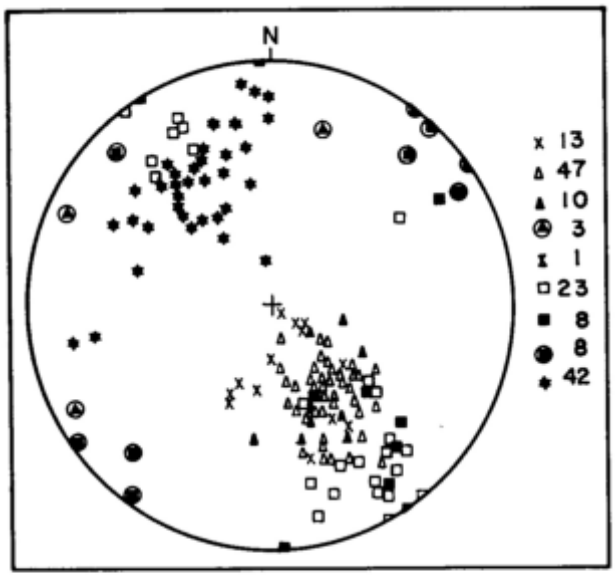

Fig. 5.3: Stereonet showing structural data from amphibolites and metasediments of the Matchless Amphibolite. Note sub-horizontal to plunging attitude of fold axes. For explanation of symbols see Table 4.3.

5.3.2 Structure

As with the surrounding Kuiseb schists, the structural geology of the Matchless Amphibolite is characterized by folding and thrusting. According to the timing of deformational events established in Chapter 4, D_2 is generally the main folding phase, which accounts for the development of strongly isoclinal, metre-scale folds and a penetrative, northwest-dipping S_2 cleavage (Fig. 5.3). Elongated biotites and hornblendes form a pronounced down-dip L_2 lineation which shows its strongest development in the Matchless Amphibolite zone relative to other areas of the study traverse as a whole. Pillow bodies are also strongly elongated down-dip on S_2 planes. Other features are the S_3 biotite fabric, which is recognizable in intercalated biotite schists, and a strong S_4 crenulation cleavage. The structural features within the Matchless Amphibolite show all characteristics of high-strain zones which have been described in the structural context of the overall study traverse in Chapter 4.4.2. On a small scale, the alternation of low- and high-strain zones in vertical profiles is illustrated in Figure 5.4 by the shape of pillows, some of which have their spheroidal shape preserved, whereas others are extremely elongated. Thrusting is generally evident from the displacement of type I and type II amphibolites, metagabbros and metasediments as well as from the development of shear zones. The pronounced L_2 lineation has been interpreted to have formed parallel to tectonic transport direction in thrust zones (Chapter 4).

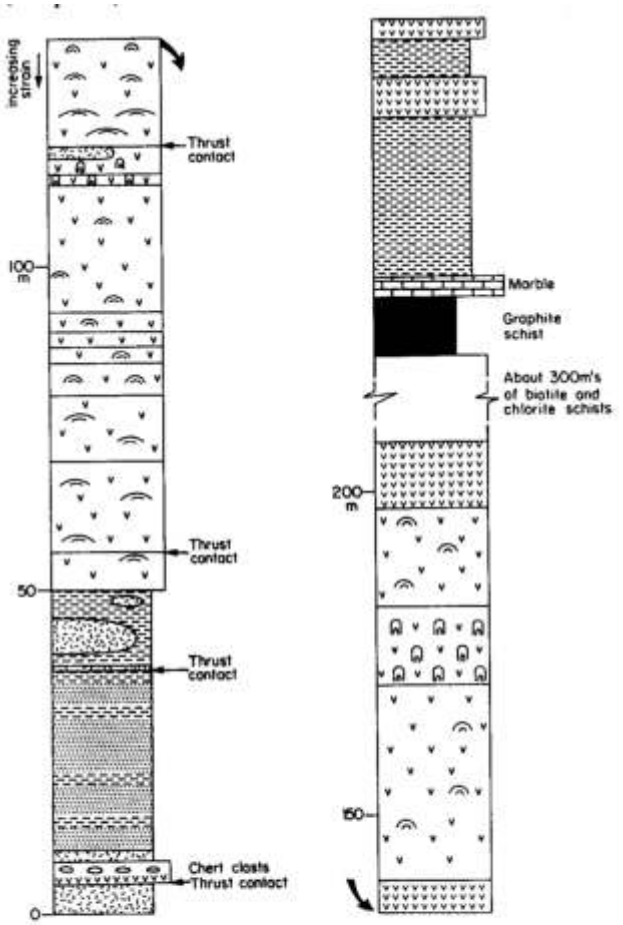

Fig. 5.4: Detailed measured section (profile A in Fig. 5.2) showing the interposition of amphibolites, metagabbros and metasediments. Major thrust contacts are indicated and the spheroidal to elongate shape of pillows (distinguishable by the degree of curvature of the pillow symbol in the figure, e.g. in the top part of the left column) is regarded as a measure of the imposed strain (for symbols see Fig. 5.2).

High-strain zones are associated with thrusting which is particularly evident in the lower part of the sequence in the Annelie section where major thrust contacts occur (Fig. 5.4). A major horizon of displacement is developed at the base of the lower most graphite schist (Fig. 5.5) with a décollement plane indicated by the disruption of layering and fabrics, silicification, quartz-segregation and sulphide precipitation (Fig. 5.1, G). Further upwards, displacements and shear zones are mainly observable at the contacts of metasediments, metabasalts and metagabbros (Fig. 5.4).

Structural displacement of the metagabbros is postulated on the basis of contact relationships between amphibolites

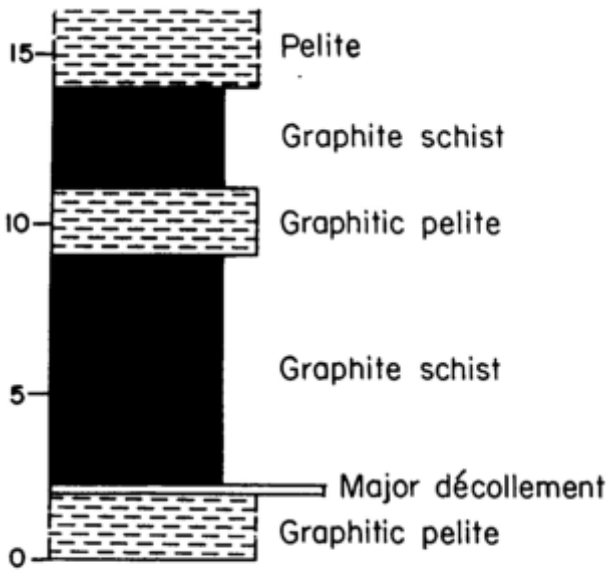

Fig. 5.5: Diagram showing graphite schists developed in the Amsas river section. A major décollement is developed in the lower part of the sequence. The location of the profile is indicated in Figure 5.2,B.

5.1, D). Some of the bodies confirm the overall southeastward-directed vergence and displacements by their overall shape and by the internal shear fabric (Fig. 5.6).

The main thrusting event has occurred syn- to post-D_2 (Figs 5.7 and 5.1, H) which is inferred from the associated shearing of the S_2 cleavage and the unaffected S_3 fabric. Post-D_3 thrusting also occurs, however, as illustrated by the shearing of D_3 structural elements in parts of the sequence. The D_4 crenulation cleavage post-dates these events.

Concluding the above, thrusting and shearing identify the Matchless Amphibolite as a highly and heterogeneously strained zone situated within pelites of the Kuiseb Formation. Graded layering suggests that the overall sequence is upward-facing. Structural dislocation is especially indicated in the lower parts of the sequence with the interposition of thinly layered amphibolites, pelitic schists, graphite schists and metagabbro bodies. Upper parts of the sequence show a more coherent relationship between carbonate-rich amphibolites and units of graphite schist and marble.

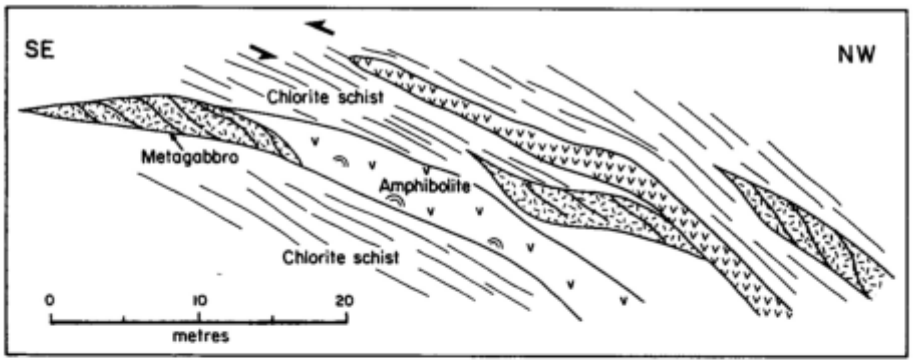

Fig. 5.6: Sketch showing the structural interposition of sheared metagabbro bodies with type I and type II amphibolites and with chlorite schists. Note sigmoidal internal shear fabric of the metagabbros. The location and symbols are shown in Figure 5.2,B.

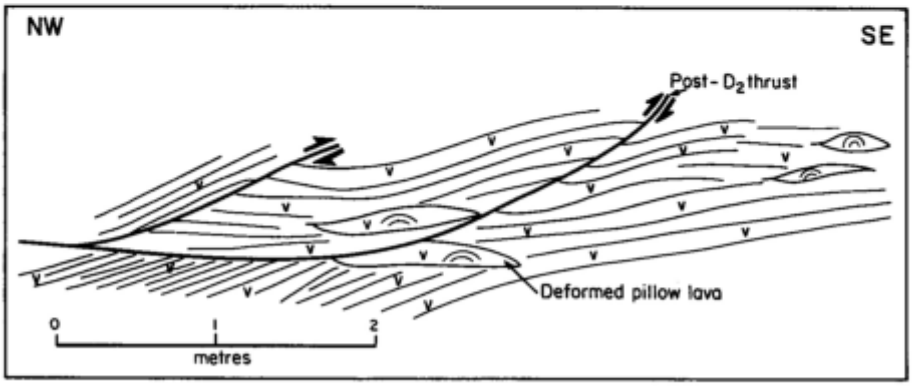

Fig. 5.7: Structural sketch showing post-D_2 thrusting within a pillow lava sequence on the farm Annelie (see Fig. 5.2,A). Note the sheared pillow structures. Form lines represent S_2 structural fabric. For symbols see Figure 5.2.

and metasediments. Metagabbro always occurs in bodies which are up to 10 m thick but which terminate mostly within the lateral extent of the outcrop (Fig. 5.6). The majority of the contacts with associated lithologies are sharp and the rims of the metagabbro lenses are extremely sheared (Fig.

5.4 Classification of metabasic rocks

Over and above the study of field relationships, a classification and chemical characterization of the amphibolites and metagabbros within the Matchless Amphibolite was

aimed at determining the nature of the Matchless metabasic rocks. Geochemical analyses of 23 major and minor elements were undertaken by XRF analysis on 14 amphibolite and metagabbro samples from along the Amsas river profile and the profile on the farm Annelie. Sample locations are indicated in Figure 5.2 and full analyses are presented in Appendix II.

The geochemistry of the Matchless metabasites has previously been investigated in detail in a number of studies (Finnemore, 1978; Miller, 1983c; Schmidt and Wedepohl, 1983; Breitkopf and Maiden, 1987; Klemd *et al.*, 1989). In particular Miller (op.cit.) and Breitkopf and Maiden (op.cit.) put emphasis on element mobility during hydro thermal alteration and metamorphism. These authors showed that the high field-strength elements (small size, high charge) such as Zr, Y, Nb, Ti, and Al may be considered to have behaved in an immobile fashion. Most major elements, on the other hand, have been considerably mobile. These results from the Matchless Amphibolite confirm the findings of Pearce (1975) and Garcia (1978) from studies of various metabasalts elsewhere. Major element mobility is also indicated by plotting data of this study in the classification diagram of Cox *et al.* (1979) which shows a wide spread of compositions for the analysed samples mostly within the basalt field (Fig. 5.8).

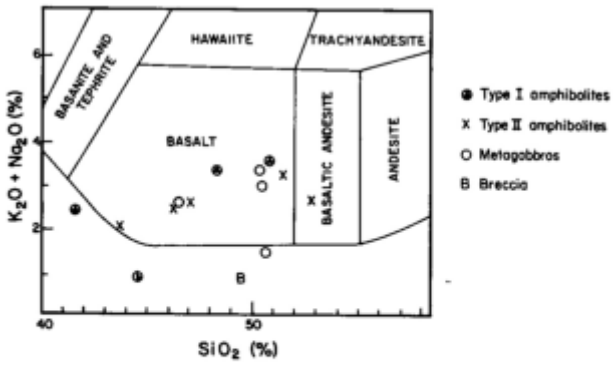

Fig. 5.8: Variation diagram $K_2O + Na_2O$ versus SiO_2 after Cox *et al.* (1979) classifying amphibolites and metagabbros of the Matchless sequence as basalts.

A distinct tholeiitic trend for the amphibolites is defined by the TiO_2 versus Zr diagram of Floyd and Winchester (1975) which shows the majority of the samples exclusively in the oceanic tholeiite field (Fig. 5.9). This is confirmed by the diagram of Miyashiro and Shido (1975) which is based on absolute contents of SiO_2 and Cr (Fig. 5.10). Judging from these data the Matchless amphibolites may be classified as tholeiitic metabasalts.

In acknowledging the problem of element mobilities, the discrimination diagrams most widely used to deduce the tectonic setting of basaltic rocks are those employing the above mentioned elements which have proved immobile in many studies. The diagram of Pearce and Cann (1973) uses Ti, Zr and Y and the Matchless samples cluster in the ocean-floor basalt, within-plate basalt (i.e. continental and ocean-island basalt), and island-arc fields (Fig. 5.11). The Zr/Y versus Zr diagram of Pearce and Norry (1979), however, characterizes all samples, apart from one metagabbro sample, as mid-ocean ridge basalts (MORB; Fig. 5.12).

In conclusion, the Matchless amphibolites represent metamorphosed equivalents of igneous rocks of tholeiitic basaltic composition. Although some of the analysed amphibolites plot close to and in the within-plate basalt field, the majority show geochemical affinities to mid-ocean ridge basalts.

A comparison of average geochemical compositions of the Matchless amphibolites with those of within-plate and plate-margin basalts, as compiled by Carmichael *et al.* (1974), Pearce (1976) and Condie (1982), shows that most elements, but especially the more immobile TiO_2, Zr, Y, Co and Cr, compare best with low-K ocean-floor basalts from diverging plate regimes.

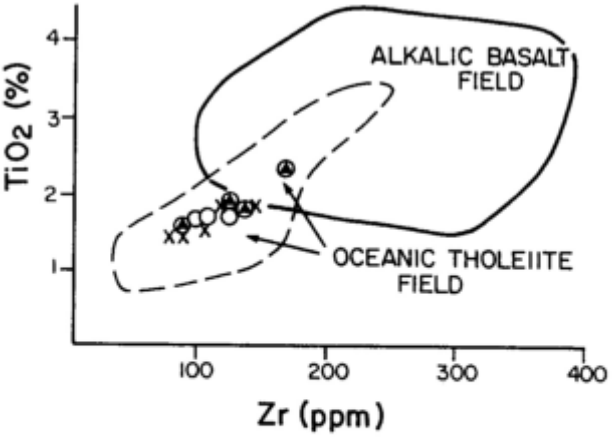

Fig. 5.9: Variation diagram TiO_2 versus Zr after Floyd and Winchester (1975). The majority of the Matchless metabasites plot within the oceanic tholeiite field. Symbols as for Figure 5.8.

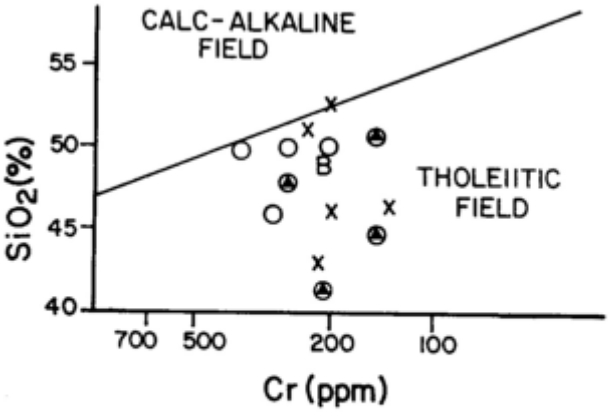

Fig. 5.10: Matchless Amphibolite samples plotted on the variation diagram SiO_2 versus Cr after Miyashiro and Shido (1975). The tholeiitic character of the Matchless metabasic rock types is evident. Symbols as for Figure 5.8.

These data confirm the results of Finnemore (1978), Miller (1983c) and Schmidt and Wedepohl (1983) who found exclusively mid-ocean ridge-type compositions for the Matchless metabasalts. This is in contrast with the findings of Breitkopf and Maiden (1987) who described within-plate compositions of metabasalts in the western Khomas Trough

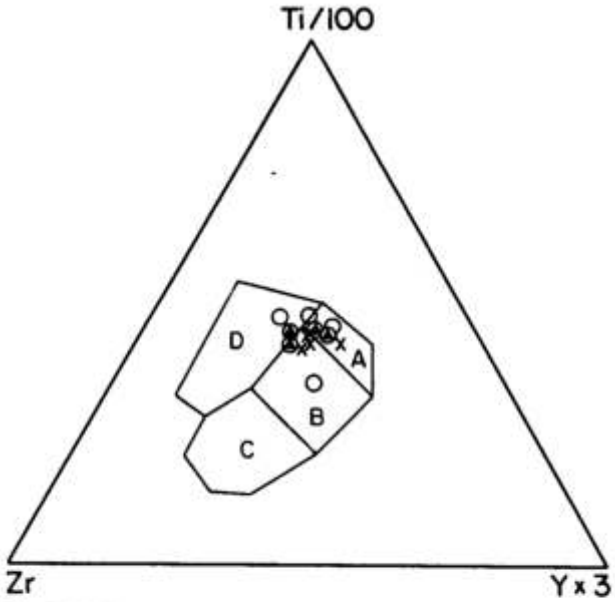

Fig. 5.11: Matchless Amphibolite samples plotted on the triangular variation diagram after Pearce and Cann (1973). Within-plate basalts plot in field D, ocean-floor basalts in field B, island-island arc tholeiites in fields A and B and calc-alkali basalts in fields C and B. Symbols as for Figure 5.8.

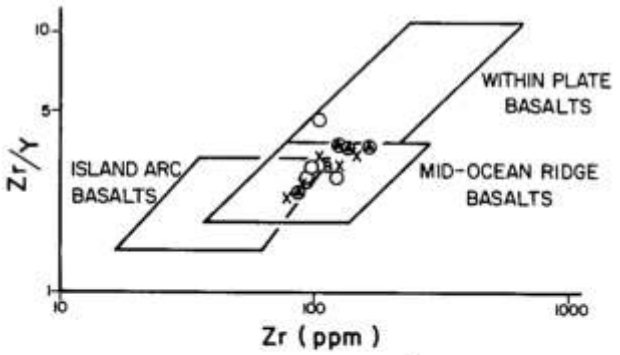

Fig. 5.12: Variation diagram Zr/Y versus Zr after Pearce and Norry (1979) showing the mid-ocean ridge basalt (MORB) affinity of the Matchless metabasites. Symbols as for Figure 5.8.

and mid-ocean ridge basaltic compositions to the east of Windhoek.

5.5 Tectonic setting of the Matchless Amphibolite with special regard to the development of the Khomas Trough

In summary, detailed sections through the Matchless Amphibolite show the sedimentological and structural interposition of various amphibolites, metagabbros, amphibolite breccias, pelitic schists, some psammitic schists, graphite schists and a marble unit. Structural emplacement is indicated especially in the lower parts of the sequence. Serpentinites which are derived from mantle harzburgites are a structurally dismembered part of the sequence as well (Barnes, 1982). Genetically, the extrusive origin of the amphibolites in a submarine environment is confirmed by pillow lavas and gradational contacts with pelitic and some psammitic sediments. Graded layering within sequences of amphibolites, metagabbros and various sediments demonstrates the generally contemporaneous aspect of turbidite and pelagic sedimentation and mafic extrusion and intrusion. Isotope signatures of graphite schist and marble (see Chapter 3) confirm, in addition, contemporaneous biogenic sedimentation and hydro thermal magmatic activity on the sea floor. Geochemical analyses reveal an oceanic tholeiitic character and a close affinity of the Matchless metabasic rocks to mid-ocean ridge basalts.

Since more detailed studies have been carried out during the last decade, the genesis and tectonostratigraphic importance of the Matchless Amphibolite has been discussed intensively and several models have been presented. The basic question which has arisen is whether or not the metabasalts are of plate-margin or intraplate origin. Finnemore (1978) concluded his initial geochemical studies, characterizing the amphibolites as having followed a tholeiitic differentiation trend but within an ensialic crust, which he interpreted because of a perceived lack of field evidence for a collisional orogeny. From geological comparisons with similar settings, Hartnady (1978) suggested that the Matchless massive sulphide deposits may have been formed both in Red Sea-type settings and also at mid-ocean ridges. Schmidt and Wedepohl (1983) found exclusively MORB major and minor element patterns along the entire Matchless Amphibolite. Furthermore, rare earth elements demonstrate a very flat element pattern i.e. a very small degree of fractionation of the light rare earth against the heavy rare earth elements. These patterns are characteristic for ocean-ridge tholeiitic basalts (Menzies, 1976). The authors concluded their study with a statement that, judging from the lack of evidence for ophiolitic suites and deep-sea sediments, the Damara Orogen must have formed on sialic crust although all geochemical signatures point towards mid-ocean ridge basalts and low-K tholeiites.

From tectonostratigraphic considerations Kasch (1983a) postulated that the Matchless Amphibolite either represents a fragment of oceanic crust emplaced in an active subduction complex or that basaltic magmas intruded into trench deposits. Miller (1983c) also found evidence for tholeiitic trends from geochemical studies and envisages the formation of the basalts and massive sulphide deposits in a Red Sea-type situation with volcanics and intrusives occurring above a buried mid-ocean ridge with minor amounts of oceanic crust. Considering the massive sulphide mineralization and their host rocks, Killick (1983) concluded that the deposits were most probably formed at a site of seafloor spreading at a constructive plate margin.

Breitkopf and Maiden (1987) found that the western Matchless Amphibolite shows a considerable amount of fractionation which they related to the presence of continental crust in this area. In contrast to this, samples from the eastern part show little fractionation and were interpreted by Breitkopf and Maiden (op. cit.) to have developed in small strike-slip related pull-apart sub-basins underlain by oceanic crust.

Klemd *et al.* (1989, p. 615) concluded their geochemical studies of the Matchless massive sulphide ore deposit with a model which involves "... seafloor precipitation of metal sulphides from convecting hydro thermal fluid generated

by reaction of seawater with sub-seafloor basalts and clastic sediments".

In view of the massive sulphide mineralization, Rona (1988), in his compilation of massive sulphide deposits associated with oceanic ridges worldwide, gives statistics concerning the tectonic settings of these deposits. These show that basalt-hosted massive sulphides, which may have formed in oceanic hydrothermal settings, constitute about 17% of the 508 deposits considered; sediment-hosted deposits associated with oceanic volcanic rocks form about 9%. The most numerous and largest deposits occur in subduction-related volcanic suites and island-arc or continental-rift tectonic settings which are associated with rhyolites. Rona (op.cit.) further states that all major massive sulphide deposits associated with basalts in the ancient record are related to oceanic ridges and rifts.

Thus, the sum of stratigraphic, sedimentological, structural and geochemical data from the Matchless Amphibolite suggests an interaction of contemporaneous pelagic sedimentation, turbiditic sedimentation and formation of massive sulphide deposits in an oceanic setting. This allows a comparison with oceanic ridge settings close to adjacent continents, such as in the eastern Pacific. There sediment-hosted massive sulphide deposits are associated with volcanics of MORB composition, such as in the Escabana Trough of the southern Gordaridge (Morton *et al.*, 1987) and in the Middle Valley (Endeavour segment) of the Juan de Fuca ridge (Davis *et al.*, 1987). Similar associations of meta-greywackes and pelagics with only minor amounts of oceanic pillow basalts, cherts and some ultramafics (without sheeted dykes) in ancient terrains are known from parts of the Cordillera Belt, such as the Slide Mountain and Quesnel terrains (Coney, 1989) and from the Central Appalachians (Lash, 1986). Judging from these data the Matchless Amphibolite is interpreted here to represent the upper part of an oceanic crustal sequence.

6. METAMORPHISM

6.1 Introduction

Studies on the metamorphic evolution of the Khomas Trough were undertaken by Hoffer (1977) as part of a large-scale investigation on the thermal evolution of the Damara Orogen. Metamorphism of the eastern Khomas Trough has been studied by Kasch (1983b, 1987); whereas Sawyer (1981) and Preussinger (1987, 1990) studied the metamorphism of the western Khomas Trough.

Taking the approach and the findings of the latter studies into account, it is the aim of this chapter to present an overview of the critical mineral assemblages and textures of pelites and calcareous rocks encountered along the study traverse and to place crystallization events within the framework of the structural development of the Khomas Trough. The pelites of the Kuiseb Formation are most suitable for studies of the stability conditions during metamorphism. Mineral compositions of pelites from crucial areas have been determined by microprobe analysis. These, together with data derived from mineral assemblages, lead to qualitative and some quantitative pressure - temperature (P-T) estimates.

6.2 Mineral textures and relationships to structural elements

Textural relationships of mineral assemblages indicate their relative time of formation during consecutive deformation phases. The study of mineral - fabric relationships is facilitated by the fact that original sedimentary layering is largely preserved in the metasediments. Figure 6.1, A shows a graded turbidite layer with psammitic compositions at the base consisting mainly of quartz, plagioclase and biotite. The thin pelitic top, however, shows staurolite strongly aligned with the bedding plane within a matrix of mainly biotite, with minor quartz and plagioclase. This is an excellent demonstration that the development of specific mineral phases and assemblages depended largely on the respective small-scale bulk rock compositions.

Modal compositions of pelites, which have also been analysed chemically (see 6.4), are shown in Table 6.1. Sample 86176 is a chlorite schist and sample 306 contains scapolite as a major constituent. The composition of an average psammite is shown for comparison (sample 816 in Table 6.1). The relative timing of deformation phases D_1 to D_4, which has proved to be associated with cleavage development (Chapter 4) and related crystallization events, is presented in Table 6.2.

6.2.1 Pelites

Quartz is a major constituent of the groundmass of pelites and occurs as recrystallized grains of variable sizes. In the southern-most part of the traverse, close to the contact with the Southern Margin Zone, as well as in shear and thrust zones throughout the traverse, quartz is highly strained, as indicated by undulous extinction and subgrain development.

Plagioclase is a common constituent in all rock types along the study traverse. The crystals are usually very small, xenomorphic and occur in clusters together with quartz. Sericitization is common and only very few twinned grains have been found.

K-feldspar occurs in coarsely recrystallized pelites as microcline, at the northernmost margin of the study traverse in the Kaan river up to several hundreds of metres south of the contact with the Donkerhuk Granite.

TABLE 6.1: Modal compositions of selected pelites (146, 86/76, 274, 109), scapolite schists (306, 308) and a psammite (816) of the Khomas Trough (sample localities are shown in Figure 6.2).

SAMPLE	146	86/76	274	306	308	109	816
quartz	22	5	26	22	16	22	61
plagioclase	7	4	2	< 1	16	14	14
biotite	36	36	27	31	35	33	24
muscovite	33	8	27	< 1	7	28	< 1
garnet	2	1	< 1		5		
staurolite					3		
andalusite			4				
sillimanite					10	2	
scapolite				39	5		
chlorite		44	13	< 1	1	< 1	
green amphibole				6			
calcite				< 1			
opaque ore	< 1	2	1		1	< 1	< 1
tourmaline	< 1	< 1	< 1		< 1	< 1	< 1
sphene				< 1			
zircon	< 1	< 1	< 1	< 1	< 1	< 1	< 1
apatite	< 1	< 1	< 1	< 1	< 1	< 1	< 1
clino-zoisite				< 1			

Biotites are subidioblastic to xenoblastic red-brown to green-brown crystals. Generally, biotite has crystallized syn- and post-kinematically during various deformation phases (Table 6.2). This is inferred from the alignment of the biotite generations within respective cleavage domains as well as from overprinting relationships of various biotite fabrics. Syn-kinematic biotites occur as small thin tablets and define the composite cleavage in the south, the S_1, S_2 and S_3 penetrative cleavages further north, as well as the distinct L_{2A} mineral lineation. The first biotite fabric formed during the D_1 deformation and has subsequently been wrapped around and enclosed by biotites formed during the main deformation D_2 (Fig. 4.10). A third biotite fabric formed during D_3 and clearly overprints earlier biotite generations (Fig. 4.10). Post-kinematic biotites occur throughout the traverse. These crystals are unoriented, up to several millimetres long and overgrow the penetrative cleavages as well as the D_4 crenulation cleavage. Biotites have also formed as reaction products around and within garnets. Frequent inclusions in biotites are quartz, zircon (with pleochroic haloes), muscovite, apatite and rutile.

Muscovites occur basically in two different modes. The

TABLE 6.2: Relative timing of deformation phases and metamorphic crystallization in the western Khomas Trough.

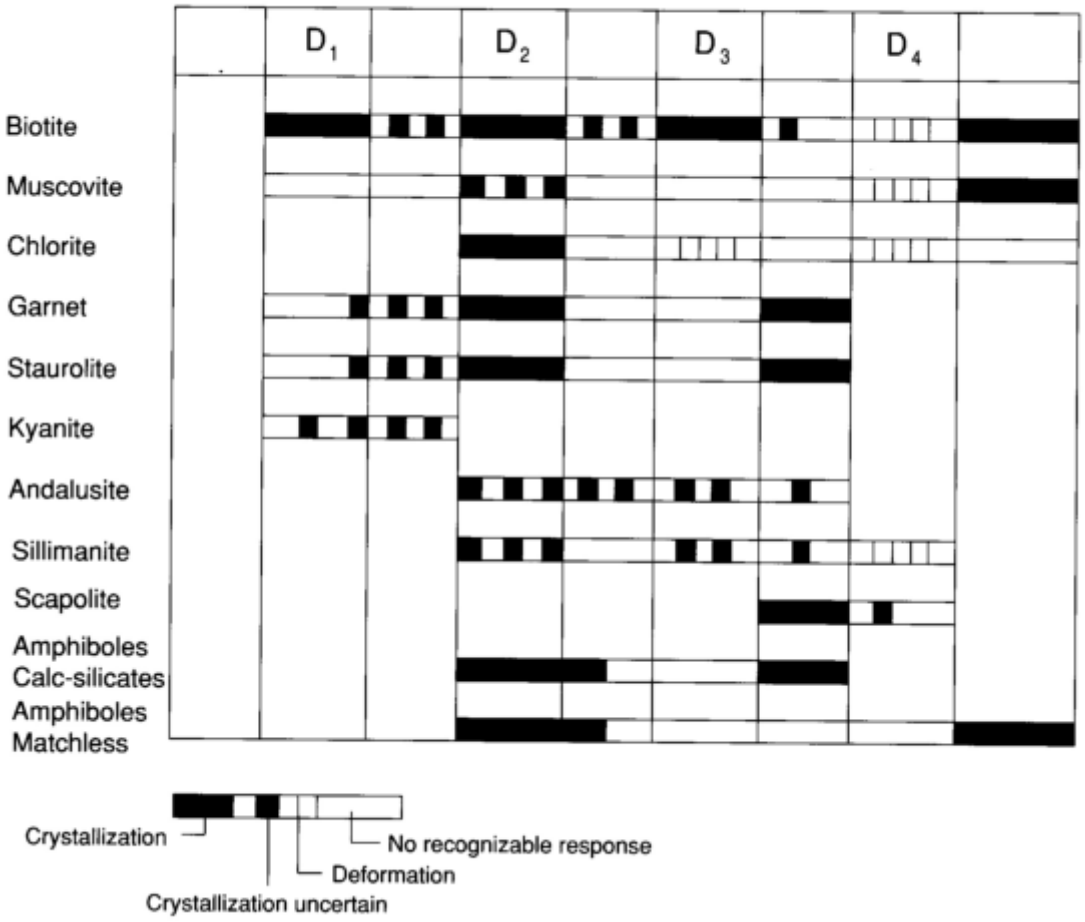

first type is that of matrix muscovites which were oriented in the composite cleavage in the southern Khomas Trough and within the S_2 cleavage in the north. These muscovites were deformed within late crenulation cleavage domains (Table 6.2). The second type of muscovite has grown after the D_4 phase of deformation and occurs as small grains within the matrix but also as large porphyroblastic crystals which are up to several millimetres long. Crystallization under stress-free conditions (post-D_4) is indicated by radial muscovite bundles. A striking and widely distributed feature of the central and northern Khomas Trough is the alteration of alumo-silicates such as andalusite and sillimanite, as well as of staurolite to muscovite.

Chlorite formation during prograde metamorphism in the southern part of the traverse is related to the D_2 deformation which is evident from assemblages containing chlorite, syn-D_2 garnet and biotite. Chlorite forms the matrix of rocks with suitable bulk compositions. Retrograde chloritization of biotite, garnet and staurolite occurs especially in the high-strain zones throughout the traverse.

Garnet occurs in three different generations. Garnet I is anhedral and poikiloblastic and is elongated within the composite fabric of the southern Khomas Trough with length/width ratios of up to 10: 1. The time of crystallization of this generation is somewhat uncertain but a pre-D_2 age is judged from textural relationships with syn-D_2 minerals and from subsequent garnet generations. Garnet II is subhedral to euhedral and shows internal snowball inclusion trails of opaque phases within the $S_{0,1,2,3}$ composite fabric (Fig. 6.1, C) and the S_2 biotite fabric, thus indicating synkinematic crystallization during D_2. Garnet III is also subhedral to euhedral and overgrows the S_3 cleavage, but pre-dates the S_4 crenulation cleavage. Sizes of garnet porphyroblasts increase northwards.

Staurolite I crystallization prior to D_2 might be indicated in the southern Khomas Trough where staurolite porphyroblasts are wrapped around by the composite cleavage (Fig. 6.1, D). Staurolite II porphyroblasts are anhedral, poikiloblastic and have formed syn-D_2 in association with garnet II. In the north, staurolite III has crystallized post-D_3 as is shown by the overgrowths on the S_3 cleavage (Fig. 6.1, E).

Kyanite is only developed in the most Al-rich pelites in the southern Khomas Trough and occurs as xenomorphic grains which are strongly elongated in the composite cleavage. Contact relationships show that this kyanite generation pre-dates garnet II. Kyanite has also been observed together with quartz and chlorite in segregational spaces. Time constraints are lacking for this kyanite generation.

Andalusite occurs within a confined area about 3 km wide in the centre of the Khomas Trough. Most of the andalusite has been replaced by muscovite and forms elongate aggregates up to 10 cm in length. The age of crystallization of the andalusite is uncertain since both orientation within S_2 cleavage domains and unoriented overgrowth on the S_2 fab-

ric have been observed. Garnet III, however, occurs in an assemblage with the andalusite, possibly indicating a syn- to post-D_3 growth of the andalusite.

Sillimanite occurs as fibrolite which is frequently intergrown with biotite. The fibrolite knots are elongated with their long axes parallel to both the S_2 and the S_3 biotite fabric. Although sillimanite is known to grow epitactic on earlier biotites, which could mistakenly be interpreted as synkinematic growth, it has been observed that S_3 biotites are wrapped around the fibrolite knots. Fibrolite is, however, mostly oriented within the S_3 cleavage. Further crystallization constraints come from contact relationships with post-D_3 staurolite III and garnet III, indicating a post-D_3 growth of the sillimanite together with these minerals. Fibrolite bundles are deformed within the D_4 crenulation cleavage.

Scapolite is the major constituent of scapolitized psammites and pelites in the northern Khomas Trough. The scapolite forms a large proportion of the total rock volume in these areas and occurs most massively along veins and fractures, thus proving discordant relationships (Fig. 6.1 ,p). The scapolite poikiloblasts are up to 1 cm across and enclose the S_2 and S_3 biotite fabrics which indicates post-D_3 crystallization (Fig. 6.1, G). The poikiloblasts enclose quartz, biotite, calcite and minor amounts of tourmaline and sphene. Plagioclase has not been observed in most massively scapolitized rocks but occurs in increasing amounts away from the scapolitized areas.

Graphite is a major constituent of the graphite schists which occur mostly in thin units «10 m) at various points through the traverse. The amount of graphite ranges from about 20% to 80% of the total rock volume.

Accessory minerals in all pelitic rocks are tourmaline, zircon, apatite and opaques.

6.2.2 Calcareous lithologies

The constituents of the *calc-silicates* throughout the traverse are quartz, plagioclase, calcite, amphiboles (common and green hornblende), biotite, muscovite, chlorite, garnet, scapolite, epidote, clinozoisite and sphene. Minor amounts of diopside, apatite, tourmaline, rutile and opaque minerals are also present. The calc-silicate layers and spindles (Chapter 3.5.5) are frequently zoned, with light cores containing mainly quartz, plagioclase, calcite, garnet and scapolite and dark rims consisting of amphiboles and epi-dote, but scapolite sometimes occurs at the rims as well.

The timing of calc-silicate formation is best constrained by the amphiboles. The first amphibole generation is strongly aligned parallel to the S_2 cleavage but has also been bent along the spindle walls. This indicates that amphibole growth started syn-kinematically and lasted until post-D_2. The second amphibole generation is poikiloblastic and overgrows the original spindle outline as well as the S_3 fabric thus indicating post-D_3 crystallization (Fig. 6.1, H; Table 6.2).

On the farm Kaan 309, aim-thick, strongly weathered *tremolite schist* has been found below the thick graphite schist (Fig. 6.2). The layer consists almost exclusively of tremolite with only minor amounts «5%) of quartz and biotite being present.

The 2 m-thick *marble* horizon overlying the Matchless Amphibolite sequence comprises a recrystallized matrix of dolomitic carbonate, which was confirmed by X-ray diffraction analysis and staining. Only minor amounts of quartz are present as well as traces of white mica.

6.3 Mineral assemblages

The mineral assemblages encountered along the study traverse are diagnostic for medium-grade metamorphic terrains as classified by Winkler (1979). Assemblage zones have been defined on the basis of Al-silicate phase changes and reaction-isograds. The assemblage zones together with the respective assemblages (a) to (i) are shown in Figure 6.2. Furthermore, mineral assemblages are illustrated in AFM diagrams and their approximate position in the Al-silicate system, as delineated by various experimentally determined reaction curves, is shown in Figure 6.3.

(a) Assemblage zone 1

Hoffer (1977) pointed out that a large part of the southern Khomas Trough is characterized by assemblages comprising kyanite, staurolite, biotite and chlorite. The southern boundary of the study traverse, at the confluence of the Kuiseb and Koam rivers, is situated close to Hoffer's (op. cit.) isograd (3) which demarcates the "kyanite-in" reaction. The diagnostic mineral species in assemblage zone 1 of this study are garnet, kyanite, staurolite, muscovite, biotite, chlorite, plagioclase and quartz in the pelitic rocks. From south to north the following mineral assemblages are developed in this zone:

(a) kyanite + garnet + biotite + plagioclase + quartz, (Fig. 6.3,11; Fig. 6.4, A),

(b) chlorite + garnet + biotite + muscovite + plagioclase + quartz, (Fig. 6.3,1; Fig. 6.4,B), and

(c) staurolite + garnet + biotite + plagioclase + quartz (Fig. 6.3,11).

Since assemblages are largely dependent on the respective bulk rock compositions, sharp boundaries may not be drawn. Primary matrix chlorite, however, does not occur north of a line indicated in Figure 6.2, a geographical position which was also suggested by Hoffer (1977). The presence of assemblage (b) and the absence of chloritoid both indicate that chlorite may have formed according to the reaction

(1) chloritoid + biotite + quartz + H_2O = garnet + chlorite + muscovite, given by Spear and Cheney (1989). The formation of staurolite in the absence of chloritoid was attributed by Hoffer (1977) to the reaction

(2) chlorite + muscovite = staurolite + biotite + quartz + H_2O which was determined by Hoschek (1969). It is further notable that kyanite has only been observed in the southern part of this assemblage zone. Hoffer (1977) suggested that kyanite formed according to the reaction

(3) staurolite + chlorite + muscovite + quartz = kyanite + biotite + H_2O, determined by Thompson and Norton (1968).

The final decomposition of prograde chlorite in the centre of the traverse might indicate that conditions were ap-

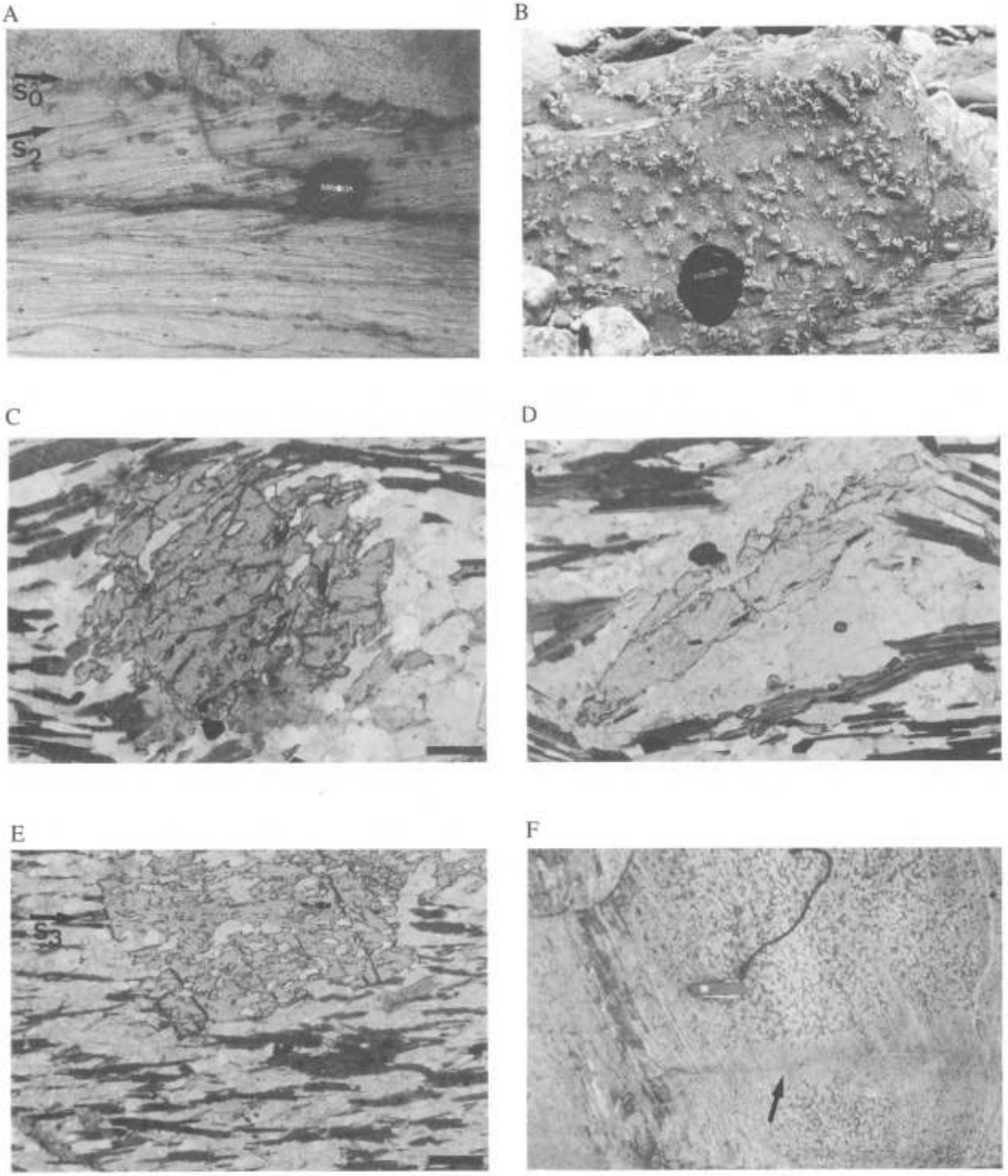

Fig. 6.1: (A) Photograph of graded turbidite bed showing the preferred crystallization of staurolite porphyroblasts in the pelitic to along the bedding plane (S_0) and within S_2 cleavage domains (indicated by arrows). The psammite at the base and the overlyin psammite contains only rare staurolite. Locality is at the northern boundary of the farm Kaan 309. (B) Photograph illustrating th pseudomorphism of muscovite after post-D_3 staurolite in the northern Khomas Trough. Locality is at the northern boundary of th farm Kaan 309. (C) Photomicrograph (plane light) showing deformed garnet II within the $S_{0,1,2,3}$ composite cleavage in the souther Khomas Trough in a pelite of assemblage zone 1 (farm Usambara 304). The metamorphic mineral assemblage is garnet + biotit + plagioclase + quartz (specimen PK 855). Scale bar is 0.2 mm. (D) Photomicrograph (plane light) showing early, possibly pre-D_2, staurolite I wrapped around by the $S_{0,1,2,3}$ composite cleavage in a pelite of the southern Khomas Trough. The metamorphic mineral assemblage is staurolite + biotite + plagioclase + quartz; the staurolite is altered to muscovite along its margins (specimen PK 855, farm Usambara 304). Scale bar is 0.2 mm. (E) Photomicrograph (plane light) illustrating the crystallization of staurolite III after the formation of the S_3 biotite fabric (indicated by arrow) in a pelite of assemblage zone 2 (specimen PK 838, farm Kaan 309). Scale bar is 0.2 mm. (F) Photograph showing psammitic schist speckled by scapolite and massive scapolitization along a fracture (indicated by arrow). The amount of scapolite decreases away from this vein. Locality is at the southern scapolite schist on the farm Dagbreek 365. Pocket knife is 8.5 cm long.

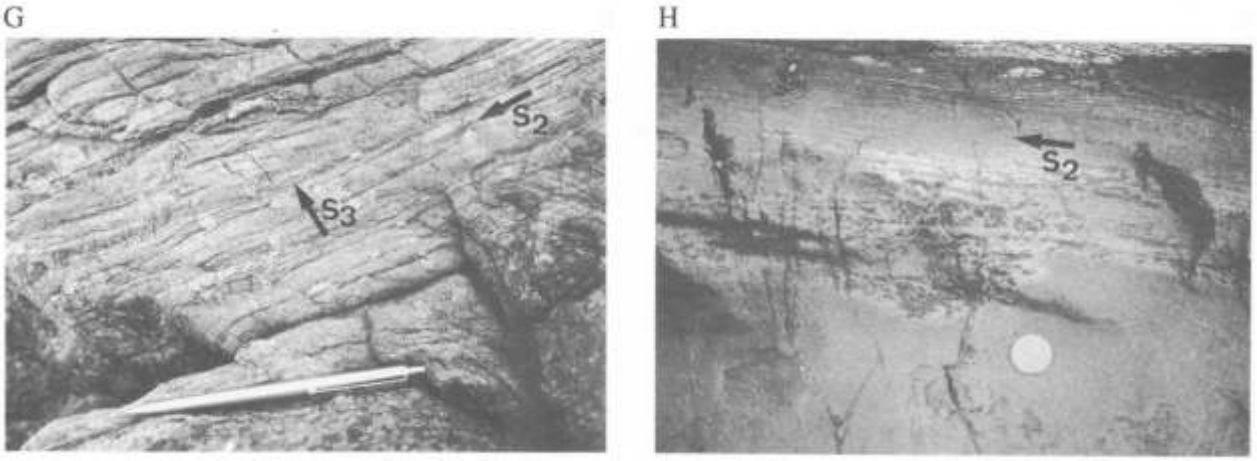

Fig. 6.1: (G) Photograph illustrating the post-D_3 crystallization of scapolite. The poikiloblasts enclose both the S_2 and S_3 biotite fabrics (indicated by arrows); pen is 14 cm long. Farm Dagbreek 365. (H) Calc-silicate concretion in psammitic schist illustrating the crystallization of first generation amphiboles parallel to the S_2 fabric. The second amphibole generation overgrows fabrics discordantly (basal part of the concretion) constraining the syn-D_2 to post-D_3 growth of amphiboles during formation of the calc-silicate lithologies. Farm Kaan 309.

propriate for the reaction

(4) garnet + muscovite + chlorite = staurolite + biotite, determined by Thompson (1976).

(b) Assemblage zone 2

This zone has been subdivided into two subzones based on the occurrence of andalusite. Pelites include andalusite from the immediate footwall of the graphite schist on the farm Kaan 309 towards the north, but only for about 3 km across strike in subzone 2A (Fig. 6.2); The critical assemblage found in subzone 2A is

(d) andalusite + garnet + biotite + muscovite + plagioclase + quartz (Fig. 6.4, C).

Hoffer (1977) argued that andalusite might have formed according to reaction (3), substituting kyanite, but under reduced pressures. Since staurolite decomposition (according to reaction (6)) has only been observed more than 20 km north of the andalusite zone, the reaction

(5) Mg-chlorite + muscovite + quartz = Al_2SiO_5 + biotite + H_2O

after Carmichael (1970) is suggested for the formation of andalusite in the presence of staurolite.

Within subzone 2B no Al-silicate has been found and the characteristic assemblage occurring for about 10 km across strike up to assemblage zone 3 is

(e) staurolite + garnet + biotite + muscovite + plagioclase + quartz (Fig. 6.4, D).

(c) Assemblage zone 3

This zone is about 20 km wide and its southern boundary delimits the first occurrence of sillimanite. Assemblages include

(f) sillimanite + staurolite + garnet + muscovite + biotite + plagioclase + quartz (Fig. 6.3, IV; 6.4, E), and

(g) sillimanite + sulurolite + biotite + plagioclase + quartz (Fig. 6.3, IV).

The assemblage (c) also occurs within this zone.

Towards the north, staurolite decreases in abundance whilst sillimanite increases. Hoffer (1977) ascribed the sillimanite formation to the reaction

(6) staurolite + muscovite + quartz = sillimanite + biotite + H_2O

experimentally determined by Hoschek (1969). Staurolite decomposition, however, has only been observed further north in assemblage zone 4. Since garnet occurs in association with sillimanite and staurolite, the reaction

(7) staurolite + muscovite + quartz = Al_2SiO_5 + almandine + biotite + H_2O

after Guidotti (1970) might have taken place. The occurrence of staurolite + sillimanite + biotite together over this wide zone was explained by Hoffer (1977) as being due to changing Fe and Mg contents of the pelites with increasing metamorphic grade.

(d) Assemblage zone 4

The last occurrence of staurolite is about 5 km south of the Donkerhuk Granite and the pelites show the assemblage

(h) sillimanite + biotite + muscovite + plagioclase + quartz in this area (Fig. 6.3, V; Fig. 6.4, F). Textures show an intergrowth of fibrolite with biotite which confirms that ideal conditions were reached for the formation of the critical assemblage sillimanite + biotite according to reaction (6) in this area.

The highest-temperature metamorphic conditions are evident at the northern margin of the Khomas Trough where partial migmatization occurred (Fig. 6.4, G). Pelites in this area contain the assemblage

(i) muscovite + biotite + K-feldspar (microcline) + plagioclase + quartz

(Fig. 6.4,H) which indicates the formation of melt according to the reaction

(8) muscovite + K-feldspar + albite + quartz + H_2O = melt,

determined by Thompson and Algor (1977).

In conclusion, the microscopic investigation confirms, to a large extent, the position of the metamorphic isograds proposed by Hoffer (1977) for the Khomas Trough. Pro-

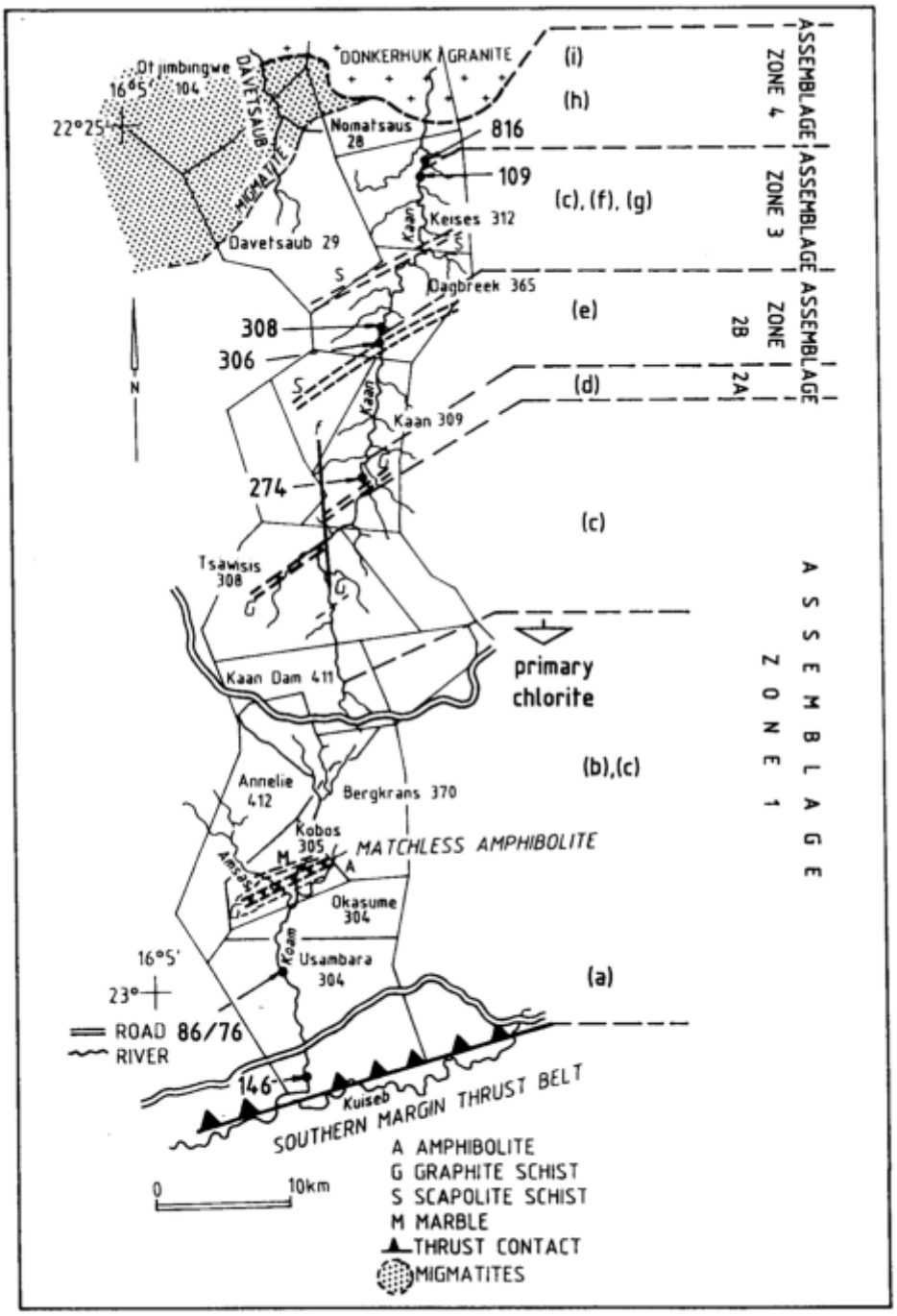

Fig. 6.2: Map of the study area showing distribution of assemblage zones with respective mineral assemblages (a) to (i), and sample localities.

nounced features of the central and northern part of the traverse are characteristic changes from a narrow andalusite zone to a wide sillimanite zone, the decomposition of staurolite and, finally, partial melting. In the south, however, mineral phase changes are much more indistinct with specific mineral assemblages occurring over wide areas.

6.4 Mineral compositions

Within the framework of this study, mineral analyses were undertaken to confirm and support indirect P-T estimates which were derived from mineral assemblages. Of additional interest was the chemical composition of the scapolites in the northern part of the traverse. With regard to these aims, six pelites from different assemblage zones were chosen. Sample numbers mark the locations shown in Figure 6.2, modal compositions are listed in Table 6.1 and analytical conditions and data may be found in Appendix III.

Plagioclases are mostly sericitized and untwinned. Four samples have been measured which did not show any significant degree of zonation. The plagioclases are generally oligoclases with An_{15} to An_{24} (Appendix III, A2).

The chemical analyses of *white micas* confirm that most are close to end-member muscovites (*sensu stricto*) (Appen-

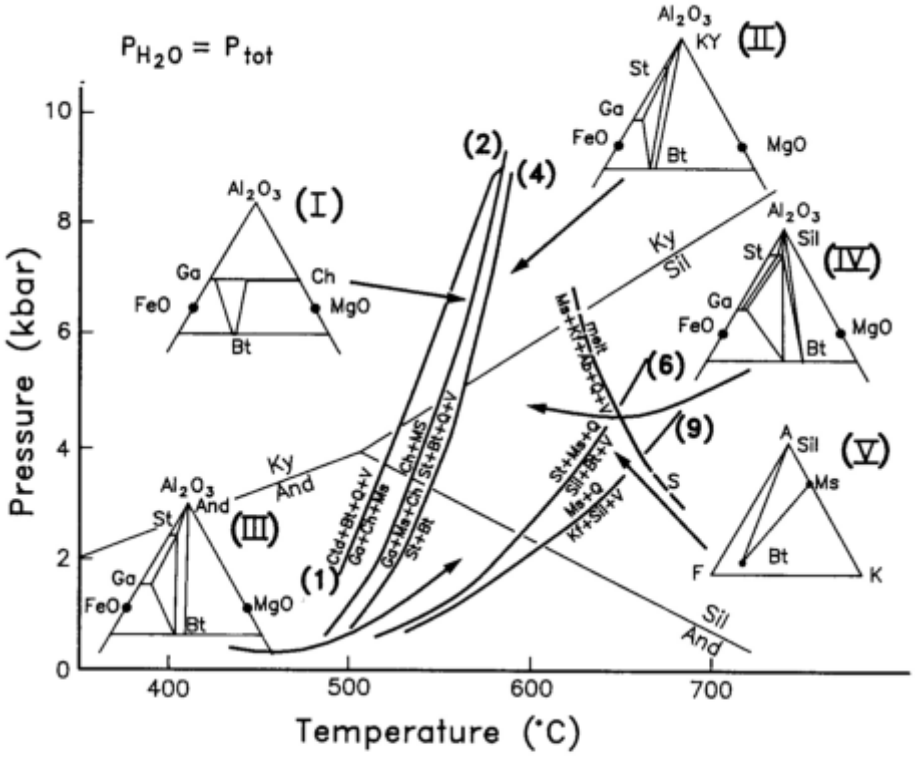

Fig. 6.3: P-T diagram showing the stability fields and assemblages for the assemblage zones 1 to 4. Upper stability limits of chloritoid + biotite + quartz + H_2O (1) after Spear and Cheney (1989); of chlorite + muscovite (2) after Hoschek (1969); of garnet + muscovite + chlorite (4) after Thompson (1976); of staurolite + muscovite + quartz (6) after Hoschek (1969); and of muscovite + quartz (9) after Chatterjee and Johannes (1974). The melting curve (S) is based on experimental data from the Khomas Trough after Hoffmann (1976) and Winkler (1983). Stability field of Al-silicates after Holdaway (1971).

dix III, B). This is shown by Si cation values of close to 6.00 and by low octahedral cation values in excess of Al. Moderate phengitic white mica is indicated in sample 86/76 (chlorite-garnet schist) which might be due to the presence of chlorite, as pointed out by Hoffer (1977). The analyses of different muscovite generations such as matrix muscovite (samples 146,86/76), porphyroblastic muscovites (samples 146, 274, 109) and late muscovites which replace Al-silicates (sample 308) and staurolite, have shown no significant differences in chemical compositions.

Biotite analyses of all six samples also show no significant variations in composition between both fabric biotites and late porphyroblastic biotites. This is demonstrated in Appendix III, C with sample 146-1 representing matrix biotites and with sample 146-2 in which porphyroblastic biotites have been analysed. There is also no systematic change of Mg-content of biotites with increasing metamorphic grade towards the north as has been observed by Hoffer (1977). However, Ti and Mn increase slightly towards the north. Sample 306 is from the scapolite schist sequence on the farm Dagbreek and shows a very different composition of biotites compared with other samples. These biotites are enclosed within the scapolite poikiloblasts.

Garnet III has been analysed from assemblage zones 1, 2 and 3 (Appendix III, D) and garnet II additionally in assemblage zone 1 (sample 146). Calculations based on 24 oxygens show good results of 6: ± 4:6. In all samples almandine garnet forms the most frequent end member of the garnet series constituting more than 60 mol-%. It is followed by spessartine and pyrope. Grossular and andradite components vary considerably. With the exception of sample 274 all garnets are distinctly zoned with Ca- and Mn-rich cores and Fe- and Mg-rich rims, zonations which are common in pelites of many metamorphic terrains.

Prograde *chlorite* has been analysed in a garnet-chlorite schist (sample 86/76; Appendix III, E). The chlorites are SiO_2 poor and the X_{Mg} of 0.58 is below the value of 0.63 which Hoffer (1977) considered to be the lower limit within his "medium-grade" assemblage zone 3.

In view of indirect P-T estimates, *staurolite* has been analysed in sample 308 to compare the composition with staurolites used for experimental studies by Hoschek (1969). The staurolite in this sample occurs in contact with garnet and sillimanite and does not show any muscovite replacement. The ratio of Mg/Mg+Fe is 0.17 (Appendix III, E) which is identical to that in staurolites used by Hoschek (1969).

Scapolites have been analysed from the southern scapolite schist sequence on the farm Dagbreek (Appendix III, E). Compositions are uniformly mizzonitic with a meionite percentage of about 64% and equivalent anorthite of about 59 (Fig. 6.5; Appendix III, E). Chlorine contents of about 0.61 wt% are characteristic for scapolites of mizzonitic compositions (Fig. 6.5; Evans *et al.*, 1969; Shaw, 1960). Employing the stoichiometry scheme of Evans *et al.* (1969) a general formula of $Na_{1.5}Ca_{2.5}Al_{4.6}Si_{7.4}O_{24}Cl_{0.2}(CO_3$

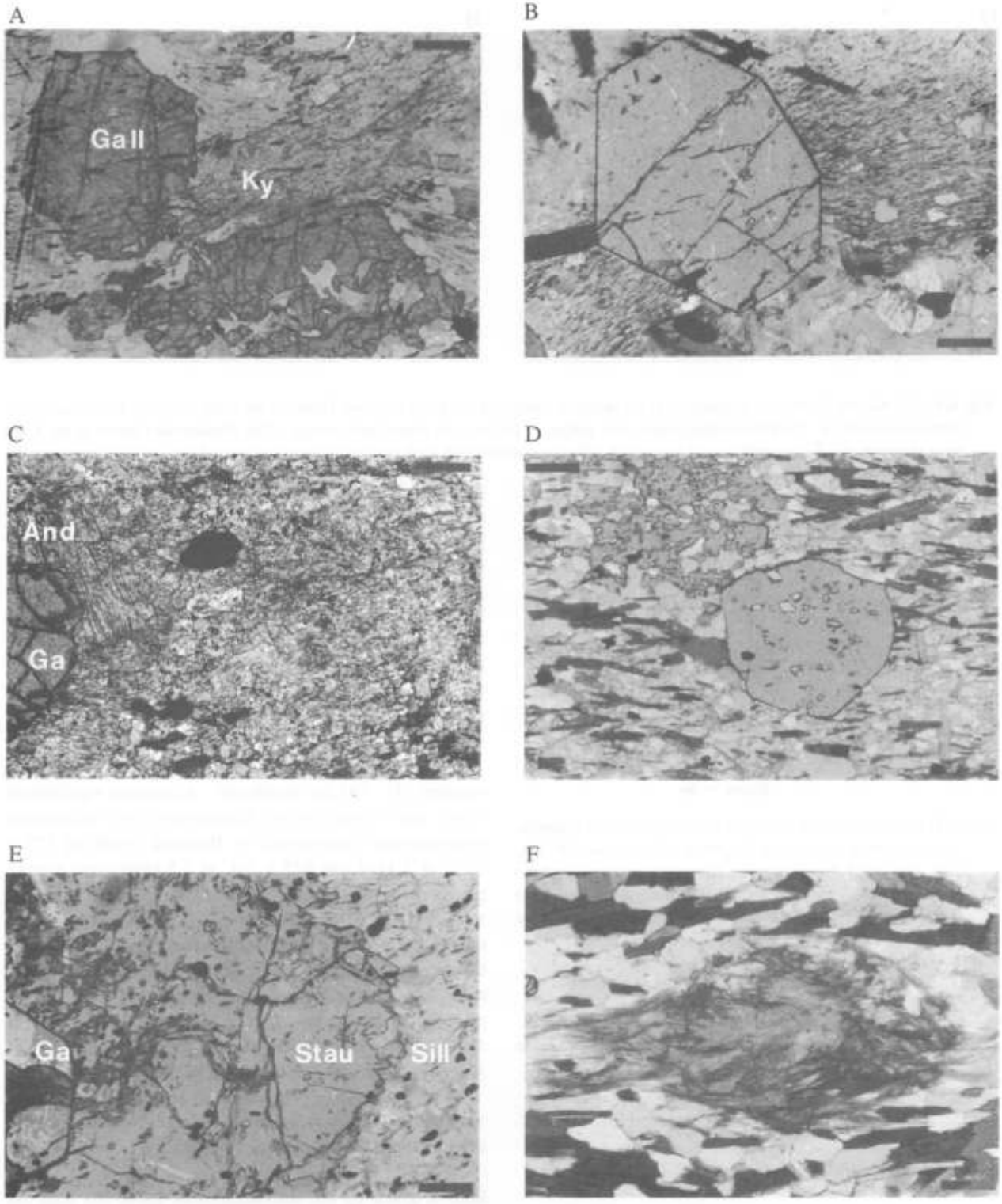

Fig. 6.4: (A) Photomicrograph (plane light) showing mineral assemblage (a) kyanite + garnet II + biotite + plagioclase + quartz of the southernmost Khomas Trough (pelite specimen PK 86/86, farm Usambara 304). Scale bar is 0.2 mm. (B) Photomicrograph (plane light) showing mineral assemblage (b) garnet III + chlorite (matrix) + biotite + plagioclase + quartz in assemblage zone 1 (pelite specimen PK 86/76, farm Usambara 304). Scale bar is 0.2 mm. (C) Photomicrograph (cross polars) showing mineral assemblage (d) garnet + andalusite (strongly altered to muscovite) + biotite + plagioclase + quartz in pelitic schist in assemblage zone 2A (pelite specimen PK 278, farm Kaan 309). Scale bar is 0.2 mm. (D) Photomicrograph (plane light) showing mineral assemblage (e) staurolite + garnet + biotite + plagioclase + quartz in assemblage zone 2B (pelite specimen PK 293, farm Kaan 309). Scale bar is 0.2 mm. (E) Photomicrograph (plane light) showing mineral assemblage sillimanite + staurolite + garnet in assemblage zone 3 (pelite specimen PK 308, farm Dagbreek 365). Scale bar is 0.2 mm. (F) Photomicrograph (plane light) showing fibrolite knot within the S_3 biotite fabric in association with biotite, plagioclase and quartz in the northern Khomas Trough (mineral assemblage (h), assemblage zone 4, pelite specimen PK 815, farm Keises 312). Scale bar is 0.2 mm.

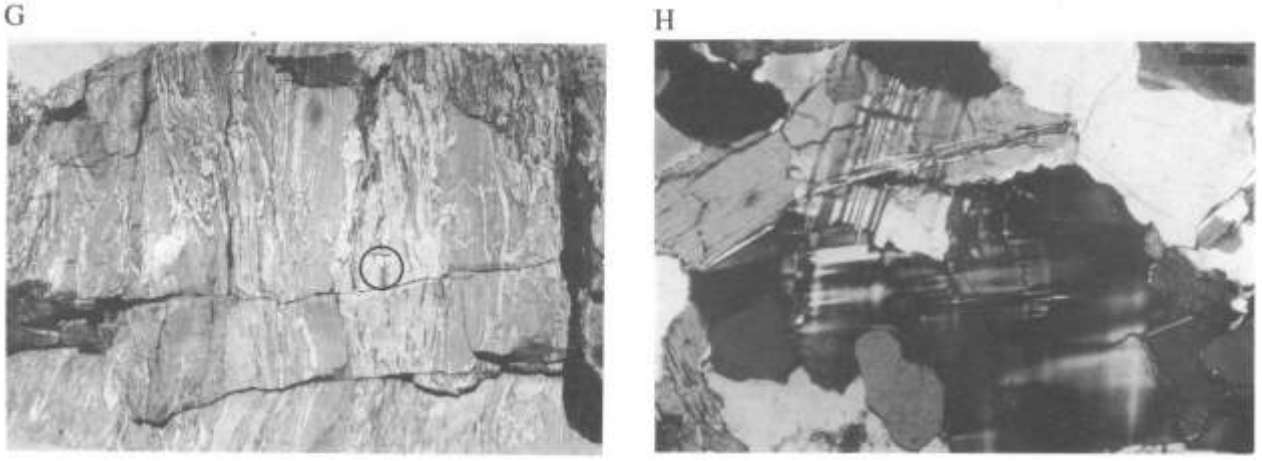

Fig. 6.4: (G) Kuiseb Formation migmatites at the northern margin of the study traverse. Hammer for scale (circled), Davetsaub river, farm Davetsaub 29. (H) Photomicrograph (cross polars) of pelite in the immediate vicinity of the Donkerhuk Granite in the Kaan river showing mineral assemblage (i) muscovite + biotite + microcline + plagioclase + quartz in assemblage zone 4 (specimen PK 344, farm Nomatsaus 28). Scale bar is 0.2 mm.

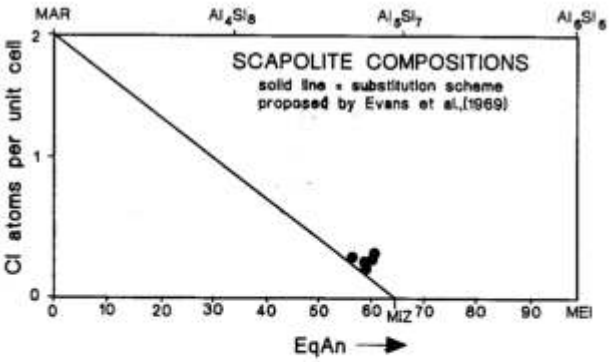

Fig. 6.5: Compositions of scapolite from the southern scapolite schist sequence on the farm Dagbreek 365 (sample 306, Fig. 6.2). The solid line represents the solid solution between marialite (MAR) and mizzonite (MIZ) as suggested by Evans *et al.* (1969). Cl-atoms per unit cell are a function of %EqAn for natural scapolites; (MEI=meijonite).

$)_{0.8}$ (Na includes K, Ca includes Sr, and CO_3 includes SO_4) is suggested by the analytical results.

6.5 The P-T evolution of metamorphism

6.5.1 Qualitative estimates of P-T conditions

Mineral assemblages and reaction-isograds allow some P-T estimates using experimentally determined reaction curves which are compiled in Figure 6.3. Judging from these reactions (and provided $P_{H2O}=P_{tot}$) the relevant P-T fields for the four assemblage zones are shown in this figure. The Al-silicate triple point of Holdaway (1971) has been employed because it best fits the evidence obtained from petrographic data and mineral analyses (see below).

The P-T field of assemblages in the southern Khomas Trough is framed by the equilibrium curve (1), by curve (2) which was experimentally determined at 540 ± 15°C at 4 kbar and 565 ± 5°C at 7 kbar water vapour pressure by Hoschek (1969), and by curve (4) determined by Thompson (1976) at 580°-590°C at 3-6 kbar. The last occurrence of primary chlorite several kilometres south of the andalusite zone indicates that P-T conditions in this area are close to reaction curve (4). The resulting P-T conditions for the south, as determined by assemblages and the latter equilibrium curves within the kyanite field, are a temperature range of about 540-590°C at water vapour pressures from 4.5 to about 9 kbars.

Conditions in the andalusite field are determined by: (i) reaction (4); (ii) the andalusite - sillimanite equilibrium curve; and (iii) reaction (6). Equilibrium curve (6) has been experimentally determined by Hoschek (1969) at 575 ± 15°C at 2 kbar and 675 ± 5°C at 5.5 kbar water vapour pressure (using a biotite with Mg/Mg+Fe = 0.48 and a staurolite with Mg/Mg+Fe = 0.17). A possible temperature range of 500-590°C is given by curves (4) and (6), and by the intersection of curve (6) with the andalusite - sillimanite equilibrium curve. A pressure range of <1-2.8 kbar is provided by the lower pressure limits of curves (4) and (6) and by the intersection of curve of (4) with the andalusite-sillimanite equilibrium curve (Fig. 6.3).

Assemblage zone 3 shows the widest possible P-T range with 550-650°C given by the intersection of curve (4) with the andalusite - sillimanite equilibrium curve, and of curve (6) with the granite solidus. A pressure range of about 2.4-6 kbar is given by the intersections of curve (6) with the andalusite - sillimanite equilibrium curve, and of the granite solidus with the kyanite - sillimanite equilibrium curve.

Further evidence for temperature conditions close to the southern boundary of zone 3 comes from scapolite stabilities (Fig. 6.6). The mizzonitic composition of the scapolite indicates a minimum formation temperature of about 470°C and a maximum of about 650°C according to studies of Oterdoom and Wenk (1983). In comparison with co-genetic silicate phases it is more likely, however, that the scapolite formed above the minimum temperature of 550°C for CO_3-scapolite as indicated in Figure 6.6.

Constraints on the P-T conditions of assemblage zone 4

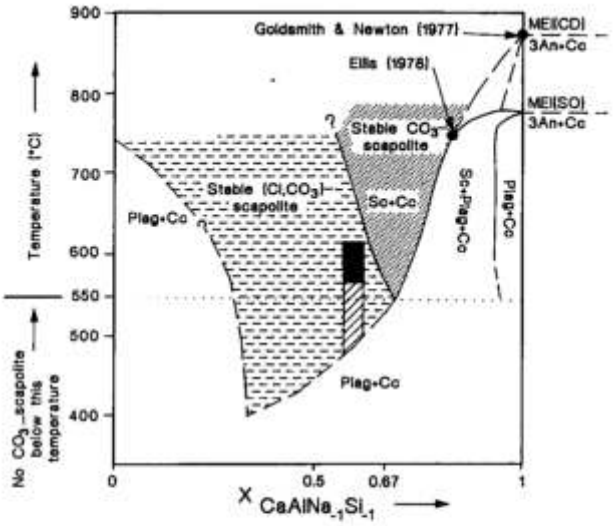

Fig. 6.6: Diagram showing isobaric temperature - composition relations between scapolite, plagioclase and calcite as well as stability conditions for stable CO_3- and Cl,CO_3-scapolite (after Oterdoom and Wenk, 1983). The possible temperature range for the formation of mizzonitic scapolite in the Khomas Trough according to this diagram is demarcated by hatched and solid black areas. The most likely temperature range for the investigated samples is shown in solid black (for details see text).

are provided by reaction curve (6) and by reaction

(9) muscovite + quartz = K-feldspar + Al-silicate + H_2O

determined by Chatterjee and Johannes (1974).

Furthermore, melting experiments in Kuiseb schists, migmatites and granites in the vicinity of the study area were undertaken by Hoffmann (1976) and Winkler (1983). The experiments show initial melting of Kuiseb pelites at 660-670°C at 4 kbar, of migmatites at 667-683°C at 4 kbar and of granite at 663°C at 4 kbar. Winkler (1983) obtained a granite solidus at 640-646°C at 5 kbar. These results are manifest in the solidus curve S in Figure 6.3 which demarcates a similar slope but at about 25°C higher than the solidus curve of Thompson and Algor (1977). The P-T conditions in the northern part of the traverse are well constrained by experimental data indicating a temperature range of 590-670°C and a pressure range of 2-4.5 kbar (Fig. 6.3). Further evidence for the pressure conditions at the northern margin comes from primary muscovite in the Donkerhuk Granite which indicates a lower pressure limit of about 3.5 kbar (experimentally determined by Storre and Karotke, 1971) for the crystallization of the granite.

An outstanding feature of the central and northern Khomas Trough is the alteration of staurolite, andalusite and sillimanite to muscovite (Fig. 6.1, B). Carmichael (1969) and Eugster (1970) ascribed this phenomenon to retrograde alteration which is dependent on fH_2O, pH, K+ concentrations, total pressure and temperature of the metamorphic fluids. These authors have formulated the reaction

(10) 2 muscovite + 2 H^+ = 3 Al_2SiO_5 + 3 SiO_2 + 2 K^+ + 3 H_2O

to account for the formation of muscovite. This process may be initiated above 600°C during regional cooling (Eugster, 1970),

6.5.2 Geothermometry and geobarometry

For a direct P-T estimate, four samples were chosen from assemblage zones 1, 2 and 3 (sample localities are shown in Figure 6.2) which allow the application of garnet-biotite- and garnet-chlorite geothermometers as well as of a garnet-biotite-muscovite-plagioclase geobarometer. All phases used for thermobarometry are in contact with each other and garnets belong mostly to the late garnet III generation. An exception is sample 146 where a spiral-shaped garnet II has also been measured.

Garnet-biotite geothermometers used are those of Ferry and Spear (1978), Hodges and Spear (1982), Perchuk and Lavrent'Eva (1983), Indares and Martignole (1985) and Hoinkes (1986), taking into account that some of these have been calibrated for specific pressures. The garnet-chlorite geothermometer of Dickenson and Hewitt (1986) has been used for sample 86/76. Pressure estimates for samples 146 and 308 are based on the garnet-biotite-muscovite-plagioclase geobarometer of Ghent and Stout (1981).

The results of the initial P-T estimates are shown in Table 6.3. Temperature ranges result from the analysis of different minerals of the same generation. Figure 6.7 illustrates the inferred P-T conditions derived from reaction curves, mineral analyses of critical assemblages in AFM diagrams as well as X_{Alm} isopleths of garnet-biotite bearing pelites after Spear and Cheney (1989). The general lack of agreement between the different garnet-biotite geothermometers proposed is confirmed by the data shown in Table 6.3. The experimental calibration of Ferry and Spear's (1978) thermometer is based on pure Fe-Mg solid solutions using Fe/Fe+Mg systems of about 0.9. The calibration of Hodges and Spear (1982) accounts for non-ideal garnet solid solution, but only the grossular-pyrope crystalline solution was assumed to behave non-ideally. Perchuk and Lavrent'Eva's (1983) experimental calibration uses Fe/Fe+Mg systems of about 0.6. Indares and Martignole (1985) have combined data of Ferry and Spear (1978) and natural biotite-garnet occurrences to derive an empirical thermometer which accounts for dilutents such as Ti, Al, Ca and Mn. Hoinkes (1986) has found non- ideal mixing of grossular with almandine-pyrope solid solution in an empirical study.

For the southern Khomas Trough, both garnet II and III (sample 146) are zoned and show a range of X_{Alm} from 0.90 (centre) to 0.85 (rim). According to the X_{Alm} isopleths given by Spear and Cheney (1989) this indicates a temperature range of about 550-570°C at pressures of 5-7.6 kbar. Mineral thermometry gave large errors with temperatures of 490-626°C at 6 kbar for garnet II-biotite pairs and of 442-533°C at 6 kbar for garnet III-biotite pairs (Table 6.3). The geobarometer of Ghent and Stout (1981) gives a range of 3.98-6.94 kbar at 550°C for garnet II. Garnet III shows 3.82-6.72 kbar at 550°C.

The distribution coefficient (KD) value of 0.17 and the high X_{Ca} value of 0.12 of sample 146 compare best with the grossular-rich samples used by Hoinkes (1986). The presence of staurolite in this area and its commonly accepted formation temperature of at least 540°C at 4 kbar (Hoschek, 1969) from chlorite + muscovite (Fig. 6.3) further suggest that the data obtained from Hoinkes (1986) record the most accurate estimate of temperatures in this area. The above

TABLE 6.3: Geothermometric and geobarometric data. Sample localities within the respective assemblage zones are shown in Figure 6.2. Modal compositions are given in Table 6.1.

SAMPLE	146	86/76	274	308
Gh&St (550°C): Ga II	3.98-6.94 (kb)			
Ga III	3.82-6.72			
Gh&St (620°C):				2.22-4.24 (kb)
F&S (6 Kb): Ga II	490-519 (°C)			
Ga III	442-451		(2 kb): 531-550 (°C)	(4 kb): 601-605 (ÉC)
H (6 kb): Ga II	588-626			
Ga III	522-533		(2 kb): 579-599	(4 kb): 637-646
I&M (6 kb): Ga II	525-550			
Ga III	470-495		(2 kb): 560-580	(4 kb): 610-627
P&L (6kb): Ga II	533-550			
Ga III	503-508			
H&S (6 kb): Ga II	490-519			
Ga III	442-451			(4 kb): 601-605
D&H (6 kb):		485-512 (ÉC)		
$K_D = (Fe/Mg)_{Bi}/(Fe/Mg)_{Ga}$	0.17		0.16	0.18

Abbreviations: Gh&St, Ghent & Stout (1981); F&S, Ferry and Spear (1978); H, Hoinkes (1986); I&M, Indares & Martignole (1985); P&L, Perchuk & Lavrent'Eva (1983); H&S, Hodges & Spear (1982); D&H, Dickenson & Hewitt (1986).

thermometric data together with suitable reaction curves for this area suggest a P-T range from about 520° to 570°C at 4-7 kbar (Fig. 6.7).

Sample 86/76 represents a garnet-chlorite schist from an area in assemblage zone 1 where no staurolite has been observed. Geothermometers for this zone give a narrow temperature range of 485-512°C at 6 kbar pressure (Table 6.3).

The thermometric analyses from assemblage zone 2, just south of the first occurrence of sillimanite, show a temperature of about 530-600°C at 2 kbar pressure which supports the use of the Holdaway Al_2SiO_5 triple point. The equilibrium curve andalusite - sillimanite is intersected at these temperatures at reasonable pressures, a result which is in contrast to the phase diagrams of Richardson *et al.* (1969) and Althaus (1969) which would hardly allow the formation of sillimanite at these temperatures. The lower Ca contents and the KD values of garnet in this area compared with samples used by the above authors for thermometric cali-brations, suggest that the geothermometer of Indares and Martignole (1985) shows the most reliable results of 560-580°C at 2 kbar in this area (Table 6.3).

Thermometric data calculated for assemblage zone 3 garnet-biotite pairs give a narrow range of 600-630°C at 4 kbar, with the exception of Hoinkes' (1986) thermometer. It is conceivable that the Ca-poor composition (X_{Ca}=0.03) of the garnets accounts for the higher reliability of other thermometers compared to the calibration of Hoinkes (op. cit.) who used garnets with X_{Ca} 0.1. Pressure estimates for this area gave 2.22-4.24 kbar at 620°C. Values of 0.84 for X_{Alm} indicate a P-T range of 590-630°C at 3.8-5.8 kbar (Fig. 6.7).

6.5.3 Summary of the P-T conditions in the Khomas Trough

Previously Hoffer (1977) interpreted a continuous development of the Al-polymorphs within the Khomas Trough from south to north showing decreasing pressure and increasing temperature conditions. This was largely an effect of the phase diagram of Althaus (1969) which permits a continuous P-T path from high-P/low-T to low-P/high-T along a simple prograde path. In addition, the andalusite and sillimanite isograds were interpreted by Hoffer (1977) to be influenced by the Donkerhuk Granite.

Using fluid inclusion data and taking the findings of Hoffer (1977,1983) into account, Behr *et al.* (1983) calculated that the southern Khomas Trough experienced pressures of 6-9 kbar at temperatures of 480-580°C, whereas the northern part was subjected to pressures of 4.5 kbar at temperatures of 650°C. As a consequence of this the latter authors showed two distinct P-T paths for these areas and explained the difference by a rapid downwarping of the southern Khomas Trough in contrast to the north.

Sawyer (1981) and Preussinger (1990) studied the metamorphic conditions of Kuiseb schists at the western end of the Khomas Trough in the Gorob mining area which is situated close to the Matchless Amphibolite. Sawyer (op.cit.) estimated about 600°C at 6-9 kbar for the peak of metamorphism in this area and Preussinger (op.cit.) established 580-630°C at 5.5-6.5 kbar from sillimanite- and kyanite-bearing assemblages. Kasch (1983b) estimated P-T conditions at the

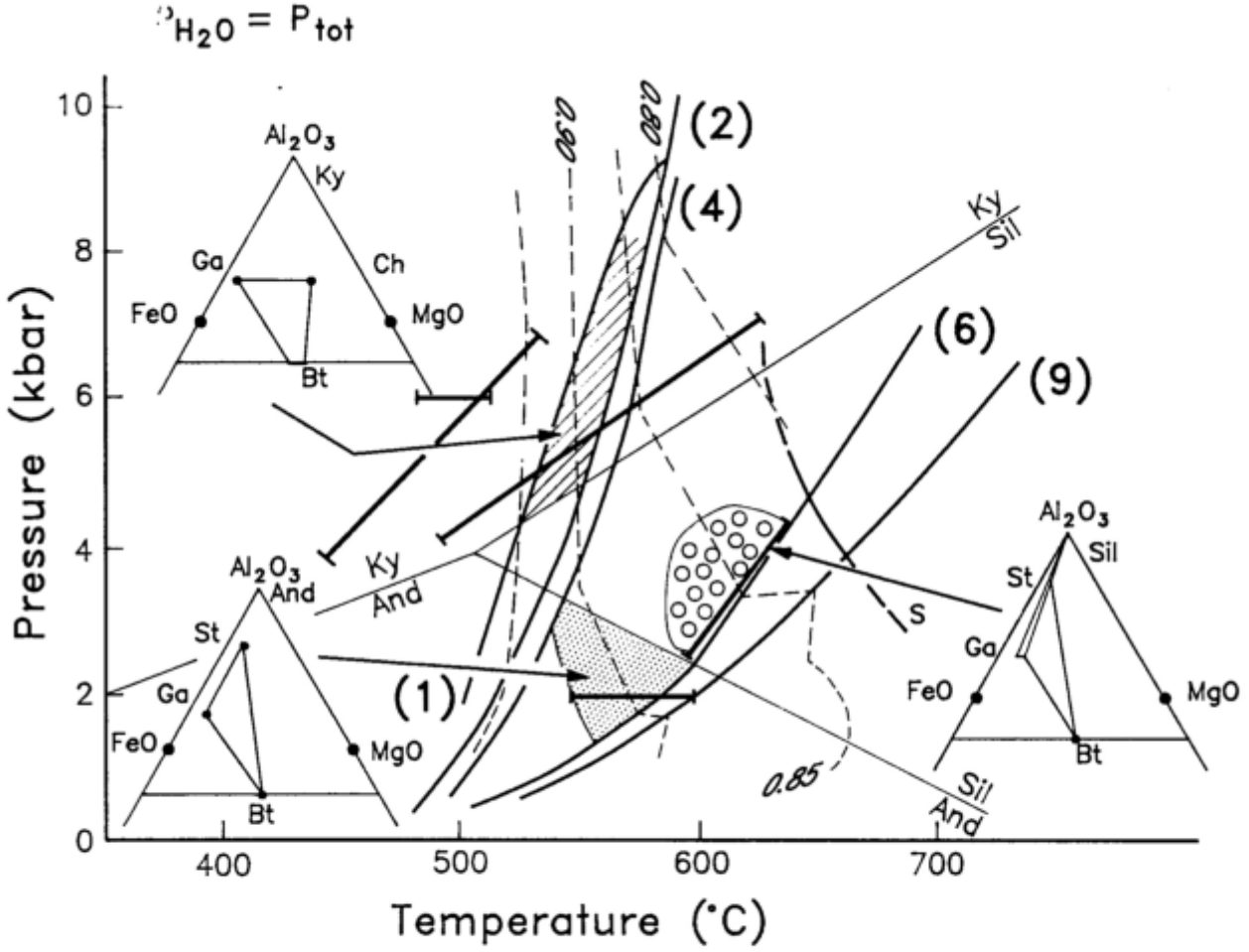

Fig. 6.7: Petrogenetic grid for the KFMASH system (modified from Spear and Cheney, 1989). Dashed lines represent contours of X_{Alm} in garnet in assemblages which contain garnet + biotite. Reaction curves are identical to those given in Figure 6.3. Bars indicate P-T range as derived from geothermometric and geobarometric calculations of samples from the respective assemblage zones (see Table 6.3). P-T conditions for assemblage zones 1 (hatched symbol), 2 (dots) and 3 (circles) result from combined geothermobarometric data and qualitative estimates.

southern margin of the Khomas Trough, 200 km east of the study traverse. He obtained about 600°C at 9 kbar for a first metamorphic event (M1) and about 600°C at 7-8 kbar for a second event (M2).

An interesting issue is the discussion of the peak conditions of regional or thermal metamorphism in the Khomas Trough. The migmatites, which partially occur close to the Donkerhuk Granite, as well as the sillimanite and andalusite isograds, have been interpreted by several authors to represent a thermal aureole of the granite (e.g. Nieberding, 1976; Jacob, 1974; Hoffer, 1977). Smith (1965) and Faupel (1974) presented arguments to discount a large thermal aureole on the basis of similar solidus temperatures for schists and granite.

The principal calculations of Jaeger (1957) on other granitic bodies have, however, shown that a large medium- to high-grade thermal aureole around a granitic pluton of 700°C which intrudes a country rock of about the same temperature at a depth corresponding to 4 kbar is unlikely. This study has presented structural evidence indicating that the migmatites occurring in the Davetsaub river profile are crosscut by granite apophyses (see Chapter 4). Furthermore, coarsely recrystallized grain sizes only occur up to about 1 km south of the granite and K-feldspar has formed in the schists only at the immediate contact in the Kaan river section. Migmatites, on the other hand, occur in well-defined zones ex tending for several kilometres south of the granite - schist contact. Partly-bent fibrolite knots within the S_2 cleavage domains and the possible formation of fibrolite syn- to post-D_3 according to reaction (6) also indicate that Al-silicates have formed prior to the intrusion.

In conclusion, the petrographic data and mineral analyses presented in this study indicate that the Kuiseb schists exposed along the study traverse do not show a coherent isograd pattern from low-grade in the south to high-grade in the north, as postulated by Hoffer (1977). The metamorphic history of the Khomas Trough is therefore not easily explained by a single, prograde P-T evolution which was influenced in the centre and north by a post-tectonic granite intrusion.

The mineral analyses, obtained from widespread post-D_3 mineral phases, reveal a temperature variation from about 500 to 660°C from south to north but pressures vary considerably in the respective assemblage zones. Maximum conditions of 7 kbar at 570°C are indicated in assemblage zone 1 which is in good agreement with the studies cited above. In contrast to this, only about 2 kbar at 570°C are recorded in the andalusite zone and, further north, pressures reached about 4 kbar at a maximum temperature of 660°C in the sillimanite zone. These pressures and temperatures

correspond to geothermal gradients of about 20° /km, 80°/km and 45°/km respectively (taking $P_{H2O} = P_{lithostatic}$, and a mean rock density of 2.80 g/cm). An earlier syn-D_2 phase of mineral growth which is evident from some preserved garnets and staurolites suggests slightly higher temperatures for garnet II than for garnet III at about the same pressures. Peak metamorphic conditions in the northern Khomas Trough have partially led to the formation of migmatites which were subsequently intruded by the Donkerhuk Granite. Throughout the Khomas Trough, late muscovites, biotites and amphiboles are evidence for elevated temperatures in a largely stress-free environment after the D_4 deformation and after the peak of metamorphism. Also at this late stage, alteration of Al-silicates and staurolite to muscovite occurred.

7. TECTONICS AND SEDIMENTATION OF A LATE PROTEROZOIC CONVERGENT CONTINENTAL MARGIN

7.1 Previous geodynamic models for the evolution of the inland branch of the Damara Orogen

Previous discussions on the geodynamic evolution of the inland branch of the Damara Orogen have concentrated mainly on whether or not oceanic crust formed during spreading and prior to subduction and continental convergence. Martin and Porada (1977) and later Porada (1983) proposed an aulacogen model which initiates the development of the Damara Orogen with three symmetrical rift grabens induced by the cooling of an asthenolith. They suggested that this was followed by a downwarping stage and a final post-geosynclinal stage. The delamination model of Kröner (1982) is similar to the latter, involving initial crustal stretching over a mantle plume situated underneath the Khomas Trough and leading to the extrusion of the Matchless Amphibolite. Further processes in this model involve lithospheric delamination, continental subduction, crustal underthrusting and high-level thrusting.

An ocean-floor subduction model on the other hand, involving the subduction of a several thousand kilometres wide ocean, was favoured by Hartnady (1978), Kasch (1979) and Barnes and Sawyer (1980). The subduction of a narrow, Red Sea-type ocean was suggested by Miller (1983b) who interprets the Matchless Amphibolite as a remnant of a spreading centre which was covered by clastic sediments. A small ocean-basin model associated with strike-slip shear movements was proposed by Downing and Coward (1981) and Coward (1983). This involves the formation of pull-apart basins which are partly floored by oceanic crust in the inland branch, the oblique subduction of these basins and the late-stage movement of the Congo Craton towards the southeast. Breitkopf and Maiden (1987) proposed a limited ocean-basin model involving the fault-related development of sub-basins in the Khomas Trough on both continental and oceanic crust. Blaine (1977) summarized his structural investigations in the eastern Khomas Trough suggesting a possible fore-arc basin on the basis of contrasting tectonic styles with the Central Zone. This was partly supported by Miller *et al.* (1983), who argued, on the basis of a geochemical maturity index, that the Khomas Trough north of the Matchless Amphibolite contains fore-arc basin deposits and older spreading-phase deposits towards the south. Downing and Coward (1981) and Hoffmann (1983) speculated upon an accretionary prism setting for the Khomas Trough.

The pronounced sedimentological and structural asymmetries within the inland branch of the orogen recently led Henry *et al.* (1990) to relate the early rifting phase to the development of two low-angle detachment systems. This ultimately resulted in the evolution of the Khomas Sea between the Kalahari and Congo Cratons.

7.2 The tectono-sedimentary evolution of the Khomas Trough

The Damara Orogen is part of the Pan-African mobile belt system and connects with the Zambezi and Mozambique Belts in Central Africa. Irrespective of which of the above geotectonic models is applied, the Khomas Trough represents a crucial area in interpreting the tectonics of the Late Proterozoic in Namibia. In previous chapters this thesis has investigated the structural, sedimentological, and metamorphic evolution as well as geochemical aspects of the Kuiseb Formation in the Khomas Trough. The synthesis of conclusions drawn from each of these aspects helps to discriminate between the various interpretations given above for the evolution of the inland branch of the Damara Orogen. Consequently, the information gathered in this study is combined in a model which involves the convergence and collision of the Kalahari and Congo Cratons following a rifting and spreading phase. The model proposes that an accretionary prism, here named Khomas Hochland accretionary prism, of Late Proterozoic age, developed in the Khomas Trough.

7.2.1 Rifting and spreading phase

The evolution of the Khomas Trough commenced with an initial rift system (Miller, 1983b) which probably developed from a northwest-dipping detachment fault as suggested by Henry *et al.* (1990). Thick volcanic sequences of the Naauwpoort Formation in the northern Damara Orogen have been interpreted by Miller (1983b) to represent the initiation of large-scale rifting in the inland branch at about 750± 65 Ma (U/Pb zircon dates). There is no evidence of rift-related volcanic rocks or sediments in the Khomas Trough. Miller (1983b), however, has reported very minor acid volcanic rocks of Nosib Group age occurring along the Okahandja Lineament. Advanced rifting led to crustal thinning and the development of an oceanic spreading centre in the Khomas Sea. This generation of oceanic crust is confirmed by tholeiitic, mid-ocean ridge-type metabasalts and pillow lavas of the Matchless Amphibolite. Breccias, meta-gabbros and ultramafic lithologies also occur within the oceanic sequence. The metabasic rocks are associated with pelagic and hemipelagic deep-sea lithologies such as pelitic schists and graphite schists, but also with turbiditic grey-wackes. Massive sulphide ore deposits in the vicinity of the Matchless Amphibolite formed as part of the hydro thermal system during spreading (Killick, 1983). A notable marble unit is most likely to have originated by carbonate precipitation, probably induced by the hydro thermal convection cells along the spreading ridge. Stable isotope signatures of associated graphite schists, however, confirm that these are organic pelagic sediments. The intercalation of spreading-ridge basalts and ore deposits with turbiditic and pelagic sediments has implications for the size of the Khomas Sea and the position of the mid-ocean ridge relative to the continental margin (see below). The amount of tectonic shortening calculated indicates that the basin had a minimum width of hundreds of kilometres once spreading ceased.

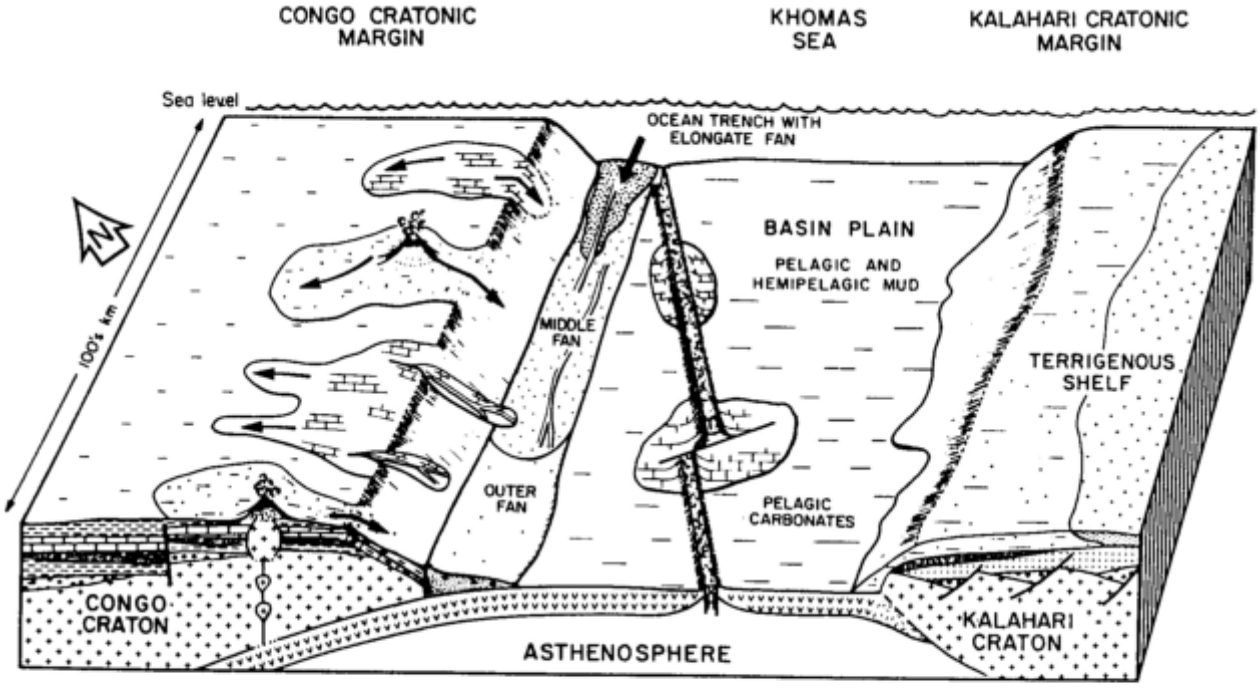

Fig. 7.1: Depositional palaeoenvironments in the southern Damara Orogen during early continental convergence. The elongate trench fan transports large amounts of clastic sediment from a northeasterly source area along the trench axis. Pelagic and hemipelagic sedimentation dominates the basin plain. Decreasing carbonate sedimentation (platform carbonates and carbonate turbidites) characterizes the northern shelf and slope. Clastic deposition occurs on the southern cratonic shelf.

7.2.2 Early subduction phase

The next phase in the evolution was characterized by convergence and subduction of Khomas Sea oceanic crust beneath the Congo Craton. The palaeo-environmental setting during the early stage of convergence is shown in Figure 7.1. Early structural vergences to the southeast confirm that subduction of the ocean and movement of the Kalahari Craton was down to the northwest. Subduction was probably initiated by extensive sediment loading along the Congo cratonic margin in a manner similar to that described by Cloetingh *et al.* (1982) for small ocean basins. The Kuiseb schists, which are partly intercalated with Tinkas Formation carbonate turbidites in the vicinity of the Okahandja Lineament (Porada and Wittig, 1983), may be regarded as remnants of these early clastic sediments entering the northern Khomas Sea. An oceanic trench developed consequently along the southern margin of the Congo Craton. Original sedimentary structures, turbidite facies, cyclic sedimentation and the lateral extent of sedimentary marker units within the Khomas Trough indicate that the sedimentary precursors of the Kuiseb schists accumulated as turbidites on an elongate submarine fan. Palaeocurrents and lateral correlation suggest that it developed as a southwestward prograding elongate trench fan which incorporated large amounts of clastic sediments (Fig. 7.1). This, together with the relative uniformity of grain sizes (i.e. no conglomeratic material), indicates that the main source area was situated a considerable distance to the northeast of the area of deposition. It is also conceivable that a volcanic arc north of the subduction zone additionally contributed towards the trench fill (Fig. 7.1). In any case, geochemical signatures such as high contents of certain immobile elements suggest an active continental-margin source for the precursor of the Kuiseb schists. Some of the metamorphosed carbonate-rich rocks (calc-silicates) in the Khomas Trough are associated with terrigenoclastic turbidites and have also been deposited by mass-flow processes.

In large parts of the basin, pelagic sediments accumulated and the intercalation of submarine fan lithologies and pelagic and hemipelagic sediments in the Khomas Trough confirms that these depositional processes were contemporaneous within the basin.

Adjacent to the Khomas Sea in the north at this early stage of subduction, platform carbonates were still being deposited (Karibib Formation) as indicated by the calcareous slope turbidites which were accumulating (Tinkas Formation; Fig. 7.1). These platform deposits were, however, soon to be totally replaced by immature terrigenous sediments of the Kuiseb Formation in the Central Zone. At the same time clastic terrigenous platform sediments were deposited on the southern passive continental margin of the Kalahari Craton.

7.2.3 Accretion phase

The further geotectonic development of the active continental margin is explained by accretion of the trench sediments against the Congo cratonic margin. This model is represented in Figure 7.2 which shows the Khomas Hochland accretionary prism evolving through the off-scraping of submarine fan lithologies from the descending oceanic slab. The dominance of metasediments relative to basalts within the present-day Khomas Trough also confirms high sediment input into the oceanic trench. Clastic sediments were therefore preferentially accreted whereas oceanic basalts and pelagics were mostly subducted, similar to the mechanism suggested by Thornburg and Kulm (1987) from the

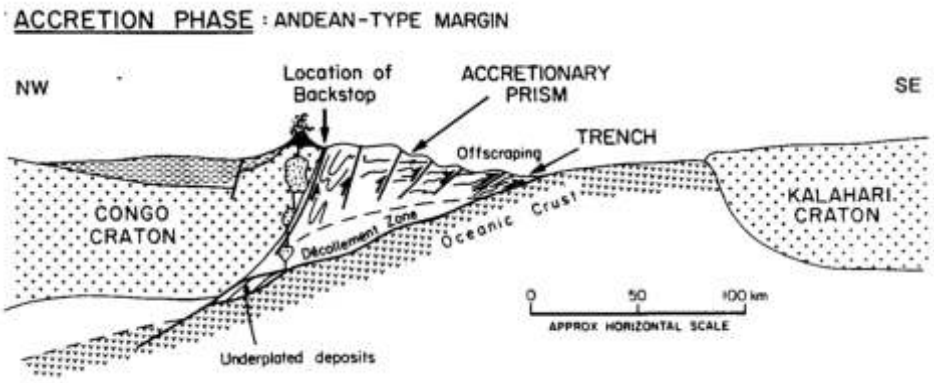

Fig. 7.2: Tectonic setting of the southern Damara Orogen during late convergence of the Congo and Kalahari Cratons. The oceanic trench contains the elongate submarine fan and the accretionary prism evolves through the off-scraping of sediment from the descending slab. Early (D_1) folding and thrusting occurs within the prism.

Peru - Chile Trench. It is thought that a continued high sediment input into the trench caused and maintained a shallow slab inclination as described by Karig *et al.* (1976) from recent subduction zones. This setting may have also included a narrow arc - trench gap and it may have inhibited the formation of a major fore-arc basin as described by Dickinson and Seely (1979) and Cross and Pilger (1982) for the Peru - Chile Trench.

One possible explanation for the emplacement of the oceanic sequence represented by the Matchless Amphibolite is that it was incorporated into the prism during the late stages of the accretionary processes by off-scraping from an oceanic crustal high such as the mid-ocean ridge, an aseismic ridge or an oceanic plateau.

During accretion, early isoclinal folding, associated with cleavage formation and thrusting, occurred within the accretionary prism. These features are represented by the relict structures preserved from the D_1 phase of deformation in the Khomas Trough. Such early compressional stresses are also characteristic of low-angle subduction zones associated with young, buoyant oceanic lithosphere (Cross and 'Pilger, 1982; Park, 1988). Similarly, early deformation involving thrusting and folding has been reported from modem accretionary prisms in the Aleutian Trench (Lewis *et al.*, 1988) and in the Mariana and Yap Trenches off Japan (Kimura *et al.*, 1989).

The backstop of the accretionary prism was located at the southern margin of the Congo Craton and it is suggested that this structure was the initial expression of the Okahandja Lineament (Fig. 7.2).

It has previously been pointed out that no obvious magmatic arc was associated with the proposed subduction zone. Miller (1983b) and Brandt (1987), however, recorded small amounts of pre-, syn-, and post-tectonic alkaline and calc-alkaline granites, diorites and metagabbros. The pre- and syn-tectonic magmatic rocks especially have I-type character, shown by low initial $^{87}Sr/^{85}Sr$ ratios and by the presence of hornblende and sphene. The majority of these intrusions occur in the southern Central Zone within 30 km of the Okahandja Lineament (Miller, 1983b).

The palaeo-environmental setting during the later stages of subduction is illustrated in Figure 7.3. To the north of the Khomas Sea, a magmatic arc is shown situated close to the trench. The shelf area on the Congo Craton became unstable during continued accretion and the carbonates were followed by clastic terrigenous sediments (Kuiseb Formation; Badenhorst, 1987). It may therefore be speculated that the Central Zone developed as a back -arc basin at this stage (Fig. 7.3). The southern terrigenous platform of the Kalahari Craton maintained its stability with local fan sedimentation occurring (Porada and Wittig, 1983).

One aspect which has repeatedly been addressed with regard to the Khomas Trough is the question of preservation of both spreading- and subduction-phase sediments, their distribution and the nature of their contact (Miller, 1983a). Judging from the data presented in this study, the southern Khomas Trough may be regarded as the most likely position in which spreading-phase sediments may have been preserved. Mainly basin-plain with minor submarine-fan associations may be found in the Matchless Amphibolite oceanic sequence and southwards of it (Fig. 3.18). These deposits contrast with the thick trench-fan associations in the central and northern Khomas Trough. With regard to the deformational patterns described previously, a possible contact between these different depositional systems is most likely to be of tectonic origin.

7.2.4 Collision phase

Post-D_1 deformation patterns in the Khomas Trough give evidence for the onset of major compressive stresses in the lithosphere. This is attributed to the next step in the geotectonic evolution involving collision between the two cratons (Fig. 7.4).

By this stage, the accretionary prism had reached a considerable size. Initial collision led to the regional D_2 deformation in the Khomas Trough producing metre- to kilometre-scale isoclinal to open folds and a penetrative, axial-planar metamorphic banding cleavage. Fold axes trend horizontally to subhorizontally to the northeast and structural vergences are consistently to the southeast, indicating tectonic transport in this direction. Folds of the D_1 phase were refolded to develop D_2 downward-facing folds in restricted parts of

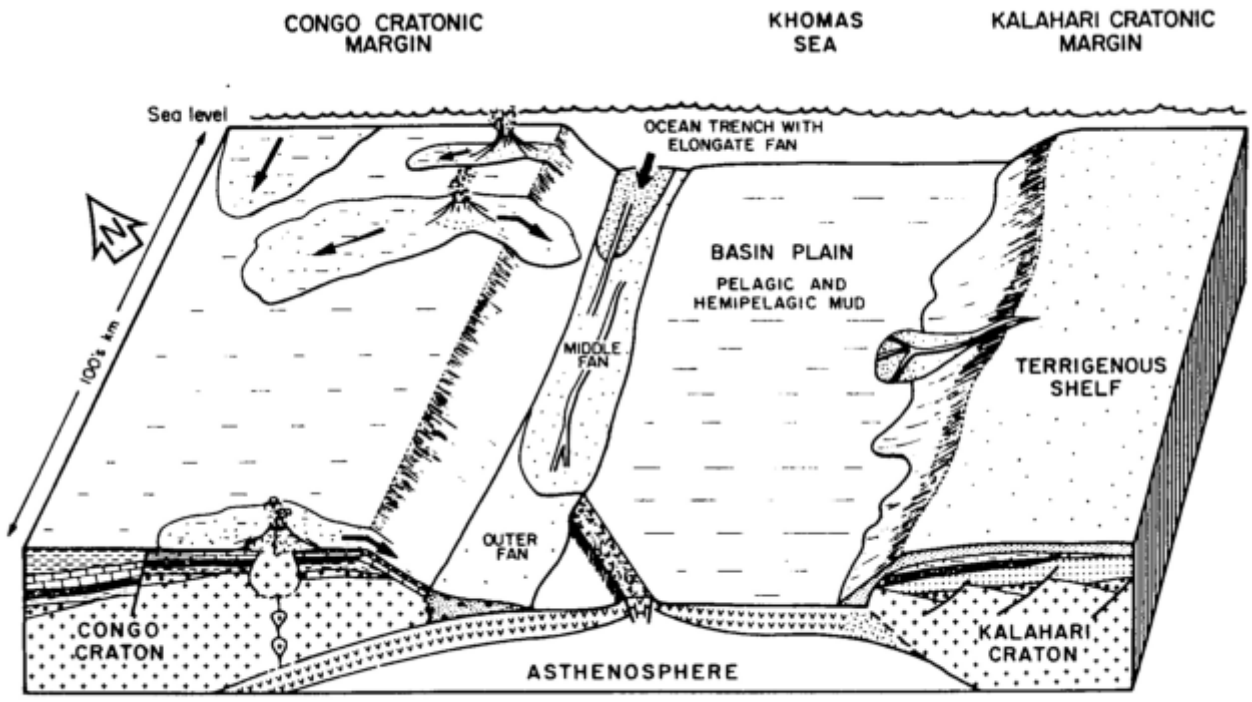

Fig. 7.3: Palaeoenvironmental setting during late continental convergence. High sediment input into the trench maintains shallow subduction and a narrow arc - trench gap. Terrigenoclastic sedimentation occurs on both adjacent shelves at this stage.

the sequence. Also associated with this deformation was a major phase of thrusting.

The continuation of collision resulted in the D_3 deformation. This was characterized by a spaced cleavage and tight to isoclinal metre-scale F_3 folds which developed preferentially in high-strain shear and thrust zones. The style and scale of folding and the subhorizontal to moderately-plunging attitude of fold axes confirm the major role of simple shear processes during this deformation. In two of the thrust zones in the northern Khomas Trough, late-tectonic scapolitization occurred, probably indicating the presence and the migration of Na- and Cl-rich fluids. This might confirm results from modem accretionary prisms which show that fluids participate actively during the development of shear zones (Peacock, 1987). The fluids are channelized and preserved in major pelagic horizons in the prism over a considerable time-span (Moore, 1989). At this stage of the geotectonic evolution, the structures within the accretionary prism defined a northward-steepening thrust pile with an overall imbricate fan geometry. The observed development from metamorphic banding cleavages (S_1 and S_2), which probably originated from pressure solution during dewatering processes (Behr *et al.*, 1983), to a shear cleavage (S_3) conforms with theoretical considerations on the dynamics of thick orogenic wedges by Platt (1986). A second possible emplacement mechanism for the Matchless Amphibolite is that it may have been structurally emplaced at this stage during abduction of the accretionary prism onto the Kalahari Craton. This explanation is fa-voured and strengthened by the emplacement of Alpine-type ultramafic bodies close to and south of the Matchless Amphibolite (Fig. 7.4) and by tectonic interleaving of basement slices and ultramafic rocks in the Southern Margin Zone (Barnes, 1982). The latter occur together with a prominent rhyolite unit close to the Schlesien-Amerongen Line (Hartnady, 1978) or Us Pass Lineament (Hoffmann, 1983) along the northern margin of the Southern Margin Zone (Fig. 7.4). This Lineament has been interpreted to represent the continental suture zone (Hartnady, Hoffmann, op.cit.) which can probably be traced into the Mwembeshi shear zone of the Zambezi Belt (Unrug, 1990).

The continental collision and subduction of the Kalahari Craton beneath the Congo Craton resulted in crustal thickening and thermal relaxation. The processes associated with a collision-related, late-tectonic regional metamorphism are reflected in the metasediments and metabasic rocks of the Khomas Trough. Growth of critical metamorphic minerals such as kyanite, sillimanite, andalusite, staurolite, garnet and amphibole started mostly during D_2 and lasted until after D_3. Scapolite in the northern Khomas Trough post-dates the D_3 deformation. There are indications, however, that biotite, garnet, kyanite and staurolite also grew prior to D_2. Geothermo-barometric calculations on post-D_3 and on some D_2 mineral assemblages show that P-T conditions within the amphibolite facies rocks varied considerably. Values of about 7 kbar and 570°C have been calculated for the southern Khomas Trough, about 2 kbar and 570°C for the centre and about 4 kbar and 660°C for the north. Partial melting of the metasediments during regional metamorphism at about 660°C occurred at the northern margin. U/Pb analyses on monazites indicate an age of about 525 Ma for this event which is also interpreted to represent the peak of metamorphism (Kukla *et al.*, 1990a). The above pressures and temperatures correspond to geothermal gradients of about 20°C/km, 80°C/km and 45°C/km from south to north and it is conceivable that these heterogeneous gradients are due to post-D_3 differential uplift of the Khomas Trough.

Late stages in the structural evolution comprise the formation of crenulation cleavages as well as kink folds in the

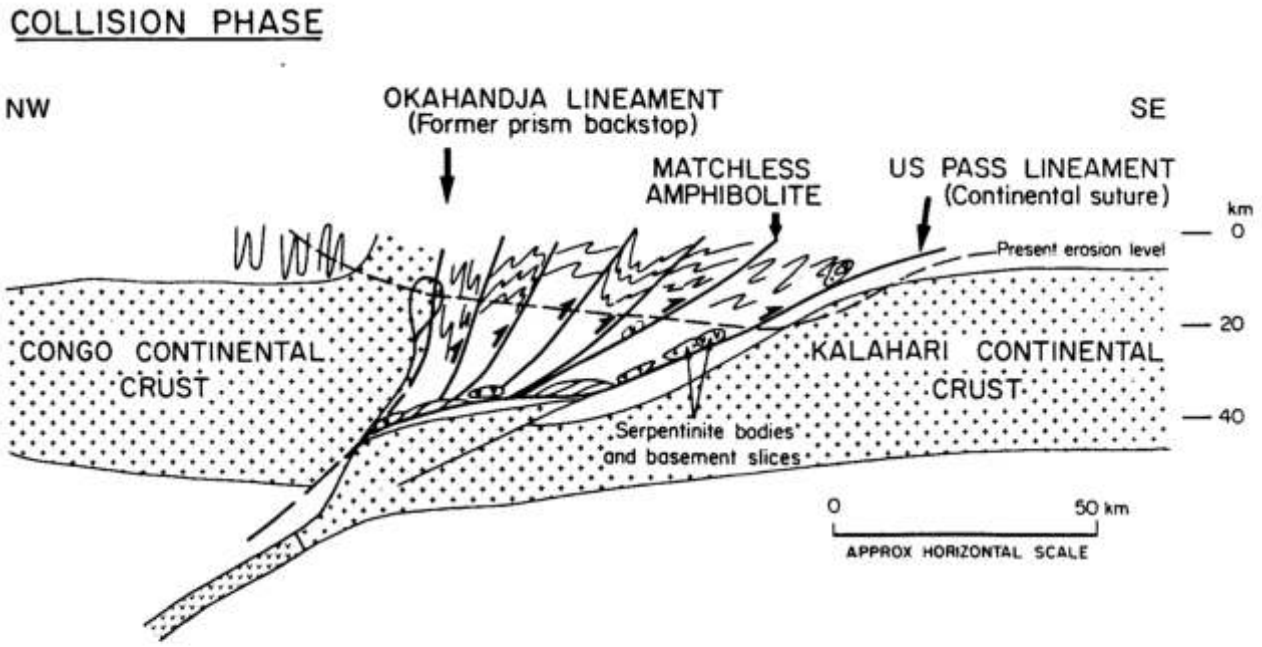

Fig. 7.4: Collision between the Congo and Kalahari Cratons. This was accompanied by strong southeast-vergent folding and thrusting, late-tectonic metamorphism, and emplacement of the accretionary prism including the Matchless Amphibolite onto the Kalahari Cratonic Foreland. The post-tectonic Donkerhuk Granite intruded partly along the Okahandja Lineament.

southern Khomas Trough. Along the Okahandja Lineament, late dextral strike-slip movements produced a clockwise rotation of D_1 to D_4 structural elements. It is suggested that this opened a path for the ascent of the post-tectonic Donkerhuk Granite at about 505 Ma (U/Pb monazite ages; Kukla *et al.*, 1990a). The retrograde path of metamorphism involved the growth of muscovite, chlorite and amphibole and textures suggest that this took place in a largely stress-free environment after the D_4 deformation.

The end of the main orogenic movements has been interpreted to be represented by the cooling of biotites below 300°C at about 485 Ma (Rb/Sr and K/Ar whole rock ages; Haack, 1983). Certainly an exception are late alaskite intrusions in the Central Zone with a Rb/Sr whole rock age of 458± 8 Ma, obtained by Kröner and Hawkesworth (1977).

7.2.5 Ancient and modern analogues

Lithologies, structural styles, sedimentation patterns, time-sequence of events and the size of the Khomas Hochland accretionary prism are most reminiscent of the Lower Palaeozoic Southern Upland accretionary prism (e.g. Leggett *et al.*, 1979; Kemp, 1987) in view of: (i) series of imbricate thrust slices steepening towards the backstop (Southern Uplands Fault here compared with the Okahandja Lineament); (ii) extreme lateral persistence (150 km) of stratigraphic marker horizons and thrust slices; (iii) the predominance of lateral trench-fill turbidite sedimentation; (iv) non-recognition of melange deposits; (v) the scarcity of arc-related magmatic rocks and (vi) the low- to medium-pressure metamorphism.

The Chugach terrain in Alaska has been explained as a Cretaceous trench-fill deposit (Nilsen and Zuffa, 1982; Sample and Moore, 1987). Broad similarities with the Khomas Trough exist in terms of: (i) linear extent (2000 km long, 100 km wide); (ii) contained lithologies such as sandstones, siltstones, shales, limestones, basalts, and ultra-mafics; (iii) late-phase granite intrusions towards the continental margin and (iv) structural style comprising coaxial deformation "seawards" and non-coaxial deformation with rotation and strike-slip faulting "landwards".

The time-sequence of events during deformation of the Shumagin region of the modem Aleutian Trench (Lewis *et al.*, 1988) can be compared with the Khomas Trough, involving successively: (i) early folding and thrust faulting; (ii) thrust faulting; and (iii) strike-slip faulting.

The inferred tectonic setting of the Khomas Sea during subduction is compared with the present situation of the southern Peru - Chile Trench (Cross and Pilger, 1982). There, the Chile Rise spreading centre passes obliquely into the trench, which causes an intercalation of turbidite trench sediments with oceanic crust, pelagic sediments and spreading centre hydro thermal deposits, similar to that observed at the Matchless Amphibolite. The subduction of young, hot and buoyant oceanic crust causes shallow slab angles, an effect which is enhanced by high sediment input into the trench. This leads consequently to a narrow arc - trench gap with no major fore-arc basin developed and finally results in a complete cessation of arc magmatism because young lithosphere may be absorbed into the asthenosphere before low-density magma is produced (Cross and Pilger, 1982). This is the case on the South American Plate where arc magmatism has ceased in the area of the subducted Chile Rise (south of 43°S). These mechanisms would explain the scarcity of arc-related magmatism in the Central Zone of the Damara Orogen (see Fig. 7.3) as well as the inferred lack of fore-arc basin deposits.

8. ACKNOWLEDGEMENTS

This study is the result of a research project which was funded by the Geological Survey of Namibia which is gratefully acknowledged. The Deutsche Forschungsgemeinschaft (DFG) and the Foundation for Research Development (FRD) of the CSIR are thanked for additional funds. The Geological Survey, Windhoek, kindly supplied four-wheel drive vehicles and field equipment.

Special thanks go to Dr Roy McG. Miller, Director of the Geological Survey of Namibia, for his generous support during the fieldwork, the fruitful discussions and the invitation to publish this memoir.

This memoir is based on a Ph.D. dissertation, submitted to the University of the Witwatersrand, Johannesburg. The Department of Geology is thanked for financial and logistical support during this period. During the project, many people gave advice and had critical discussions with the writer who would like to thank all of them sincerely for their help. In particular my supervisor Dr Ian Stanistreet is thanked for his encouragement, his great support and his never ending willingness for discussions. Dr Guy Charlesworth is thanked for his enthusiastic supervision of the structural geology. Special thanks are extended to Prof. Martin Okrusch of the Mineralogy Institute of the University of Würzburg, Germany for his challenging criticism and for his great support during my research leave from his department. I thank Dr Ken Maiden, Mount Isa, for the original initiation of this project.

I am thankful for the discussions and field trips with Geological Survey of Namibia staff, in particular Dr Roger Swart, Mr Karl Hoffmann and Mr Frickie Badenhorst.

The work has benefited from discussions with colleagues in the Geology Department, particularly Prof. Spike McCarthy, Drs Michael Meyer and Thomas Wallmach, Mr Tony Cadle, Mr George Henry, Dr Sharad Master, Mr Rudi Boer and Ms Gil Drennan. I especially thank George Henry for his patient introduction to Namibia and the long discussions on the Damara. Thanks are extended to the staff of the Mineralogy Institute, Würzburg University, in particular Dr Horst Häussinger who is thanked for providing a computer-programme which helped to process microprobe analyses, and Mr Bernd Bühn. Prof. Peter Richter and Mrs R. Baur are thanked for their support during geochemical studies at this department, and Dr Uli Schüssler for his assistance during the microprobe analyses. Many thanks to Mrs Angelika Kirchner for her administrative assistance.

Prof. Bault Verhagen of the Schonland Research Centre for Nuclear Sciences, University of the Witwatersrand, is thanked for the stable isotope analyses carried out in his laboratory.

I also acknowledge useful discussions with Prof. Arnold H. Bouma (Louisiana State University, Baton Rouge, USA), Mr Dudley Corbett and Mr Louis Kruger (Gold Fields Botswana and N arnibia Ltd), Mr Rainer Schneeweiss (Rössing Uranium Ltd), Dr Tim Smalley, and Dr Gregor Borg (Bundesanstalt für Geowissenschaften und Rohstoffel Hannover/ Germany). Many thanks go to Dudley Corbett for the dedication of his “calc-silicate song”, developed around the fire over long ponderings on the Kuiseb schists.

Special thanks are addressed to the farming families in the Khomas Hochland whose hospitality and support were fabulous. In particular Hardus and Anita Myburgh (Okasume), Mr and Mrs Jacob (Kaan Dam) and Mrs Johnston (Kaan) are thanked for their friendship.

Thanks also to Ms Judy Wilmot for her administrative help, to Mrs Nellie Day for her assistance in providing the geochemical data, to Mrs Lyn Whitfield for the line drawings and to Mr Mark Hudson and Mr Klaus-Peter Kelber (Würzburg) for the photographic work. Messrs Mitch Miles, Matt Kitching, Alex Mathebula, the late John Molotsi and Peter Spathe (Würzburg) are thanked for technical support and the preparation of thin and polished sections.

A special word of thanks goes to my parents for their support and encouragement. I am deeply indebted to my wife and “colleague” Christine for her great scientific and moral support during this project, and for always being a cheerful partner during our joint fieldwork in the Khomas Hochland which also included beat, frost, flash floods and beautiful wildlife.

9. REFERENCES

Ahrendt, H., Hunziker, J.C. and Weber, K. (1977). Age and degree of metamorphism and time of nappe emplacement along the southern margin of the Damara Orogen/Namibia (SW-Africa). *Geol. Rdsch.*, **67**, 719-742.

Althaus, E. (1969). Das System Al_2O_3-SiO_2-H_2O. Experimentelle Untersuchungen und Folgerungen für die Petrogenese der metamorphen Gesteine. *Neues Jb. Miner. Abh.*, **111**, 74-161.

Anderson, T.B. (1974). The relationship between kink bands and shear fractures in the experimental deformation of slate. *J. geol. Soc. Lond.*, **130**, 367-382.

Arthur, M.A., Dean, W.E. and Stow, D.A.V. (1984). Models for the deposition of Mesozoic-Cenozoic fine-grained organic-carbon-rich sediment in the deep sea. *In*: Stow, D.A.V. and Piper, D.J.W., (Eds), *Fine-grained sediments: deep-water processes and facies*. Spec. Publ. geol. Soc. Lond., **15**, 527-560.

Badenhorst, F.P. (1987). Lithostratigraphy of the Damara Sequence in the Omaruru area of the northern Central Zone of the Damara Orogen and a proposed correlation across the Omaruru Lineament. *Communs geol. Surv. S.W.Afr./Namibia*, **3**, 3-8.

Baier, B., Berckhemer, H., Gajewski, D., Green, RW., Grimsel, Ch., Prodehl, C. and Vees, R. (1983). Deep seismic sounding in the area of the Damara Orogen, Namibia, South West Africa, 885-900. *In*: Martin, H. and Eder, F.W., (Eds), *Intracontinental Fold Belts - Case Studies in the Variscan Belt of Europe and the Damara Belt in Namibia*. Springer-Verlag, Berlin, 945pp.

Barnes, N.E. and Normark, W.R. (1983/84). Diagnostic parameters for comparing modern submarine fans and ancient turbidite systems. *Geo-Marine Lett*., **3**, Map.

Barne, S.-J. (1982). Serpentinites in central South West Africa/ Namibia - a reconnaissance study. *Mem. geol. Surv. S.W.Afr./Namibia*, **8**, 90pp.

Barnes, S.-J. and Sawyer, E.W. (1980). An alternative model for the Damara Mobile Belt. Ocean crust subduction and continental convergence. *Precambrian Res.*, **13**, 297-336.

Behr, H.-J., Horn, E.E. and Porada, H. (1983). Fluid Inclusions and Genetic Aspects of the Damara Orogen, 611-654. *In*: Martin, H. and Eder, F.W., (Eds), *lntracontinental FoldBelts - Case Studies in the Variscan Belt of Europe and the Damara Belt in Namibia*. Springer-Verlag, Berlin, 945pp.

Berner, RA. and Honjo, S. (1981). Pelagic sedimentation of aragonite: its geochemical significance. *Science*, **211**, 940-942.

Bhatia, M.R. (1983). Plate tectonics and geochemical composition of sandstones. *J. Geol*., **91**, 611-627.

Bhatia, M.R and Crook, K.A.W. (1986). Trace element characteristics of greywackes and tectonic setting discrimination of sedimentary basins. *Contr. Miner. Petrol*., **92**, 181-193.

Blaine, J.L. (1977). Tectonic evolution of the Waldau Ridge structure and the Okahandja Lineament in part of the Central Damara Orogen, west of Okahandja, South West Africa. *Bull. Precambrian Res. Unit, Univ. Cape Town*, **21**, 99pp.

Blaxland, A., Gohn, E., Haack, U. and Hoffer, E. (1979). Rb/Sr ages of late-tectonic granites in the Damara Orogen, Southwest Africa/Namibia. *Neues Jb. Miner. Mh*., **11**, 498-508.

Bouma, A.H. (1962). *Sedimentology of some flysch deposits: a graphic approach to facies interpretation*. Elsevier, Amsterdam, 168pp.

Bouma, A.H., Normark, W.R. and Barnes, N.E., (Eds), (1985). *Submarine fans and related turbidite systems*. Springer-Verlag, New York, 351pp.

Bowles, F.A., Ruddiman, W.F. and Jahn, W.H. (1978). Acoustic stratigraphy, structure and depositional history of the Nicobar fan, eastern Indian ocean. *Marine Geology*, **26**, 269-288.

Boyer, S.E. and Elliot, D. (1982). Thrust systems. *Bull. Am. Ass. Petrol. Geol.*, **66**, 1196-1230.

Brandt, R. (1987). Evolution of the Pan-African granitic rocks of the Damara Orogen, Namibia, 121-125. *In*: Matheis, G. and Schandelmeier, H.S., (Eds), *Current research in African earth-sciences*. Balkema, Rotterdam.

Breitkopf, J.H. (1986). *Iron formations and associated amphibolites in the southern part of the Damara Orogen of South West Africa/Namibia*. Ph.D. thesis (unpubl.), Univ. Witwatersrand, Johannesburg, 350pp.

Breitkopf, J.H. and Maiden, K.J. (1987). Geochemical patterns of metabasites in the southern part of the Damara Orogen, SW A/Namibia: applicability to the recognition of tectonic environment. *In*: Pharaoh, T.C., Beckinsale, R.D. and Rickard, D., (Eds), *Geochemistry and Mineralization of Proterozoic Suites*, Spec. Publ. geol. Soc. Lond., **33**, 355-361.

Breitkopf, J.H. and Maiden, K.J. (1988). Tectonic setting of the Matchless pyritic copper deposits, Namibia. *Econ. Geol.*, **83**, 710-723.

Briqueu, L., Lancelot, J.P., Valois, J.P. and Walgenwitz, F. (1980). Géochronologie U-Pb et genèse d'un type de minéralisation uranifère: les alaskites de Goanikontes (Namibie) et leur encaissant. *Bull. Cent. Réch. Explor.-Prod., Elf-Aquitaine*, **4**, 759-811.

Carmichael, D.M. (1969). On the mechanism of prograde metamorphic reactions in quartz-bearing pelitic rocks. *Contr. Miner. Petrol*., **20**, 244-267.

Carmichael, D.M. (1970). Intersecting isograds in the Whetstone Lake area, Ontario. *Petrology*, **11**, 147-181.

Carmichael, I., Turner, F. and Verhoogen, J. (1974). *Igneous Petrology*. McGraw Hill, New York, 739pp.

Chatterjee, N.D. and Johannes, W. (1974). Thermal stability and standard Thermodynamics Properties of synthetic $2M_1$-muscovite, $KAl_2[AlSi_3O_{10}(OH)_2]$. *Contr. Miner. Petrol.*, **48**, 89-114.

Clifford, T.N. (1967). The Damara episode in the Upper Proterozoic - Lower Paleozoic structural history of southern Africa. *Spec. Pap. geol. Soc. Amer*., **92**, 100pp.

Cloetingh, S.A.P.L., Wortel, M.J.R. and Vlaar, N.J. (1982). Evolution of passive continental margins and initiation of subduction zones. *Nature*, **297**, 139-142.

Cocker, J.D., Griffin, B.J. and Muehlenbachs, K. (1982). Oxygen and carbon isotope evidence for sea-water-hydro-thermal alteration of the Macquarie Island ophiolite. *Earth Planet. Sc. Lett*., **61**, 112-122.

Condie, K.e. (1982). *Plate tectonics and crustal evolution*. 2nd ed., Pergamon, New York, 310pp.

Coney, P.J. (1989). Structural aspects of suspect terranes and accretionary tectonics in western North America. *J. Struct. Geol*., **11**, 107-125.

Cook, H.E., Field, M.E. and Gardner, L.V. (1982). Characteristics of sediments on modern and ancient continental slopes. *In*: Scholle, P.A. and Spearing, D., (Eds), *Sandstone depositional environments*. Mem. Am. Ass. Petrol. Geol., **31**, 329-364.

Cordani, U.G., Figueiredo, M.C.H., Teixeira, W., Basei, M.A.S. and Solianijr, E. (1990). Geotectonic evolution of the Dom Feliciano Belt in South America. *Abstr. Geocongress '90*, Geol. soc. S. Afr., 111.

Corner, B. (1983). An interpretation of aeromagnetic data covering the western portion of the Damara Orogen in South West Af-

rica/Namibia. *Spec. Publ. geol. Soc. S. Afr.*, **11**, 339-354.

Coumes, F., Delteil, G.H., Ravenne, C. and Cremer, M. (1983). Cap Ferret Deep-Sea Fan. *In*: Watkins, J.S. and Drake, C.L., (Eds), *Studies in continental margin geology*. Mem. Am. Ass. Petrol. Geol., **34**, 583-592.

Coward, M.P. (1983). The tectonic history of the Damara Belt. *Spec. Publ. geol. Soc. S. Afr.*, **11**, 409-421.

Cox, K.G., Bell, J.D. and Pankhurst, R.J. (1979). *The interpretation of igneous rocks*. Allan and Unwin, London, 450pp.

Crook, K.A.W. (1974). Lithogenesis and geotectonics: the significance of compositional variations in flysch arenites (greywackes). *In*: Dott, R.H. and Shaver, R.H., (Eds), *Modern and Ancient Geosynclinal sedimentation*. Spec. Publ. Soc. Econ. Paleont. Miner., 19, 304-310.

Cross, T.A. and Pilger, R.H. Jr. (1982). Controls on subduction geometry, location of magmatic arcs, and tectonics of arc and back-arc regions. *Bull. geol. Soc. Am*., **93**, 545-562.

Davis, E.E., Goodfellow, W.O., Bornhold, B.D., Adshead, J., Blaise, B., Villinger, H. and Le Cheminant, G.M. (1987). Massive sulfides in a sedimented rift valley, northern Juan de Fuca ridge. *Earth Planet. Sc. Lett*., **82**, 49-61.

De Kock, G.S. (1985). Die geologie van'n gebied suidoos van Karibib, Suidwes-Afrika/Namibie. *Communs geol. Surv. S.W. Afr./Namibia*, **1**, 45-55.

De Kock, W.P. (1934). The Geology of the Western Rehoboth, an explanation of sheet F33-W3. *Mem. Dept. Mines, S.W.Afr*., **1**, 148pp.

De Waal, S.A. (1966). *The Alberta Complex, a metamorphosed layered intrusion north of Nauchas, South West Africa, the surrounding granites and repeated folding in the younger Damara System*. D.Sc. thesis (unpubl.), Univ. Pretoria, 207pp.

Dickenson, M.P. and Hewitt, D.A. (1986). A garnet-chlorite geothermometer. *Geol. Soc. Am. Abstracts with Programs*, **18**, 584.

Dickinson, W.R. and Seely, D.R. (1979). Structure and stratigraphy of forearc regions. *Bull. Am. Ass. Petrol. Geol.*, **63**, 2-31.

Donath, F.A. (1961). Experimental study of shear failure in anisotropic rocks. *Bull. geol. Soc. Am*., **72**, 985-990.

Downing, K.N. (1983). The stratigraphy and palaeoenvironment of the Damara Sequence in the Okahandja Lineament area. *Spec. Publ. geol. Soc. S. Afr.*, **11**, 37-41.

Downing, K.N. and Coward, M.P. (1981). The Okahandja Lineament and its significance for Damaran tectonics in Namibia. *Geol. Rdsch.*, **70**, 972-1000.

Ellis, D.E. (1978). Stability and phase equilibria of chloride and carbonate bearing scapolites at 750°C at 4.000 bar. *Geochim. cosmochim. Acta*, **42**, 1271-1281.

Esquevin, J. and Menendez, R. (1975). *Radiodatation sur roches du permis Diana*. S.N.P.A Rep. for Elf Aquitaine S.W.Afr., Mineral Exploration (unpubl.), 12pp.

Eugster, H.P. (1970). Thermal and ionic equilibria among muscovite, K-feldspar and alumosilicate assemblages. *Fortschr. Miner.*, **47**, 106-123.

Evans, B.W., Shaw, D.M. and Haughton, D.R. (1969). Scapolite stoichiometry. *Contr. Miner. Petrol*., **24**, 293-305.

Faupel, J. (1974). Geologisch-mineralogische Untersuchungen am Donkerhoek-Granit (Karibib-Distrikt, Südwestafrika). *Göttinger Arb. Geol. Palaeont*., **15**, 95pp.

Faure, G. (1986). *Principles of isotope geology*. J. Wiley and Sons, New York, 589pp.

Ferry, J.M. and Spear, F.S. (1978). Experimental calibration of the partitioning of Fe and Mg between biotite and garnet. *Contr. Miner. Petrol*., **66**, 113-1l7.

Finnemore, S.H., (1978). The geochemistry and origin of the Matchless amphibolite belt, Windhoek district, South West Africa. *Spec. Publ. geol. Soc. S. Afr*., **4**, 433-477.

Fleuty, M.J. (1964). The description of folds. *Proc. Geol. Ass. Lond*., **75**, 461-492.

Floyd, P.A. and Winchester, J.A. (1975). Magma type and tectonic setting discrimination using immobile elements. *Earth Planet. Sc. Lett*., **27**, 211-218.

Frets, D.C. (1969). Geology and structure of the Huab-Welwitschia area, South West Africa. *Bull. Precambrian Res. Unit, Univ. Cape Town*, **5**, 235pp.

Garcia, M.O. (1978). Criteria for the identification of ancient volcanic rocks. *Earth-sc. Rev*., **14**, 147-165.

Gevers, T.W. (1931). An ancient tillite in South West Africa. *Trans. geol. Soc. S. Afr*., **34**, 1-17.

Gevers, T.W. (1963). Geology along the northwestern margin of the Khomas Highlands between Otjimbingwe-Karibib and Okahandja, South West Africa. *Trans. and Proceed. geol. Soc. S. Afr.*, **66**, 199-258.

Ghent, E.D. and Stout M.Z. (1981). Geobarometry and geothermometry of plagioclase-biotite-garnet-muscovite assemblages. Contr. Miner. Petrol., 76, 92-97.

Goldsmith, J.R and Newton, R.C. (1977). Scapolite-plagioclase stability relations at high pressures and temperatures in the system $NaAlSi_3O_8$-$CaAl_2Si_2O_8$-$CaCO_3$-$CaSO_4$. *Am. Miner*., **62**, 1063-1081.

Gorsline, D.S. (1984). A review of fine-grained sediment origins, transport and deposition. *In*: Stow, D.A.V. and Piper, D.J.W., (Eds), *Fine-grained sediments: deep-water processes and-facies*. Spec. Publ. geol. Soc. Lond., **15**, 17-34.

Graham, S.A. and Bachman, S.B. (1983). Structural controls on submarine-fan geometry and internal architecture: upper La Jolla fan system, offshore Southern California. *Bull. Am. Ass. Petrol. Geol*., **67**, 83-96.

Green, R.W.E. (1983). Seismic refraction observations in the Damara Orogen and flanking craton and their bearing on deep seated processes in the orogen. *Spec. Publ. geol. Soc. S. Afr.*, **11**, 355-367.

Gressly, A. (1838). Observations géologique sur le Jura Soleurois. *Neue Denkschr. Allg. Schweiz. Ges. Naturwiss*., 2, 1-112.

Guidotti, C.V. (1970). The mineralogy and petrology of the transition from the lower to upper sillimanite zone in the Oquossoc Area, Maine. *J. Petrol.*, **11**, 277-336.

Haack, U. (1983). Reconstruction of the cooling history of the Damara Orogen by correlation of radiometric ages with geography and altitude, 873-884. *In*: Martin, H. and Eder, F.W., (Eds), *Intracontinental FoldBelts - Case Studies in the Variscan Belt of Europe and the Damara Belt in Namibia*. Springer-Verlag, Berlin, 945pp.

Haack, U. and Martin, H. (1983). Geochronology of the Damara-Orogen - A Review, 839-846. *In*: Martin, H. and Eder, F.W., (Eds), *Intracontinental Fold Belts - Case Studies in the Variscan Belt of Europe and the Damara Belt in Namibia*. Springer Verlag, Berlin, 945pp.

Hälbich, I.W. (1970). *The geology of the western Windhoek and Rehoboth Districts, a stratigraphic-structural analysis of the Damara System*. D.Sc. thesis (unpubl.), Univ. Stellenbosch, 199pp.

Hälbich, I.W. (1977). Structure and tectonics along the southern margin of the Damara mobile belt, South West Africa. *Annale Univ. Stellenbosch, Ser. Al(Geol*), **2**, 149-247.

Häussinger, H. (1990). *Geochemische und petrologische U ntersuchungen an metasedimentären Nebengesteinen und assoziierten Metabasiten der Sulfiderzvorkommen von Gorob, Damara Orogen, Namibia*. Ph.D. thesis (unpubl.), Univ. Würzburg, 258pp.

Häussinger, H. and Kukla, P.A. (1990). The interpretation of geochemical data from metaturbidites using the TiO_2/Zr ratio. *Europ. J. Miner*., **2**, Beih. 1,87.

Hahn-Weinheimer, P. (1966). Die isotopische Verteilung von Kohlenstoff und Schwefel in Marmor und anderen Metamor-

phiten. *Geol. Rdsch*., **55**, 197-209.

Hartmann, O., Hoffer, E. and Haack, U. (1983). Regional metamorphism in the bamara Orogen: interaction of crustal motion and heat transfer. *Spec. Publ. geol. Soc. S. Afr*., **11**, 233-241.

Hartnady, C.J. (1978). The stratigraphy and structure of the Naukluft nappe complex. *14th and 15th an. Rep. Precambrian Res. Unit*, Univ. Cape Town, 163-170.

Hartnady, C.J.R, Joubert, P. and Stowe, C. (1985). Proterozoic crustal evolution in southwestern Africa. *Episodes*, **8**, 236-244.

Hawkesworth, C.J., Kramers, K.D. and Miller, R. McG. (1981). Old model Nd ages in Namibian Pan-African rocks. *Nature*, **289**, 278-282.

Hawkesworth, C.J., Gledhill, A.R., Roddick, J.C., R. McG. Miller, and Kröner, A. (1983). Rb/Sr and Ar/Ar Studies bearing on Models for the Thermal Evolution of the Damara Belt, Namibia. *Spec. Publ. geol. Soc. S. Afr*., **11**, 323-339.

Heath, K.C. and Mullins, H.T. (1984). Open-ocean, off-bank transport of fine-grained carbonate sediment in the Northern Bahamas. *In*: Stow, D.A.V. and Piper, D.J.W., (Eds), *Fine-grained sediments: deep-water processes and facies.* Spec. Publ. geol. Soc. Lond., **15**, 199-208.

Henry, G., Stanistreet, I.G. and Maiden, K.J. (1986). Preliminary results of a sedimentological study of the Chuos Formation in the Central Zone of the Damara Orogen: evidence for mass flow processes and glacial activity. *Communs geol. Surv. S.W.Afr./Namibia*, **2**, 75-92.

Henry, G., Clendenin, C.W., Stanistreet, I.G. and Maiden, K.J. (1990). A multiple detachment model for the early rifting stage of the Late Proterozoic Damara Orogen in Namibia. *Geology*, **18**, 67-71.

Hiscott, R.N. and Middleton, G.V. (1979). Depositional mechanics of thick-bedded sandstones at the base of a submarine slope, Tourelle Formation (Lower Ordovician), Quebec, Canada. *Spec. Publ. Soc. Econ. Paleont. Miner.*, **27**, 307-326.

Hobbs, B.E., Means, W.D. and Williams, P.F. (1976). *An outline of structural geology*. John Wiley, New York, 571pp.

Hodges, K.V. and Spear, F.S. (1982). Geothermometry, geobarometry and the Al_2SiO_5 tripple point at Mt. Moosilauke, New Hampshire. *Am. Miner.*, **67**, 1118-1134.

Hoefs, J. (1980). *Stable isotope geochemistry*. Springer-Verlag, Berlin, 208pp.

Hoffer, E. (1977). *Petrologische Untersuchungen zur Regionalmetamorphose Al-reicher Metapelite im südlichen Damara-Orogen (Südwest-Afrika)*. Habilitationsschrift (unpubl.), Univ. Göttingen, 150pp.

Hoffer, E. (1983). Compositional Variations of Minerals Involved in Low to Medium Grade Isograd Reactions in the Southern Damara Orogen, Namibia, South West Africa, 745-767. *In*: Martin, H. and Eder, F.W., (Eds), *Intracontinental Fold Belts - Case Studies in the Variscan Belt of Europe and the Damara Belt in Namibia*, Springer Verlag, Berlin, 945pp.

Hoffmann, C. (1976). Granites and migmatites of the Damara Belt, South West Africa. Petrography and melting experiments. *Geol. Rdsch*., **65**, 939-966.

Hoffmann, K.H. (1983). Lithostratigraphy and facies of the Swakop Group of the Southern Damara Belt, SWA/Namibia. *Spec. Publ. geol. Soc. S. Afr.*, **11**, 43-63.

Hoffmann, K.H. (1987). Stratigraphic subdivision and sedimentary facies of the Duruchaus Formation in the Geelkop Dome and Nauaspoort-Wortelpoort area north of Rehoboth, southern Damara Belt. *Communs geol. Surv. S.W.Afr./Namibia*, **3**, 9-18.

Hoinkes, G. (1986). Effect of grossular-content in garnet on the partitioning of Fe and Mg between garnet and biotite. *Contr. Miner. Petrol*., **92**, 393-399.

Holdaway, M.J. (1971). Stability of andalusite and the aluminium silicate phase diagram. *Am. J. Sc.*, **271**, 97-131.

Hoschek, G. (1969). The stability of staurolite and chloritoid and their significance in metamorphism of pelitic rocks. *Contr. Miner. Petrol.*, **22**, 208-232.

Indares, A. and Martignole, J. (1985). Biotite-garnet geothermometry in the granulite facies: the influence of Ti and Al in biotite. *Am. Miner*., **70**, 272-278.

Jacob, R.E. (1974). Geology and metamorphic petrology of part of the Damara Orogen along the lower Swakop river, South West Africa. *Bull. Precambrian Res. Unit, Univ. Cape Town*, **17**, 185pp.

Jaeger, J.C. (1957). The temperature in the neighbourhood of a cooling intrusive sheet. *Am. J. Sc.*, **255**, 306-318.

Karig, D.E., Caldwell, J.G. and Parmentier, E.M. (1976). Effects of accretion on the geometry of the descending lithosphere. *J. geophys. Res*., **81**, 6281-6291.

Kasch, K.W. (1975). A preliminary report on the geology of the southern margin of the Damara Orogen around Omitara, South West Africa. *13th an. Rep. Precambrian Res. Unit*, Univ. Cape Town, 102-138.

Kasch, K.W. (1979). A continental collision model for the tectono-thermal evolution of the (southern) Damara belt. *16th an. Rep. Precambrian Res. Unit*, Univ. Cape Town, 101-107.

Kasch, K.W. (1983a). Continental collision, suture progradation and thermal relaxation: a plate tectonic model for the Damara Orogen in central Namibia. *Spec. Publ. geol. Soc. S. Afr*., **11**, 423-429.

Kasch, K.W. (1983b). Regional P-T variations in the Damara Orogen with particular reference to early high-pressure metamorphism along the southern margin. *Spec. Publ. geol. Soc. S. Afr.*, **11**, 243-253.

Kasch, K.W. (1983c). Folding and thrust tectonics in the southeastern portion of the Damara Orogen around Omitara, Namibia. *Spec. Publ. geol. Soc. S. Afr.*, **11**, 175-184.

Kasch, K.W. (1986). Tectonic subdivision, lithostratigraphy and structural geology of the Upper Black Nossob River area. *Communs geol. Surv. S.W.Afr./Namibia*, **2**, 117-129.

Kasch, K.W. (1987). Metamorphism of pelites in the Upper Black Nossob River area of the Damara Orogen. *Communs geol. Surv. S.W.Afr./Namibia*, **3**, 63-81.

Kemp, A.E.S. (1987). Tectonic development of the Southern Belt of the Southern Uplands accretionary complex. *J. geol. Soc. Lond.*, **144**, 827-838.

Killick, A.M. (1983). Sulphide mineralization at Gorob and its genetic relationship to the Matchless Member, Damara Sequence, SWA/Namibia. *Spec. Publ. geol. Soc. S. Afr.*, **11**, 381-384.

Kimura, G., Koga, K. and Fujioka, K. (1989). Deformed soft sediments at the junction between the Mariana and Yap Trenches. *J. Struct. Geol.*, **11**, 463-472.

Klemd, R. and Okrusch, M. (1990). Phase relationships and fluid-inclusion characteristics of the metamorphosed, stratiform sulfide deposit Matchless, Namibia. *Geol. Rdsch*., **79**, 433-449.

Klemd, R., Maiden K.J. and Okrusch, M. (1987). The Matchless copper deposit SWA/Namibia: A deformed and metamorphosed massive sulfide deposit. *Econ. Geol.*, **82**, 163-171.

Klemd, R., Maiden K.J., Okrusch, M. and Richter, P. (1989). Geochemistry of the metamorphosed massive sulphide deposit Matchless, South West Africa/Namibia: wallrock alteration during submarine ore-forming processes. *Econ. Geol*., **84**, 603-617.

Kröner, A. (1982). Rb-Sr geochronology and tectonic evolution of the Pan-African Damara Belt of Namibia, southwestern Africa. *Am. J. Sc*., **282**, 1471-1507.

Kröner, A. and Hawkesworth, C. (1977). Late Pan-African em-

placement ages for Rössing alaskitic granite (Damara Belt) and Rooi Lepel bostonite (Gariep Belt) in Namibia and their significance for the timing of metamorphic events. *20th an. Rep. Res. Inst. Afr. Geol*., Univ. Leeds, 14-17.

Kukla, C. (in prep.). *Geochronological and isotope geochemical studies on the Kuiseb Formation metasediments in the southern Damara Orogen, Central Namibia*. Ph.D; thesis (unpubl.), Univ. Würzburg.

Kukla, C., Kramm, U., Okrusch, M. and Grauert, B. (1990). Isotope studies and their implication for the metamorphic processes in the Kuiseb Formation of the southern Damara Orogen, Namibia. *Ext. Abstract, Geocongress '90*, geol. Soc. S. Afr., 305-308.

Kukla, P.A, Opitz, e., Stanistreet, I.G. and Charlesworth, E.G. (1988). New aspects of the sedimentology and structure of the Kuiseb Formation in the western Khomas Trough, Damara Orogen, SWA/Namibia. *Communs geol. Surv. S.W.Afr./Namibia*, **4**, 33-42.

Kukla, P.A., Charlesworth, E.G., Stanistreet, I.G. and Kukla, C. (1989). Downward-facing structures in the Khomas Trough of the Damara Orogen, Namibia. *Communs geol. Surv. Namibia*, **5**, 53-57.

Kukla, P.A., Kukla, C., Stanistreet, I.G. and Okrusch, M. (1990). Unusual preservation of sedimentary structures in sillimanite-bearing metaturbidites of the Damara Orogen, Namibia. *J. Geol.*, **98**, 91-99.

Land, L.S. (1980). The isotopic and trace element geochemistry of dolomite: the state of the art. *Spec. Publ. Soc. Econ. Paleont. Miner.*, **28**, 87-110.

Lash, G.G. (1986). Sedimentology of channelized turbidite deposits in an ancient (early Palaeozoic) subduction complex, central Appalachians. *Bull. geol. Soc. Am.*, **97**, 703-710.

Leggett, J.K., McKerrow, W.S. and Eales, M.H. (1979). The Southern Uplands of Scotland; a Lower Palaeozoic accretionary prism. *J. geol. Soc. Lond.*, **136**, 755-770.

Lewis, S.D., Ladd, J.W. and Bruns T,R. (1988). Structural development of an accretionary prism by thrust and strike-slip faulting: Shumagin region, Aleutian Trench. *Bull. geol. Soc. Am.*, **100**, 767-782.

Löffler, T. and Porada, H. (1987). Fazielle Untersuchungen an Metapsammiten der Duruchaus Formation (Geelkop-Aufwölbung, südliches Damara Orogen, Namibia/Südwestafrika). *Communs geol. Surv. S.W.Afr./Namibia*, **3**, 119-127.

Lowe, D. R. (1982). Sediment gravity flows: II. Depositional models with special references to the deposits of high density turbidity currents. *J. sedim. Petrol.*, **52**, 279-297.

MacKinnon, T.C. and Howell, D.G. (1983/84). Turbidite facies in an ancient subduction complex: Torlesse Terrane, New Zealand. *Geo-Marine Lett*., **3**, 211-216.

Maldonado, A. and Stanley, D.J. (1978). Nile Cone depositional processes and patterns in the Late Quaternary, 239-257. *In*: Stanley, D.J. and Kelling, G., (Eds), *Sedimentation in submarine canyons, fans, and trenches*. Dowden, Hutchinson and Ross, Stroudsburg, Pennsylvania., 395pp.

Martin, H. (1965). *The Precambrian Geology of South West Africa and Namaqualand*. Precambrian Res. Unit, Univ. Cape Town, 159pp.

Martin, H. (1983). Overview of the Geosynclinal, Structural and Metamorphic Development of the Intracontinental Branch of the Damara Orogen, 473-502. *In*: Martin, H. and Eder, F. W., (Eds), *Intracontinental Fold Belts - Case Studies in the Variscan Belt of Europe and the Damara Belt in Namibia*. Springer Verlag, Berlin, 945pp.

Martin, H. and Porada, H. (1977). The intracratonic branch of the Damara Orogen in South West Africa. 1. Discussion of the geodynamic models. II. Discussion of relationships with the Pan-African Mobile Belt system. *Precambrian Res*., **5**, 311-357.

Mattes, B.W. and Mountjoy, E.W. (1980). Burial dolomitization of the Upper Devonian Miette Buildup, Jasper National Park, Alberta. *Spec. Publ. Soc. Econ. Paleont. Miner*., **28**, 259-297.

McWilliams, M.O. and Kröner, A. (1981). Paleomagnetism and tectonic evolution of the Pan-African Damara belt, southern Africa. *J. geophys. Res*., **86**, 5147-5162.

Menzies, M. (1976). Rare-earth geochemistry of fused ophiolitic and alpine Iherzolites, 1. Othris, Lanzo and Troodos. *Geochim. cosmochim. Acta*, **40**, 645-656.

Middleton, G.V. and Hampton, M.A. (1973). Sediment gravity flows: mechanics of flow and deposition. *In*: Middleton, G.V. and Bouma, A.H., (Eds), *Turbidites and deep water Sedimentation:* Soc. Econ. Paleont. Miner., Pacific sect., Short course, Anaheim, California, 1-38.

Middleton, G.V. and Hampton, M.A. (1976). Subaqueous sediment transport and deposition by sediment gravity flows, 197-217. *In*: Stanley, D.G.and Swift, D.J., (Eds), *Marine sediment transport and environmental management*. John Wiley, New York, 602pp.

Miller, R.McG. (1979). The Okahandja Lineament, a fundamental tectonic boundary in the Damara Orogen of South West Africa/ Namibia. *Trans. geol. Soc. S. Afr*., **82**, 349-361.

Miller, R.McG. (Ed.), (1983a). Evolution of the Damara Orogen of South West Africa/Namibia. *Spec. Publ. geol. Soc. S. Afr*., **11**, 515pp.

Miller, R.McG. (1983 b). The Pan-African Damara Orogen of South West Africa/Namibia. *Spec. Publ. geol. Soc. S. Afr*., **11**, 431-515.

Miller, R.McG. (1983 c). Tectonic implications of the contrasting geochemistry of Damaran mafic volcanic rocks, South West Africa/Namibia. *Spec. Publ. geol. Soc. S. Afr*., **11**, 115-139.

Miller, R.McG. and Hoffmann, K.H. (1981). Geology of the Damara Belt. *Excursion Guide, Geocongress '81*, geol. Soc. S. Afr., 115pp.

Miller, R.McG. and Burger, A.J. (1983). U-Pb zircon age of the early Damaran Naauwpoort Formation. *Spec. Publ. geol. Soc. S. Afr.*, **11**, 267-272.

Miller, R.McG. and Grote, W. (1988). *Geological Map of the Damara Orogen 1: 500 000*. Geol. Soc. S. Afr., Johannesburg.

Miller, R.McG., Barnes, S.-J. and Balkwill, G. (1983). Possible active margin deposits within the Southern Damara Orogen: The Kuiseb Formation between Okahandja and Windhoek. *Spec. Publ. geol. Soc. S. Afr*., **11**, 73-88.

Miyashiro, A and Shido, F. (1975). Tholeiitic and calc-alkalic series in relation to the behaviours of titanium, vanadium, chromium and nickel. *Am. J. Sc*., **275**, 265-277.

Moore, J.C. (1989). Tectonics and hydrogeology of accretionary prisms: role of the décollement zone. *J. Struct. Geol*., **11**, 95-106.

Morton, J.L., Holmes, ML and Koski, R.A (1987). Volcanism and massive sulfide formation at a sedimented spreading centre, Escabana Trough, offshore northern California. *EOS, Trans. Am. geophys. Un*. **67**, 769-772.

Mottl, M.J., Lawrence, J.R. and Keigwin, L.D. (1983). Elemental and stable-isotope composition of pore waters and carbonate sediments from deep-sea drilling project sites 501/504 and 505. *Init. Repts. DSDP*, **69**, 461-473.

Muhongo, S. (1990). Late Proterozoic collision tectonics in the Mozambique Belt of East Africa. *Abstr.15th Colloquium on African Geology*, Nancy, 276.

Mutti, E. and Sonnino, M. (1981). Compensation cycles: A diagnostic feature of turbidite sandstone lobes. *Abstr. 2nd European Regional Meeting of IAS*, Bologna, 120-123.

Mutti, E. and Ricci Lucchi, F. (1972). Le torbiditi dell' Appenino

settentrionale: introduzione all' analisi di facies. *Mem. Soc. geol. Ital*., **11**, 161-199.

Mutti, E. and Ricci Lucchi, F. (1975). Turbidite facies and facies associations. *In*: Mutti, E. *et al.*, (Eds), *Examples of turbidite facies and associations from selected formations of the Northern Apennines*. Field Trip Guidebook A-II, 9th IAS Congress, Nice, 21-36.

Nelson, C.H. (1983/84). The Astoria Fan: An Elongate Type Fan. *Geo-Marine Lett*., **3**, 65-70.

Nelson, C.H. and Nilsen, T. (1974). Depositional trends of modem and ancient deep-sea fans. *In*: Dott, RH. and Shaver, R.H., (Eds), *Modern and Ancient Geosynclinal Sedimentation*. Spec. Publ. Soc. Econ. Pa1eont. Miner., **19**, 54-76.

Nelson, C.H. and Nilsen, T. (1984). Modern and ancient deep-sea fan sedimentation. *Soc. Econ. Paleont. Miner. Short course*, **14**, 404pp.

Neumann, A.C. and Land, L.S. (1975). Lime mud deposition and calcareous algae in the Bight of Abaco, Bahamas. *J. sedim. Petrol*., **51**, 999-1013.

Nieberding, F. (1976). Die Grenze der Granitzone Südwestlich Otjimbingwe (Karibib-District, Südwestafrika): Intrusionsverband, Tektonik, Petrographie. *Göttinger Arb. Geol. Palaeont.*, **19**, 78pp.

Nilsen, T.H. and Zuffa, G.G. (1982). The Chugach Terrane, a Cretaceous trench-fill deposit, southern Alaska. *In*: Leggett, J.K., (Ed.), Trench-Forearc Geology. *Spec. Publ. geol. Soc. Lond*., **10**, 213-227.

Normark, W.R. (1970). Growth patterns of deep-sea fans. *Bull. Am. Ass. Petrol. Geol.*, **54**, 2170-2195.

Normark, W.R. and Piper, D.J.W. (1972). Sediments and growth pattern of Navy deep-sea fan, San Clemente Basin, California Borderland. *J. Geol*., **80**, 192-223.

Normark, W.R, Mutti, E. and Bouma, A.H., (Eds), (1983/84). *Geo-Marine Lett.*, **3**. Springer-Verlag, New York, 224pp.

Orville, P.M. (1975). Stability of scapolite in the system Ab-An-NaCI-$CaCO_3$ at 4 kb and 750°C. *Geochim. cosmochim. Acta*, **39**, 1091-1105.

Oterdoom, W.H and Wenk, H.-R. (1983). Ordering and composition of scapolite: Field observations and structural interpretations. *Contr. Miner. Petrol.*, **83**, 330-341.

Park, R.G. (1988). *Geological structures and moving plates*. Blakie and Sons, Glasgow and London, 337pp.

Peacock, S.M. (1987). Thermal effects of metamorphic fluids in subduction zones. *Geology*, **15**, 1057-1060.

Pearce, J.A. (1975). Basalt geochemistry used to investigate post tectonic environment on Cyprus. *Tectonophysics*, **25**, 41-67.

Pearce, J.A. (1976). Statistical analysis of major element patterns in basalts. *J. Petrol*., **17**, 15-43.

Pearce, J.A. and Cann, J.R. (1973). Tectonic setting of basic volcanic rocks determined using trace element analyses. *Earth Planet. Sc. Lett*., **19**, 290-300.

Pearce, J.A. and Norry, M.J. (1979). Petrogenetic implications of Ti, Zr, Y and Nb variations in volcanic rocks. *Contr. Miner. Petrol*., **69**, 33-47.

Perchuk, L.L. and Lavrent'Eva IV (1983). Experimental investigation of exchange equilibria in the system cordierite-garnet-biotite, 199-239. *In*: Saxena, S.K., (Ed.), *Kinetics and equilibrium in mineral reactions*. Springer- Verlag, Berlin-Heidelberg-New York, 273pp.

Pettijohn, F.J. (1963). Chemical composition of sandstones excluding carbonate and volcanic sands. *Geol. Surv. Prof Pap*., **440-S**, 1-21.

Pettijohn, F.J. (1975). *Sedimentary rocks*. Harper and Row, New York, 628pp.

Pfurr, N., Ahrendt, H. and Weber, K. (1990). U/Pb and Rb/Sr isotopic study of red granitic gneisses and associated meta-volcanics in the area of the Rostock Massifs, Southern Margin Zone of the Damara Orogen, Namibia and their implications for the Lithostratigraphy of this crustal segment. *Abstr. 15th Colloquium on African Geology*, Nancy, 185.

Phillips, G.N., Groves, D.I. and Reed, K. (1989). Geochemical evolution of the Kuiseb schists, Windhoek, Namibia. *Communs geol. Surv. Namibia*, **5**, 19-30.

Pickering, K.T. (1981). Two types of outer fan lobe sequence from the Late Precambrian Kongsfjord Formation submarine fan, Finnmark, North Norway. *J. sedim. Petrol.*, **367**, 77-104.

Pickering, K.T. (1984). Facies, facies associations and sediment transport/deposition processes in a late precambrian upper basin-slope/pro-delta, Finnmark, N. Norway. *In*: Stow, D.A.V. and Piper, D.J.W., (Eds), *Fine-grained sediments: deep-water processes and facies*. Spec. Publ. geol. Soc. Lond., **15**, 343-362.

Pickering, K.T. (1985). Kongsfjord turbidite system, Norway, 237-244. *In*: Bouma, A.H., Normark, W.R. and Barnes, N.E., (Eds), *Submarine fans and related turbidite systems*. Springer-Verlag, New York, 351pp.

Pickering, K.T. and Hiscott, R.N. (1985). Contained (reflected) turbidity currents from the Middle Ordovician Cloridorme Formation, Quebec, Canada: an alternative to the antidune hypothesis. *Sedimentology*, **32**, 373-394.

Pickering, K.T., Stow, D.A.V., Watson, M.P. and Hiscott, R.N., (1986). Deep-water facies, processes and models: a review and classification scheme for modem and ancient sediments. *Earth-sc. Rev.*, **23**, 75-174.

Piper, D.J.W. (1978). Turbidite muds and silts on deep-sea fans and abyssal plains, 163-176. *In*: Stanley, D.J. and Kelling, G., (Eds), *Sedimentation in submarine canyons, fans, and trenches*. Dowden, Hutchinson and Ross, Stroudsburg, Pennsylvania.

Piper, J.D.A., Briden, J.C. and Lomax, K. (1973). Precambrian Africa and South America as a single continent. *Nature*, **245**, 244-248.

Platt, J.P. (1986). Dynamics of orogenic wedges and the uplift of high-pressure metamorphic rocks. *Bull. geol. Soc. Am*., **97**, 1037-1053.

Porada, H. (1973). Tektonisches Verhalten und geologische Bedeutung von Kalksilikatfels-Lagen und Spindeln im Damara-Orogen Südwest-Afrikas. *Geol. Rdsch*., **62**, 918-938.

Porada, H. (1979). The Damara-Ribeira orogen of the Pan-African Brasiliano cycle in Namibia (South-West Africa) and Brazil as interpreted in terms of continental collision. *Tectonophysics*, **57**, 237-265.

Porada, H. (1983). Geodynamic Model for the Geosynclinal Development of the Damara Orogen, Namibia, South West Africa, 503-541. *In*: Martin, H. and Eder, F.W., (Eds), *Intracontinental Fold Belts - Case Studies in the Variscan Belt of Europe and the Damara Belt in Namibia*, Springer-Verlag, Berlin, 945pp.

Porada, H. and Wittig, R (1975). Zur Tektonik des südlichen Damara- Belts. *Ber. Sond. Forsch. Bers. 48 (unpubl.*), Univ. Göttingen, 51-70.

Porada, H. and Wittig, R. (1983). Turbidites in the Damara Orogen, 543-576. *In*: Martin, H. and Eder, F.W., (Eds), *Intracontinental Fold Belts - Case Studies in the Variscan Belt of Europe and the Damara Belt in Namibia*, Springer-Verlag, Berlin, 945pp.

Preussinger, H. (1987). *Die geologische Situation der Erzlinse Vendome im Gorob-Bezirk, SWA/Namibia*. Diploma thesis (unpubl.), Univ. Würzburg, 137pp.

Preuss inger, H. (1990). Host-rock geology of the metamorphosed massive sulfide deposits at Gorob in the Pan-African Damara Orogen, Namibia. *Afr. J. Earth Sc*., **10**, 717-732.

Preussinger, H., Maiden, K. and Okrusch, M. (1987). Contrasting styles of sedimentation in metasediments of the Kuiseb Formation near Gorob, SWA/Namibia. *Communs geol. Surv.*

S.W.Afr./Namibia, **3**, 105-109.

Ramsay, I.G. (1967). *Folding and Fracturing of Rocks*. Mc Graw-Hill, New York, 568pp.

Ramsay, I.G. and Huber M.J. (1987). *The techniques of modern structural geology. Vol. 2: folds and fractures*. Academic press, London, 391pp.

Reeves, C. V. (1978). Interpretation of the reconnaissance aeromagnetic survey of Botswana. *Rep. geol. Surv. Botswana*, 199pp.

Reuning, E. (1923). Pegmatit und Pegmatitmineralien in Südwestafrika. *Zeitschr. Kristall*., **58**, 448-459.

Ricci Lucchi, F. and Valmori, E. (1980). Basin-wide turbidites in a Miocene, over-supplied deep-sea plain: a geometrical analysis. *Sedimentology*, **27**, 241-270.

Richardson, S.W., Gilbert, M.C. and Bell, P.M. (1969). Experimental determination of kyanite-anda1usite and anda1usite-sillimanite equilibria: The aluminium silicate triple point. *Am. J. Sc*., **267**, 259-272.

Rona, P.A. (1988). Hydro thermal mineralization at oceanic ridges. *Can. Miner.*, **26**, 431-465.

Roser, B.P. and Korsch, R.I. (1986). Determination of tectonic setting of sandstone-mudstone suites using SiO_2 content and K_2O/Na_2O ratio. *J. Geol.*, **94**, 635-650.

Sample, J.C. aand Moore, J.C. (1987). Structural style and kinematics of an underplated slate belt, Kodiak and adjacent islands, Alaska. *Bull. geol. Soc. Am.*, **99**, 7-20.

Sanderson, D.J. and Marchini, W.R.D. (1984). Transpression. *J. Struct. Geol.*, **66**, 449-458.

Saquaque, A., Admou, H., Karson, J., Hefferan, K. and Reuber, J. (1989). Precambrian accretionary tectonics in the Bou Azzer-E1 Graara region, Anti-Atlas, Morocco. *Geology*, **17**, 1107-1110.

Sawyer, E.W. (1981). Damaran structural and metamorphic geology of an area southeast of Walvis Bay, SW A/Namibia. *Mem. geol. Surv. S.W.Afr./Namibia*, **7**, 94pp.

Sawyer, E.W. (1983). Structures in the contact strain aureole of the Donkerhoek Granite, Gross Barmen area, South West Africa/Namibia. *Spec. Publ. geol. Soc. S. Afr*., **11**, 209-217.

Schalk, K. (1970). Some late Precambrian formations in central South West Africa. *Annale geol. Surv. S. Afr.*, **8**, 29-47.

Schmidt, A. and Wedepohl, K.H. (1983). Chemical composition and genetic relations of the Matchless Amphibolite (Damara Orogenic Belt). *Spec. Publ. geol. Soc. S. Afr*., **11**, 139-145.

Schneider, A. (1983). The chemical composition of the common metamorphic sediments of the Damara Orogen, 655-677. *In*: Martin, H. and Eder, F.W., (Eds), *Intracontinental FoldBelts - Case Studies in the Variscan Belt of Europe and the Damara Belt in Namibia*. Springer-Verlag, Berlin, 945pp.

Selley, RC. (1976). Subsurface environmental analysis of North Sea sediments. *Bull. Am. Ass. Petrol. Geol.*, **66**, 1489-1498.

Shackleton, R.M. (1976). Pan-African structures. *Phil. Trans. R. Soc. Lond.*, **A 280**, 491-497.

Shackleton, RM. and Ries, A.C. (1984). The relation between regionally consistent stretching lineations and plate motions. *J. Struct. Geol*., **6**, 111-117.

Shanmugam, G. and Moiola, R.J. (1988). Submarine fans: Characteristics, models, classification, and reservoir potential. *Earth-sc. Rev.*, **2**, 383-428.

Shanmugam, G., Moiola, R.J., McPherson, J.G. and O'Connell, S. (1988). Comparison of turbidite facies associations in modern passive-margin Mississippi fan with ancient active-margin fans. *Sedim. Geol*., **58**, 63-77.

Shaw D.M. (1960). The geochemistry of scapolite. *J. Petrol*., **1**, 218-285.

Smith, D.A.M. (1965). The geology of the area around the Khan and Swakop rivers in South West Africa. *Mem. geol. Surv. S. Afr., S.W.Afr. Ser.*, **3**, 113pp.

South African Committee for Stratigraphy (SACS), (1980). *Stratigraphy of South Africa*. Part 1 (Comp. L.E. Kent). *Lithostratigraphy of the Republic of South Africa, South West Africa/Namibia and the Republics of Bophuthatswana, Transkei and Venda*. Handb. geol. Surv. S. Afr., 8, 690pp.

Spear, F.S. and Cheney, J.T. (1989). A petrogenetic grid for pelitic schists in the system SiO_2-Al_2O_3-FeO-MgO-K_2O-H_2O. *Contr. Miner. Petrol.*, **101**, 149-164.

Spry, A. (1963). The chronological analysis of crystallization and deformation of some Tasmanian Precambrian rocks. *J. geol. Soc. Australia*, **10**, 193-209.

Stanley, D.J. (1981). Unifites - structureless muds of gravity flow origin in Mediterranean basins. *Geo-Marine Lett.*, **1**, 77-83.

Stokke, P., Carson, B. and Baker, E. (1977). Comparison of the bottom nepheloid layer and Late Holocene deposition of Nitinat fan: Implications for lutite dispersal and deposition. *Bull. geol. Soc. Am.*, **88**, 1586-1592.

Storre, B. and Karotke, E. (1971). Experimentelle Anatexis von Glimmerschiefern in Modellsystemen. *Fortschr. Miner*., **49**, 56-58.

Stow, D.A.V. (1984). Turbidite facies, associations, and sequences in the southeastern Angola Basin. *In*: Hay, W.W., Sibuet, J.-C. *et al.*, (Eds), *Init. Repts. DSDP*, **75**, 785-799.

Stow, D.A.V. (1985). Deep-sea clastics: where are we and where are we going? *In*: Brenchley, P.J. and Williams, B.P.I., (Eds), *Sedimentology: Recent developments and applied aspects.* Spec. Publ. geol. Soc. Lond., **18**, 67 -93.

Stow, D.A.V. (1986). Deep clastic seas, 399-444. *In*: Reading, H.G., (Ed.), *Sedimentary environments and facies*. Blackwell, London, 615pp.

Stow, D.A.V. and Bowen, A.J. (1978). Origin of lamination in deep-sea fine-grained sediments. *Nature*, **274**, 324-328.

Stow, D.A.V. and Bowen, A.J. (1980). A physical model for the transport and sorting of fine-grained sediment by turbidity currents. *Sedimentology*, **27**, 31-46.

Stow, D.A.V. and Dean, W.E. (1984). Middle Cretaceous black shales at site 530 in the southeastern Angola Basin. *In*: Hay, W.W., Sibuet, J.-C. *et al.*, (Eds), *Init. Repts. DSDP*, **75**, 809-817.

Stow, D.A.V. and Piper, D.J.W. (1984). Deep-water fine-grained sediments: facies models. *In*: Stow, D.A.V. and Piper, D.J.W., (Eds), *Fine-grained sediments: deep-water processes and facies*. Spec. Publ. geol. Soc. Lond., **15**, 611-646.

Stow, D.A.V. and Shanmugam, G. (1980). Sequence of structures in fine-grained turbidites: Comparison of rccent and ancient flysch sediments. *Sedim. Geol*., **2**, 23-42.

Stow, D.A.V., Howell, D.G. and Nelson, C.H. (1983/84). Sedimentary, tectonic, and sea level controls on submarine fan and slope-apron turbidite systems. *Geo-Marine Lett*., **3**, 57-64.

Taira, A., Okada, H., Whitaker, J.H.McD. and Smith, A.J. (1982). The Shimanto Belt of Japan: Cretaceous-lower Miocene active margin sedimentation. *In*: Leggett, J.K., (Ed), *Trench-Forearc Geology.* Spec. Publ. geol. Soc. Lond., **10**, 537-550.

Thompson, A.B. (1976). Mineral reactions in pelitic rocks: II. Calculations of some P-T-X (Fe-Mg) phase relations. *Am. J. Sci,* **276**, 401-454.

Thompson, A.B. and Algor, J.R. (1977). Model systems for anatexis of pelitic rocks. 1. Theory of melting reactions in the system $KAlO_2$ - $NaAlO_2$ - Al_2O_3 - SiO_2 - H_2O. *Contr. Miner. Petrol.*, **63**, 247-269.

Thompson, A.B. and Norton, S.A. (1968). Paleozoic regional metamorphism in New England and adjacent areas, 319-327. *In*: Zen E-an, White, W.S, Hadley, J.B. and Thompson, J.B, Jr, (Eds), *Studies of the Appalachian geology, northern and maritime*. Wiley, New York.

Thornburg, T.M. and Kulm, L.D. (1987). Sedimentation in the Chile trench: Depositional morphologics, lithofacies, and stratigraphy. *Bull. geol. Soc. Am.*, **98**, 33-52.

Thornton, S.E. (1984). Basin model for hemipelagic sedimentation in a tectonically active continental margin: Santa Barbara Basin, California Continental Borderland. *In*: Stow, D.A.V. and Piper, D.J.W., (Eds), *Fine-grained sediments: deep-water processes and facies*. Spec. Publ. geol. Soc. Lond., **15**, 377-394.

Tissot, B., Demaison, G., Masson, P., Delteil, J.R. and Combaz, A. (1980). Paleoenvironment and petroleum potential of middle Cretaceous black shales in Atlantic basins. *Bull. Am. Ass. Petrol. Geol*., **64**, 2051-2063.

Turner, F.J. and Weiss, L.E. (1963). *Structural analysis of metamorphic tectonites*. McGraw-Hill, New York, 545pp.

Underwood, M.B. and Bachman, S.B. (1982). Sedimentary facies associations within subduction complexes. *In*: Leggett, J.K., (Ed), *Trench-Forearc Geology*. Spec. Publ. geol. Soc. Lond., **10**, 537-550.

Unrug, R. (1990). The Transcontinental Schlesien-Mwembeshi-Chimaliro Dislocation Zone of South-Central Africa. *Abstr. 15th Colloquium on African Geology*, Nancy, 175.

Valley, J.W. (1984). Fluid heterogeneity during granulite facies metamorphism in the Adirondacks: stable isotope evidence. *Contr. Miner. Petrol.*, **85**, 158-173.

Veizer, J. and Hoefs, J. (1976). The nature of $^{18}O/^{16}O$ secular trends in sedimentary carbonate rocks. *Geochim. cosmochim. Acta*, **40**, 1387-1395.

Walker, R. G. (1976). Facies models, 2. Turbidites and associated coarse clastic deposits. *Geosci. Can*., **3**, 25-36.

Walker, R.G. (1978). Deep-water sandstone facies and ancient submarine fans; models for exploration/or stratigraphic traps. *Bull Am. Ass. Petrol. Geol.*, **62**, 932-966.

Ward, J.D. (1987). The Cenozoic succession in the Kuiseb Valley, Central Namib Desert. *Mem. geol. Surv. S.W.Afr./Namibia*, **9**, 124pp.

Weber, K., Ahrendt, H. and Hunziker, J.C. (1983). Geodynamic aspects of structural and radiometric investigations on the northern and southern margins of the Damara Orogen, South West Africa/Namibia. *Spec. Publ. geol. Soc. S. Afr*., **11**, 307-319.

Williams, P.P. (1985). Multiply deformed terrains - problems of correlation. *J. Struct. Geol*., **7**, 269-280.

Wimmenauer, W. (1984). Das pravariskische Kristallin im Schwarzwald. *Fortschr. Miner., Beih*., **62**, 69-86.

Winkler, H.G.F. (1979). *Petrogenesis of metamorphic rocks*. Springer-Verlag, Berlin, 348pp.

Winkler, RG.F. (1983). A survey of granitic rocks of the Damara Orogen and considerations on their origin, 817-837. *In*: Martin, H. and Eder, F.W., (Eds), *IntracontinentalF oldBelts - Case Studies in the Variscan Belt of Europe and the Damara Belt in Namibia*. Springer Verlag, Berlin, 945pp.

Woodcock, N.H. (1976). Ludlow series slumps and turbidites and the form of the Montgomery Trough, Powys, Wales. *Proc. geol. Ass*., **87**, 169-182.

APPENDIX I,A: Table of XRF-analyses (major elements) of psammites along the study traverse, (samples are arranged from north to south, nd = not determined).

SAMPLE NO	SiO_2	TiO_2	Al_2O_3	Fe_2O_3	FeO	MnO	MgO	CaO	Na_2O	K_2O	P_2O_5	H_2O	Loi	TOTAL	Farmname
PK 348	73.29	1.03	10.54	5.52	nd	.08	1.87	1.38	2.11	2.68	.19	nd	1.21	99.90	Nomatsaus
86/1	72.45	.77	11.48	5.34	nd	.07	2.02	1.51	2.80	2.14	.17	nd	.46	99.22	Keises
86/4	73.76	.94	10.27	5.30	nd	.09	1.95	1.58	2.45	1.94	.12	nd	.60	99.00	
PK/814	74.20	.71	10.91	5.33	nd	.12	2.02	1.71	2.59	2.04	.17	nd	.51	100.30	
PK/816	74.02	.76	10.77	5.07	nd	.06	1.81	1.48	2.56	1.97	.16	nd	.66	99.31	
86/5	74.32	.70	10.75	4.33	nd	.09	1.73	2.57	1.97	1.64	.16	nd	.69	98.96	
PK 114	72.88	.77	12.05	4.88	nd	.07	2.03	.73	2.73	3.40	.18	nd	.92	100.64	
86/6	70.33	1.13	11.44	6.11	nd	.06	2.09	1.06	2.05	3.95	.24	nd	.58	99.03	
86/7	70.80	1.09	11.55	5.76	nd	.09	1.97	1.47	2.63	2.27	.25	nd	.51	98.38	
86/14	73.07	.94	11.01	5.08	nd	.09	1.82	1.47	3.18	1.89	.26	nd	.52	99.32	Dagbreek
86/15	73.06	.95	10.95	5.13	nd	.07	1.99	1.03	2.37	2.57	.19	nd	.84	99.13	
86/16	71.09	1.01	11.03	5.58	nd	.09	2.03	1.52	2.85	2.14	.24	nd	.79	98.37	
PK 312	74.14	.74	11.21	4.54	nd	.11	2.06	2.61	2.50	1.65	.21	nd	.85	100.62	
86/19	71.80	.68	11.35	5.07	nd	.06	2.20	.74	3.36	2.19	.19	nd	.90	98.53	
PK 356	73.17	.84	11.51	4.87	nd	.08	1.75	1.21	3.01	2.83	.23	nd	.59	100.09	
PK 354	73.61	.74	10.62	4.69	nd	.09	1.71	1.59	3.00	2.06	.17	nd	.52	98.80	
PK 364	72.34	.91	12.19	5.31	nd	.08	2.45	1.59	2.93	2.10	.21	nd	.72	100.83	Kaan
PK/803	71.17	1.02	11.70	5.90	nd	.09	3.48	.90	1.62	2.42	.20	nd	1.07	99.57	
PK/805	71.38	.82	11.90	4.94	nd	.14	3.08	1.57	2.84	2.19	.19	nd	.69	99.73	
PK/806	70.35	1.03	12.34	5.35	nd	.10	2.99	1.53	2.88	2.19	.22	nd	.68	99.65	
86/24	73.90	.86	10.86	4.80	nd	.09	1.81	2.06	2.19	1.76	.23	nd	.47	99.02	
86/25	71.65	.76	11.31	4.86	nd	.06	1.82	.97	2.05	2.85	.21	nd	2.92	99.46	
86/26	72.27	.71	11.78	4.75	nd	.06	1.98	1.12	2.41	2.83	.17	nd	.81	98.88	
86/27	70.07	.95	12.35	5.67	nd	.07	2.11	1.05	3.50	2.65	.23	nd	.63	99.29	
86/29	72.55	.85	10.88	5.07	nd	.07	1.66	1.11	2.52	2.50	.21	nd	.73	98.15	
86/30	70.62	.68	12.20	5.10	nd	.08	2.29	2.00	3.43	2.04	.16	nd	.55	99.15	
86/31	73.68	.67	10.51	4.23	nd	.08	1.77	1.83	3.03	1.53	.19	nd	.58	98.09	
86/34	72.25	.85	11.36	5.01	nd	.06	1.69	.71	2.85	2.55	.19	nd	.98	98.50	
86/37	71.89	1.00	11.31	4.81	nd	.06	1.94	1.17	2.39	2.51	.26	nd	1.49	98.81	
86/39	73.16	.71	10.96	4.99	nd	.08	2.20	1.44	3.72	1.78	.15	nd	.55	99.74	
86/40	68.63	.72	13.11	5.64	nd	.09	2.47	1.71	3.23	2.25	.17	nd	.71	98.72	
86/41	70.12	.96	12.27	5.44	nd	.08	2.24	1.57	3.94	2.20	.23	nd	.83	99.88	
86/42	75.65	.49	9.38	3.35	nd	.14	1.39	2.85	2.59	1.31	.14	nd	1.55	98.83	Tsawisis
86/44	73.47	.79	10.47	4.40	nd	.07	1.64	1.00	3.34	1.87	.18	nd	.62	97.85	
86/45	71.40	.76	12.05	5.16	nd	.08	1.81	.75	2.52	2.86	.23	nd	.96	98.58	
86/48	74.65	.67	11.20	4.51	nd	.08	1.86	2.02	3.56	1.60	.17	nd	1.48	101.80	
86/50	73.31	.79	10.94	4.70	nd	.07	1.54	1.57	3.33	2.56	.20	nd	1.17	100.17	
86/51	73.59	.83	11.02	4.79	nd	.07	1.70	1.10	2.89	2.61	.21	nd	.87	99.67	Kaan Dam
86/52	72.91	1.13	11.10	4.63	nd	.07	1.86	1.48	3.06	2.22	.23	nd	.68	99.37	
86/53	74	.99	10.82	4.77	nd	.07	1.83	.86	2.37	2.42	.27	nd	.97	99.37	
86/54	70.17	.69	11.91	5.80	nd	.07	2.45	1.75	3.01	2.08	.15	nd	.73	98.80	
PK/871	72.31	.81	12.10	5.16	nd	.08	2.09	1.09	2.66	2.36	.17	nd	1.67	100.50	
86/55	70.13	.71	12.51	5.93	nd	.07	2.31	1.72	2.72	2.45	.18	nd	.90	99.62	
86/59	71.07	1.19	11.17	6.08	nd	.06	1.94	.98	2.46	2.66	.20	nd	.94	98.76	
86/60	69.53	.88	12.49	5.84	nd	.09	2.40	.94	3.15	1.95	.22	nd	1.44	98.92	Annelie
86/62	72.97	.96	10.90	5.00	nd	.08	1.73	1.84	3.27	1.68	.20	nd	.50	99.13	
86/65	68.12	.89	12.63	6.34	nd	.15	2.63	2.95	2.68	1.90	.27	nd	.60	99.16	
PK 209	72.71	1.16	10.93	5.86	nd	.07	2.05	1.99	2.18	2.64	.19	nd	1.40	101.18	Kobos
PK 199	71.67	1.02	11.79	5.51	nd	.06	2.20	2.48	3.28	1.72	.21	nd	.77	100.71	
PK 955	71.56	.69	11.16	3.85	nd	.15	2.78	1.26	3.46	1.26	.10	nd	4.21	100.48	
PK/824	72.65	.98	10.00	4.65	nd	.11	1.98	5.07	2.11	1.41	.22	nd	1.31	100.50	Annelie
PK 196	73.98	.73	11.23	3.89	nd	.09	2.07	1.79	3.12	1.77	.16	nd	.92	99.75	Okasume
PK 197	74.48	.86	10.67	4.85	nd	.09	2.15	1.83	3.19	1.85	.19	nd	1.15	101.31	
86/71	71.97	.72	11.53	4.20	nd	.10	2.19	1.47	2.33	2.48	.17	nd	1.19	98.34	
PK 193	72.18	1.03	10.32	5.76	nd	.11	2.26	1.79	2.64	1.97	.20	nd	1.28	99.55	
PK/821	75.42	.74	9.95	4.55	nd	.08	1.48	1.84	2.48	1.90	.14	nd	1.42	100.00	
PK/822	72.52	.66	9.94	4.14	nd	.12	1.51	2.97	3.14	1.63	.13	nd	2.96	99.71	
86/72	72.64	.79	10.95	4.90	nd	.08	1.98	1.58	3.03	1.97	.18	nd	.75	98.83	
PK 189	75.43	.94	9.35	4.40	nd	.09	1.80	2.04	2.56	1.51	.14	nd	.98	99.24	
86/73	69.44	.92	10.71	5.24	nd	.12	2.14	3.26	2.73	1.83	.19	nd	2.74	99.31	Usambara
86/74	72.37	.80	10.62	4.81	nd	.07	1.71	1.67	2.94	2.18	.17	nd	1.52	98.85	
PK 182	73.39	.76	10.83	4.27	nd	.08	1.75	2.05	3.00	2.26	.15	nd	2.00	100.54	
86/75	73.14	.80	11.60	5.09	nd	.08	1.86	1.96	3.54	2.02	.18	nd	1.49	101.76	
86/80	70.94	.68	10.78	4.55	nd	.11	1.80	3.56	2.52	1.84	.15	nd	2.57	99.50	
86/81	70.34	1.14	10.99	5.92	nd	.10	2.17	2.52	2.62	1.87	.21	nd	1.06	98.94	
86/84	73.80	.77	10.99	4.94	nd	.06	1.82	1.63	2.77	2.11	.15	nd	.76	99.78	
86/85	72.65	1.02	10.77	5.44	nd	.07	1.95	1.58	2.84	2.07	.19	nd	.56	99.14	
PK/856	74.78	.69	10.65	4.78	nd	.06	2.00	1.80	2.23	1.99	.14	nd	.84	99.97	
PK 152	72.49	.93	11.26	5.64	nd	.08	1.96	2.20	2.55	2.14	.16	nd	1.02	100.43	
PK 149	72.49	1.10	11.27	5.87	nd	.06	2.18	2.07	2.33	2.22	.19	nd	1.04	100.82	

APPENDIX I,B: Table of XRF-analyses (trace elements) of psammites along the study traverse, (samples are arranged from north to south, nd = not determined; bd = below detection limit).

SAMPLE NO	Rb	Sr	Y	Zr	Nb	Ba	V	Cr	Co	Ni	Cu	Zn	Farmname
PK 348	119	121	42	355	14	498	105	78	10	23	34	65	Homatsaus
86/1	81	131	28	181	9	463	104	76	11	27	bd	71	Keises
86/4	75	109	32	272	9	457	102	80	9	26	12	69	
PK/814	88	119	36	193	10	272	82	66	11	26	53	74	
PK/816	83	114	32	217	11	331	86	71	11	24	30	70	
86/5	66	118	27	187	9	401	85	65	7	25	36	62	
PK 114	119	109	31	229	12	949	92	69	12	28	6	75	
86/6	112	118	35	347	9	731	119	91	10	28	bd	73	
86/7	86	135	37	332	12	610	108	96	11	30	bd	76	
86/14	74	117	33	289	11	317	97	84	12	26	9	69	Dagbreek
86/15	83	101	34	273	11	559	87	80	10	24	37	62	
86/16	75	143	35	317	10	351	93	87	11	29	bd	73	
PK 312	86	141	37	222	12	252	85	68	12	28	9	66	
86/19	81	82	26	169	8	341	87	69	14	46	6	114	
PK 356	127	144	37	273	13	704	101	78	10	25	19	68	
PK 354	95	133	37	256	12	428	87	67	12	23	7	66	
PK 364	89	339	36	304	12	607	111	82	14	26	25	71	Kaan
PK/803	105	240	34	351	14	653	98	90	13	35	21	98	
PK/805	99	382	34	235	12	505	107	80	15	33	53	83	
PK/806	100	396	37	350	13	646	124	95	12	33	142	77	
86/24	75	100	29	255	9	399	95	83	10	24	41	77	
86/25	91	106	31	198	10	624	101	75	18	51	bd	115	
86/26	94	104	26	180	9	655	94	71	13	27	bd	74	
86/27	111	162	33	257	11	505	117	86	18	43	bd	119	
86/29	97	112	32	244	9	565	96	77	18	47	bd	72	
86/30	82	136	29	172	8	286	103	70	11	44	11	97	
86/31	65	116	32	187	8	242	77	63	12	25	bd	72	
86/34	82	77	29	243	9	546	98	79	13	23	10	75	
86/37	82	119	34	301	10	432	98	85	12	26	bd	72	
86/39	67	126	29	178	9	395	88	69	13	24	8	70	
86/40	87	155	26	140	9	582	106	81	11	28	bd	86	
86/41	75	136	33	226	11	538	105	87	13	30	42	61	
86/42	54	338	17	125	4	417	72	60	10	24	bd	60	Tsawisis
86/44	70	119	31	227	9	370	96	79	15	14	16	13	
86/45	100	236	29	207	10	717	115	75	9	24	9	71	
86/48	65	132	22	163	7	403	91	70	12	31	bd	82	
86/50	91	223	28	213	8	829	92	71	10	24	bd	47	
86/51	96	140	29	224	10	484	96	81	13	27	9	62	Kaan Dam
86/52	83	131	40	373	12	465	106	93	11	27	bd	74	
86/53	86	77	31	303	11	454	94	86	16	42	21	121	
86/54	81	146	27	156	9	443	98	77	9	25	bd	69	
PK/871	87	121	33	212	10	513	104	81	12	26	17	37	
86/55	88	144	30	155	9	419	108	70	10	23	bd	59	
86/59	93	82	37	366	12	556	112	101	11	26	8	71	
86/60	68	88	31	200	11	331	113	84	12	25	bd	66	Annelie
86/62	75	146	32	255	10	353	97	89	15	31	bd	52	
86/65	84	75	34	187	11	307	118	88	13	31	bd	60	
PK 209	107	58	45	374	15	502	121	92	11	27	bd	67	Kobos
PK 199	95	238	38	319	11	423	110	83	12	27	16	72	
PK 955	95	157	31	174	11	185	95	65	11	23	132	87	
PK/824	34	346	38	300	13	775	70	75	9	28	26	81	Annelie
PK 196	86	151	33	213	10	302	95	63	10	22	27	71	Okasume
PK 197	81	115	34	267	12	314	106	72	10	22	6	70	
86/71	92	87	29	179	9	391	108	70	15	29	bd	83	
PK 193	93	124	41	384	13	303	101	79	12	21	bd	80	
PK/821	82	119	29	218	10	343	88	64	11	22	9	57	
PK/822	65	138	29	190	11	296	89	65	10	20	:d	56	
86/72	74	107	30	196	10	397	111	80	12	25	17	68	
PK 189	64	124	38	290	12	283	92	70	10	20	20	65	
86/73	64	116	31	253	11	284	106	79	15	29	18	85	Usanbara
86/74	83	124	29	199	9	506	103	72	11	24	bd	66	
PK 182	101	170	34	221	11	528	99	69	9	21	bd	62	
86/75	74	122	30	175	8	426	104	75	10	24	bd	65	
86/80	73	123	27	159	8	399	99	68	11	24	bd	67	
86/81	76	165	38	297	11	496	116	89	13	28	bd	82	
86/84	74	117	30	184	8	487	100	66	12	24	bd	67	
86/85	77	90	35	291	11	374	100	93	11	27	bd	78	
PK/856	98	192	28	178	9	429	85	62	12	27	bd	40	
PK 152	104	139	40	269	13	531	108	73	11	27	bd	64	
PK 149	110	158	41	381	15	463	110	87	12	27	6	46	

APPENDIX I,C: Table of XRF-analyses (major elements) of pelites along the study traverse, (samples are arranged from north to south; nd = not determined).

SAMPLE NO	SiO_2	TiO_2	Al_2O_3	Fe_2O_3	FeO	MnO	MgO	CaO	Na_2O	K_2O	P_2O_5	H_2O	Loi	TOTAL	Farmname
PK 349	68.23	1.02	13.35	6.54	nd	.09	3.34	.70	.80	3.43	.22	nd	1.59	99.31	Nomatsaus
86/2	56.32	.96	18.07	9.23	nd	.12	4.32	1.33	1.81	4.98	.22	nd	1.72	99.09	Keises
PK/815	56.05	1.13	19.81	9.25	nd	.11	4.15	.51	1.25	5.34	.25	nd	2.32	100.16	
PK 109	57.12	.93	19.96	9.82	nd	.09	3.89	.31	.59	6.23	.16	nd	2.66	101.76	
86/8	60.88	.93	17.60	7.72	nd	.08	3.75	.88	1.19	4.36	.23	nd	2.47	100.07	
PK 327	59.26	.86	16.48	7.55	nd	.15	4.59	5.28	1.05	3.29	.21	nd	.86	99.58	
PK 328	61.92	.97	17.65	7.55	nd	.09	3.83	.87	1.42	4.08	.22	nd	2.19	100.79	
PK/849	54.84	1.08	20.83	9.51	nd	.10	4.75	.64	1.17	4.64	.26	nd	2.49	100.32	
PK 324	54.74	.86	20.63	8.85	nd	.05	4.77	.66	.95	6.69	.19	nd	2.50	100.89	
PK/883	50.49	1.18	21.71	9.83	nd	.14	4.95	.69	1.41	6.66	.30	nd	2.79	100.14	Dagbreek
PK/881	50.02	1.16	23.08	8.58	nd	.07	4.67	.43	.90	7.87	.21	nd	2.39	99.37	
PK/843	46.44	1.24	25.30	6.71	nd	.06	5.60	1.67	2.93	7.26	.23	nd	2.56	100.00	
PK 315	60.76	.88	17.55	8.28	nd	.08	3.73	.35	1.07	5.18	.17	nd	2.06	100.11	
86/18	54.44	1.04	19.25	8.90	nd	.10	4.04	.78	1.81	5.83	.24	nd	2.23	98.64	
PK 357	51.97	1.07	21.04	9.31	nd	.12	4.81	1.34	2.60	5.41	.28	nd	2.23	100.18	
PK 355	58.66	.87	18.07	7.62	nd	.08	4.01	1.64	4.31	3.33	.22	nd	1.34	100.15	
PK 358	53.47	.83	16.76	7.54	nd	.08	7.31	5.21	1.26	4.66	.20	nd	1.57	98.89	
PK 359	52.00	.82	15.80	7.37	nd	.07	7.88	7.76	1.30	3.46	.20	nd	1.61	98.27	
PK 360	45.44	1.15	23.16	9.90	nd	.07	6.79	5.90	1.43	5.10	.24	nd	1.20	100.38	
86/22	60.53	.78	15.71	7.16	nd	.09	4.52	5.37	.68	3.55	.19	nd	1.14	99.70	Kaan
86/23	57.98	.93	17.66	8.82	nd	.07	3.62	.96	1.38	5.49	.22	nd	1.84	98.98	
PK/804	67.64	.91	14.45	5.59	nd	.09	3.58	1.35	2.69	2.55	.20	nd	1.02	100.06	
PK 299	59.56	.91	18.08	8.23	nd	.06	3.64	.93	1.38	5.67	.18	nd	1.77	100.41	
PK/880	60.26	.92	17.68	8.01	nd	.09	3.62	.59	1.90	4.41	.14	nd	2.49	100.10	
PK/879	60.11	.93	17.21	8.32	nd	.08	3.48	.86	2.04	4.87	.13	nd	2.05	100.07	
PK 277	56.51	.91	17.80	8.22	nd	.05	4.07	2.05	2.33	4.97	.25	nd	3.27	100.43	
86/38	62.49	.88	17.69	2.50	nd	.01	1.25	.15	.62	5.16	.07	nd	7.11	97.93	
PK/807	57.92	.89	18.37	8.01	nd	.09	3.82	.86	.93	6.07	.16	nd	2.72	99.84	
PK/808	58.98	.94	18.09	7.98	nd	.08	3.72	.82	.94	5.99	.19	nd	2.33	100.05	
PK/835	48.82	1.13	22.12	10.87	nd	.15	5.27	.75	1.57	5.47	.24	nd	3.73	100.12	Tsawisis
PK/874	59.67	.93	17.82	7.88	nd	.12	3.68	1.40	2.02	3.98	.17	nd	2.35	100.03	
86/47	58.35	.95	17.80	7.76	nd	.12	3.60	1.38	1.96	3.97	.20	nd	2.53	98.59	
PK 852	65.19	.94	15.81	1.42	nd	.02	.67	.11	.69	5.03	.09	nd	9.30	99.26	Kwaggafontein
PK/873	58.56	.86	18.20	8.96	nd	.08	3.68	.38	1.29	5.08	.13	nd	2.80	100.00	Kaan Dam
PK/872	56.03	.95	19.32	9.16	nd	.10	4.34	.42	1.14	5.27	.17	nd	3.65	100.55	
86/57	60.37	.97	17.08	7.73	nd	.10	3.36	.90	1.91	3.69	.23	nd	2.65	98.99	
PK 248	49.22	1.19	22.75	10.20	nd	.11	5.51	.65	1.39	5.39	.35	nd	4.63	101.39	Annelie
PK 246	57.43	.92	19.03	8.19	nd	.09	5.01	.45	.92	4.56	.18	nd	3.68	100.46	
PK/870	55.77	1.08	20.33	8.36	nd	.09	4.07	.44	1.15	5.70	.20	nd	3.34	100.51	Bergkrans
PK/869	57.64	1.00	18.03	7.65	nd	.09	4.00	2.03	2.59	4.41	.21	nd	1.95	99.59	Kobos
PK/954	63.76	.91	16.44	4.78	nd	.08	3.62	.49	1.78	3.95	.07	nd	4.57	100.45	Annelie
PK 215	56.76	1.06	17.94	8.69	nd	.13	4.97	2.38	1.55	3.52	.21	nd	3.17	100.38	Kobos
PK 208	49.45	1.13	20.43	10.70	nd	.15	6.55	1.70	1.38	4.40	.26	nd	3.84	99.99	
PK 131	63.94	.82	13.49	6.86	nd	.08	2.05	8.86	3.10	.32	.16	nd	1.08	100.76	
PK 130	55.57	1.04	18.85	9.97	nd	.11	4.98	.81	.87	4.47	.23	nd	3.50	100.41	
PK 198	58.11	1.03	17.67	9.10	nd	.10	4.39	.73	1.14	4.88	.24	nd	2.71	100.10	
PK 210	59.08	1.03	16.75	8.84	nd	.09	4.84	1.65	1.57	3.11	.23	nd	2.51	99.70	
PK 195	62.25	.96	16.09	7.29	nd	.11	3.76	2.03	2.35	3.09	.20	nd	1.79	99.92	Okasume
PK 190	57.69	.99	18.32	8.60	nd	.08	4.50	.91	1.39	5.22	.24	nd	2.54	100.48	
PK 183	60.70	1.17	17.13	7.99	nd	.08	3.77	.51	1.24	4.59	.28	nd	2.68	100.14	Usambara
86/76	39.93	1.55	25.90	12.11	nd	.16	6.38	.61	.91	6.70	.26	nd	4.55	99.06	
PK/862	54.87	1.16	19.23	8.46	nd	.10	4.38	.51	1.49	4.74	.24	nd	3.30	98.48	
PK/863	66.88	.93	13.96	6.83	nd	.07	3.27	.92	1.68	3.47	.20	nd	1.71	99.93	
PK/864	66.58	.94	13.39	6.62	nd	.12	3.17	1.87	3.30	2.79	.21	nd	1.02	100	
PK/861	47.81	1.29	21.88	10.64	nd	.18	5.78	1.55	3.07	3.78	.24	nd	3.78	100.00	
86/79	65.35	.78	13.77	8.11	nd	.08	3.89	.91	1.25	3.03	.21	nd	2.06	99.43	
PK/858	54.63	1.16	19.61	9.37	nd	.15	4.85	.73	1.01	5.40	.25	nd	2.93	100.06	
86/83	63.20	1.04	15.27	7.17	nd	.17	3.92	1.37	2.05	3.35	.23	nd	1.41	99.17	
PK 153	65.21	.81	15.22	8.08	nd	.12	3.29	1.88	2.20	3.37	.26	nd	.09	100.53	
86/87	58.40	1.35	15.73	7.96	nd	.18	4.13	4.03	2.70	2.26	.20	nd	.95	97.88	
PK/855	54.50	1.05	19.15	9.55	nd	.11	5.14	1.09	2.15	4.97	.19	nd	2.51	100.42	
PK/854	49.54	1.17	21.39	11.96	nd	.15	5.44	.69	.78	6.37	.20	nd	2.24	99.91	

APPENDIX I,D: Table of XRF-analyses (trace elements) of pelites along the study traverse, (samples are arranged from north to south; nd = not determined; bd = below detection limit).

SAMPLE NO	Rb	Sr	Y	Zr	Nb	Ba	V	Cr	Co	Ni	Cu	Zn	Farmname
PK 349	137	61	47	291	15	724	131	89	16	36	bd	97	Nomatsaus
86/2	180	97	37	170	11	732	204	125	19	51	bd	144	Keises
PK/815	203	80	44	216	17	849	202	140	20	61	bd	150	
PK 109	258	60	36	208	15	769	197	138	21	63	91	165	
86/8	144	75	33	179	10	647	196	127	10	26	bd	71	
PK 327	169	206	48	208	15	394	147	91	16	50	6	122	
PK 328	160	63	40	221	16	557	177	121	19	50	10	130	
PK/849	185	50	43	217	16	682	221	150	21	59	27	159	
PK 324	279	93	36	160	17	765	199	123	21	61	35	163	
PK/883	226	73	52	225	18	1255	244	149	20	68	20	183	Dagbreek
PK/881	381	40	39	238	17	1148	223	152	20	62	bd	51	
PK/843	324	184	47	240	11	1486	262	166	11	38	46	48	
PK 315	218	47	34	191	15	686	165	111	19	46	49	119	
86/18	185	82	38	198	13	1023	237	131	12	28	bd	77	
PK 357	220	179	43	233	18	1169	270	151	22	68	bd	154	
PK/355	164	228	38	185	15	478	204	126	17	50	21	90	
PK 358	244	160	34	171	15	491	171	108	17	49	7	72	
PK 359	208	162	36	182	15	550	137	109	13	45	33	63	
PK 360	215	297	26	210	20	1187	211	160	18	53	186	169	
86/22	175	151	36	152	10	254	136	96	10	24	13	67	
86/23	208	215	33	169	9	787	222	120	10	23	bd	71	Kaan
PK/804	108	388	64	208	13	742	139	94	17	43	235	104	
PK 299	253	228	40	196	16	599	180	130	20	56	bd	129	
PK/880	175	80	36	192	13	562	170	120	18	49	bd	137	
PK/879	218	91	34	196	15	590	160	114	17	48	30	134	
PK 277	269	188	42	196	10	812	199	126	16	54	9	42	
86/38	149	94	32	169	9	924	165	127	11	29	bd	82	
PK/807	205	78	30	173	14	1167	189	125	17	48	8	103	
PK/808	222	84	31	183	12	843	185	126	17	51	8	59	
PK/835	199	99	30	215	13	1152	195	142	24	59	56	102	Tsawisis
PK/874	161	119	31	190	13	667	181	123	13	43	32	121	
86/47	136	104	26	178	9	648	191	130	11	36	bd	88	
PK 852	136	116	32	190	14	733	156	120	6	bd	bd	14	Kwaggafontein
PK/873	214	81	32	166	12	755	186	128	20	52	26	150	
PK/872	201	78	31	182	13	842	194	137	20	51	60	91	Kaan Dam
86/57	112	85	33	183	11	771	154	110	12	24	bd	69	
PK 248	175	99	53	231	11	1152	240	157	19	58	46	158	
PK 246	176	67	39	194	13	674	223	144	19	62	25	152	Annelie
PK/870	186	65	43	199	18	1153	229	145	11	47	22	114	
PK/869	192	170	42	207	15	761	175	125	16	48	14	69	Bergkrans
PK/954	154	109	34	201	14	499	140	102	17	35	27	89	Kobos
PK 215	125	56	39	209	14	619	205	129	21	56	43	143	Annelie
PK 208	147	46	43	220	14	950	240	146	27	69	131	171	Kobos
PK 131	14	338	38	175	14	79	140	91	13	44	11	59	
PK 130	174	44	45	214	16	563	211	130	23	60	14	159	
PK 198	202	41	36	215	14	796	214	126	20	56	31	143	
PK 210	104	70	53	228	17	642	164	109	19	54	7	127	
PK 195	133	119	42	214	15	493	173	110	19	45	21	120	
PK 190	205	80	47	188	16	864	200	123	17	56	34	141	Okasume
PK 183	192	93	44	270	17	869	182	113	20	52	36	127	
86/76	184	68	32	238	11	1427	304	187	32	79	121	194	Usambara
PK/862	146	83	42	215	14	911	219	142	18	53	20	141	
PK/863	128	70	32	189	12	563	121	88	17	38	52	108	
PK/864	128	171	31	178	12	425	136	92	17	36	7	107	
PK/861	133	138	58	269	15	745	194	117	26	70	18	193	
86/79	103	80	33	161	6	505	127	85	20	45	119	130	
PK/858	181	63	43	215	16	782	228	144	22	60	22	153	
86/83	122	124	34	191	10	533	183	116	19	46	15	116	
PK 153	148	124	38	171	11	438	162	97	18	49	43	63	
86/87	70	118	42	213	11	279	137	108	16	41	19	98	
PK/855	188	79	40	195	13	593	217	136	23	66	16	151	
PK/854	228	55	46	214	16	856	249	144	24	74	88	212	

APPENDIX II: Table of XRF-analyses of amphibolites and metagabbros from the Matchless Amphibolite sequenee. Sample localities are indicated in Figure 5.2; (nd = not determined).

SAMPLE NO	867	230	228	221	222	219	220	217	214	213
SiO_2	51.37	41.47	44.51	46.21	46.47	52.87	50.81	49.32	43.43	48.19
TiO_2	1.46	2.37	1.90	1.52	1.95	1.85	1.90	1.68	1.43	1.59
Al_2O_3	13.39	14.97	14.65	13.24	13.78	15.03	13.99	13.35	11.95	14.97
Fe_2O_3	10.65	13.54	11.68	9.62	11.91	12.20	11.81	11.20	11.11	11.76
FeO	nd	nd	nd	nd	nd	nd	nd	nd	nd	nd
MnO	.22	.22	.17	.16	.20	.18	.15	.19	.21	.18
MgO	5.18	6.93	4.23	6.84	6.28	6.21	5.63	8.27	7.91	7.55
CaO	10.74	13.99	18.50	12.35	10.89	7.81	10.04	10.82	14.94	13.13
Na_2O	3.16	2.14	.79	2.27	2.43	2.58	3.28	.86	1.80	3.15
K_2O	.14	.23	.07	.25	.28	.22	.26	.15	.21	.17
P_2O_5	.13	.30	.25	.17	.22	.19	.20	.21	.12	.18
H_2O	nd	nd	nd	nd	nd	nd	nd	nd	nd	nd
Loi	3.43	5.00	5.44	7.41	6.49	2.05	1.67	4.85	7.40	.00
TOTAL	99.88	101.16	102.19	100.04	100.90	101.19	99.74	100.90	100.51	100.88
Rb	5	10	6	12	8	8	10	5	7	6
Sr	156	239	334	192	142	107	175	59	145	143
Y	34	42	35	31	37	39	34	35	33	35
Zr	88	165	134	104	139	123	130	110	77	87
Nb	2	28	26	14	15	8	9	13	4	11
Ba	74	61	37	52	48	26	46	22	42	41
V	313	341	376	310	312	386	339	316	299	343
Cr	239	215	150	198	131	199	147	215	222	278
Co	39	42	20	29	33	32	39	31	37	36
Ni	85	134	80	75	61	61	70	95	82	67
Cu	91	7	11	7	5	5	33	8	56	62
Zn	108	110	62	61	64	84	87	95	99	89
amphibolite type	II	type I	type I	type II	type II	type I	type II	breccia	type II	type I

SAMPLE NO	86/66	86/68	201	895
SiO_2	46.31	50.25	50.62	50.45
TiO_2	1.64	1.67	1.86	1.71
Al_2O_3	14.98	15.10	13.27	13.32
Fe_2O_3	11.19	12.06	13.23	11.97
FeO	nd	nd	nd	nd
MnO	.15	.19	.27	.21
MgO	7.21	7.61	7.63	8.84
CaO	12.35	10.16	8.84	9.20
Na_2O	2.35	3.14	1.45	2.87
K_2O	.19	.24	.19	.22
P_2O_5	.20	.16	.19	.14
H_2O	nd	nd	nd	nd
Loi	3.15	1.05	3.62	1.35
TOTAL	99.71	101.62	101.17	100.29
Rb	3	5	8	7
Sr	183	162	91	168
Y	24	31	42	33
Zr	105	98	121	96
Nb	13	3	9	3
Ba	29	24	45	58
V	315	334	360	340
Cr	290	204	270	240
Co	9	13	38	36
Ni	19	28	102	112
Cu	0	4	11	34
Zn	32	75	175	88
amphibolite type	gabbro	gabbro	gabbro	gabbro

APPENDIX III,A1: Analytical conditions for microprobe analyses. Analyses were made on a CAMECA XS 50 electron microprobe at the Mineralogical Institute of the University of Würzburg/FRG. Acceleration potential used was 15 kV and a sample current of 10 nA. Counting time for each mineral was 10s per spot (number of spots are given with analyses in Appendices III,A-E). Natural crystalline and synthetic standards, feldspar-glasses, and metals were used for calibration. Only minerals were analysed which are in direct contact parageneses but avoiding edge effects. H_2O in biotite, muscovite, chlorite, and staurolite has been calculated from stoichiometry. Calculations and corrections were made with the Cameca "Geo" software (based on PAP).

SAMPLE	146	86/76	308	109
SiO_2	61.09	62.83	61.53	63.55
Al_2O_3	24.07	22.81	23.97	22.47
MgO	.02	0	0	.01
CaO	4.63	3.70	4.97	3.04
MnO	.02	.02	0	.01
FeO	.12	.16	.12	.16
BaO	.06	.01	.02	.04
Na_2O	8.76	9.45	8.68	9.63
K_2O	.28	0.07	.14	.13
Total	99.03	99.05	99.44	99.04
Atomic porportions based on 8 <0>				
Si	2.74	2.81	2.74	2.83
Al	1.27	1.20	1.26	1.18
	4.01	4.00	4.01	4.01
Mg	0	0	nd	0
Ca	.22	.18	.24	.15
Mn	0	0	nd	0
Fe^{2+}	0	.01	.01	.01
Ba	0	0	0	0
Na	.77	.82	.75	.83
K	.02	0	.01	.01
	1.01	1.01	1.01	.99
Total	5.02	5.01	5.01	5.00
An	22	18	24	15
grains/points	3/10	3/8	2/7	1/4

APPENDIX III,B: Table of average muscovite analyses.

SAMPLE	146	86/76	274	308	109
SiO_2	44.59	45.81	45.15	44.47	45.16
TiO_2	.44	.44	.19	.33	.41
Al_2O_3	36.24	33.55	37.33	37.04	36.19
MgO	.74	1.24	.54	.55	.67
CaO	.01	0	.03	.01	.01
MnO	.03	0	.05	.01	.01
FeO	1.03	3.03	.87	.85	1.11
BaO	.21	.23	.10	.40	.21
Na_2O	.98	.86	1.37	1.27	.80
K_2O	9.84	9.84	9.46	9.39	9.98
H_2O	4.45	4.45	4.51	4.47	4.47
Total	98.56	99.45	99.60	98.78	99.02
Atomic porportions based on 22 <0>					
Si	6.00	6.17	5.99	5.97	6.05
Ti	.05	.06	.02	.04	.05
Al	5.75	5.33	5.84	5.86	5.71
Mg	.15	.25	.11	.11	.13
Ca	0	0	0	0	0
Mn	0	0	0	0	0
Fe	.12	.34	.10	.10	.13
Ba	.01	.01	0	.02	.01
Na	.26	.23	.35	.33	.21
K	1.69	1.69	1.60	1.61	1.71
Tetr. Z	8.00	8.00	8.00	8.00	8.00
Oct. Y	4.08	4.15	4.06	4.07	4.07
Interl. X	1.96	1.93	1.95	1.96	1.94
Total	14.03	14.08	14.01	14.03	14.01
grains/points	4/11	1/2	1/3	2/5	4/11

APPENDIX III,C: Table of average biotite analyses.

SAMPLE	146-1	146-2	86/87	274	306	308	109
SiO_2	34.69	34.28	35.05	34.33	37.07	35.01	34.00
TiO_2	1.59	1.56	1.61	1.60	1.82	1.48	1.96
Al_2O_3	18.69	18.66	18.10	19.28	16.73	19.68	19.73
MgO	10.34	10.39	11.59	10.34	15.48	10.93	9.13
CaO	.03	.01	.01	.01	.02	0	.01
MnO	.10	.08	.13	.12	.14	.17	.20
FeO	19.88	19.66	18.36	19.50	13.85	18.26	20.14
BaO	.06	.09	.05	.03	.04	.07	.01
Na_2O	.20	.22	.24	.18	.09	.09	.24
K_2O	9.22	9.33	9.12	9.18	9.38	9.25	9.00
H_2O	3.90	3.87	3.92	3.90	4.02	3.95	3.89
Total	98.68	98.14	98.17	98.47	98.64	98.89	98.31
Atomic porportions based on 22 <0>							
Si	5.31	5.28	5.36	5.26	5.51	5.30	5.22
Ti	.23	.23	.23	.23	.25	.21	.28
Al	3.38	3.40	3.26	3.48	2.93	3.51	3.57
Mg	2.36	2.39	2.64	2.36	3.43	2.47	2.09
Ca	0	0	0	0	0	0	0
Mn	.01	.01	.02	.02	.02	.02	.03
Fe	2.55	2.54	2.34	2.50	1.72	2.31	2.59
Ba	0	.01	0	0	0	0	0
Na	.06	.06	.07	.05	.03	.03	.07
K	1.80	1.84	1.78	1.79	1.78	1.79	1.76
Tetr. Z	8.00	8.00	8.00	8.00	8.00	8.00	8.00
Oct. Y	5.84	5.84	5.84	5.84	5.86	5.82	5.78
Interl. X	1.87	1.91	1.85	1.85	1.81	1.82	1.84
Total	15.70	15.75	15.70	15.69	15.67	15.64	15.62
grains/points	3/7	3/6	3/8	2/6	2/6	2/6	4/11

146-1 = matrix biotites

146-2 = Late, porphyroblastic biotites

APPENDIX III,D: Table of average garnet analyses.

SAMPLE	146 Ga II		146 Ga III		86/87 Ga III		274	308 Ga III	
	rim	centre	rim	centre	rim	centre	Ga III	rim	centre
SiO_2	35.77	36.07	35.73	35.66	36.11	36.10	35.42	36.29	36.61
TiO_2	.01	.05	.06	.11	.03	.06	.07	0	.07
Al_2O_3	21.51	21.70	21.76	21.59	21.11	21.18	21.58	21.64	21.78
Cr_2O_3	0	0	0	0	0	0	0	0	0
Fe_2O_3	2.37	1.75	1.77	1.37	1.57	1.31	1.09	.27	.58
MgO	3.11	2.07	3.05	1.83	2.61	2.62	2.64	3.38	2.89
CaO	4.70	5.51	4.26	4.85	1.72	2.12	1.85	1.19	1.75
MnO	.90	2.17	1.37	5.87	8.19	9.90	7.08	6.42	9.05
FeO	32.26	31.92	32.38	28.89	29.26	26.94	29.77	30.28	28.28
Total	100.63	101.23	100.39	100.18	100.60	100.23	99.50	99.47	101.01
Atomic proportions based on 24 <0>									
Si	5.736	5.768	5.741	5.772	5.836	5.842	5.777	5.876	5.858
Ti	.001	.006	.007	.013	.004	.007	.009	0	.008
Al	4.065	4.090	4.121	4.119	4.021	4.040	4.149	4.130	4.108
Cr	0	0	0	0	0	0	0	0	0
Fe^{3+}	.286	.210	.215	.167	.191	.160	.134	.033	.069
Mg	.743	.493	.730	.442	.629	.632	.642	.816	.689
Ca	.808	.944	.733	.841	.298	.368	.323	.206	.300
Mn	.122	.294	.186	.805	1.121	1.357	.978	.881	1.227
Fe^{2+}	4.326	4.269	4.351	3.912	3.955	3.646	4.060	4.100	3.785
X_{Fe}	.85	.90	.86	.90	.86	.85	.86	.83	.85
X_{Mn}	.02	.06	.04	.16	.20	.24	.17	.15	.22
Tetr.Z	6.00	6.00	6.00	6.00	6.00	6.00	6.00	6.00	6.00
Oct.Y	4.09	4.08	4.08	4.07	4.05	4.05	4.07	4.04	4.04
X	6.00	6.00	6.00	6.00	6.00	6.00	6.00	6.00	6.00
Total	16.09	16.08	16.08	16.07	16.05	16.05	16.07	16.04	16.04
AD	7.18	5.41	5.545	4.52	4.86	4.18	3.57	.83	1.94
GR	6.28	10.32	6.68	9.51	.11	1.95	1.82	2.61	3.06
AL	72.11	71.14	72.50	65.20	65.89	60.74	67.63	68.30	63.07
SP	2.04	4.90	3.11	13.42	18.68	22.61	16.29	14.67	20.44
PY	12.39	8.22	12.17	7.32	10.47	10.53	10.69	13.59	11.49
grains/points	1/10		1/7		2/16		3/14	3/14	

APPENDIX III,E: Table of average staurolite, scapolite and chlorite analyses.

STAUROLITE		SCAPOLITE		CHLORITE	
SAMPLE	308	SAMPLE	306	SAMPLE	86/87
SiO_2	26.39	SiO_2	47.37	SiO_2	23.88
TiO_2	.46	Al_2O_3	26.51	TiO_2	.08
Al_2O_3	55.43	TiO_2	.02	Al_2O_3	22.61
MgO	1.36	FeO	.06	MgO	17.32
MnO	.52	MgO	0	CaO	.02
FeO	11.96	MnO	.03	MnO	.39
ZnO	1.23	CaO	15.76	FeO	22.25
H_2O	2.13	Na_2O	4.71	Na_2O	.02
F	.03	K_2O	.41	K_2O	.04
Cl	.02	Cl	.61	H_2O	11.36
		F	.01		
		SO_3	.21		
Total	99.53	Total	95.71	Total	97.97
Atomic proportions based on 24 <O, OH, F, Cl>		Atomic proportions based on 12 <Si+Al>		Atomic proportions based on 36 <O, OH>	
Si	3.68	Si	7.23	Si	5.04
Al	9.11	Al	4.77	Ti	.02
Ti	.05			Al	5.63
Mg	.28			Mg	5.45
Mn	.06			Ca	0
Fe	1.40			Mn	.07
Zn	.13			Fe	3.93
				Na	0
				K	.01
Total	14.71		12.00	Total	20.15
Mg/Mg+Fe	.17	Ti	0	^{X}Mg	.58
		Fe	.01		
		Mg	0		
		Mn	0		
		Ca	2.58		
		Na	1.39		
		K	.08		
		Cl	.13		
		F	0		
		S	.04		
grains/points	1/10	cat[a]	4.07	grains/points	1/17
		% Mej[b]	63.75		
		EqAn[c]	59.05		
		grains/points	1/8		

[a] = (Ti+Fe+Mg+Mn+Ca+Na+K)
[b] = Shaw (1960)
[c] = 100 (Al-3)/3 Orville (1975)